THE THERMAL BEHAVIOUR AND ISOTHERMAL CRYSTALLISATION OF CYCLIC POLY (BUTYLENE TEREPHTHALATE) AND ITS BLENDS

By:

SANI AMRIL SAMSUDIN

UNIVERSITY OF BIRMINGHAM

A thesis submitted to the University of Birmingham

for the degree of

Doctor of Philosophy

School of Metallurgy and Materials

College of Engineering and Physical Sciences

University of Birmingham

August 2010

Synopsis

This thesis concerns the thermal behaviour and isothermal crystallisation kinetics study of cyclic polyesters and its blends, in particular cyclic poly (butylene terephthalate) (c-PBT). The production of c-PBT is interesting; in fact it is different from production of conventional linear PBT since c-PBT is produced by *in situ* polymerisation of cyclic butylene terephthalate oligomers (CBT) in the presence of suitable initiators or catalysts. These relatively novel materials, i.e. CBT offer many advantages in properties and the most unusual and useful is that they can be processed at low viscosity (water like) and exhibit rapid crystallisation. The thermal behaviour and isothermal crystallisation kinetics of CBT and c-PBT were analysed.

The most significant achievement of this project is blending where blends of c-PBT and styrene maleimide (SMI) were prepared by simultaneous *in situ* polymerisation and melt blending of solid dispersion CBT/SMI powder. This is unique and novel and the results show consistency and signs of miscibility although there are no external forces applied during the melt blending. It was found that the presence of 30 wt % and above of SMI impeded the crystallisation of c-PBT. This suggests that miscibility occurred. The miscibility of these c-PBT/SMI blends was support with the presence of a single composition-dependent glass transition temperature and negative Flory-Huggins interaction parameter (χ_{12}).

Studies on crystallisation kinetics of c-PBT were also done by Avrami analysis and using the Hoffman-Lauritzen theory. Previously there have been very limited studies of the crystallisation kinetics of PBT produced from its oligomer. Further work on crystallisation of c-PBT/SMI blends was also performed.

To my father and mother…

and especially to my beloved wife and children..

Niza, Awatif, Adam and Arfan..

Acknowledgements

I wish to express my sincere thanks to my supervisors, Dr. Stephen Kukureka and Dr. Mike Jenkins, who provided invaluable guidance and profound expertise and wisdom throughout the course of my studies. Without their constant encouragement and support, this work would not have been possible and accomplished.

I also would like to thank Mr. Frank Biddlestone who always gave valuable advice and technical support throughout this project. His wide experience, ideas and constructive comments always helped me to solve experimental difficulties.

I am deeply indebted to all my colleagues for support, sharing their knowledge and precious friendships that made my life abroad so enjoyable. Without them I would have felt very lonely on the way to accomplish my mission.

A scholarship from the Higher Education Ministry of Malaysia (MOHE) and financial support from Universiti Teknologi Malaysia (UTM) are gratefully acknowledged.

Finally, I would like to give my special thanks to my wife Siti Zurainiza Ibrahim and my children Awatif, Adam and Arfan, for always being there for me. Thank you for sharing my difficulties and supporting me with endless love and patience to realise this dream.

Contents

List of Figures

List of Tables

Abbreviations

ABS	*Acrylonitrile butadiene styrene*
ATR	*Attenuated total reflectance*
BPACY	*Cyclic oligomers of bis-phenol A polycarbonates*
CBT	*Cyclic butylene terephthalate oligomers*
CEO	*Cyclic ester oligomers*
CL	*Caprolactone*
CMC	*Critical monomer concentration*
COOH	*Carboxyl*
c-PBT	*Cyclic poly (butylene terephthalate)*
DMAPA	*Dimethylaminopropylamine*
DSC	*Differential scanning calorimetry*
EMAA	*Ethylene-methacrylic acid*
EVA	*Poly (ethylene-co-vinyl acetate)*
FTIR	*Fourier transform infrared spectroscopy*
GPC	*Gel permeation chromatography*
HDT	*High heat-deflection temperatures*
HFIP	*1,1,1,3,3,3-hexafluoro-2-propanol*
HIPS	*High impact polystyrene*
IEC	*International electrotechnical commission*
IPN	*Interpenetrating polymer network*
ISO	*International organization for standardisation*
KOH	*Potassium hydroxide*

MA	*Maleic anhydride*
o-DCB	*o-dichlorobenzene*
OH	*Hydroxyl*
PAr	*Polyarylate*
PBT	*Poly (butylene terephthalate)*
PDMS	*Poly (dimethyl siloxane)*
PEEK	*Poly (ether ether ketone)*
PEI	*Poly (ether imide)*
PEO	*Poly (ethylene oxide)*
PET	*Poly (ethylene terephthalate)*
PMMA	*Poly (methyl methacrylate)*
p.p.m	*Parts per millions*
PS	*Polystyrene*
PTFE	*Poly (tetra fluoro ethylene)*
PTMEG	*Poly (tetra methylene ether glycol)*
PTT	*Poly (trimethylene terephthalate)*
PVAc	*Poly (vinyl acetate)*
PVB	*Poly (vinyl butyral)*
ROP	*Ring opening polymerisation*
RRIM	*Reinforced reaction injection molding*
RTM	*Resin transfer molding*
SAN	*Styrene-acrylonitrile copolymer*
SAXS	*Small-angle X-ray scattering*
SEC	*Size exclusion chromatography*

SEM	*Scanning electron microscopy*
SHS	*Styrene-hydroxystyrene copolymer*
SMA	*Styrene maleic anhydride copolymer*
SMI	*Styrene maleimide copolymer*
TBTE	*Tributyltin ethoxide*
TGA	*Thermogravimetric analysis*
THF	*Tetrahydrofuran*
US	*United States*
VOC	*Volatile organic compounds*

Symbols

α	*Empirical constant which depends on the chemical structure of the polymers*
σ	*Lateral surface energy*
σ_e	*Folding chain surface energy*
$\sigma\sigma_e$	*Surface free energy product*
ϕ	*Volume fraction*
χ_{12}	*Flory-Huggins interaction parameter*
ρ	*Density*
%	*Percentage*
B	*Interaction energy density*
b_o	*Molecular thickness, separation between two adjacent fold planes*
°C	*Degree Celsius*
C_p	*Specific heat per unit mass*
ΔE	*Activation energy for viscous flow*
f	*Correction factor,* $(\frac{2T}{T+T_m^o})$
ΔG_n	*Free energy of nucleus formation*
ΔG_n^*	*Free energy of formation of a critical size secondary nucleus*
ΔG_v	*Free enthalpy change between solid and liquid phase*
g	*Steady-state growth rate of a crystal*

g_o	*Temperature-independent constant*
ΔH_f^o	*Heat of fusion for 100% crystalline polymer*
ΔH_v	*Enthalpy of crystallisation*
K	*Kelvin*
K_g	*Nucleation constant*
k	*Boltzmann constant (1.380×10^{-23} JK^{-1})*
M_w	*Molecular weight*
µm	*Micrometer*
m	*Mass, also Degree of polymerisation*
mg	*Milligram*
mL	*Millilitre*
n	*Avrami's exponent, also number of molecular strands*
Q	*Energy*
R	*Gas constant (8.314 $JK^{-1}mol^{-1}$)*
ΔS_v	*Entropy of crystallisation*
T	*Temperature*
T_c	*Crystallisation temperature*
T_g	*Glass transition temperature*
T_m	*Melting point temperature*
T_m^o	*Equilibrium melting temperature*
T_∞	*Temperature below which the motions of crystallisable segments to the crystallisation face cease*

t	*Time*
ΔT	*Degree of super-cooling* $(\Delta T = T_m^o - T_c)$
$t_{1/2}$	*Crystallisation half-life*
U^*	*Activation energy for viscous flow*
V	*Molar volume*
wt %	*Weight percentage*
w	*Weight fraction*
X_t	*Fractional crystallinity*
Z	*Composite rate constant*

Chapter One

INTRODUCTION

1.1 Cyclic Polyesters

1.1.1 Evolution: Past and current research

The first publications on synthetic polymers with macrocyclic structures were reported for poly (dimethyl siloxane) (PDMS) by Scott [1] in 1946. The series of publications [2-5] on the preparation and characterisation of cyclic PDMS was followed by the reporting of cyclic polystyrene (PS) by Gieser and Hocker in 1980 [6, 7]. Studies on the macrocyclic structures of synthetic polymer then continued with reports of macrocyclic structures in engineering thermoplastics, i.e., polymers with high melting temperatures such as polyesters [8-16]. The early work mostly focussed on the preparation of macrocyclic structures from engineering thermoplastics, but since the syntheses were inefficient, purification of the products was needed [10-12, 15, 17-25].

After the process for preparing cyclic ester oligomers (CEO) was patented in 1995 [11], further work then focussed on the polymerisation processes of these cyclic oligomers and the availability or effectiveness of catalysts to initiate the polymerisation [13, 18, 21, 26-44]. The early polymerisation of these materials used tin and titanium catalysts as initiators and this has been extensively investigated by the Cyclics Corporation and the General Electric Company [45-48].

Two types of polymerisation processes were reported during conversion of these cyclic oligomers to polymers, i.e. ring opening polymerisation (ROP) [13, 24, 27, 28, 32, 49] and ring expansion polymerisation [13, 14, 26, 41]. Polymerisation routes depend on which types of catalysts are used in the polymerisation process. The use of cyclic catalyst such as stannoxane lead to ring expansion polymerisation and leads to the production of macrocyclic polymers, while linear catalyst e.g. tributyltin ethoxide (TBTE) lead to the production of linear polymers through ring opening polymerisation (ROP) [14]. Work to introduce new types of catalysts which could initiate CEO still carries on. In a recent example, Tripathy *et al.* [34] studied the effect of catalyst, i.e. stannoxane, butyltin chloride dihydroxide and tetrakis-(2-ethylhexyl) titanate on polymerisation of CEO in particular cyclic butylene terephthalate oligomers (CBT). Furthermore, they also investigated the effect of polymerization temperature on the *in situ* polymerization of CBT for composite applications.

After studies of polymerisation of these cyclic oligomers, researchers discovered the unique properties of these materials, which became a reason why interest in CEO has increased dramatically over the last few years. The advantages of these materials are they

have a low melt viscosity (water-like), rapid isothermal bulk polymerisation, rapid crystallisation with a high degree of crystallinity, and they do not produce chemical emissions during processing [50-52]. Moreover, their molecular weight can be tailor made for specific application and/or manufacturing processes [52]. The polymerisation and crystallisation have been found to occur simultaneously, and the mechanisms involved have been studied [13, 14], while the industrialists are more focussed to exploit the advantage of the low melt viscosity of this material in order to suit current needs.

The creation of these cyclic oligomers and their associated advantages solved some problems in thermoplastic composites [33, 51, 53-63]. It is known that the main limitation in fabricating continuous fibre thermoplastic composites is the high melt viscosity of the thermoplastic itself. The presence of low viscosity pre-polymers of cyclic oligomers however gives the best option for thermoplastic composites. These cyclic oligomers should be able to be processed reactively like a thermoset but retain their behaviour as a thermoplastic in the final state. This means that they are capable of being reground, re-melted and reprocessed again for recycling purposes. At the present time, the industrial trend is to replace thermosets by thermoplastics due to recycling problems and this is a prime strategy of polymer life-cycle engineering [64]. Their low melt viscosity (which is reported as low as 17 centipoises) [50-52] could overcome the problems in impregnation of fibers, flow of resin and removal of bubbles which are usually found in the use of thermoplastics for fiber-reinforced polymer composite applications. Moreover, cyclic polymers were suggested for processing with reinforced reaction injection moulding (RRIM) or resin transfer moulding (RTM) which has been traditionally monopolised by thermosets resins [65].

These novel materials are not only limited to liquid composite moulding applications. Recently, many studies of cyclic oligomers have been concerned with blending with other thermoplastics which have potential for novel structures and which cannot be achieved by conventional blending method [50, 66-71]. These blends may result in miscible or immiscible forms. Tripathy *et al.* [50] found that the blends of *in situ* polymerised PBT from cyclic oligomers (c-PBT) and poly(vinyl butyral) (PVB) show evidence of miscibility, where the blend shows only one glass transition temperature. However, blends of linear PBT with PVB did not show any sign of miscibility during the investigation. They concluded that the cause of miscibility in the *in situ* prepared c-PBT/PVB blends was thought to be the formation of a graft copolymer.

The *in situ* polymerisation of cyclic oligomers inside the blend system also offers the possibility of producing nanostructured composites. It was reported that cyclic carbonate oligomers (BPACY) blended with styrene-acrylonitrile copolymer (SAN) produced on unique nanostructure by liquid-liquid phase separation during *in situ* polymerisation of BPACY [66]. Tripathy *et al.* [51] in 2003 reported that the production of c-PBT nanocomposites prepared by *in situ* polymerisation of CBT. They successful produced the c-PBT/clay nanocomposite by an *in situ* polymerisation in the presence of cyclic stannoxane catalyst and sodium montmorillonite. In the latest publication on nanocomposites based on CBT, Jiang *et al.* [63] reported the production of c-PBT/silica nanocomposites prepared *via* high speed stirring followed by subsequent *in situ* polymerisation. Furthermore, the work of Bahloul *et al.* [70] in 2009 found that the morphology of poly(ethylene-co-vinyl acetate) (EVA)/PBT blends prepared by the *in situ*

polymerisation of CBT in the presence of molten EVA copolymer had a fine dispersion of PBT phase with sizes ranging from 100 to 500 nm in diameter.

Further reasons for blending these materials are typical for polymer blends; that is for property enhancement. c-PBT has been reported to have excessive crystallinity compared with conventional PBT [13, 14, 16]. This results from rapid concurrent crystallisation during the polymerisation process of CBT. It is known that the amount of polymer crystallinity can have an effect on the physical properties of the material, i.e., brittleness and ductility [43, 72-74]. The technique of copolymerisation can be used to control the properties of the polymer, i.e., crystallinity and melting point (T_m). For example, Tripathy *et al.* [67] controlled the excessive crystallinity in c-PBT by ring-opening copolymerisation CBT with caprolactone (CL). They successfully eliminated the typical brittle nature of c-PBT polymers by the incorporation of a small amount of CL.

1.2 Poly (butylene terephthalate) and its cyclic oligomers

Poly (butylene terephthalate) (PBT), an alkylene phthalate polyester is prepared commercially through the transesterification reaction (polycondensation) of 1,4-butanediol with either terephthalic acid or dimethyl terephthalate [14, 75]. The chemical structure for this polymer is shown in Figure 1.1. This polymer consists of both a flexible link and a rigid segment, i.e., four methylene groups and a terephthalate group, respectively [14, 43]. The chemical structure also shows this polymer to have hydroxyl and carboxylic acid end groups. PBT is a semi crystalline polymer with crystallinity reported in the range 35 to

45% [14] and can achieve 55 to 60% through annealing [76]. The typical glass transition temperature (T_g) of PBT is in the range from 30 to 50 °C, depending on the degree of crystallinity, annealing, amount and type of fillers, and measuring method [75]. This T_g can shift to lower temperatures (15 °C) if the PBT is fully amorphous [77]. The melting and crystallisation behaviour of this polyester is strongly dependent on the thermal history. Usually, the crystalline melting temperature was reported to be in the range 225 to 232 °C [77-79], while the equilibrium melting temperature (T_m^o) was estimated to be 245 °C [80].

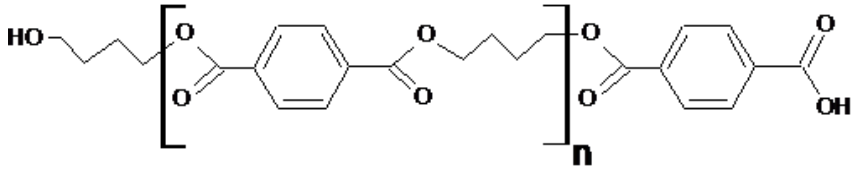

Figure 1.1: Chemical structure of linear poly (butylene terephthalate)

This type of polyester was introduced to the commercial market in the late 1960s by Celanese [75]. PBT is classified as an engineering thermoplastic due to its performance. It is in very good demand by industry [75, 80, 81] for its excellent thermoplastic processing capabilities boosted by its rapid crystallisation kinetics and semi-crystalline characteristics. These characteristics allow PBT to be used in harsh environments which require chemical resistance, thermal resistance, low friction and wear characteristics [14]. Other advantages of this polyester are high stiffness and strength, high toughness at low temperatures, high heat-deflection temperatures (HDT), high stress-cracking resistance, high resistance to fuels, oils and fats, and good processability [52, 75, 82].

PBT is a mature material widely used in the automotive industry (interior and exterior parts), household electrical appliances and connectors, telecommunications, machine component, food and medical applications. Given the pressure to re-cycle in these industries especially in the automotive sector [14, 50, 75], a recycling process has been explored. This process involves the conversion of waste polyesters to cyclic ester oligomers (CEO) through ring-chain equilibration of polymer in dilute solution (depolymerisation) with various catalysts [15, 20, 25, 83].

The idea of depolymerisation as a way to produce CEO was introduced by the pioneering work of Spanagel and Carothers [8, 16] in the 1930s. This method was found to be effective for the preparation of small-ring esters and carbonates. However, the researchers found limitations for commercial exploitation of this method such as long reaction times and large amounts of solvent needed to achieve high yields. Jacobson and Stockmayer [16, 84] in their theory state that the ring-chain equilibration of a polymer will lead to a mixture of cyclic oligomers and polymer in which a critical monomer concentration (CMC) can be defined for each monomer structure. A cyclic structure can only be achieved if the concentration of polymer is lower than the CMC, while the mixture of cyclics and polymer will be present if the concentration of polymer is above the CMC.

Early work to convert linear PBT into CBT was reported by Brunelle and Bradt [17, 19]. They patented their work on preparation of macrocyclic polyesters *via pseudo* high dilution condensation of butanediol with terephthaloyl chloride using catalyst as shown in Figure 1.2. They successfully produced cyclic oligomers through this process but because of the high cost of acid chloride this process was not commercially economical.

Also this process has other limitations such as the need to maintain rigorously dry conditions in the solvents and reactor.

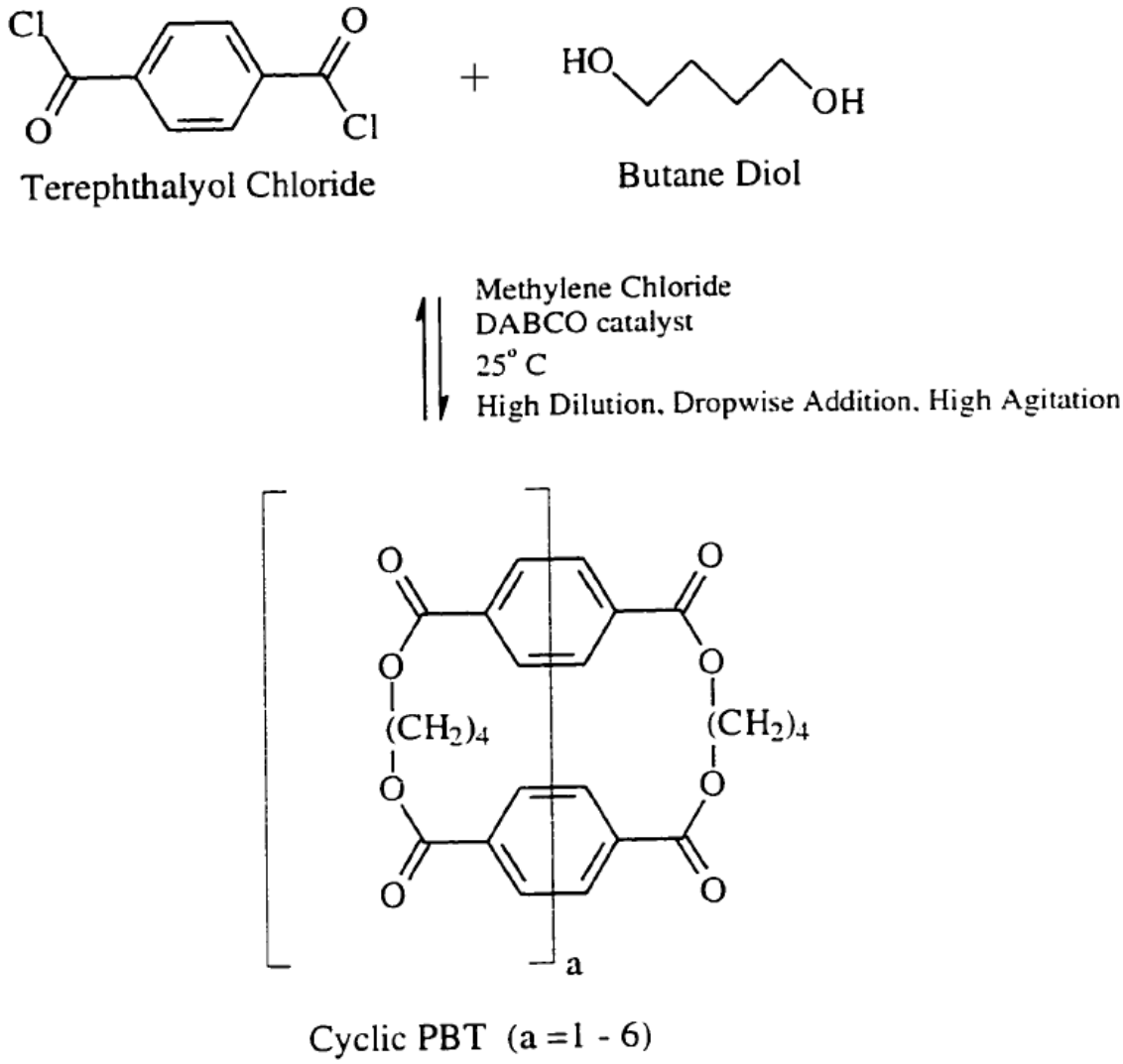

Figure 1.2: Preparation of CBT through direct condensation reaction [14, 19]

Finally, Brunelle and Takekoshi [11] patented their findings on efficient preparation of alkylene phthalate cyclic oligomers *via* ring-chain equilibration in 1995. They dissolved PBT in dry o-dicholorobenzene (o-DCB) and then added the equilibration catalyst (Figure 1.3). Most of the early work used tin catalysts since these types of catalyst were found more effective than titanates for the ring-chain equilibration reaction. They also found that a large amount of dilute solution is not necessary to form reasonable yields of cyclic oligomers. However, based on their observation 100% yields of cyclics can never be achieved at very low reaction concentration (CMC) since the starting material (polymer) has end groups [11]. The work of Brunelle *et al.* [13] continued three years later (1998) with the publication on the preparation of alkylene phthalate cyclic oligomers *via* a novel *pseudo* high dilution condensation reaction.

The cyclic oligomers produced are then readily polymerized to high molecular weight polyesters in the presence of suitable catalysts within a few minutes. Polymerisation of CBT was reported over the range 160 °C to 200 °C [13, 26, 29-31]. Before that temperature was reached, the CBT began to melt at about 140 °C, and it was completely molten at 160-190 °C. Al-Zubi *et al.* [52] reported that the melt viscosity of this material reduced as the temperature increased. They found that at 180 °C the melt viscosity is 28 centipoises and reduced to 22 and 17 centipoises upon heating to 190 °C and 200 °C, respectively.

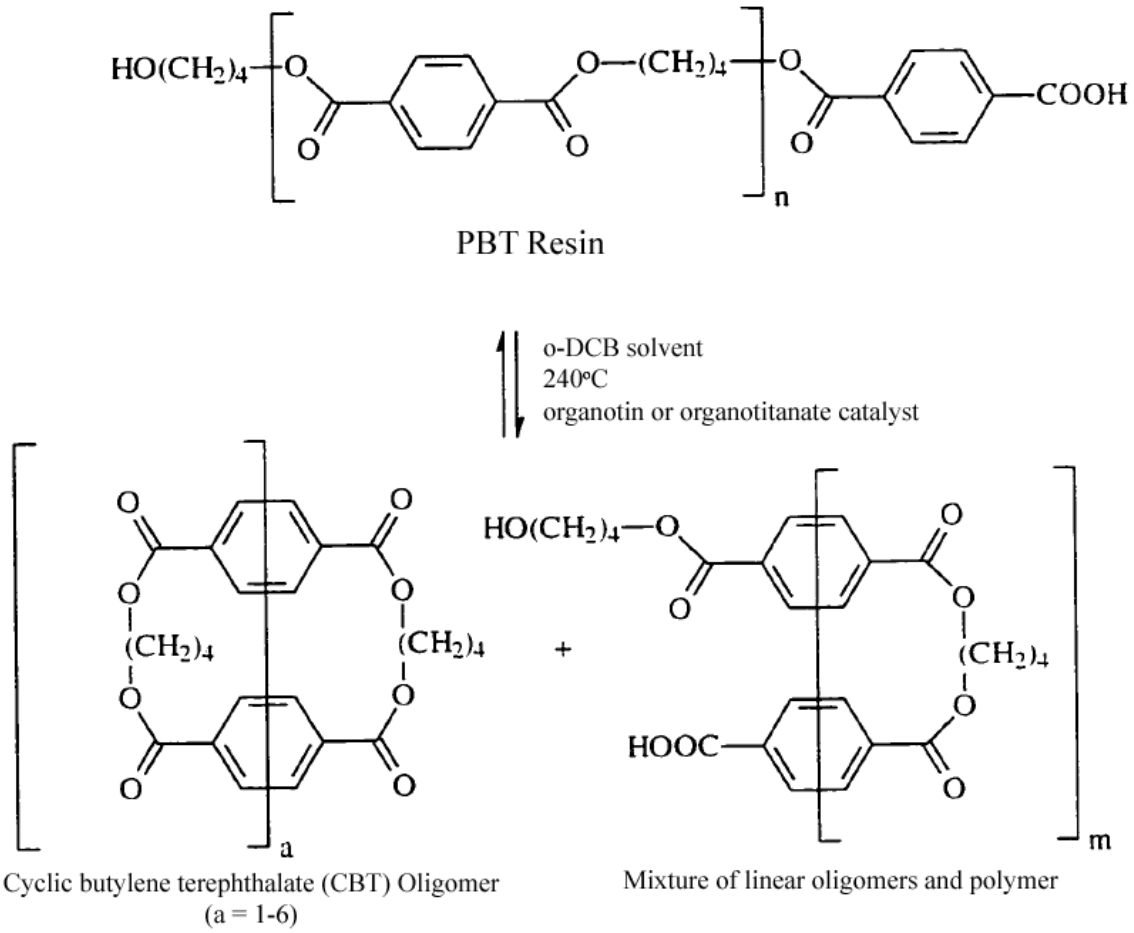

Figure 1.3: Ring-chain equilibration reaction of Brunelle and Takekoshi [11, 14]

1.3 Stannoxane

As mentioned earlier, CBT need a suitable catalyst to perform *in situ* polymerisation in order to produced polymer. Tin and titanium initiator have been reported to be efficient catalysts which successfully convert CBT into polymer [13, 45-48]. One of the most suitable tin initiators is butyltin alkoxides [26]. The tin initiator is known to be stabilised by two or three short alkane structures which are typically butyl groups [14].

Ramsden *et al.* [85] have introduced the dimer of dibutyl tin dioxide (Figure 1.4) in cyclic form [26] which was used in the polymerisation of CBT. Technically this initiator is 1, 1, 6, 6-tetra-n-butyl-1, 6-distanna-2, 5, 7, 10-tetraoxyacyclodecane and it also known as stannoxane. The used of this cyclic initiator will lead to ring expansion polymerisation which produces macrocyclic polymers as a result [13, 16, 26, 41]. Other tin compounds (such as dibutyltin oxide and tributyltin ethoxide) as catalysts will lead to production of linear polymers through ring opening polymerisation [14, 16, 26].

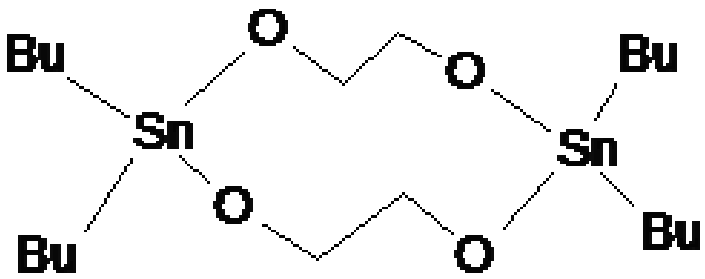

Figure 1.4: The dimer of dibutyl tin dioxide (stannoxane)

1.3.1 Polymerisation of CBT using stannoxane

Brunelle *et al.* [13] found that certain tin and titanium catalysts were most effective in initiating polymerisation of CEO although many types of compounds are available. With 0.05-1.0 mol % cyclic stannoxane based on monomer units used the CBT polymerisation is believed to undergo ring expansion polymerisation [13, 14, 26, 41].

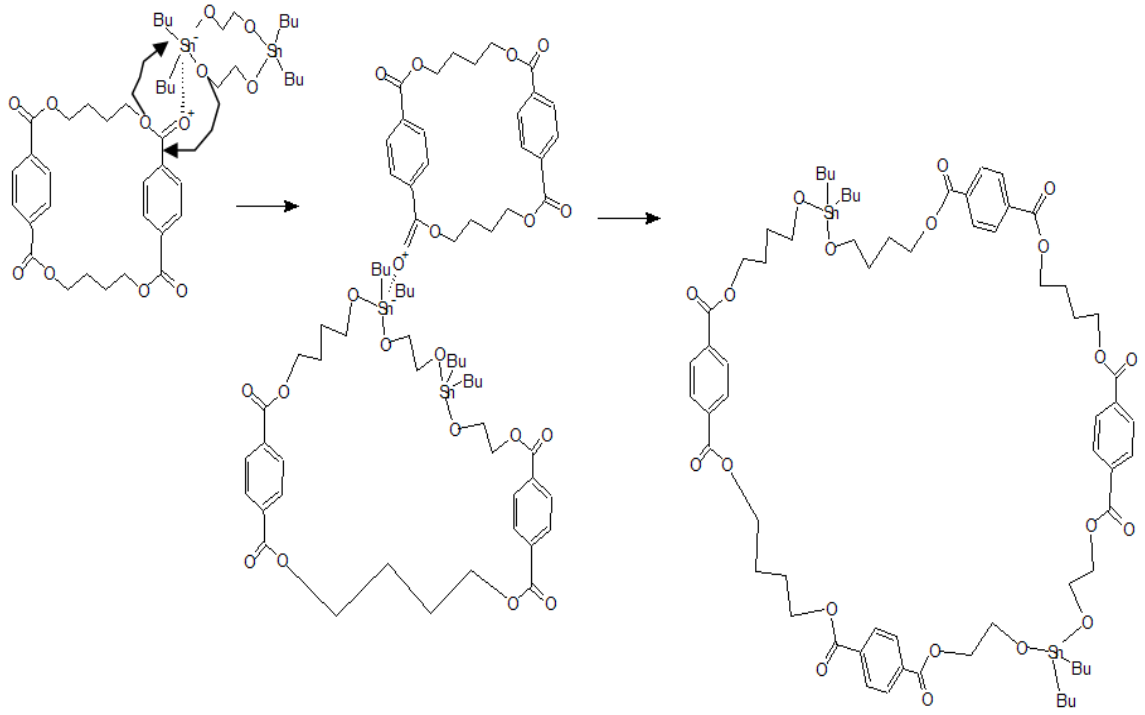

Figure 1.5: Ring expansion polymerisation of CBT using stannoxane

Figure 1.5 illustrates the ring expansion polymerisation process of CBT which occurs using stannoxane as an initiator. As stated earlier the Sn-O bonds of the cyclic stannoxane are known to be the active polymerization sites. These are active throughout the entire polymerisation. A bond exchange takes place which results in the breaking and reforming of one Sn-O bond in the stannoxane and one C-O bond in the ester group of the CBT, leading to insertion of the stannoxane initiator in the ring molecule [14]. Once the first ring has been opened, oligomers and other stannoxane containing rings are added, increasing the size of the ring. The ring expansion is entropy driven (only a little strain in the CBT) and as consequence the process is athermal [13, 16, 50] . The resulting chain structure is that of large ring (a macrocycle) consisting of PBT repeat units and the

stannoxane initiator. Throughout the entire polymerisation the Sn-O remains unbroken where the reactivity of that bond is not altered by the expansion reaction.

Ideally, the incorporation of the stannoxane catalysts into the CBT results in cyclic polymer (c-PBT) with no end groups and by-products. The c-PBT produced by ring expansion polymerization with stannoxane initiators has higher molecular weight, greater crystallinity and more perfect crystalline morphology than linear PBT [13, 14, 16].

However, the use of stannoxane in the polymerisation of CBT has limitations. This is because stannoxane has been found to be sensitive to moisture and thermally unstable at high temperature (> 230^{o}C) [13, 14, 16, 31]. Miller [14] in his thesis reported that stannoxane could exhibit two types of degradation which can cause the macrocyclic polymer chain to break and result in linear polymers. Degradation of stannoxane may occur because of thermal instability and the presence of moisture. He suggested that water degradation of cyclic chains resulting in only hydroxyl end groups as shown in Figure 1.6.

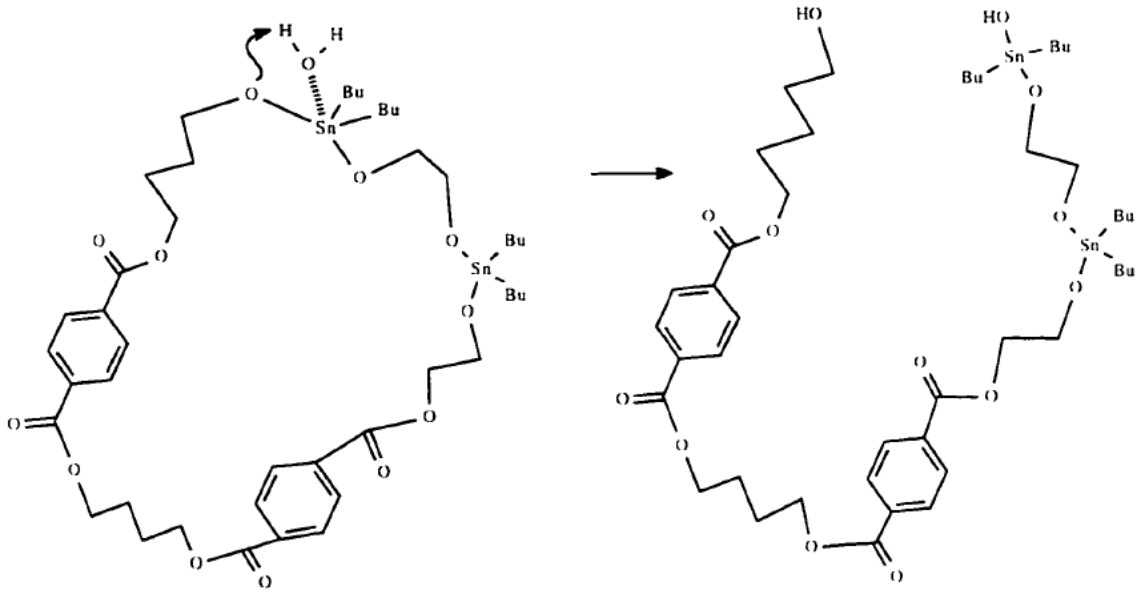

Figure 1.6: Mechanism for water degradation of stannoxane [14]

1.4 Styrene Maleimide (SMI) copolymer

Copolymers of styrene and maleic anhydride (MA) were prepared in order to improve the heat resistance of PS [86]. The further work of Moore (1986) [87] found that the copolymer of styrene and maleimide could offer more heat resistance. Styrene maleimide (SMI) is a low molecular weight (M_w = 5,000 to 10,000) synthetic copolymer that is composed of styrene and dimethylaminopropylamine (DMAPA) maleiamide [88]. This copolymer is formed by a radical polymerisation using organic peroxide as the initiator. The chemical structure of SMI has tertiary amine functional groups as shown in Figure 1.7.

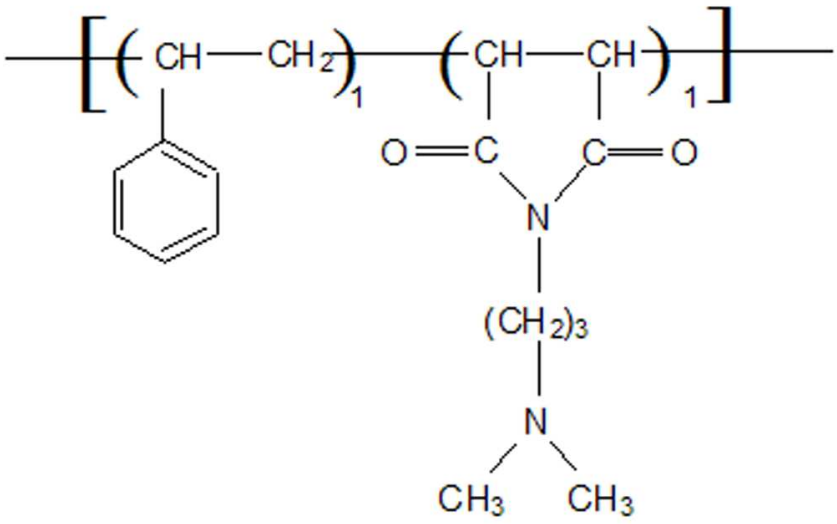

Figure 1.7: Structure of styrene maleimide (SMI)

SMI copolymer has a low melt viscosity, high thermal stability (decomposition temperature greater than 300 °C), and a low volatile organic compounds (VOC) content [87, 88]. The glass transition and softening point temperatures of this copolymer are less than 100 °C. SMI can also function as a polyimide or polyamine additive, serving as a cross-linking agent, curing catalyst or surface modifying agent. This synthetic copolymer can perform a variety of functions in water-based applications i.e. serving as an emulsifying agent, cationic dispersant, flocculating or coagulating agent as they easily form cationic salts. The typical uses of this copolymer include paper manufacture, alkaline resistant coatings, adhesives and polymer modification [88].

1.4.1 Solubility of SMI copolymer

The SMI copolymer has good solubility in organic solvents with at least moderate polarity. The solubility characteristics of SMI at room temperature ($25^{o}C$) in a variety of solvents are listed in Table 1.1.

Table 1.1: Solubility of SMI in organic solvents [88]

Solvent	**Type**	**Solubility** (insoluble = <5 wt. %, very soluble= >40 wt. %)
Cyclohexane	Aliphatic	Insoluble
Toluene	Aromatic	Very soluble
Methanol	Alcohol	Soluble
Acetone	Ketone	Very soluble
Tetrahydrofuran (THF)	Ether	Very soluble
Ethyl acetate	Ester	Very soluble
Chloroform	Chlorinated	Very soluble

Ref: Sartomer Company, Inc.

1.4.2 Applications of SMI copolymer

In applications such as printed circuit boards and powder coatings, styrene maleic anhydride (SMA) has been used as curing agent with epoxy resin formulation. The SMI copolymer can then be used as a catalyst for these formulations (containing (SMA) resin and epoxy resin). In general, the epoxy-anhydride cross-linking reaction can be speeded up with the presence of the small molecule additives such as imidazoles or tertiary amines. Since the SMI copolymers contain tertiary amine functionality, they are suitable to act as

anhydride-epoxy catalysts and offer the advantages of no migration or volatility from formulation. This copolymer is also found to be miscible in the anhydride-epoxy formulations [88].

The high solubility of SMI copolymers in various organic solvent makes them useful in many applications. This can be enhanced by the resin's excellent water resistance, alkali resistance and thermal stability properties.

The surface adhesion between the polyolefin and water-based inks and paints can be improved by the addition of SMI copolymer. In general procedure, the SMI copolymer is added during melt processing of the polyolefin. They should be compatible with other additives and fillers typically used in the production of polyolefin parts or films.

1.5 Background of the studies

PBT is well known to be among the easiest of the semi-crystalline polymers to crystallise [13, 14, 75, 89]. This makes PBT difficult to produce amorphous structures unless specimens are very thin and quenching is very rapid [14]. Miller [14] in his thesis discussed how PBT can form two types of spherulites during isothermal crystallisation depending on the rate of crystallisation. At a low rate of crystallisation and small degree of under-cooling (where crystallisation takes place at temperatures above 180^{o}C), the crystallisation of linear PBT resulted in the 'usual' spherulites. While, below the temperature of 180^{o}C, at which the highest rate of crystallisation occurred, 'unusual'

spherulites will be formed. Stein and Misra [90] have defined ‘usual’ spherulites as the one with the Maltese cross is dark arms positioned at 0° and 90° to the optical axes of polarisation when examined in polarized optical microscopy as shown in Figure 1.8 (i), while the ‘unusual’ spherulites is indentify by a 45° rotation of the Maltese cross . They also found that the ‘usual’ spherulites produces a small angle light scattering (SALS) pattern with intensity lobes at 45° to the polarised light (Figure 1.8 (ii)) and the ‘unusual’ spherulites produces a SALS pattern with intensity lobes at 0° and 90° to the polarisation planes.

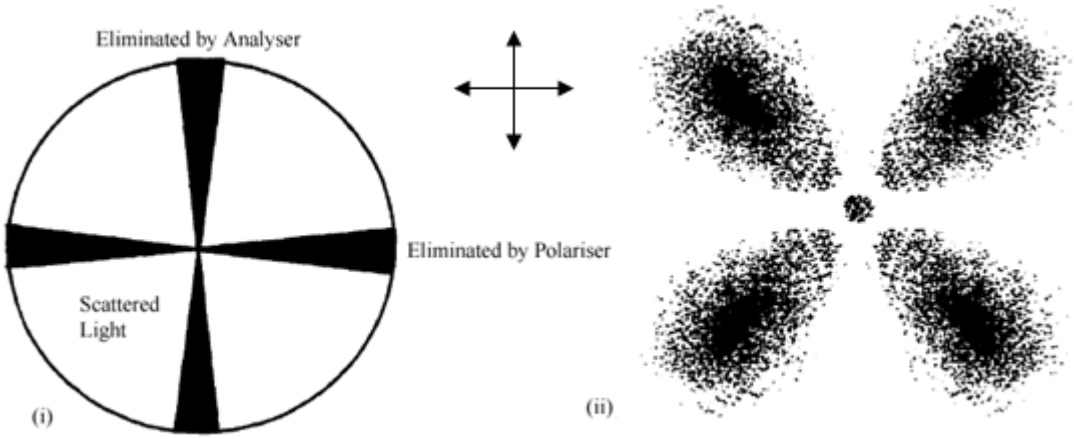

Figure 1.8: (i) Illustration of PBT’s usual spherulites examined by polarized optical microscopy, (ii) Illustration of the clover-leaf pattern of PBT’s usual spherulites examined by SALS. Arrows show the direction of polarisation axes [90]

However, it is found that cyclic PBT, produced by isothermal polymerisation and crystallisation at 190 °C, is composed only of the 'usual' spherulites [14]. They are small (approximately 2-3 µm diameter) and appear to be produced by very rapid crystallisation. This suggests that cyclic PBT crystallises easily and there are clear differences in kinetics compared with linear PBT. This behaviour is not fully understood and is further complicated by the fact that for the cyclic PBT, crystallisation and polymerisation are taking place at the same time.

Cyclic oligomers also have enormous potential for novel structures when blended with other thermoplastics [50, 66, 68, 91, 92]. These blends may be as miscible [50, 66, 68, 91] or immiscible [92] and both types may have useful properties and structures inaccessible by other means. For instance blends of c-PBT with poly(vinyl butyral) (PVB) have successfully been made where PVB is an industrially important polymer widely used in laminated safety glass and surface treatment. Preliminary work has also been done with ε-caprolactones (biodegradable polymers with applications in drug delivery) [67, 68]. Cyclic oligomers of PBT have successfully been copolymerized in situ with ε-caprolactones in the presence of stannoxane catalysts. Another interesting finding during blends cyclic oligomers with other polymer is possibility to form nanocomposites by liquid-liquid phase separation. An example of this case is cyclic carbonate oligomers blended with styrene-acrylonitrile copolymer (SAN) [66]. This blends system (CBT/SAN) shows nanostructures where unobtainable with blends based on conventional linear polymers. Moreover, the morphology of the resulting nanocomposites has been shown to have interesting effects on mechanical properties with potential applications. There are

also more general effects of the topology of cyclic polymers on blend miscibility and hence on the production of nanocomposites [18, 91, 93, 94].

Therefore, the investigation of the thermal behaviour and crystallisation kinetic study of c-PBT and its blends will form the basis in this present study. The knowledge extension on this material could be aspect from the blends of c-PBT with amorphous polymers (i.e. SMI). To date, the c-PBT/SMI blend system has not received any attention in the literature.

1.6 Aims and objectives

The study is divided into two sections. In the first section, the aim is focused on understanding the thermal behaviour of CBT and c-PBT. Since the polymerisation and crystallisation are reported to occur simultaneously, the investigations will concentrate on understanding these phenomena by various thermal analysis techniques.

Differential scanning calorimetry (DSC) techniques will be fully utilised to examine the thermal behaviour of the CBT and the polymer produced, as well as to explore the optimum polymerisation conditions (i.e. temperature and time) for production of c-PBT. This introductory exploration of the thermal behaviour of CBT and c-PBT also has the aim of gaining useful results in terms of crystallisation kinetics.

Several other characterisation techniques will be used in addition to DSC, in order to have a better understanding on the thermal behaviour of the cyclic polymer. Fourier transform infrared spectroscopy (FTIR) will be used to identify the functional groups in the CBT. Furthermore, the FTIR technique also will be used to study the effect of *in situ* polymerisation to the functional groups in CBT as well as understanding the mechanism of ring expansion polymerisation with the presence of stannoxane initiator.

Other objectives in the first section are to gather information on molecular weight development during *in situ* polymerisation process and the thermal stability of the materials. This information can be achieved with the gel permeation chromatography (GPC) and thermogravimetric analysis (TGA) experiments, respectively.

Information on characterisation of CBT and c-PBT will lead to the second section of the study which is to blend c-PBT with other polymers i.e. SMI (amorphous polymer). In the first instance, this second section work is to see if the blend systems studied are miscible or immiscible, and how this is affected by composition. The objective is also to investigate the effect of miscibility of blends of c-PBT with amorphous polymer on the rapid crystallisation process which found in c-PBT. The crystallisation kinetics of the blends will be examined.

Chapter Two

MATERIALS AND METHODOLOGY

2.1 Materials

2.1.1 Cyclic butylene terephthalate oligomers (CBT)

The CBT (grade XB2-CA4) of molecular weight (M_w = (220) $_n$ (with n=2-7)) in powder form was provided by the Cyclics Corporation (2135, Technology Drive, Schenectady, New York 12308, USA). The XB2-CA4 system contained the stannoxane catalyst and was termed a one-component CBT, where the resin and catalyst were premixed. The general procedures for combining CBT and catalyst are described in a US patent assigned to Cyclics Corporation [95]. The CBT was dried in a vacuum oven for 24 hours at 90 °C prior to processing. The general properties and typical values for CBT resin (with polymerisation catalyst for use with composite) are shown in Table 2.1.

Table 2.1: CBT® resin general properties and its typical values

Property	**Value**
Appearance	White pellets or powder
Melting range	120 to 200 °C
Heat of melting	64 J/g
Density 20 °C (solid)	1.3 g/cm^3
Bulk density (as pellets)	0.7 g/cm^3
Water content	<1000 p.p.m
Specific heat	1.25 J/(g.°C) solid 1.96 J/(g.°C) liquid
Typical Processing Temperature	180 to 250 °C
Maximum Processing Temperature	260 °C
Decomposition Temperature	290 °C (air) 370 °C (nitrogen)
Polymerisation molecular weight (gel permeation chromatography (GPC) relative to polystyrene standard)	>100,000

*Ref: Product information from Cyclics Corporation.

2.1.2 Stannoxane

The initiator which is stannoxane (technically known as 1, 1, 6, 6-tetra-n-butyl-1, 6-distanna-2, 5, 7, 10-tetraoxyacyclodecane) in white powder form was also supplied by the Cyclics Corporation (2135, Technology Drive, Schenectady, New York 12308, US).

2.1.3 Poly (butylene) terephthalate (PBT)

The linear poly (butylene) terephthalate (PBT) (PF100NT) in pellet form was purchased from Polyram through Plastribution Limited (81 Market Street, Ashby de la Zouch, Leicestershire, LE65 1AH United Kingdom). This PBT is a high viscosity grade which is formulated for general purpose and injection moulding applications. This material was also dried in a vacuum oven for 24 hours at 90 °C prior to processing. The general properties and typical values for PBT resin supplied by its manufacturer are shown in Table 2.2.

2.1.4 Styrene maleimide (SMI)

Styrene maleimide (SMA® 1000I) resin in a powder form was supplied by the Sartomer Company (502 Thomas Jones Way Exton, PA 19341, US). The SMA® 1000I is a low molecular weight copolymer of styrene and dimethylaminopropylamine maleimide, with an approximate 1:1 mole ratio. The typical physical and chemical properties from the manufacturer are shown in Table 2.3.

Table 2.2: Datasheet of PBT (PF100NT) from Polyram

PHYSICAL PROPERTIES	UNIT	TEST METHOD	VALUES
DENSITY	g/cm^3	ISO-1183	1.3
WATER ABSORPTION	%	ISO-62	0.6
MOULD SHRINKAGE	%	ISO-2577	2.1-2.3
MFI	g/10 min	ISO-1133 250/2.16	25
MOISTURE ABSORPTION 23 °C, 50% RH	%	ISO-62	0.25
MECHANICAL PROPERTIES	UNIT	TEST METHOD	VALUES
TENSILE YIELD STRENGTH	MPa	ISO-527	55
ELONGATION AT BREAK	%	ISO-527	60
FLEXURAL STRENGTH	MPa	ISO-178	95
FLEXURAL MODULUS	MPa	ISO-178	3000
NOTCHED IZOD IMPACT STRENGTH +23 °C	kJ/m^2	ISO-180	5
THERMAL PROPERTIES	UNIT	TEST METHOD	VALUES
HDT AT LOAD 1.8 MPa	°C	ISO-752	70
HDT AT LOAD 0.45 MPa	°C	ISO-752	170
GLOW WIRE TEST	°C	IEC 60695	750
MELTING POINT	°C	DSC	225
ELECTRICAL PROPERTIES	UNIT	TEST METHOD	VALUES
VOLUME RESISTANCE	Ohm x m	IEC 60093	10^16
DIELECTRIC STRENGTH	kV/mm	IEC 60250	30
DIELECTRIC CONSTANT AT 1MHZ	kV/mm	IEC 60250	3.2

Table 2.3: Typical physical and chemical properties of SMA® 1000I

Properties	Values
Acid Number (mg KOH/g)	<1
Appearance	Pale yellow solid
Color, Gardner	<5
Solubility in Acetone, g/100 ml. @ 23 °C	>40
Solubility in Ethyl Acetate, g/100 ml. @ 23 °C	>40
Solubility in Methyl Ethyl Ketone, g/100 ml. @ 23 °C	>40
Solubility in THF, g/100 ml. @ 23 °C	>40
Solubility in Toluene, g/100 ml. @ 23 °C	>40
Glass transition temperature, T_g °C	70 - 90

2.2 Summary of the experimental work

Overall, this study consist of two sections i.e., characterisation of materials and blends of c-PBT. The summarries of both sections are illustrated in Figure 2.1 and Figure 2.2, respectively.

2.3 Preparation of the blends by solid dispersion

A powder mix of CBT and SMI was produced at various compositions ranging from 90 to 10 wt% of CBT. The powder blends were mixed in an agate mortar and pestle until a homogeneous blend was observed. This observation was facilitated due to the colour difference between the component powders: SMI was pale yellow and CBT was white.

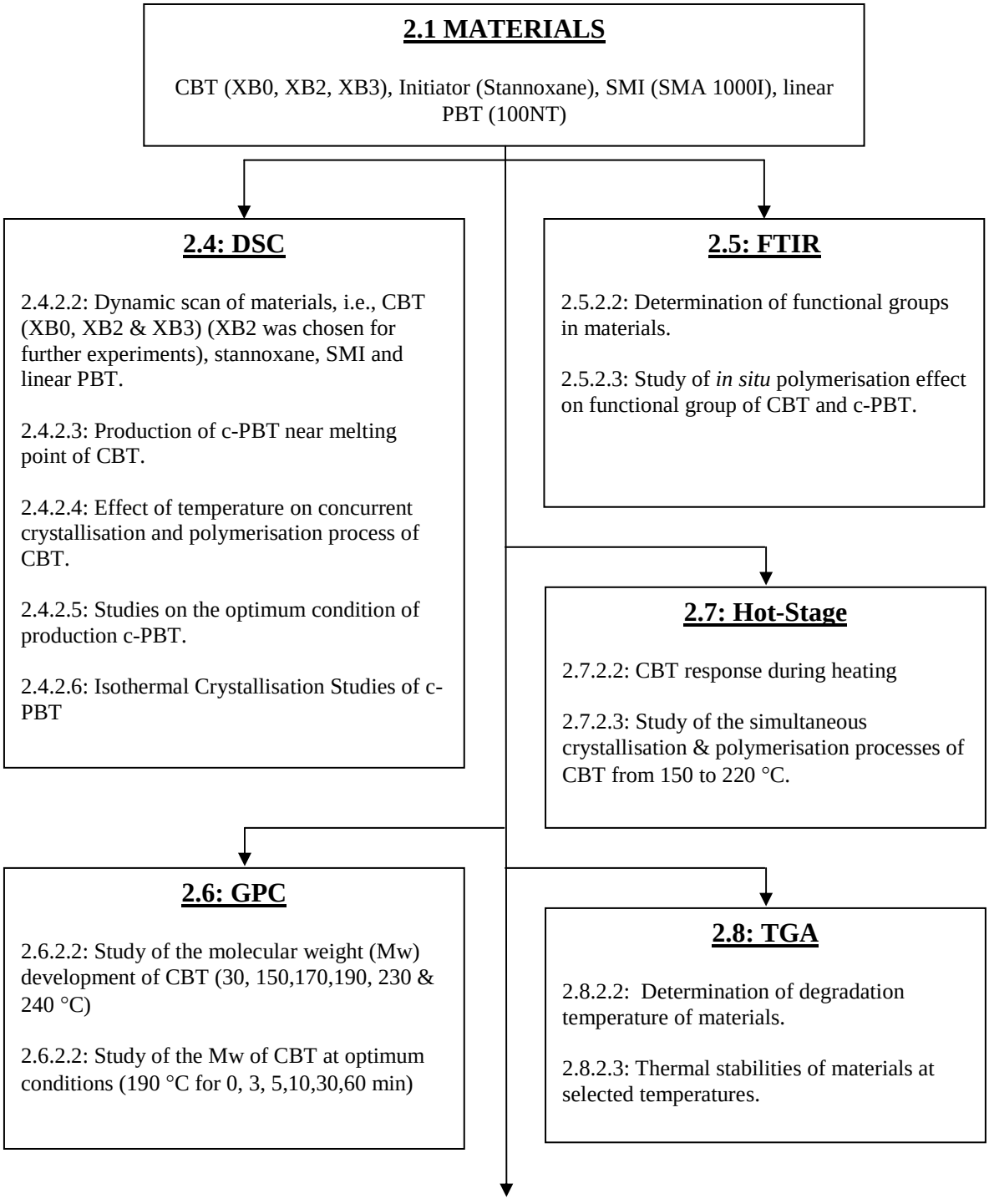

Figure 2.1: Schematic diagram of materials characterisation

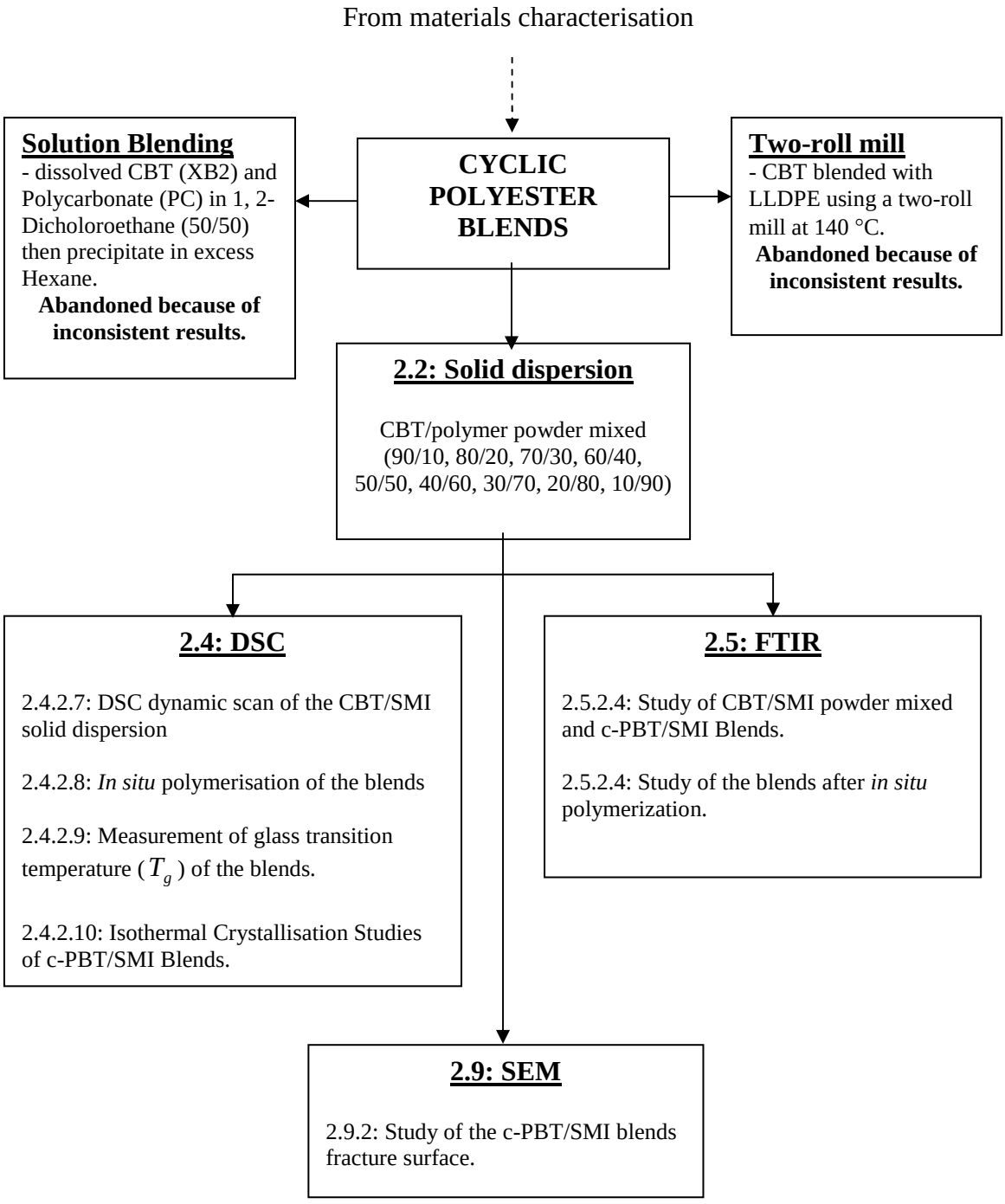

Figure 2.2: Schematic diagram of c-PBT blends study

2.4 Differential scanning calorimetry (DSC)

2.4.1 Introduction

Differential scanning calorimetry (DSC) is one of the thermal analysis techniques usually used to identify the thermal transitions and measure the heat capacity of a specimen as a function of time or temperature. The DSC experiment provides qualitative and quantitative information about physical and chemical changes which involve endothermic and exothermic processes using a minimal amount of sample. It is typically done at atmospheric pressure. That means DSC measures the constant-pressure heat capacity. At constant pressure, the DSC measures the amount of heat input required to raise the temperature of the specimen by 1 °C. This heat capacity is normally normalized by dividing the specimen heat capacity by the number of grams to know the heat required to raise 1 g of specimen by 1 °C. In general, DSC can be used to determine the glass transitions, crystallisation point, and degree of crystallinity, melting point and heats of fusion. DSC also can be used to study crystallisation and reaction kinetics, as well as thermal stabilities.

2.4.2 DSC experimental procedures

2.4.2.1 General

The thermal analysis of the materials used in this study was performed using a Perkin–Elmer differential scanning calorimeter (DSC-7). The DSC consists of two sample chambers where an empty pan is placed in the reference chamber and a pan with a polymer

specimen is placed in the sample chamber as shown in Figure 2.3. In the initial step to perform a DSC experiment, the sample and reference chamber need to be heated or cooled until they each reach the selected starting temperature. The experiment is then begun and the temperature increased at fixed number of degree Celsius per minute. During an experiment, the DSC control will monitor the temperature in each chamber where if the temperature differs from the programmed temperature in either chamber, more or less energy, Q is be supplied to the sample holder to maintain its temperature the same as that of the reference holder. This rate is registered by the instrument and plotted either against temperature, T or against time, t. It is generally possible to assume that, away from any transitions in the sample, the sample and the sample pan are at the same temperature and that the sample and reference pans are identical. It then follows that $dQ/dt = mC_p$, where m is the mass of the sample and C_p is the specific heat per unit mass. Generally in the DSC experiment, the difference in the energy supplied to the two chambers per unit time (or dQ/dt) is proportional to the heat capacity of the sample. This energy difference is then monitored electronically.

To ensure accuracy and reliability of the data obtained, this machine was temperature calibrated with pure indium and tin standards having equilibrium melting temperatures (T_m^o) of 156.67 °C and 231.97 °C, respectively. The indium equilibrium enthalpy of fusion (ΔH_f^o) is 28.5 Jg^{-1} was used for power calibration. Experiments were run with sample weights of 15 to 20 mg under argon gas with flowing rate of 20 cm^3 min^{-1} to prevent moisture and oxidative degradation. The heat flow of the samples was corrected by measured a baseline for the instrument using two empty aluminium pans.

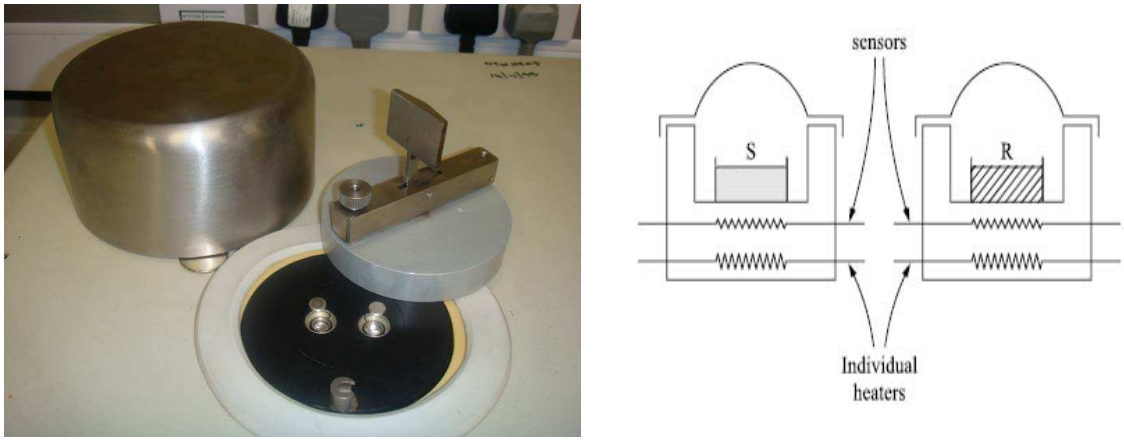

Figure 2.3: The photograph and schematic diagram of DSC head [74]

2.4.2.2 DSC dynamic scan of materials

To study the thermal behaviour of materials (i.e. CBT, stannoxane and SMI), the sample was subjected to the following heating and cooling steps:

(1) Heated to 240 °C at a 10 °C/min heating rate and kept for 1 min at 240 °C;

(2) Cooled to 30 °C at a 10 °C/min cooling rate.

The melting trace of c-PBT was obtained by a second heating of CBT sample at 10 °C/min to 240 °C. The melting transition of linear PBT was obtained from heating the sample from 30 °C to 250 °C at 10 °C/min and subsequently cooled to the starting temperature, followed by a second heating to 250 °C at 10 °C/min.

Figure 2.4 depicts the melting transition of semi-crystalline polymers. The melting temperature is sometimes taken as the onset temperature, the peak temperature, or the end temperature (last trace of crystallinity). In this study, we considered the end temperature as melting point since it defines the temperature at which all crystals disappear. The area under a melting transition curve is the total amount of heat absorbed during the melting process. The relevant area is shown as the shaded portion in Figure 2.4.

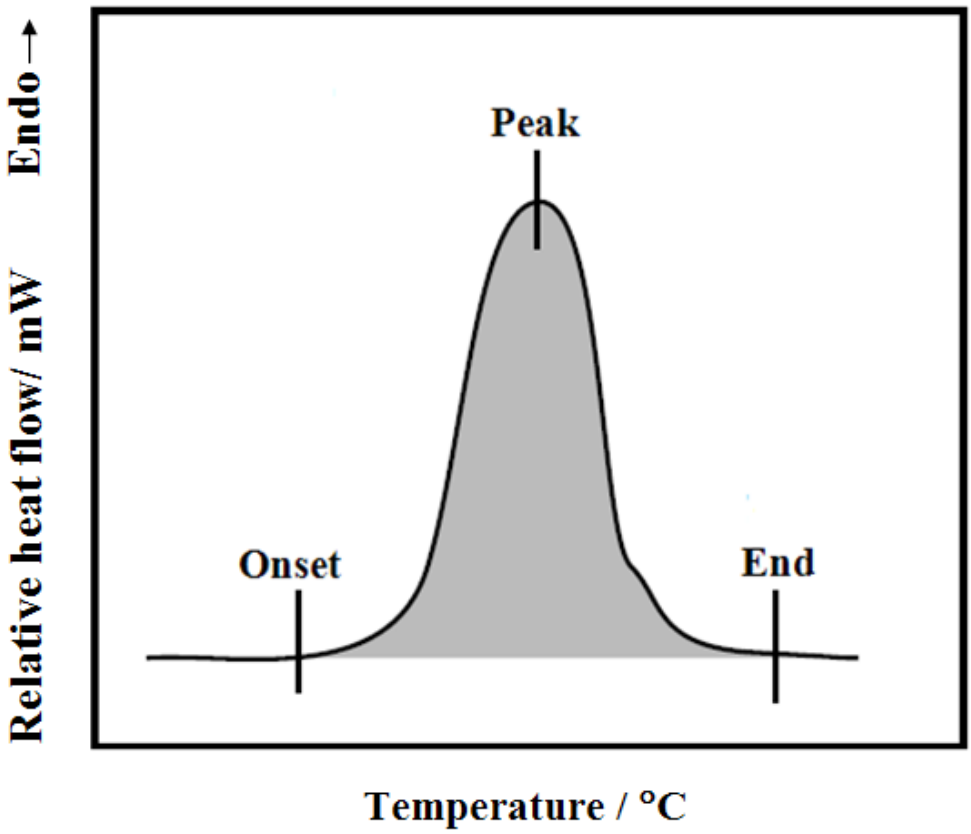

Figure 2.4: The typical melting transition of semi-crystalline polymer

2.4.2.3 Production of c-PBT near melting point of CBT

To study the production of c-PBT near the melting point of the CBT (142 °C) three temperatures were selected, i.e. 150 °C, 155 °C, and 160 °C. The CBT samples were heated to the target temperature from a starting temperature of 30 °C at 10 °C/min. The sample was then held at various times (5 to 60 minutes) at the target temperature. After that, the sample was cooled back to room temperature. The same sample was subsequently heated again to 240 °C at 10 °C/min to record the melting transition of c-PBT.

2.4.2.4 Effect of temperature on simultaneous polymerisation and crystallisation

With the aim of understanding the simultaneous crystallisation and polymerisation processes which occur after the melting of CBT, a sample of CBT was rapidly heated (100 °C/min) to a temperature above the melting peak of CBT, i.e. 150 °C, 160 °C, 170 °C, 180 °C, 190 °C, 210 °C, and 220 °C. The sample then was held at the target temperature until the crystallisation curve was completed i.e., the trace back to baseline. The sample was cooled back to room temperature and heated again to 240 °C at 10 °C/min to record the melting of the resulting c-PBT.

2.4.2.5 Studies on the optimum condition for production of c-PBT

A temperature of 190 °C was selected to study the formation of c-PBT. A sample of CBT was rapidly heated (100 °C/min) to 190 °C and held for various times (i.e., 0, 3, 5, 10, 30 and 60 minutes). This sample was cooled back to room temperature after holding at various time and heated again to 240 °C at 10 °C/min to study the melting of c-PBT.

2.4.2.6 Isothermal crystallisation studies of c-PBT

The isothermal crystallisation experiments were started as follows: the CBT sample (20 mg) was heated at 100 °C/min and held at 190 °C for 10 minutes to polymerise CBT to c-PBT. The sample was then rapidly heated (100 °C/min) to 10 °C above the observed melting point and held at this temperature for 5 minutes to ensure complete melting. Then the sample was quench-cooled to the desired crystallisation temperature (T_c) at 160 °C/min and held at the crystallisation temperature until the calorimeter response returned to the baseline. The melting trace was then determined from the heating run after each complete crystallisation. Isothermal melt crystallisations were carried out in the temperature range of 197 to 201 °C. The crystallisation and melting processes were analysed using the Avrami and Hoffman-Weeks methods [96-99], respectively.

2.4.2.7 DSC dynamic scan of the CBT/SMI solid dispersion

To study the thermal behaviour of CBT/SMI solid dispersion, about 20 mg of the sample was heated to 240 °C at a 10 °C/min heating rate and kept for 1 min at 240 °C. The sample was then cooled to 30 °C at a 10 °C/min cooling rate to detect any crystallisation transition occurring. After holding for 1 minute at 30 °C, the sample was heated again to 240 °C at a 10 °C/min heating rate to study the thermal behaviour of resulted c-PBT/SMI blends.

2.4.2.8 *In situ* polymerisation of the blends

As the optimum condition to produce c-PBT was found to be 190 °C isothermal hold for 10 minutes, this condition was adopted to produce c-PBT/SMI blends. The solid dispersion of CBT/SMI in various composition ranging from 90 wt % to 10 wt % of CBT was heated rapidly (100 °C/min) to the polymerisation temperature (190 °C) and held at that temperature for 10 minutes. This step allowed the *in situ* polymerisation of c-PBT within the SMI copolymer. The samples were then cooled back to 30 °C followed by heating the same sample to 240 °C at a 10 °C/min rate to study the effect of composition on thermal behaviour of the blends.

2.4.2.9 Measurement of glass transition temperature (T_g) of the blends

Blend samples were heated rapidly to the polymerisation temperature (190 °C) and held at that temperature for 10 minutes. Following this isothermal hold, the sample was then heated to above the c-PBT melting point and removed from the DSC to enable a rapid quench into liquid nitrogen. The sample was then immersed in the liquid nitrogen until further DSC experiment to measure the glass transition (T_g) and the specific heat of the sample (ΔC_p). This ensured that both blend components were amorphous since c-PBT could crystallise at room temperature.

The experiment begun with the empty pan to obtain the baseline of the experiment (heating from -10 °C to 240 °C at 10 °C/min and cooled back to -10 °C at 10 °C/min). After temperature reached -10 °C, the sample which had been immersed in liquid nitrogen was quickly and carefully transfers to the sample pan. The sample was re-run under same experiment condition (heating from -10 °C to 240 °C at 10 °C/min). The DSC trace obtained was then subtracted with the baseline. The T_g was measured from the midpoint of the inflection of the specific heat plot with temperature, using Pyris software [100, 101] and the ΔC_p was taken as the size of the step as illustrate in Figure 2.5.

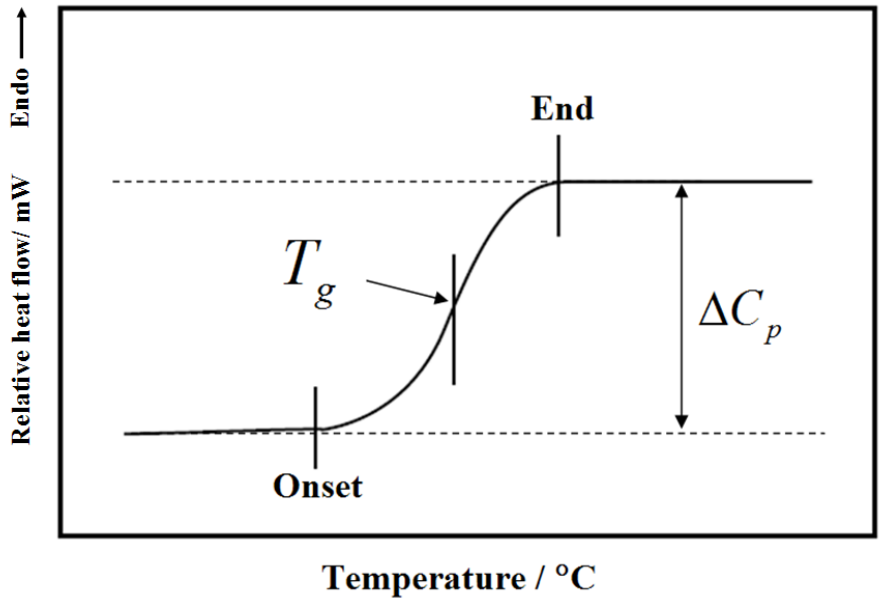

Figure 2.5: The determination of T_g

2.4.2.10 Isothermal crystallisation studies of c-PBT/SMI blends

For the c-PBT blends, the isothermal crystallisation experiment followed these procedures: 20 mg of a powder mixture of CBT with SMI was heated at 100 °C/min and held at 190 °C for 10 minutes to produce c-PBT blends *via in situ* polymerisation. The blend sample was then rapidly heated (at 100 °C/min) to 10 °C above the observed melting point and held at this temperature for 5 minutes to ensure complete melting. The blend sample was then quench-cooled at 160 °C/min to the desired T_c and held at this temperature until the calorimeter response returned to the baseline. The melting trace was then determined from the heating run after each complete crystallisation. Isothermal melt crystallisations were carried out over the temperature range of 197 to 201 °C for the blend samples. The crystallisation and melting processes of the c-PBT blends were also analysed using the Avrami and Hoffman-Weeks methods [96-99], respectively.

2.5 Fourier Transform Infrared Spectroscopy (FTIR)

2.5.1 Introduction

Fourier Transform Infrared (FTIR) is the preferred method of infrared spectroscopy for polymer work. In general, IR radiation is passed through a sample. Some of the infrared radiation is absorbed by the sample and some of it passes through (transmitted). The resulting spectrum represents the molecular absorption and transmission, creating a molecular fingerprint of the sample. No two unique molecular structures produce the same infrared spectrum. This makes infrared spectroscopy useful for several types of analysis. FTIR is used to identify unknown materials, determine the quality or consistency of a sample, and determine the amount of components in a mixture.

2.5.2 FTIR experimental procedures

2.5.2.1 General

FTIR spectra were obtained on Nicolet Magna IR-860 FTIR spectrometer. Two methods were adopted to measure the FTIR spectra, i.e. transmission and attenuated total reflectance (ATR) using the 'Golden-Gate' accessory (Specac, UK) [102] as shown in Figure 2.6. In the transmission technique, IR radiation is passed through a sample. While, in the ATR technique, IR radiation is reflected backwards and forwards between the crystal and the surface of the sample. Approximately 5 to 10 microns is the length over which radiation is able to penetrate in the sample using this technique. The absorption of

radiation at the corresponding wavelengths depends on the incident angle and the refractive indices where the beam is reflected from the surface of the sample.

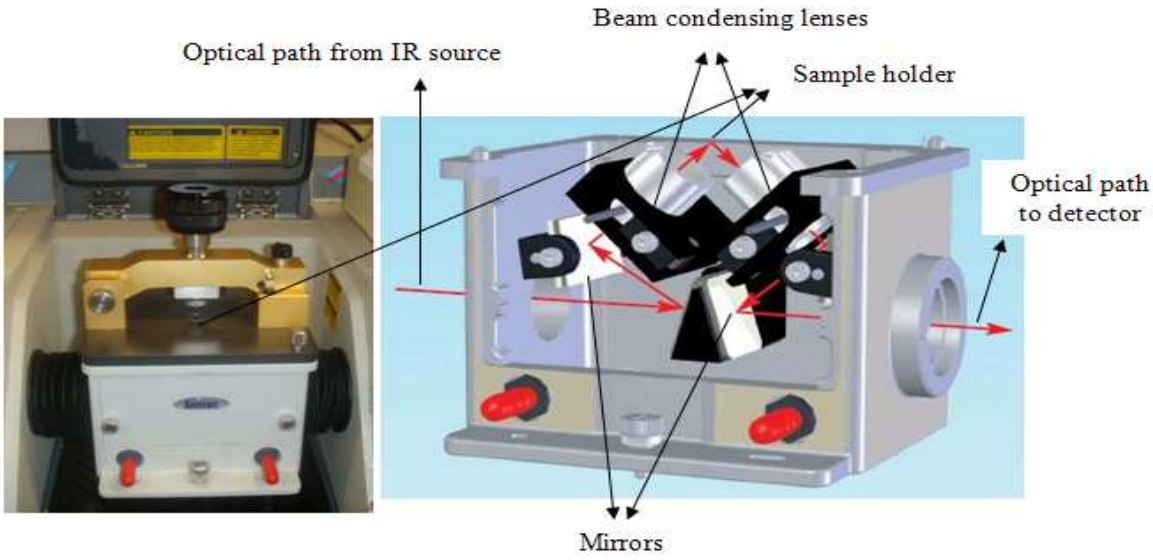

Figure 2.6: The 'Golden-Gate' accessory for ATR technique (left picture from www.specac.com)

2.5.2.2 Determination of functional groups in materials

A background absorption spectrum was taken before each run and subtracted from the sample spectrum. Then, the samples of CBT (powder), linear PBT (sheet), c-PBT (taken from the DSC pan), stannoxane (powder) and SMI (powder) were placed on the Golden Gate accessory sample holder using an ATR technique. All spectra were recorded from 750-4000 cm^{-1}. A total of 100 scans at a resolution of 2 cm^{-1} were averaged.

2.5.2.3 Study of *in situ* polymerisation effect on functional group of CBT and c-PBT

A sample of CBT on a KBr disc (0.5 wt % CBT) was placed on the hot-stage sample holder. This hot-stage was then attached to the Nicolet Magna IR-860 FTIR spectrometer to measure FTIR spectra using transmission technique. To study the effect of *in situ* polymerisation on functional groups of the CBT, FTIR spectra were taken every 10 °C interval starting at 30 °C and from 100 °C to 240 °C. All spectra were recorded from 750-4000 cm^{-1} at a resolution of 2 cm^{-1} and a total of 100 scans were accumulated. The spectra were also taken during the cooling process of c-PBT from 240 °C to 100 °C and at 30 °C. The experiment was repeated with the same procedure using the same sample to study effect of temperature on functional group of c-PBT.

2.5.2.4 Study of CBT/SMI solid dispersion and c-PBT/SMI Blends

The samples of CBT and SMI powder mixed at various compositions were placed on the Golden Gate sample holder for the ATR technique. All spectra were recorded from 750-4000 cm^{-1}. A total of 100 scans at a resolution of 2 cm^{-1} were signal averaged. The background absorption spectrum was taken before each run and subtracted from the sample spectrum. The experiment were then repeated with the c-PBT/SMI blends at various compositions which *in situ* polymerized first in the DSC. Both spectra were analysed to study the effect of *in situ* polymerisation in production of c-PBT/SMI blends and their composition.

2.6 Gel Permeation Chromatography (GPC)

2.6.1 Introduction

The common way to determining the molecular weight (M_w) of polymer is using gel permeation chromatography (GPC) also called size exclusion chromatography (SEC). In gel phase chromatography technique, a dilute polymer solution is introduced into the column which filled with beads of a rigid porous gel. These beads are selected such that the sizes of its pores are in the range of the sizes of polymer molecules. As the polymer solution passes through the column, the larger polymer molecules pass out through the bottom of the column faster than smaller molecules as they do not fit into the pores. The smaller molecules are spend more time in the column before coming out at the bottom as they diffuse in and out of the pores via Brownian motion and are delayed. To measure the molecular weight, the elution fractions from the bottom of the column were collected. In theory, the first fractions will be more concentrated in high molecular weight polymers and the elution fraction will be more concentrated in increasingly lower molecular weight polymer with time. The complete molecular weight distribution can be gain by plotting these concentrations as a function of time or elution volume. The illustration of GPC experiment is shown in Figure 2.7. The retention time is the length of time that a particular fraction remains in the columns [103].

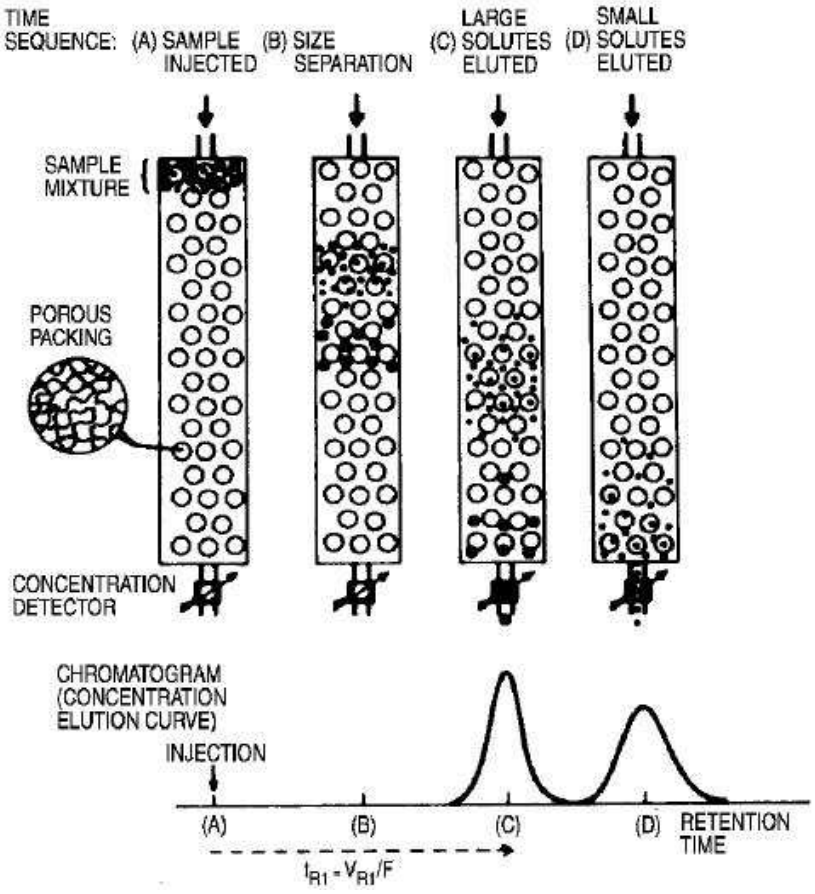

Figure 2.7: Illustration of the GPC experiment [103]

2.6.2 GPC experimental procedures

2.6.2.1 General

The samples were sent to Smithers Rapra Technology Ltd. (Shropshire, SY4 4NR, UK) to determine the M_w development upon polymerisation of CBT to c-PBT using GPC. This technique also used to study the effect of c-PBT held at high temperatures for various times. The samples have been analysed using 1,1,1,3,3,3-hexafluoro-2-propanol (HFIP) as

the solvent. The data were collected and analysed using Polymer Laboratories 'Cirrus' software [104].

2.6.2.2 Sample preparation

In order to study the development of M_w, the sample was first conditioned using the DSC as described in Table 2.4. A single solution of each sample was prepared by adding 10 mL of solvent to 20 mg of sample and leaving it overnight to dissolve. The solutions were well mixed and filtered through a 0.45 μm polytetrafluoroethylene (PTFE) membrane prior to the chromatography. All masses and volumes in this section are only approximate.

The sample descriptions of the study M_w development during production of c-PBT under optimum condition (polymerised at 190 °C) are shown in Table 2.5. The sample was rapid heated (100 °C/min) to 190 °C using the DSC, and held at various time.

Table 2.4: Conditioning of CBT for M_w determination

Sample	Sample Description
1	CBT in powder form.
2	CBT heated to 150 °C at 10 °C/min. (Melting temperature of cyclic oligomers is 142 °C)
3	CBT heated to 170 °C at 10 °C/min. (Crystallisation and polymerisation occur at this temperature)
4	CBT heated to 190 °C at 10 °C/min. (Crystallisation and polymerisation occur at this temperature)
5	CBT heated to 210 °C at 10 °C/min. (Crystallisation complete at this temperature)
6	CBT heated to 230 °C at 10 °C/min. (c-PBT formed. The T_m of c-PBT is 225 °C)
7	CBT heated to 240 °C at 10 °C/min.

Table 2.5: M_w of c-PBT produced at optimum condition

SAMPLE	TEMPERATURE HELD (°C)	HOLDING TIME (Min)	SAMPLE DESCRIPTION
1	190	0	Polymerisation not yet complete.
2	190	3	Polymerisation occurs.
3	190	5	Polymerisation occurs.
4	190	10	Optimum polymerisation time for production of c-PBT.
5	190	30	Polymerisation complete but causes double melting peak on re-melting c-PBT.
6	190	60	Polymerisation complete. Double melting peak on re-melting c-PBT shifts

2.7 Hot Stage Microscopy

2.7.1 Introduction

The development of crystallinity with time and temperature was recorded using a Zeiss polarizing microscope equipped with a Linkam TMHS 600 hot stage as shown in Figure 2.8. In this technique, we are able to record the photomicrographs of the melting process and the development of crystallites during the crystallisation process.

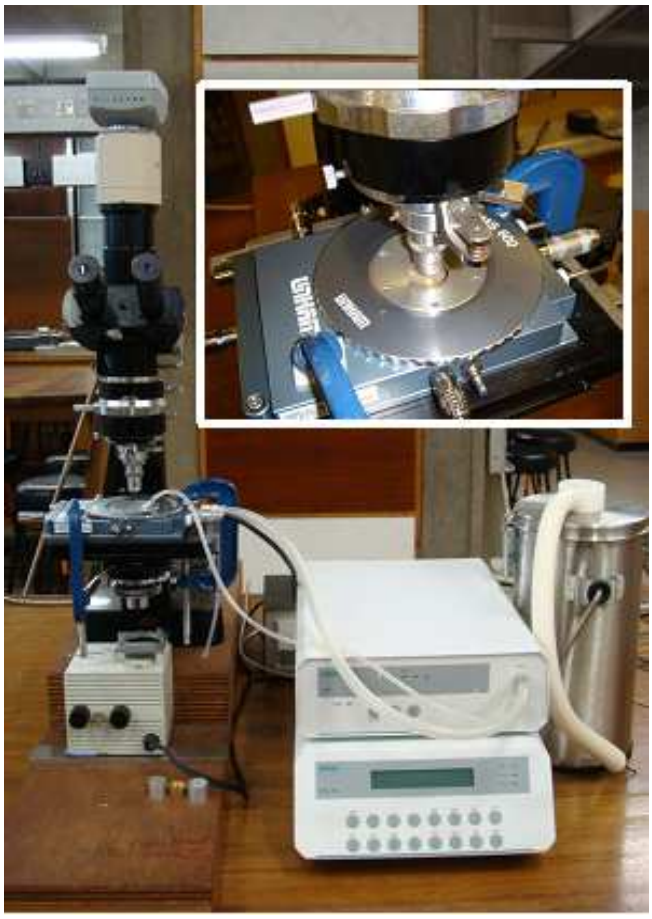

Figure 2.8: A Zeiss polarizing microscope equipped with a Linkam TMHS 600 hot stage (inset shows the hot-stage unit)

2.7.2 Hot-stage microscope experimental procedures

2.7.2.1 General

A sample of CBT powder (>5 mg) was compressed between two microscope slides then inserted in the hot stage. Photomicrographs at appropriate intervals of time were captured using a Pixelink PL-A662 digital camera coupled with the software LINKSYS 32 [105].

2.7.2.2 CBT response during heating

The sample was heated to 240 °C at a 10 °C/min heating rate and kept for 1 min at 240 °C, then cooled to 30 °C at a 10 °C/min cooling rate. The experiment was repeated under the same conditions with the same sample to study the crystallisation and melting of c-PBT.

2.7.2.3 Simultaneous polymerisation and crystallisation of CBT

The sample of CBT was rapidly heated (100 °C/min) to temperatures above the melting peak of CBT, starting at 150 °C up to 220 °C with 10 °C interval. The sample was then held at the target temperature and the photomicrographs were recorded at appropriate intervals of time were captured until the crystallisation process was completed (based on DSC results in section 2.3.2.4).

2.8 Thermogravimetric Analysis (TGA)

2.8.1 Introduction

In thermogravimetric (TGA) experiments, the mass of sample is measured as a function of temperature and time [106, 107]. The experiment is performed in a defined atmosphere, usually in argon, nitrogen or in air (or oxygen) which can be carried out in a dynamic mode at a controlled heating rate or isothermally as for DSC experiment [106, 107]. During heating, the mass of sample is measured using a highly sensitive electronic microbalance. In general, TGA is used to determine polymer degradation temperatures, residual solvent levels, absorbed moisture content, and the amount of inorganic filler in a polymer [107]. Thermal degradation reactions typically cause the weight to decrease and thus decreases in weight are a sign of thermal instabilities [106].

2.8.2 TGA experimental procedures

2.8.2.1 General

The TGA experiments were carried out using a Netzsch Jupiter STA 449C thermogravimetric analyser in an air atmosphere which flowed at 50 cm^3min^{-1}. Before every experiment, two empty ceramic crucibles were place in the TG analyser sample holder and scanned to the same temperature as the experimental conditions. This step is essential for a baseline correction. A sample of 8.0 ± 0.5 mg were used for all measurements.

2.8.2.2 Determination of degradation temperature of materials

The sample was heated in the dynamic mode from 30 °C to 800 °C at 10 °C/min with the aim to find the degradation temperature for each material. The weight of the sample as a function of temperature was recorded during the experiment. The temperature of degradation was considered as the onset of the point where the mass of the sample dropped from the baseline.

2.8.2.3 Thermal stabilities of materials at selected temperatures

The material was heated from 30 °C to the target temperature (190 or 240 °C) at 10 °C/min. This sample was then held in isothermal mode for 60 minutes. The weight of the sample as a function of time was recorded during the experiment. The thermal stabilities of each material at that temperature were analysed with Proteus Analysis software [108].

2.9 Scanning Electron Microscopy (SEM)

2.9.1 Introduction

The scanning electron microscope (SEM) is a type of electron microscope. The SEM can capture the sample surface images by scanning it with a high-energy beam of electrons in a raster scan pattern. SEM can produce information about the sample's surface topography, composition and other properties such as electrical conductivity [109].

Photomicrographs from SEM are also widely used in polymer work especially during the study of polymer morphology.

2.9.2 SEM experimental procedures

A solid dispersion of CBT/SMI was place in a small rectangular shape mould. The mould then heated to 190 °C by hot plate to perform *in situ* polymerisation of the blends. The effect of *in situ* polymerisation were studies in various time; 5, 10, 30, 60 minutes. The sample was quenched in an ice bath to freeze the morphology after a desired time. The rectangular shaped bar of the c-PBT/SMI blend samples were taken out from the mould and was broken into two pieces to form a fracture surface. The fracture surfaces of the samples then were gold coated. Scanning electron microscopy (SEM) photos of the fracture surfaces of c-PBT/SMI blends were taken on a JEOL JSM-6060LV.

Chapter Three

CHARACTERISATION OF c-PBT: THERMAL BEHAVIOUR

3.1 Introduction

3.1.1 Background of CBT polymerisation

From previous work it was known that CEO could be prepared by pseudo-high dilution techniques [13, 16], and also by ring-chain equilibrium (depolymerisation) [14, 16]. Most of the early work of preparation of CEO was carried out using various types of tin and titanium catalysts. Brunelle *et al.* in 1998 patented the efficient use of a titanate catalyst for the preparation of CBT *via* depolymerisation in a continuous reactor [45].

The ring opening polymerisation (ROP) of CBT involves initiation to form an active chain end, followed by a propagation reaction as shown in Figure 3.1. This process will continue until all the cyclic oligomers are depleted and the ring chain equilibration becomes degenerate [16]. The initiator becomes built into the polymer. This process only terminates if the sample is quenched. Because of their size, the cyclic oligomers are nearly strain free which causes the polymerisation process to be almost thermo-neutral [13, 16, 50].

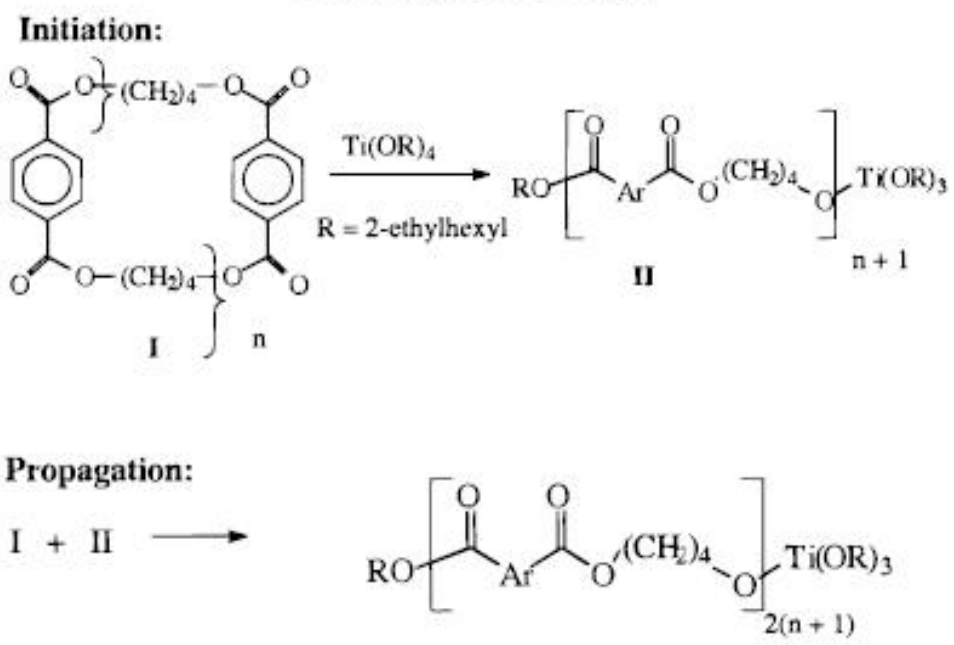

Figure 3.1: Ring opening polymerisation of CBT [16]

On the other hand, Miller [14] in his PhD study focused on the polymerisation of CBT using a stannoxane cyclic initiator. He believed that the unique ring expansion polymerisation of use in his research produced simpler cyclic molecules having no

catenation or knotting. The use of stannoxane as initiators leads to ring expansion polymerisation (Figure 3.2). With this type of initiator, the process allows for rapid growth of the ring as four active initiation sites may remain in the cyclic structure during polymerisation. This mechanism suggests a back-biting reaction that expels a large cyclic structure containing one or no initiator fragments. The reversible side reaction allow for a distribution of active and inactive macro-rings and a possible living system which reaches an equilibrium distribution of molecular weight.

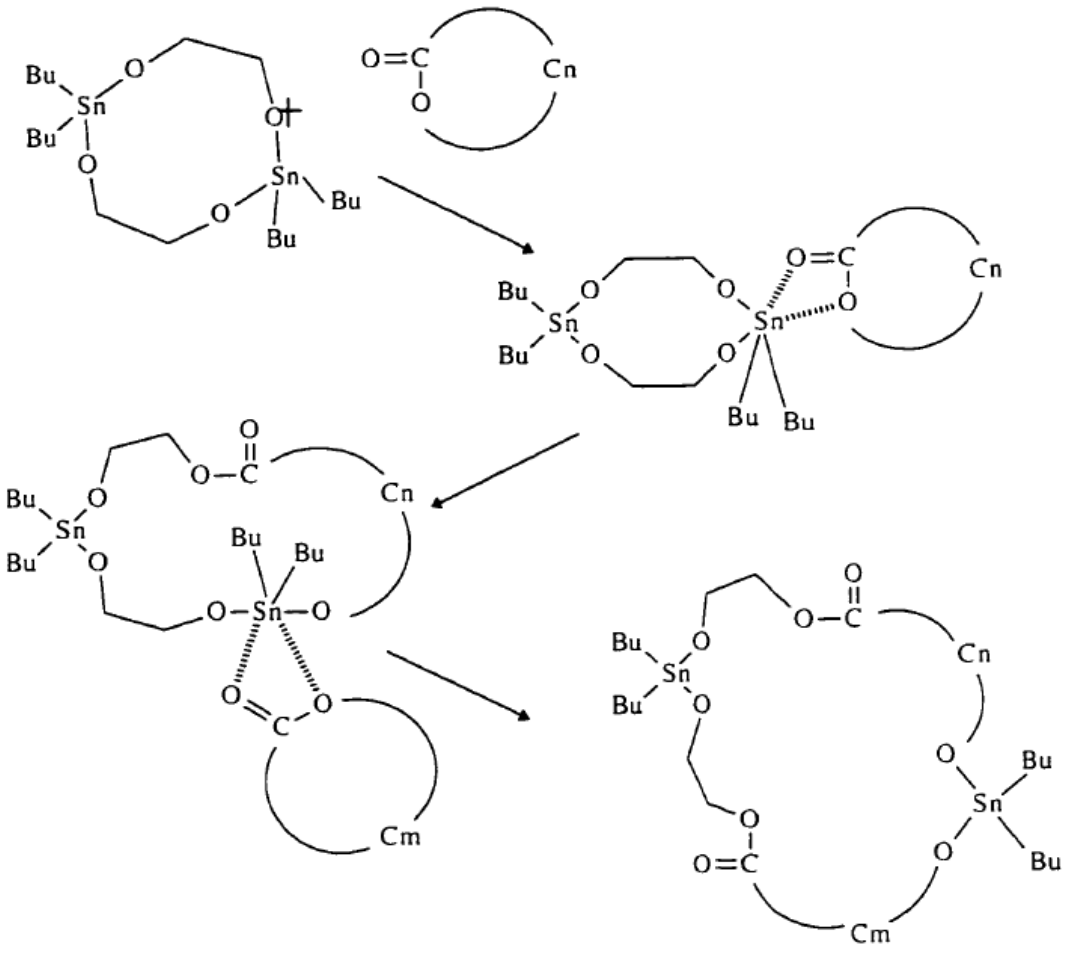

Figure 3.2: Ring expansion polymerisation of CBT [13, 14]

Previous studies [13, 14, 34-36, 50, 51] also concluded that the polymerisation reaction was typically carried out at 180-200 °C, just below the melting point of PBT (225 °C). According to Brunelle *et al*. [13, 16], the completeness of polymerisation was controlled by three factors: 1) purity of the monomers, 2) complete mixing of initiator before polymerisation which caused the viscosity to increase to the point where mixing stopped (the initiator needs to be intimately mixed with the molten cyclic), and 3) polymerisation at a high enough rate that it was essentially complete before crystallisation occurred.

3.2 Results and discussion

3.2.1 Thermal behaviour of CBT, c-PBT, catalyst (stannoxane) and linear PBT

Figure 3.3 illustrates the heating trace of CBT without any catalyst at a rate of 10 °C/min. The melting peak was observed at 142 °C. It is well known that this peak corresponds to the melting of CBT as many earlier researchers [12-14, 34-36, 50, 51, 67] found and concluded that the peak was due to the melting of the oligomers. From Figure 3.3, it can be seen that CBT is found to melt over a broad range. The start of melting process was observed from 120 °C and the process completed at 172 °C. Mohd Ishak *et al.* [35] concluded that the broadening of the shoulder resulted from different melting temperatures of the oligomers present in the CBT. A previous study found that CBT obtained *via* depolymerisation comprised of different proportions of oligomers indicated by slightly different melting temperatures [21].

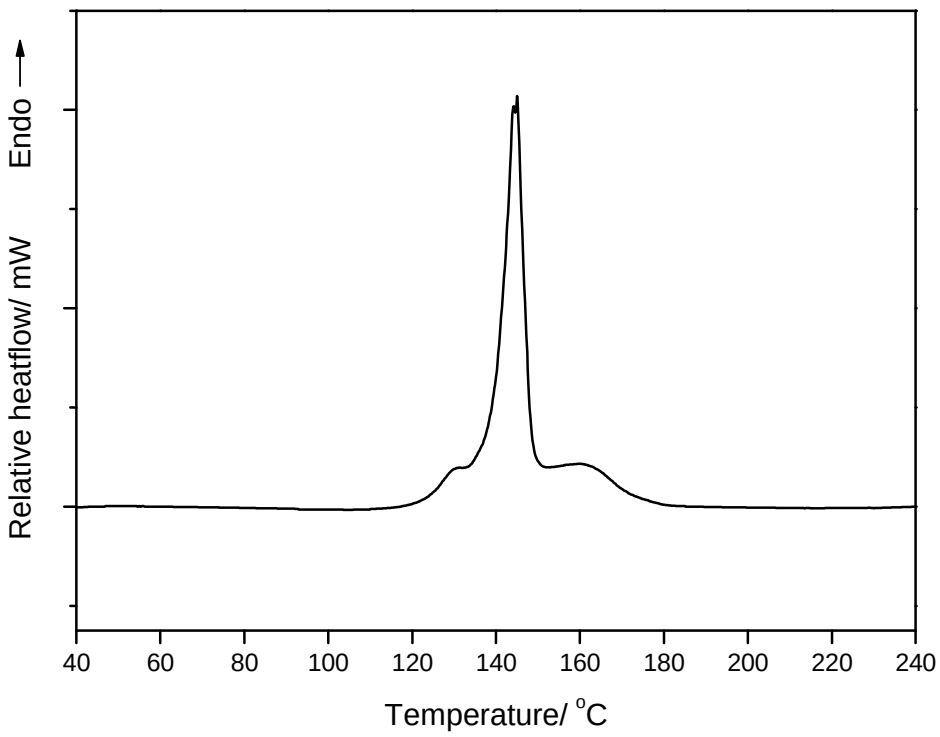

Figure 3.3: Typical DSC heating trace of CBT (XB0 – without catalyst)

The typical DSC heating traces of CBT in the presence of stannoxane (0.25 wt %) for the first dynamic scan at a rate of 10 °C/min, is shown in Figure 3.4. Obviously, it can be seen that two melting peaks were observed in this heating trace. With the presence of a suitable catalyst such as stannoxane, CBT is understood to undergo simultaneous polymerisation and crystallisation processes [13, 29, 34, 39, 67, 110] . This is believed to occur over the temperature range of 172 to 215 °C. However, only the crystallisation transition appears as a dip at 180 °C in this temperature region since the polymerisation is an entropically driven ring-expansion polymerisation, resulting in an almost thermo-neutral reaction [13, 16, 50].

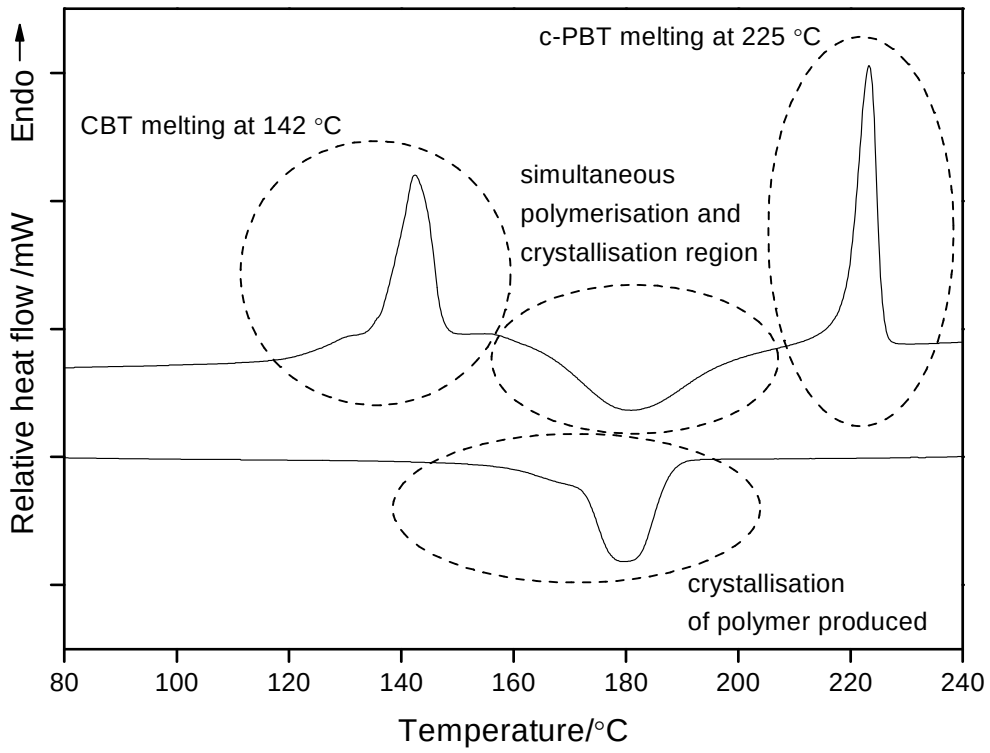

Figure 3.4: Typical DSC heating and cooling trace of CBT (XB2 - containing stannoxane)

Brunelle *et al.* [13, 45], who extensively investigated the polymerisation of CBT using tin and titanium catalysts found that the 0.25 wt % of stannoxane catalyst allowed the CBT polymerisation to be completed within 2 to 3 minutes at 190 °C. While Miller [14] in his thesis also concluded that CBT polymerised and crystallised at 190 °C. He found that both processes produced a cyclic PBT which has a 50 % crystalline structure. This structure consisted of lamella which exhibited a single melting peak at 225 °C [14]. On the cooling of this sample, the re-crystallisation process occurred in the region 190 °C to 160 °C.

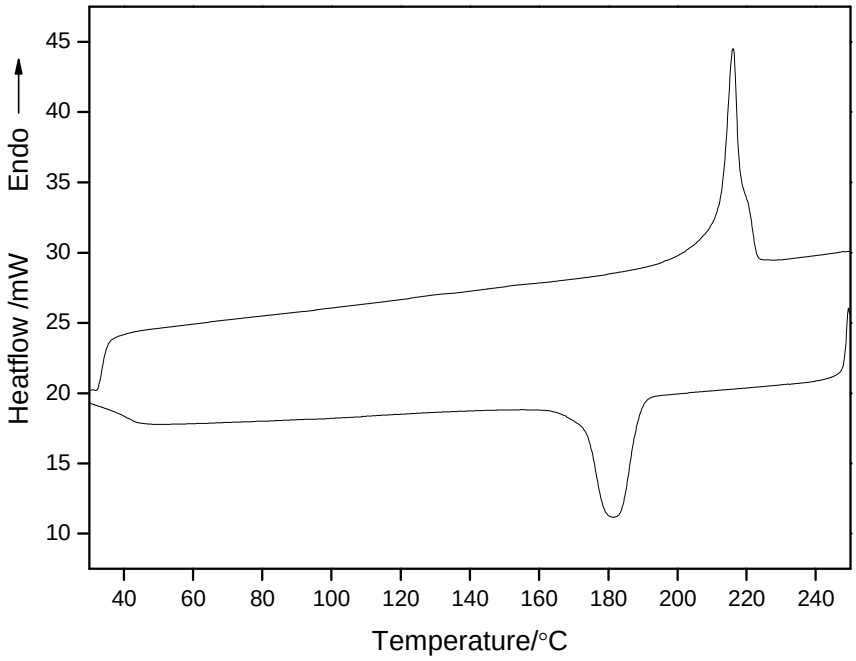

Figure 3.5: Typical DSC re-heating of c-PBT

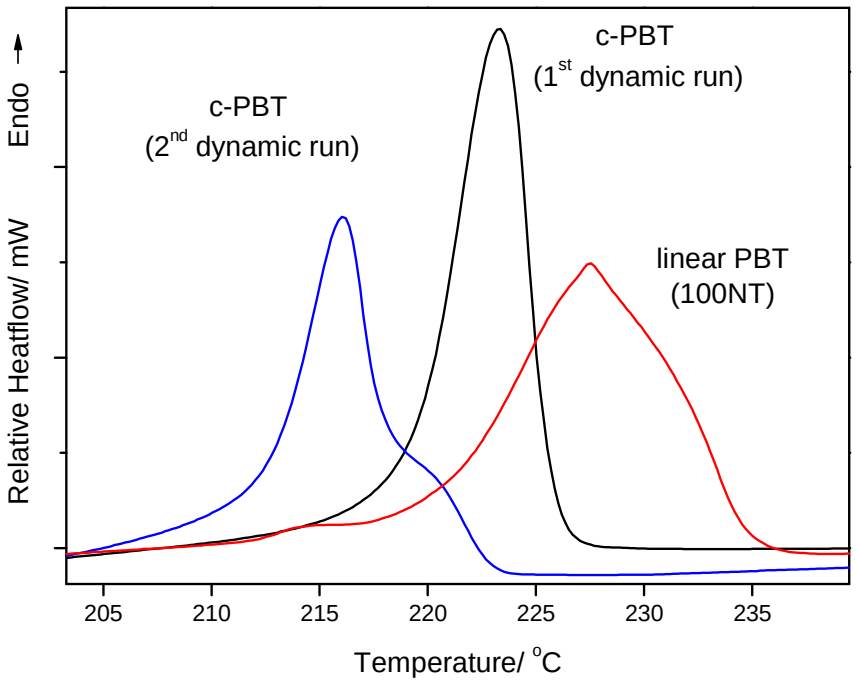

Figure 3.6: Analyses of melting transition of c-PBT and linear PBT

The second dynamic run of the c-PBT (Figure 3.5) shows no oligomers melting peak suggesting that the oligomers converts to polymer upon the first dynamic run of CBT. Figure 3.6 compares the heating transition of c-PBT produced from CBT with commercial linear PBT. The melting transition of commercial grade PBT was found to be 10 °C higher than the c-PBT which was produced from CBT. The observed melting peak for c-PBT in the first dynamic run of CBT is very sharp and symmetrical which suggests that the spherulites have a high degree of uniformity in size and perfection. High degrees of crystal perfection are reported in the literature for c-PBT [13, 14] and are an interesting result since such perfection in linear PBT can only be achieved with large cooling times [90].

The degree of crystallinity (χ_c) of c-PBT which was formed in this study was calculated according to Equation 3.1:

$$\chi_c = \frac{\Delta H_f}{\Delta H^o{}_f} \text{X100} \qquad \text{(Equation 3.1)}$$

where, ΔH_f is the measured (by the DSC) heat of fusion for the sample and $\Delta H^o{}_f$ is the heat of fusion for 100% crystalline polymer. According to work published earlier, $\Delta H^o{}_f$ which used to calculate the degree of crystallinity of c-PBT is 85.75 J/g [34, 35, 67, 111, 112]. From the calculation, we observed that the degree of crystallinity (χ_c) of c-PBT which was formed during dynamic heating of CBT at rates of 10 °C/min was 57 ± 1 % and this result is higher than the degree of crystallinity of linear PBT which was 51 ± 1%. This finding is in agreement with previous studies on degree crystallinity of c-PBT [34, 35, 67]

.

On the other hand, in the second dynamic run the main melting peak shifts to a lower temperature, closer to 224 °C. This suggests that after heating above the melting temperature lamellar thickness and hence spherulite perfection and melting temperature decrease. The degree of crystallinity on re-heating c-PBT was reduced to 53 ± 1%. An interesting result is the double melting behaviour suggested by the shoulder on the main melting peak. This situation is believed to arise from the melting and re-crystallisation of imperfect crystals during the re-heat [113-115]. It is consistent with the behaviour observed by Mohd Ishak *et. al* [36] when the CBT are heated above T_m. Kong and Hay [115] in their work on investigation of poly(ethylene terephthalate) (PET) melting behaviour indicates that further crystallisation took place above the isothermal crystallisation temperature (T_c) which caused the multiple melting endotherms. They concluded that the multiple melting phenomenon is a consequence of the balance between melting and re-crystallisation and the lamella thickness distribution existing within the sample, prior to heating.

Since stannoxane is involved during ring expansion polymerisation of CBT, an examination of the thermal behaviour of stannoxane was carried out in the temperature range of the study. Figure 3.7 illustrates the typical DSC thermogram of stannoxane. The melting peak of stannoxane was observed at 230 °C, which agreed with previous studies [14]. As the stannoxane undergoes a drying process before DSC experiments, the first endotherm peak is suspected to be the monomer (Bu_2Sn (O $(CH_2)_2O$) melting transition. This melting peak still appears in the second DSC heating trace using the same sample. However, the presence of this stannoxane monomer is believed not to give a significant effect as the quantity of stannoxane used in the *in situ* polymerisation process of CBT was

low (0.25 wt %) [18]. The stannoxane heating trace in the Figure 3.7 shows signs of instability above 170 °C. The thermal stability of this material will be further examined with TGA experiments discussed at the end of this chapter.

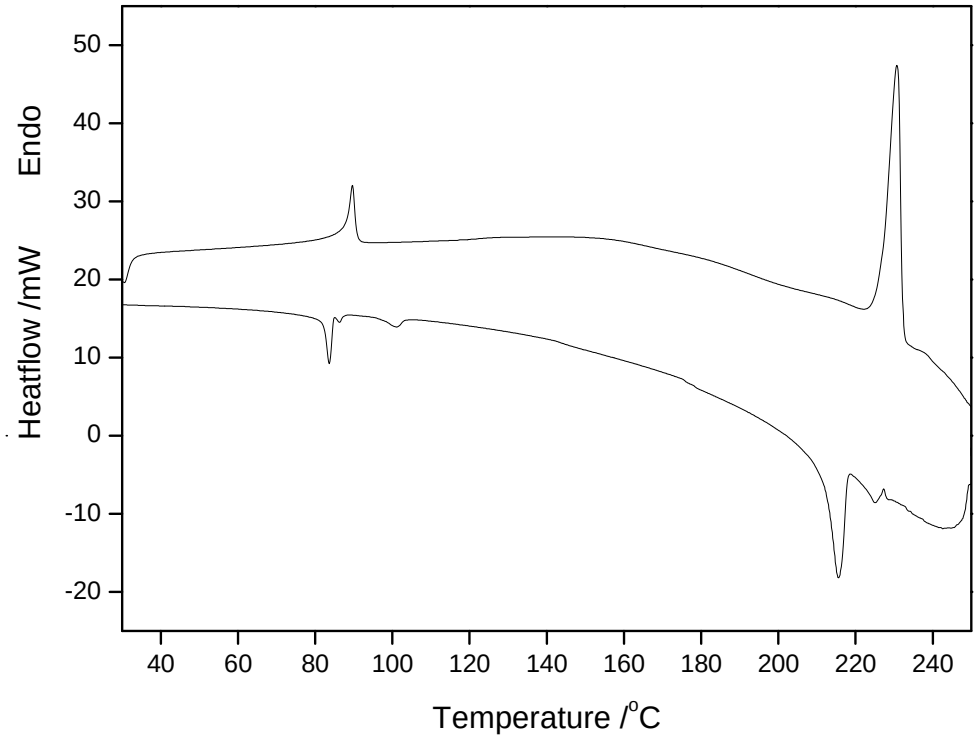

Figure 3.7: Typical DSC heating and cooling trace of stannoxane (catalyst)

3.2.2 Polymerisation near the melting point of CBT

The previous studies found that the polymerisation of CBT was typically carried out between 160 and 200 °C [13, 14]. It has been reported that stannoxane will be actively involved in the polymerisation reaction at temperatures as low as 160 °C [14]. With the aim to investigate the ring expansion polymerisation of CBT at low temperature, a study of

polymerisation near melting point of CBT was performed. Three temperatures i.e. 150, 155 and 160 °C were selected in this experiment.

Figure 3.8 shows the study of CBT polymerisation at 150 °C at various times. After 5 minutes, it was found that the ring expansion polymerisation was not complete. It can be seen that a melting peak of CBT still appeared in the heating trace from the second dynamic run of that sample. This trend continues even when more time is allowed for the polymerisation process. However, when more time is allowed (more than 10 minutes) for the polymerisation process, the melting peak of the polymer shifts to lower temperature. This effect is believed to be related to the imperfection of crystallites formed after the polymerisation process as discussed earlier.

An unknown peak also appeared before the melting peak of the polymer for 30 minutes and 40 minutes holding times at 150 °C. This unknown peak was probably a consequence of multiple oligomers in the CBT, since it was prepared by the *pseudo*-high dilution technique [13, 16]. Through this technique, cyclic oligomers mixtures can be prepared in yields as high as 90 % with excellent selectivity over the formation of linear oligomers [16]. On analysis of degree of crystallinity it was discovered that polymerisation for 20 minutes at 150 °C yields a higher crystallinity which is 57 ± 1 % as shown in Figure 3.11. However, the degree of crystallinity of the polymer produced was reduced when above 30 minutes was allowed for polymerisation at this temperature. Polymerisation of CBT at 155 °C gives the same situation as polymerisation at 150 °C (Figure 3.9). This suggests that at both temperatures, the CBT are not completely melted and not really active for ring expansion polymerisation.

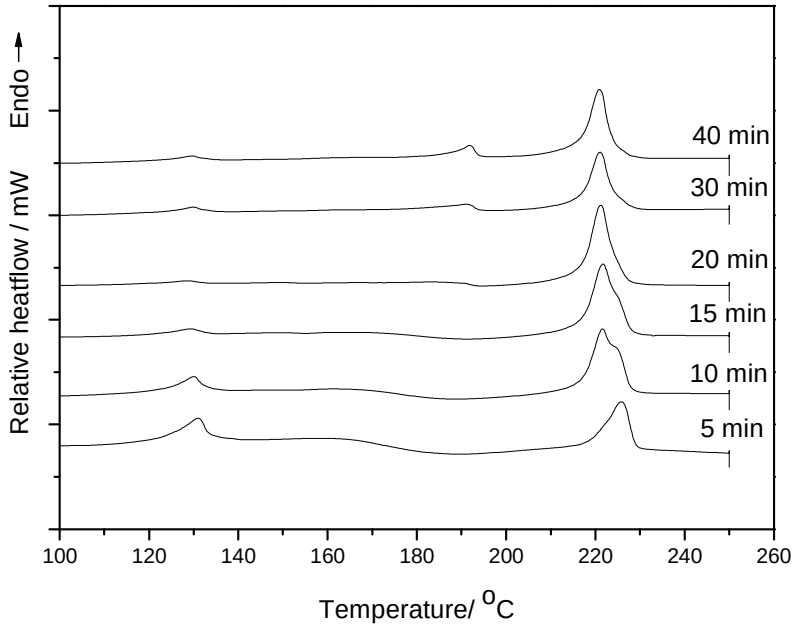

Figure 3.8: Polymerisation of CBT at 150 °C in various times

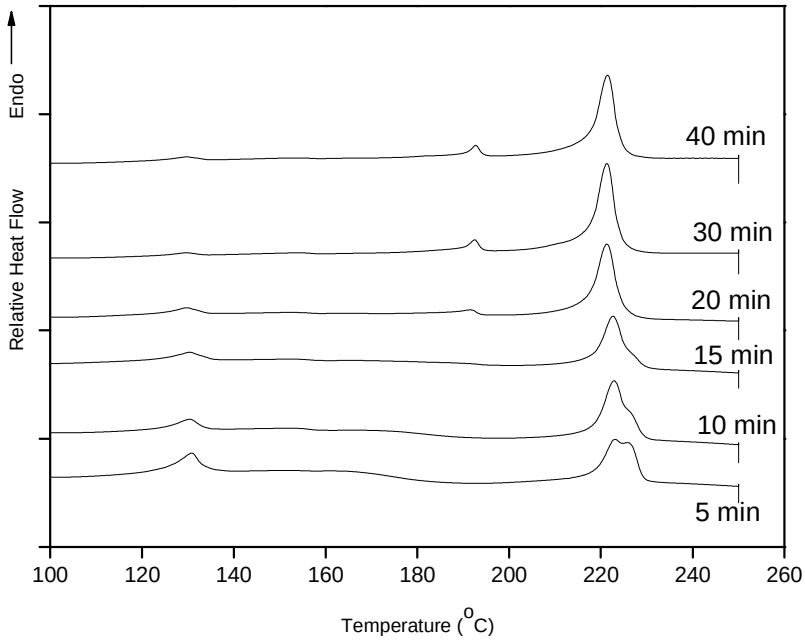

Figure 3.9: Polymerisation of CBT at 155 °C in various times

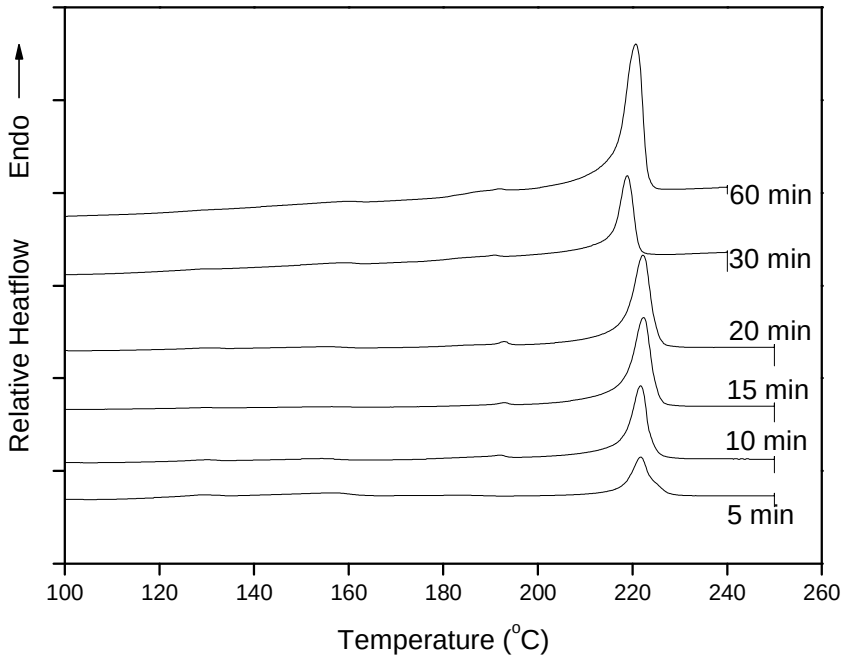

Figure 3.10: Polymerisation of CBT at 160 °C and various times

Figure 3.10 presents the finding for polymerisation of CBT at 160 °C conducted at various times. All the heating traces show no melting transition in the region of CBT melting. These results are consistent with Miller's [14] finding, where the ring expansion polymerisation of CBT was active at temperatures as low as 160 °C. However, the polymerisation took a long time to complete (up to 60 minutes) as shown in Figure 3.10. The c-PBT produced under this condition (60 minutes at 160 °C) yields 61 ± 1 % degree of crystallinity.

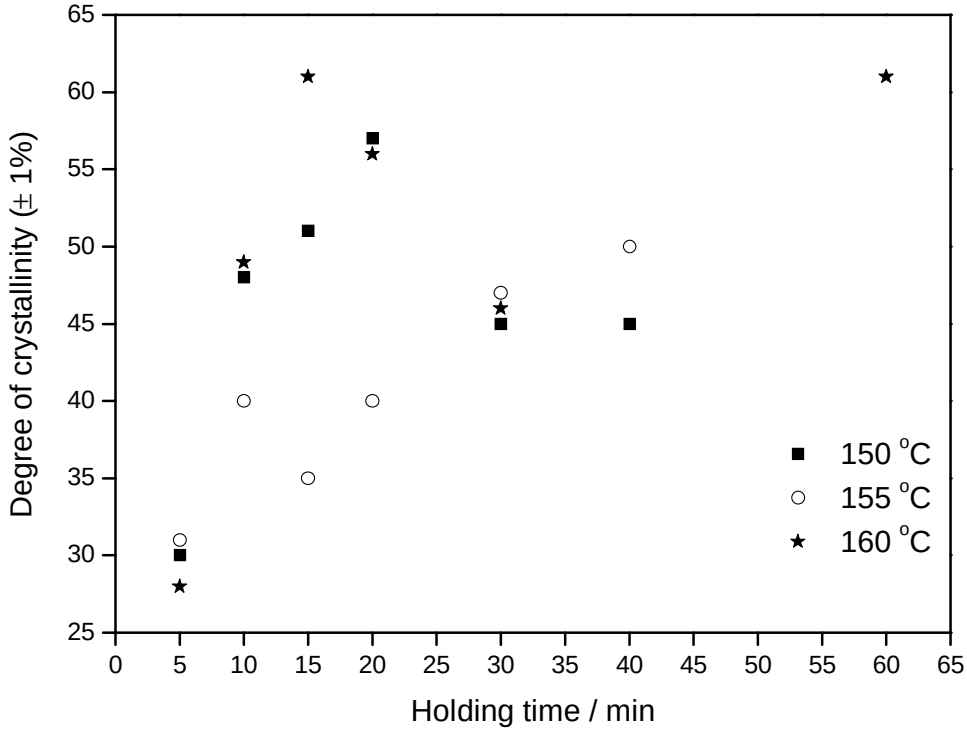

Figure 3.11: Degree of crystallinity of c-PBT produced after polymerisation near oligomers melting

3.2.3 Effect of temperature on simultaneous crystallisation and polymerisation processes of CBT

From the studies of polymerisation near the melting point of CBT, we saw that the active temperature for the ring expansion polymerisation could begin at 160 °C. It is known that the *in situ* polymerisation of CBT occurred simultaneously with the crystallisation process [13, 29, 34, 39, 67, 110]. These interesting phenomena in cyclic

oligomers have attracted many researchers to explore and do scientific research. Since the melting point of the CBT is below that of c-PBT and the conversion from CBT to c-PBT is sufficiently rapid at relatively low temperatures, isothermal processing below the melting point of PBT is possible. Depending on the degree of supercooling and the reaction speed, this isothermal processing may result in simultaneous polymerisation and crystallisation [53].

However, with thermal analysis techniques such as DSC, only the crystallisation process could be monitored since the cyclic oligomers are nearly strain-free which means their polymerisation is almost thermo-neutral [13, 16, 50]. It is also believed that CBT must be converted to a polymer of sufficiently high molecular weight before crystallisation can commence [39, 53].

An experiment to understand the behaviour of concurrent polymerisation and crystallisation of this CBT in the temperature range 160 °C to 210 °C at 10 °C intervals was carried out. Figure 3.12 shows the crystallisation process of CBT in this temperature range. From the isothermal DSC trace at 160 °C, the low dip of the crystallisation process was observed after 1-2 minutes. At 170 °C the crystallite development was observed clearly after 3 minutes as shown in Figure 3.13 (a). The DSC traces also show strong evidence that the crystallisation process occurred after 1.5 minutes at 170 °C. When the trace returns to the baseline after 5 minutes, the crystallites start to saturate and thicken (Figure 3.13 (b)).

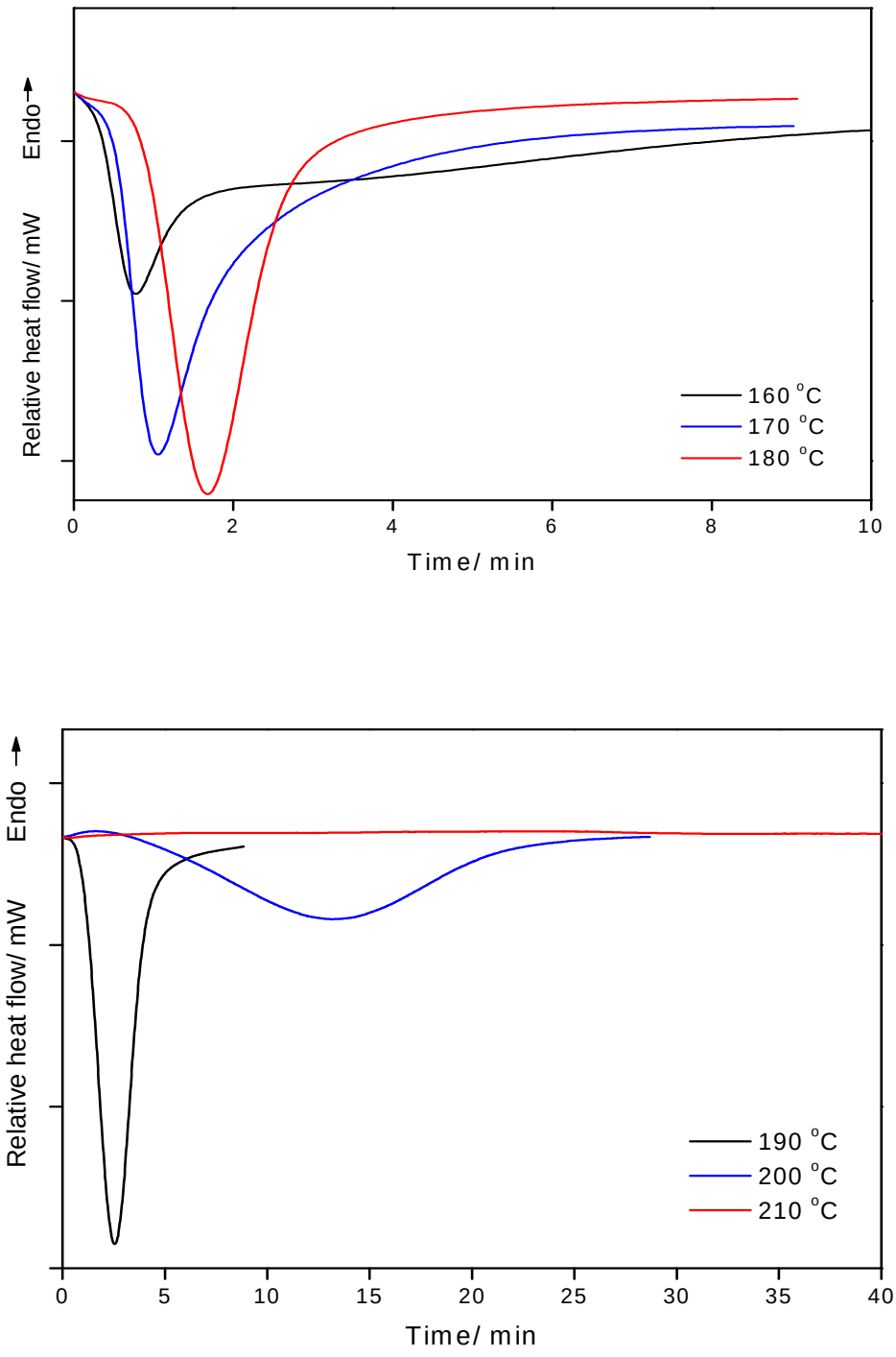

Figure 3.12: Simultaneous polymerisation and crystallisation of CBT at various temperatures

The faster crystallisation speed at lower temperatures is characteristic of crystalline lamellar growth during isothermal crystallisation [39]. However, in some cases it was reported that premature crystallisation (temperatures below 185 °C) or inefficient mixing of catalyst could lead to incomplete polymerisation [16]. The typical and strongest crystallisation was found at 180 and 190 °C. It started at 2.5 minutes and was completed after about 7 minutes.

Figure 3.14 (a) and (b) depict the crystallisation process of c-PBT at 190 °C. It was observed that the crystallites appeared after 2 minutes and this finding is in agreement with the previous finding where c-PBT is a material which has rapid crystallisation process and high crystallinity content [14]. Results from this experiment suggest that the *in situ* ring expansion polymerisation occurred in a short period of time. It was reported that 0.25 wt % of stannoxane which is considered a fast catalyst, has been found capable of completing c-PBT polymerisation within 2 to 3 min at 190 °C [34, 50].

On the other hand, from the results of DSC experiments and hot-stage microscope examination, crystallisation processes were found to become slower above 200 °C. For example, the photograph (Figure 3.15 (a) and (b)) of hot-stage microscope examination shows crystallites starting to appear after 1 hour and it is still developing after 1 hour 30 min at 220 °C. Slow crystallisation allows for a high degree of crystallinity and crystal perfection. These large and perfect crystals may cause polymer brittleness [53].

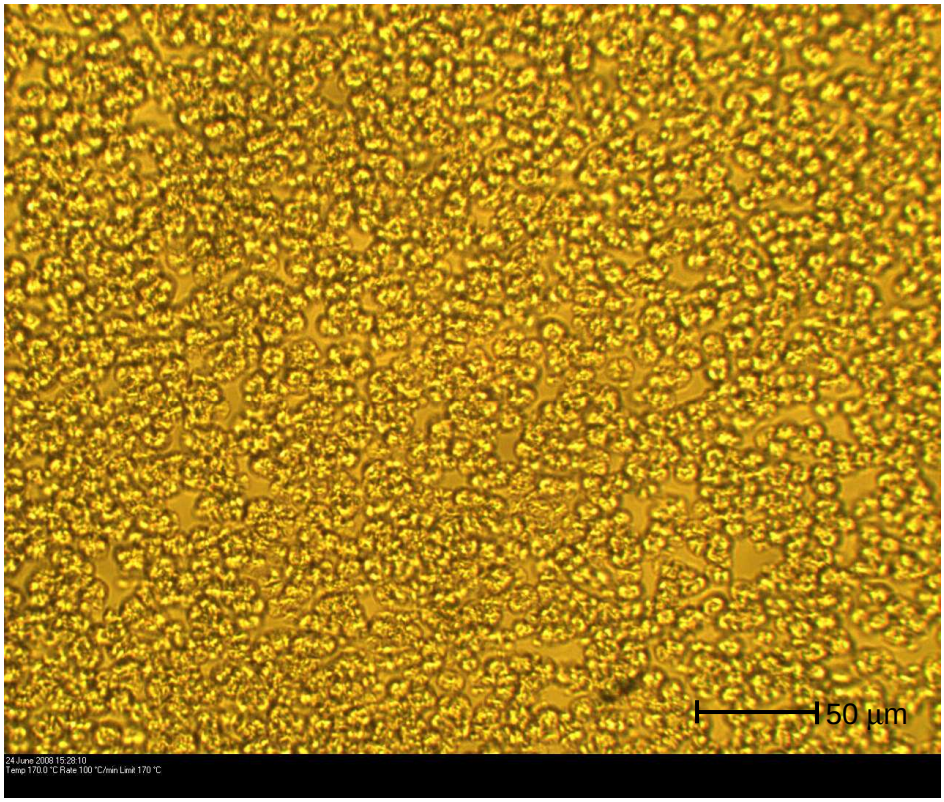

(a)

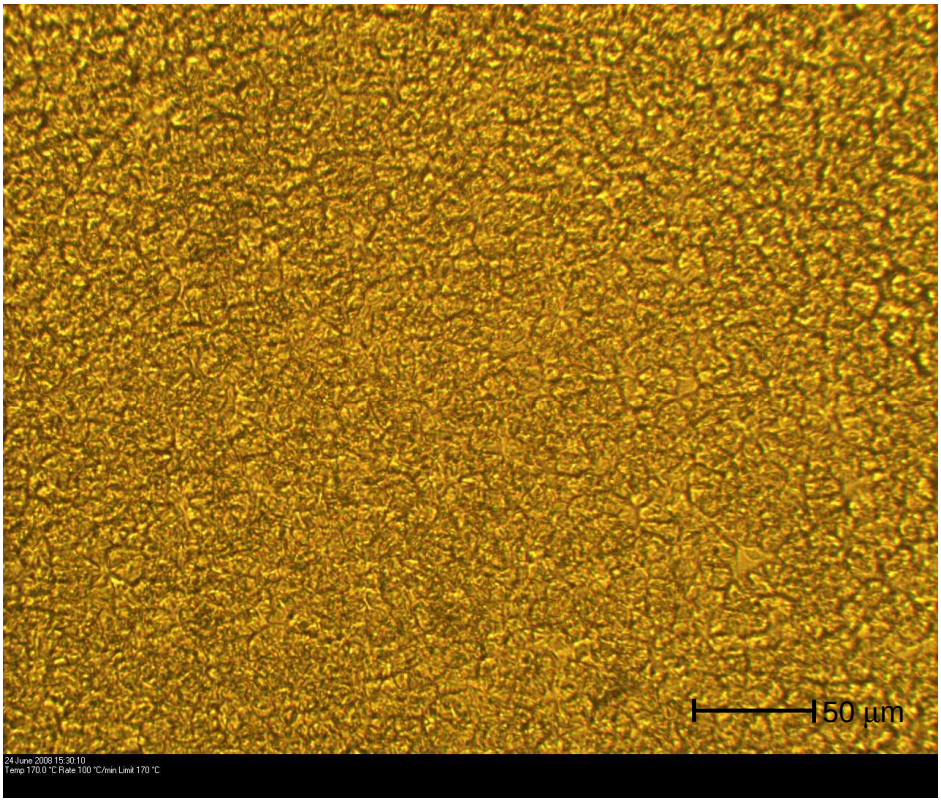

(b)

Figure 3.13: The crystallisation process at 170 ^{o}C; (a) 3 min and (b) 5 min

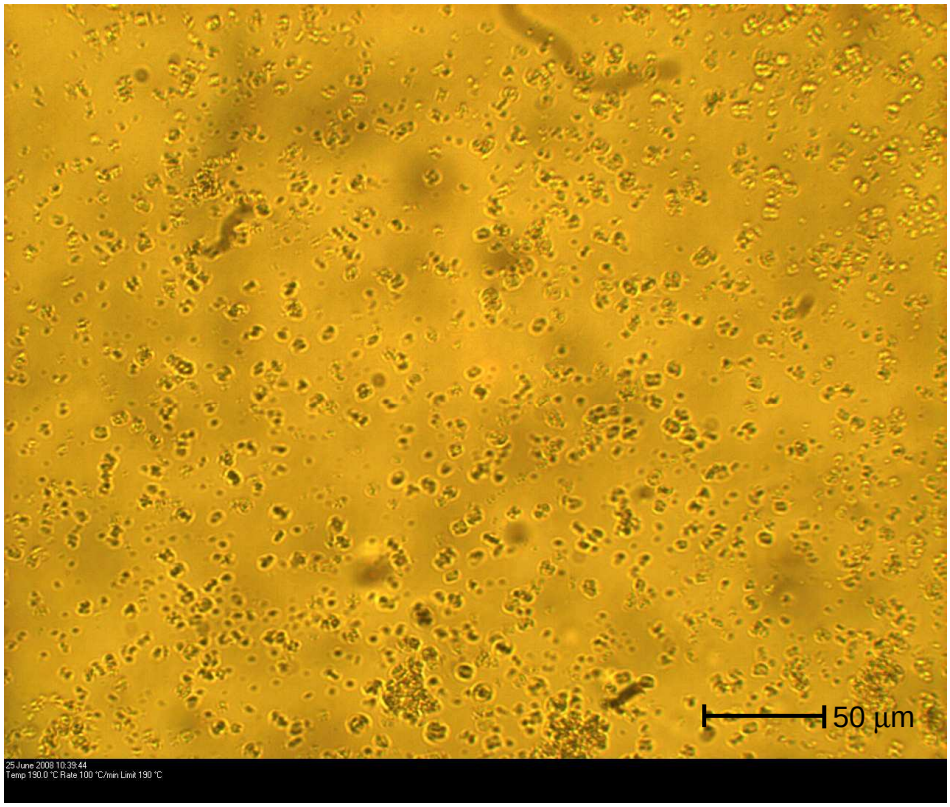

(a)

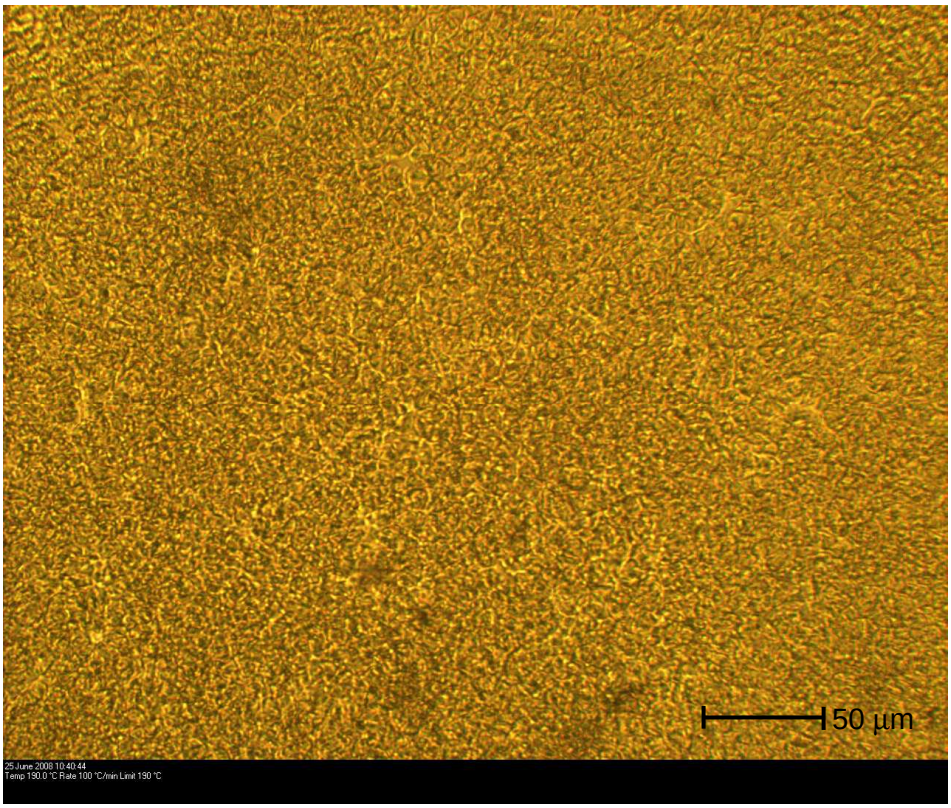

(b)

Figure 3.14: The crystallisation process at 190 ^{o}C; (a) 2 min and (b) 3 min

Hakme *et al.* [39], who investigated the polymerisation of CBT by dielectric sensing claimed that polymerisation and crystallisation occured simultaneously at lower temperatures (< 210 °C). They also observed that the crystallisation becomes slower above 210 °C. Also, Parton *et al*. [53] claimed that polymerisation of CBT occurred simultaneously with crystallisation at 190 °C but polymerisation and crystallisation were consecutive at 230 °C. However, the choice of catalyst has a large effect on the polymer conversion and the time required for polymerisation [34]. Both the Hakme *et al.* [39] and Parton *et al*. [53] studies used a catalyst which leads the CBT to undergo ring opening polymerisation to produce linear polyester. In contrast, stannoxane enabled the CBT to produce a macrocyclic polymer through ring expansion polymerisation [13, 14].

Figure 3.16 illustrates the melting transition of c-PBT produced in the temperature range 160 to 210 °C. In the range of rapid simultaneous polymerisation and crystallisation (160 °C to 190 °C), the melting transition of c-PBT only showed a single peak. This signifies satisfactory crystal quality achieved during production c-PBT. Patron *et al.* [33, 53] have characterised the crystalline structure of c-PBT and have shown that c-PBT has thick and well oriented crystalline lamellae. Miller [14] concluded that if oligomers were added to polymer chains that have already begun to crystallize, then only short amorphous segments are attached to crystal growth fronts, which in turn have a low probability of becoming part of more than one lamellae thus forming tie molecules.

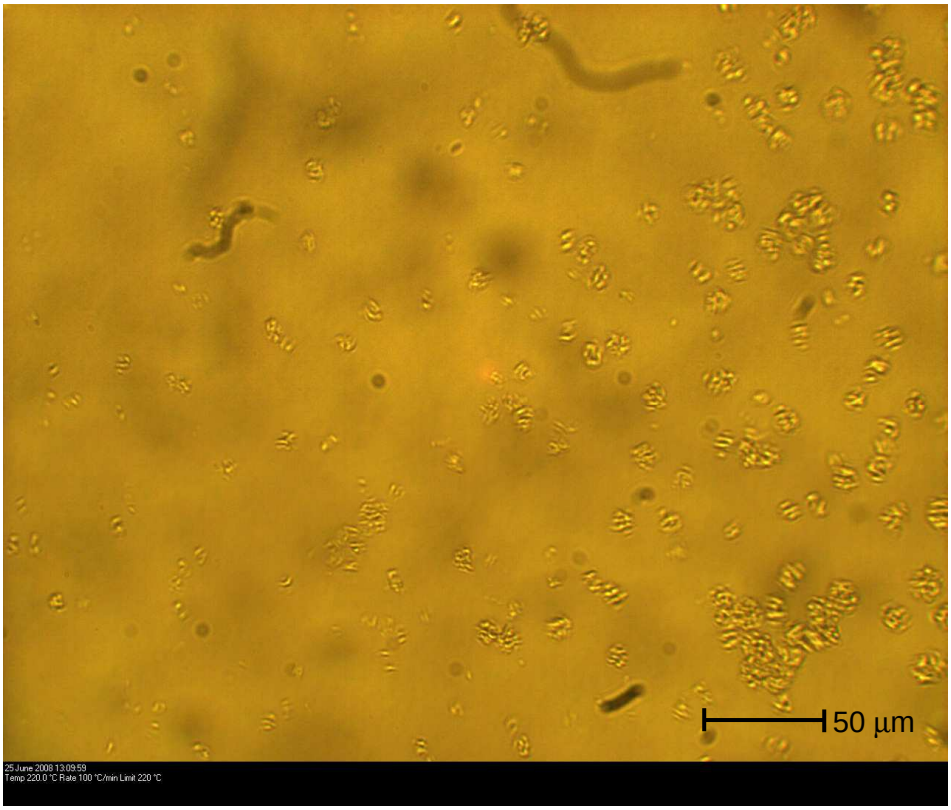

(a)

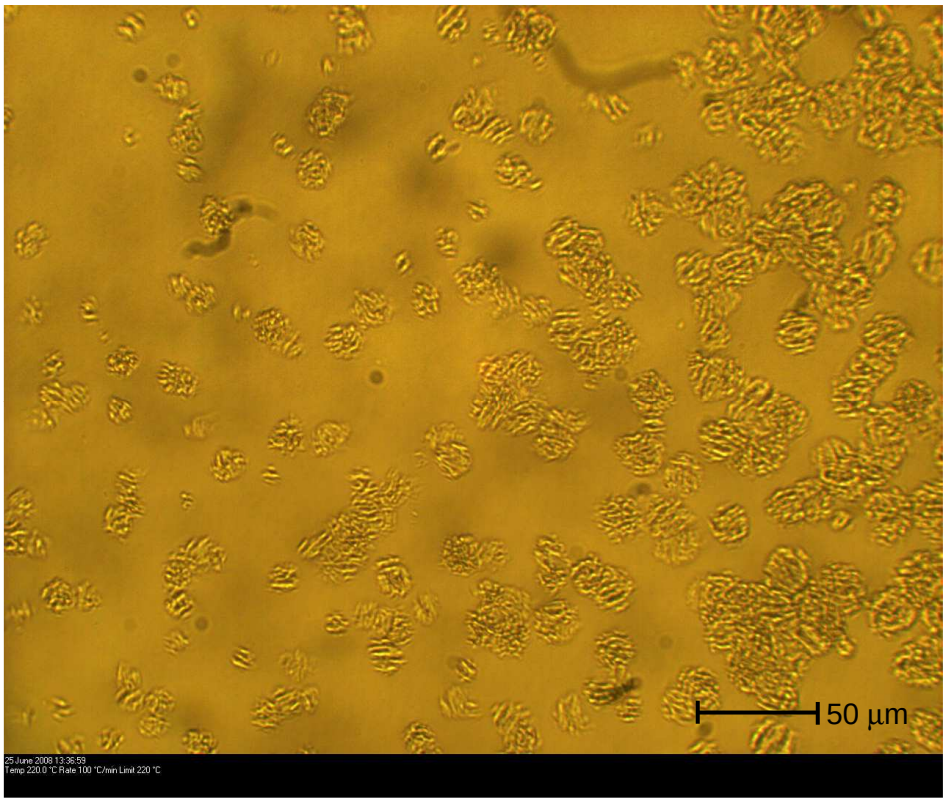

(b)

Figure 3.15: The crystallisation process at 220 ^{o}C; (a) 60 min and (b) 90 min

Moreover, he claimed that the tie molecule density is influenced by simultaneous polymerisation and crystallisation. The transesterification catalyst remaining in the polymer might also influence the amount of tie molecules. The catalyst molecules cannot be included into the polymer crystal, but probably concentrate at the surface of the growing crystals. As a consequence of mechanical tensions arising from packing density differences at the crystal boundaries, such a local transesterification enhancement would drastically decrease the amount of tie molecules [53].

In that region (160 to 190 °C) the melting transitions switch to lower temperatures and an increase in the degree of crystallinity is also observed. As reported earlier, the CBT with 0.25 wt % of stannoxane was found to polymerised within 2 to 3 min at 190 °C [34, 50] and it was believed that the *in situ* ring expansion polymerisation could be performed under optimum condition at this temperature as the resulting c-PBT showed only a single melting peak and a high degree of crystallinity. These characteristics were reported for c-PBT, where there is only a single melting peak due to the 'usual' crystallites and higher degree of crystallinity than the linear PBT [10, 13, 14]. The temperature of 190 °C then was chosen to polymerise CBT in order to produce c-PBT.

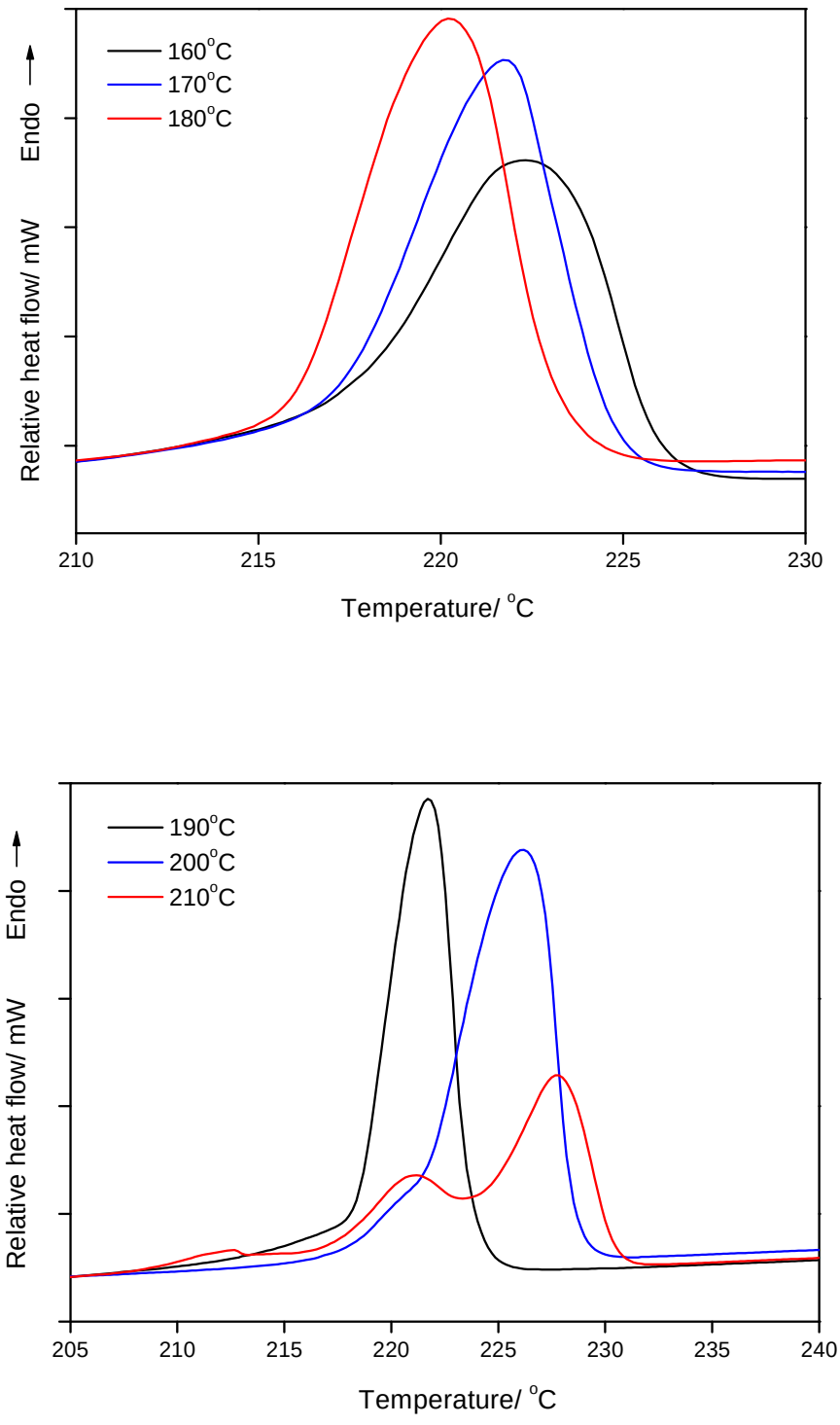

Figure 3.16: The melting point of c-PBT after simultaneous *in situ* polymerisation and crystallisation of CBT at various temperatures

In contrast, when CBT polymerised above 190 °C the melting point increased to a higher temperature which is near to the melting point of linear PBT. In the case of polymerisation of CBT at 210 °C where the crystallisation process is slow and not complete (Figure 3.12) in the time given, the polymer produced will show double melting (Figure 3.16). It is believed that the ring expansion polymerisation is also not complete which leads production of mixed spherulites or mixed cyclic and linear structures. With this assumption, it was suggested that the simultaneous polymerisation and crystallisation process in the production of c-PBT from CBT with the presence of cyclic catalyst (stannoxane) could not be separated. It starts with polymerisation and when the molecular weight reaches an appropriate level the crystallisation process can begin. That means that the crystallisation process began before the polymerisation process was complete. In the assessment of melting behaviour of c-PBT and perfection of crystallites formed, it was believed that polymerisation and crystallisation are completed in the same region.

3.2.4 Studies on the optimum condition for production of c-PBT

An investigation of the production of c-PBT at the ideal temperature (190 °C) over various polymerisation times (0 to 60 minutes) was done. Figure 3.17 presents the crystallisation process for *in situ* polymerisation of CBT at 190 °C. From that figure we know that the crystallisation process has still not begun after 1 minute. The crystallisation process only undergoes half after 3 minutes and was observed back to the baseline after 5 minutes. The resulting polymer melting transition is shown in Figure 3.18. It was observed that the polymerisation process was begun before crystallisation started as can be seen in

holding CBT for 1 minute. However, the polymer produced shows double melting. It is believed that the ring expansion polymerisation is not complete and produced mixed cyclic and linear PBT.

The double melting phenomenon was still found for sample held for 3 minutes. It is interesting to observe that the higher melting peak was reduced and the lower melting peak increased. Below 3 minutes the crystallisation is incomplete. Therefore, during the re-heat the process can continue, giving rise to an additional melting peak. However, a single melting transition was found for the sample which allowed 5 minutes polymerisation time. When the holding time was increased to 10 minutes, the single melting peak of c-PBT was found to be more sharp and symmetrical. It is suggested that the 10 minutes polymerisation time could produce a high degree of uniformity in size and perfection spherulites. It was calculated that the degree of crystallisation of c-PBT which produced under these conditions (polymerised at 190 °C for 10 minutes) is 80 ± 1 %.

In the other hand, the longer polymerisation times (i.e. 30 and 60 minutes) leads the production of double melting and the melting transition shifted to higher melting peak. As shown in Figure 3.18, the CBT samples which allowed polymerised for 30 and 60 minutes shows broad melting peak and the degree of crystallinity was reduced. This situation occurred, it is believed, because of the stability of catalyst used in this study. The stability of stannoxane will be further discussed in the thermal stability study (Section 3.27). The instability of catalyst could break the cyclic structure and resulted in mixed structure between cyclic and linear PBT. It is also suggest that the form of imperfection spherulites upon 30 and 60 minutes polymerisation times is also another possibility to cause the

double melting to reappear and shift in position. From this study, it could suggest that the best condition to produce c-PBT via *in situ* ring expansion polymerisation is at 190 °C for 5 to 10 minutes.

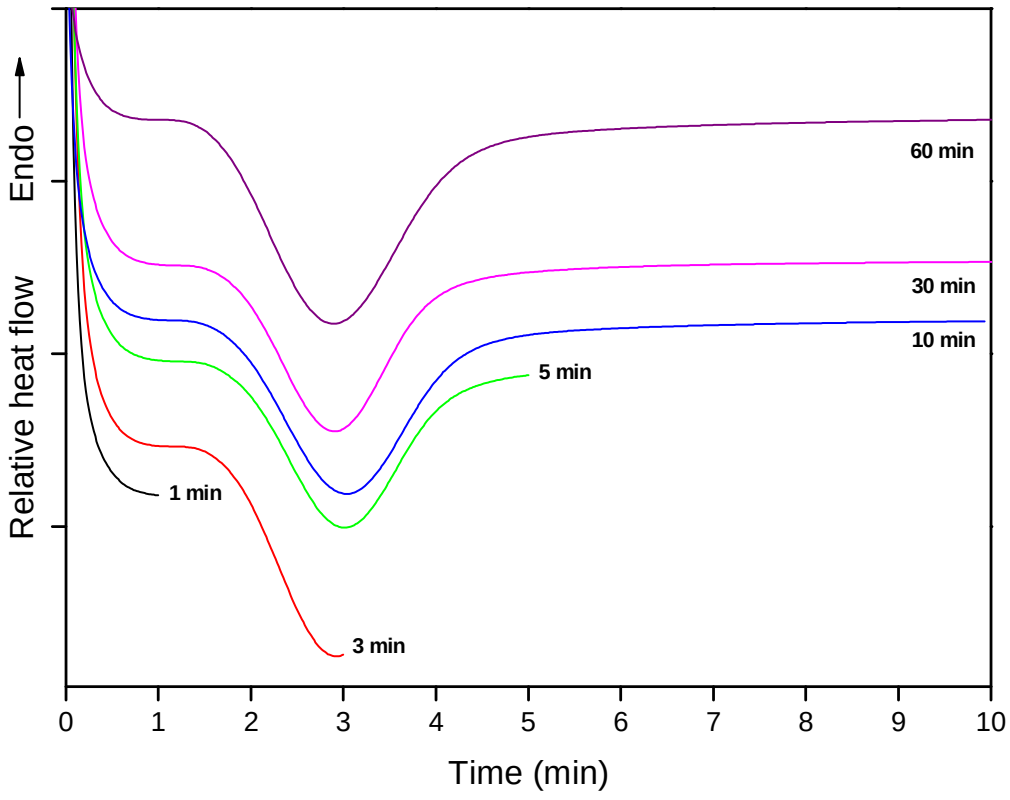

Figure 3.17: The effect of time on simultaneous *in situ* polymerisation of CBT and crystallisation of c-PBT at 190 °C

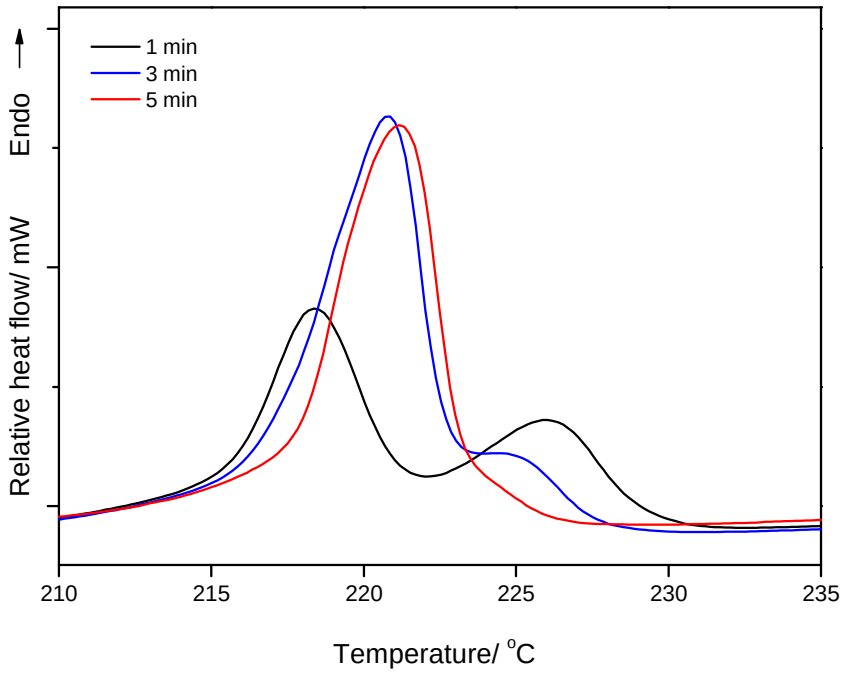

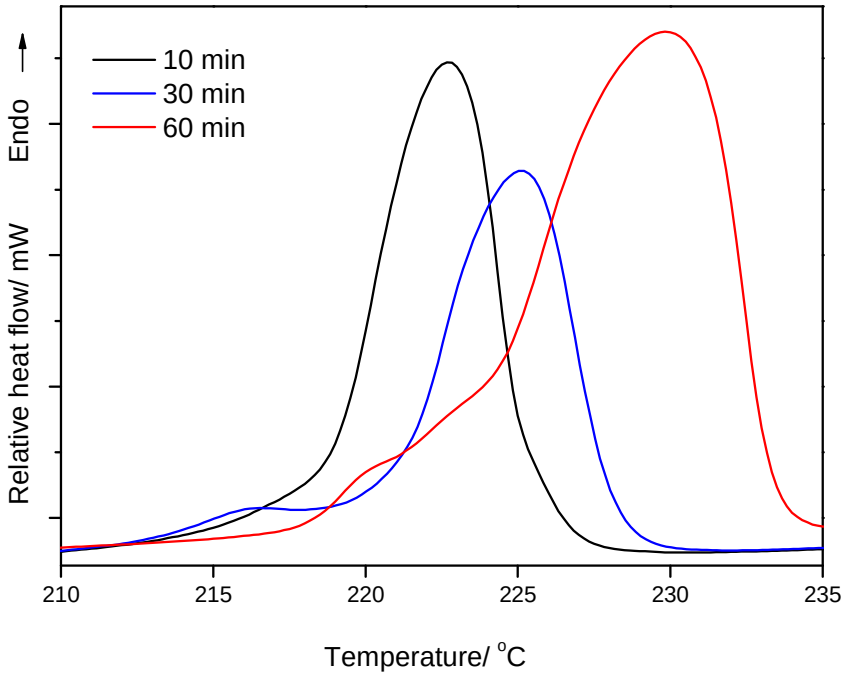

Figure 3.18: The melting of c-PBT after simultaneous *in situ* polymerisation of CBT and crystallisation of c-PBT at 190 °C at various times

3.2.5 FTIR examination

3.2.5.1 Determination of functional groups

Figure 3.19 displays the FTIR spectra of CBT from a total of 100 scans at a resolution of 2 cm^{-1} by the Attenuated Total Reflectance (ATR) technique [102]. The entire CBT structure was determined from the FTIR spectra from the following peak assignments [116, 117]:

CBT wavenumbers (cm^{-1})	Assignment
3000 to 2800	$(CH_2)_4$ stretching
1750 to 1600	C=O stretching
1300 to 1100	C-O stretching
800 to 700	Benzene bending

The spectra of the CBT and c-PBT were expected to be similar. It is clear that all peaks for both the CBT and c-PBT spectra remain in the same position except for the C-O stretching and C=O stretching band. The effect of conversion CBT into c-PBT on these peaks will be discussed in following section.

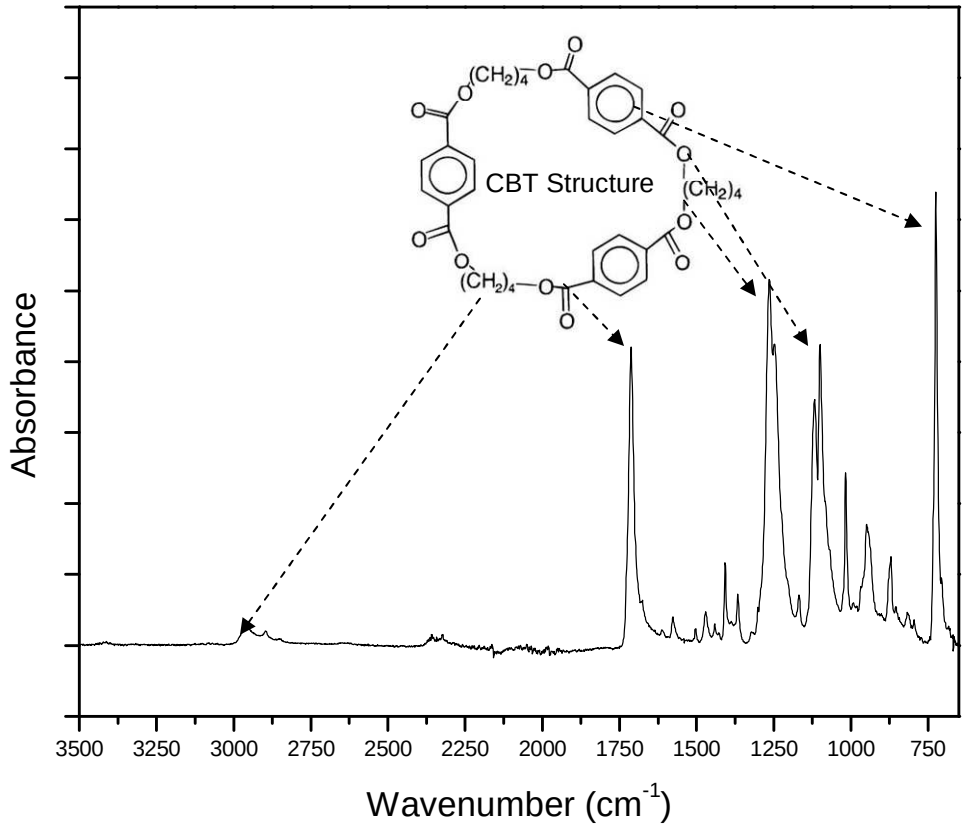

Figure 3.19: FTIR Spectra of CBT

3.2.5.2 The effects of *in situ* polymerisation of CBT on functional groups

It is believed that the polymerisation process of CBT will affect the ester group (i.e. C-O stretching and C=O stretching band). An investigation was done to study the effect of CBT polymerisation on the FTIR spectra. Data for the spectra have been normalised with the peak correlating to deformation of the benzene ring. This is because benzene was not involved in the polymerisation reaction and the peak was assumed to remain constant.

Figure 3.20 and Figure 3.21 show the changes in C-O stretching band during heating and subsequent polymerisation of CBT. The spectra show two distinct peaks which correspond to amorphous and crystalline arrangements. When the sample starts to melt, intensity of the peak drops as shown in the CBT melting region (140 to 160 °C). In this region, it can be seen that the amorphous and the crystalline arrangements have equal intensity. Subsequent temperature increases will then develop the crystalline region as polymerisation occurs and forms the semi-crystalline polymer. In the Figure 3.20, it could be observed that the peak around 1260 ± 2.5 cm^{-1} wavenumber is greater for CBT whereas the peak around 1243 ± 3.5 cm^{-1} is greater for c-PBT. This suggests that some conformational change occurs during the polymerisation reaction around the C-O stretching band. Rotation about the C-O stretching band is known to be possible in PET [117]. Conformational changes around the C-O stretching band are to be expected from the CBT ring expansion polymerisation. Jang and Sim [118], found shifts to lower wavenumbers to correlate with the progression of a more ordered structure. The shift observed between CBT and c-PBT indicates that the crystalline structure of c-PBT is more ordered than that of the CBT.

This situation can also be seen in Figure 3.21, which shows the changes in the C-O stretching band which appeared at lower wavenumber (1116 ± 1.5 to 1095 ± 3 cm^{-1}). In the active simultaneous polymerisation and crystallisation region (170 °C to 200 °C), it was observed that the crystalline peak becomes dominant since c-PBT formed. However, when the samples continue to be heated to higher temperatures (210 °C to 240 °C) the peak intensity of the spectra recorded is reduced as degradation of the catalyst expected.

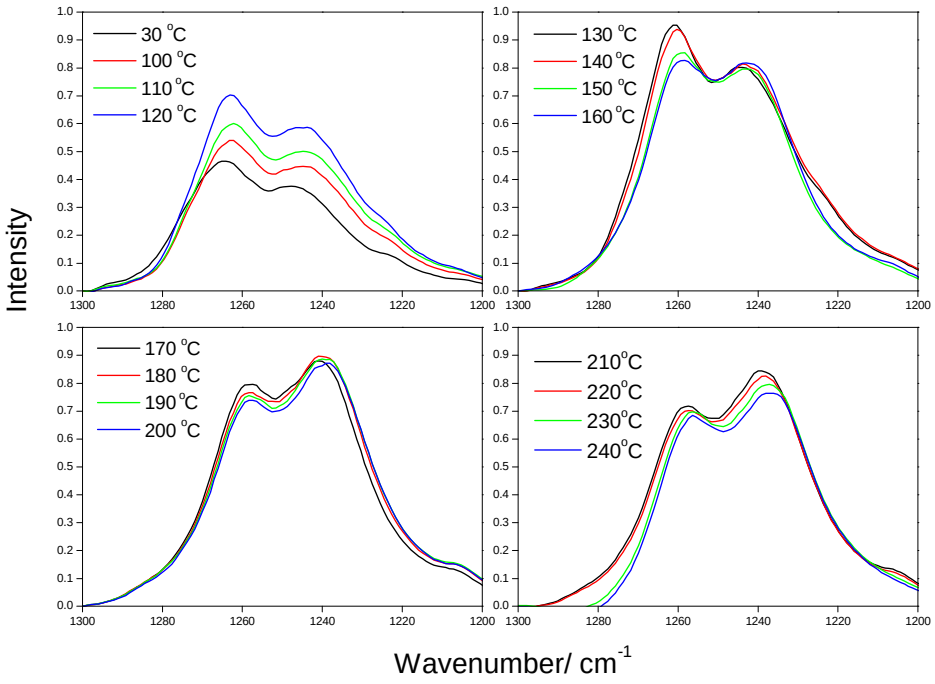

Figure 3.20: Changes in C-O *str*. band (1260 to 1243 cm^{-1}) upon heating of CBT

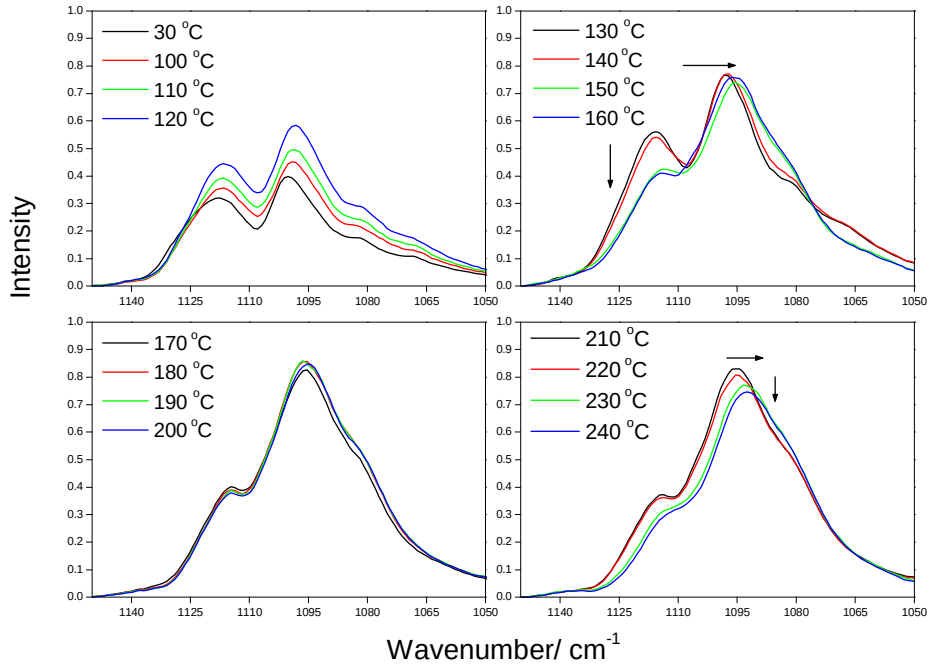

Figure 3.21: Changes in C-O *str*. band (1116 to 1095 cm^{-1}) upon heating of CBT

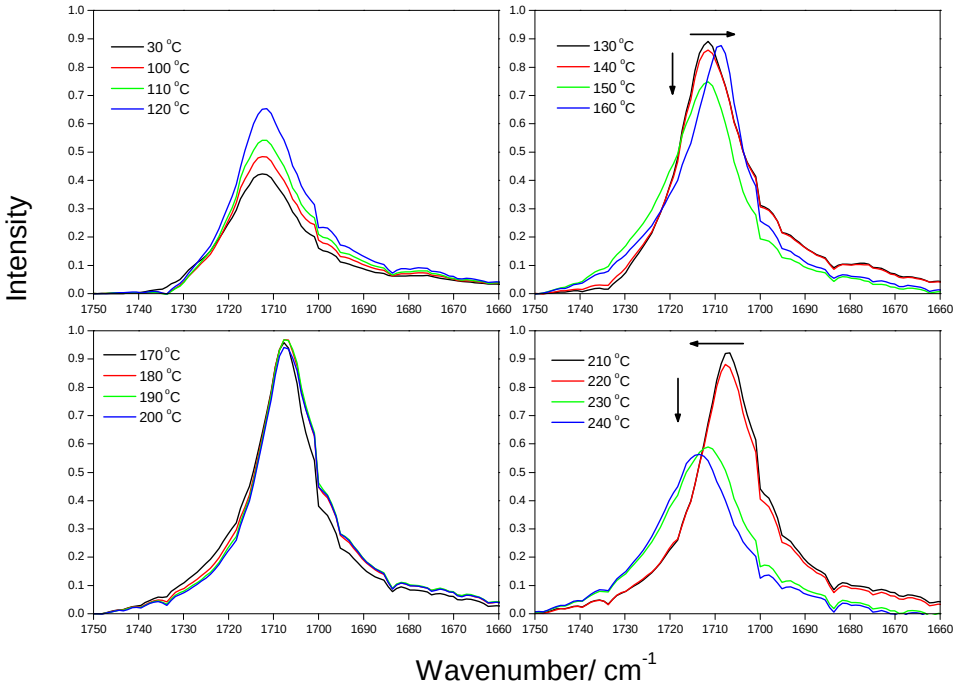

Figure 3.22: Changes in C=O *str.* band (1712 to 1709 cm^{-1}) upon heating of CBT

Figure 3.22 shows the changes in C=O stretching band upon heating of the CBT. Analysis of C=O stretching band is quite different; it only has a single peak centred at 1712 ± 1 cm^{-1} before the CBT melts. Once the CBT starts to melt the peak intensity falls and above 160 °C the peak centre was observed to shift to 1709 ± 1 cm^{-1}. This suggests that before the CBT melts, it is amorphous and after it melts polymerisation occurs and the structure changes to crystalline form as the polymer develops. Hopfe *et. al* [119] found that C=O strecthing band shifts also coincided with changes in the conformation (trans and gauche) of the tetramethylene ($(CH_2)_4$) sequences.

The phase transition from the solid to melt state also can be seen during analysis of this C=O strecthing band. Upon the first heating, we observe that after the polymer (c-PBT) melts above 230 °C the peak intensity decreases dramatically and the sample reverts to the amorphous arrangement. Logically, when the polymer melts, there is movement and the crystallites disappeared which leads to the amorphous arrangement.

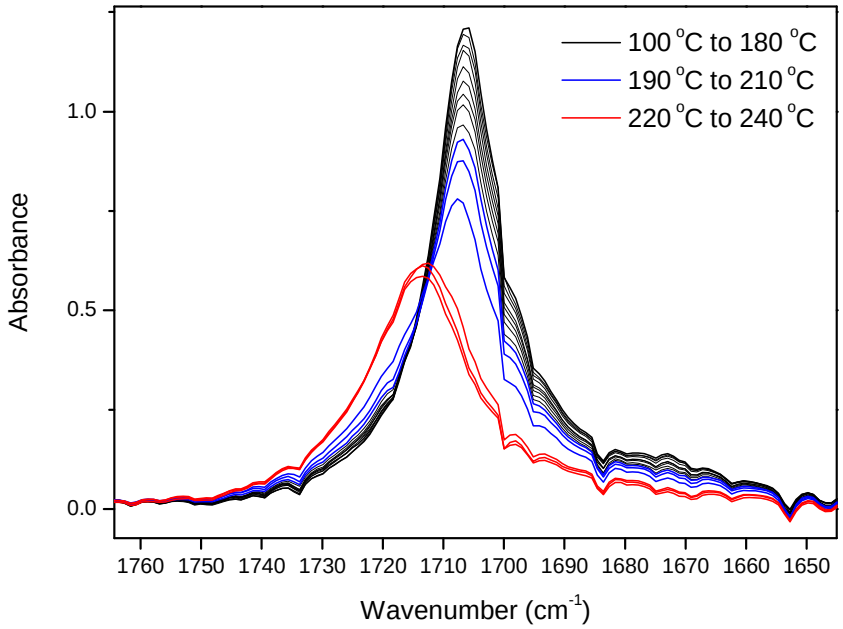

Figure 3.23: Changes in C=O group upon cooling of c-PBT

The phase transitions are illustrated in Figure 3.23 and Figure 3.24, respectively. During cooling, we observe that the sample slowly changes to solid again below 210 °C and re-heating the sample confirms that the polymer formed will melt above 230 °C. All these finding are in agreement with the DSC results. In general, the C-O stretching and C=O stretching band are involved in the polymerisation reaction of the CBT since their peaks changed after *in situ* polymerisation.

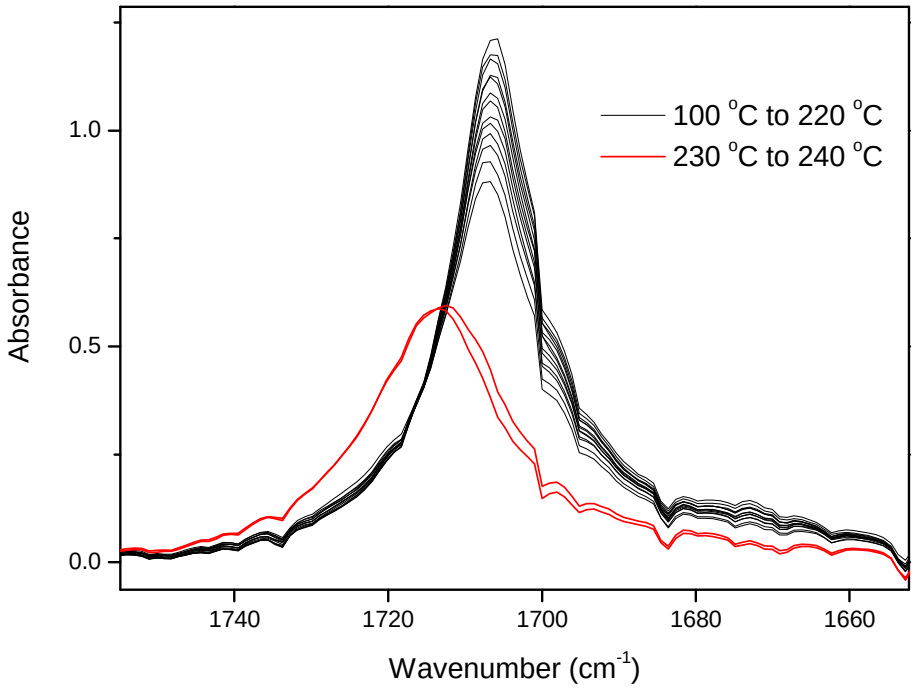

Figure 3.24: Changes in C=O group upon re-heating of c-PBT

3.2.6 The molecular weight of c-PBT

3.2.6.1 The development of M_w upon heating of CBT

As mentioned earlier, the production of c-PBT begins with a low molecular weight CBT and the molecular weight of these cyclic materials can be tailor made for a specific application and manufacturing process [52]. Gel permeation chromatography (GPC) was used to study the development of molecular weight upon heating the CBT at various temperatures. This study will contribute more understanding to the c-PBT molecular weight development as well as the conversion of CBT to c-PBT. The molecular weight distribution of c-PBT at various temperatures is shown in Figure 3.25.

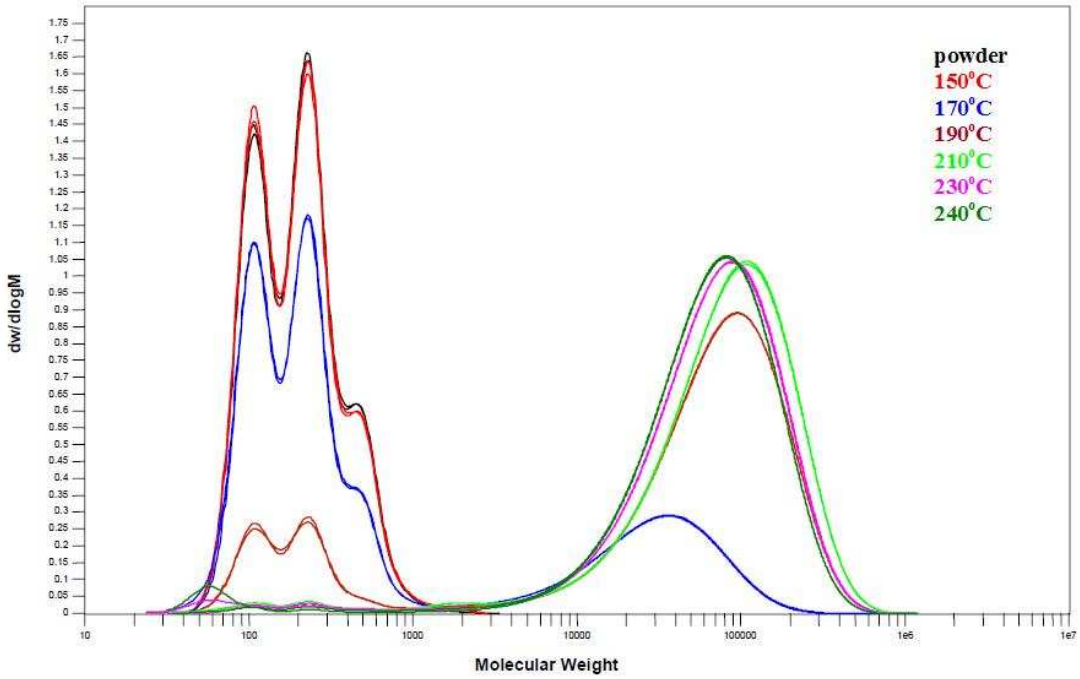

Figure 3.25: The molecular weight distribution of c-PBT at various temperatures

The GPC results indicate that the CBT actually contains three components, presumably different oligomers. This finding is in agreement with DSC results where a broad melting transition was found for CBT. The chromatograms for CBT powder samples and 150 °C only shows the low molecular weight component which believed to be due to cyclic oligomers. For samples which heat up to 170 °C and, to a lesser extent, 190 °C the chromatograms show earlier retention time peaks due to polymer as well as peaks due to the oligomers. However the chromatograms of the samples heat up to 210 °C, 230 °C and 240 °C (these temperatures are above simultaneous polymerisation and crystallisation region) just show polymer.

Table 3.1: Summaries of c-PBT molecular weight at various temperatures

Sample conditions	M_w	M_n	M_w/M_n
CBT powder	n.a.	n.a.	n.a.
Heat up to 150 ^oC	n.a.	n.a.	n.a.
Heat up to 170 ^oC	42,400	18,400	2.3
Heat up to 190 ^oC	82,500	29,600	2.8
Heat up to 210 ^oC	117,000	41,900	2.8
Heat up to 230 ^oC	101,000	39,400	2.6
Heat up to 240 ^oC	93,100	39,500	2.4

Note: 1) n.a. – not available.
2) This results is provided by Smithers Rapra Technology Ltd. (Shropshire, SY4 4NR, UK).

Average molecular weights and polydispersity (M_w/M_n) have been computed for the polymer component alone in samples which heat up to 170 °C to 240 °C. These results are summarised as the calculated molecular weight averages and polydispersity (M_w/M_n) as shown in Table 3.1. The results show that the highest polydispersity was 2.8 when the CBT was heated to 190 to 210 °C. However, the polydispersity reduces after the CBT was heated above the melting point of the polymer.

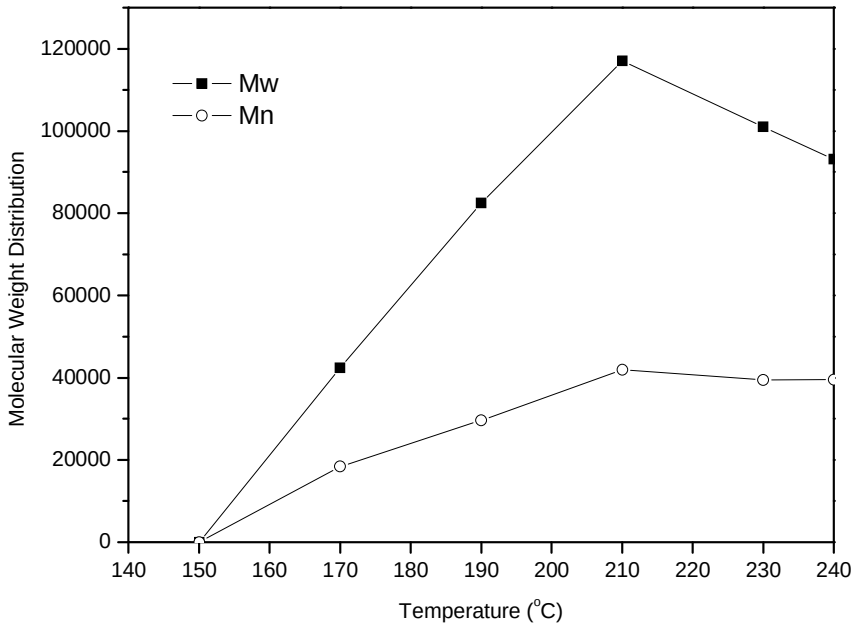

Figure 3.26: The molecular weight development of c-PBT at various temperatures

Figure 3.26 illustrates the molecular weight development of c-PBT during dynamic heating from CBT powder to 240 °C. Nothing happens to the CBT when heated up to 150 °C but a proportion of polymer is clearly produced when heated to 170 °C. At higher temperatures, the CBT is mainly polymerised and to higher molecular weight. The highest molecular weight was found in the sample which was heated to 210 °C. Although the 190 °C is claimed as the best temperature to polymerise the CBT where it should give the highest molecular weight, but the samples was prepared in the dynamic mode (the sample was cooled down after reaching the target temperature). That means the polymerisation is not complete when the sample just reaches 190 °C. Further discussion on molecular weight development at 190 °C will be developed in the following section.

The reduction in the molecular weight of polymer produced when samples are heated to higher temperatures (>210 °C) is believed due to thermal stability of the catalyst (stannoxane). The degradation of catalyst could reduce the molecular weight of polymer. On the other hand, hydrolysis of c-PBT in the presence of water could also decreased its molecular weight [14]. Moreover, the rather high level of catalyst still present in the c-PBT samples might have a negative effect on the molecular weight by a transesterification reaction [53].

3.2.6.2 The effect of polymerisation time at optimum temperature on molecular weight

Figure 3.27 shows the molecular weight distribution of c-PBT at the optimum production temperature (190 °C) for various polymerisation times. The chromatograms for the various samples showed early elution components, due to polymer and late elution components presumed to be due to the cyclic oligomers. These GPC results are also in agreement with the DSC which discussed in section 3.2.4. Again the results show that the polymerisation process will not be complete before the crystallisation process is complete. This can be found in the samples which allowed polymerisation at 190 °C for less than 5 minutes. The GPC results show these samples still have oligomers present. The proportion of residual cyclic oligomers however was found to decrease with time.

Table 3.2 summarises the calculated molecular weight averages and polydispersity (M_w/M_n) for the studies at 190 °C in various polymerisation times. A maximum molecular weight appears to be reached at 5 to 10 minutes holding time (Figure 3.28). The polymerisation of CBT for 30 and 60 minutes seems to be some decrease in molecular weight. This will particularly decrease the calculated number average molecular weights and increase the polydispersity. This finding could also explain the shift of melting peak and decrease of crystallinity for the samples polymerised for more than 30 minutes at 190 °C. Examination on molecular weight development at 190 °C also suggests that the best production time is in the 5 to 10 minutes range.

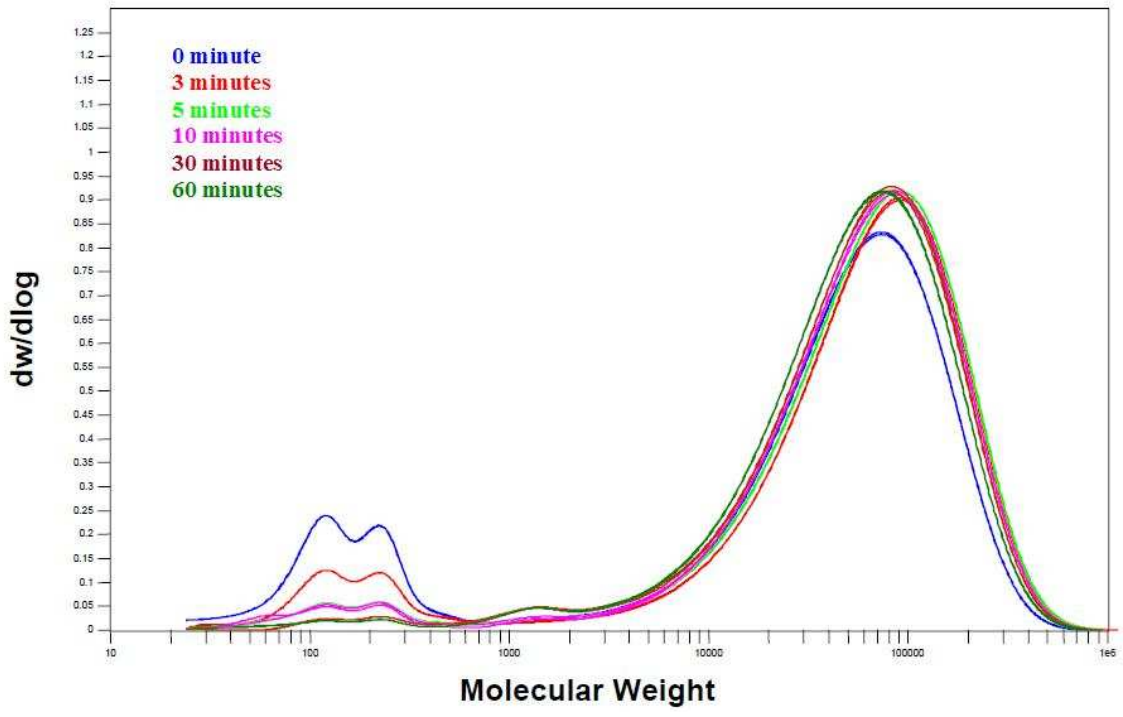

Figure 3.27: Molecular weight distribution of c-PBT at 190 °C for various polymerisation times

Table 3.2: Summary of c-PBT molecular weight distribution at 190 °C for various polymerisation times

Sample conditions	M_w	M_n	M_w/M_n
Hold 0 minutes	82,500	29,600	2.8
Hold 3 minutes	94,000	31,100	3.0
Hold 5 minutes	99,100	32,700	3.0
Hold 10 minutes	99,700	33,300	3.0
Hold 30 minutes	90,600	27,800	3.3
Hold 60 minutes	85,200	26,000	3.3

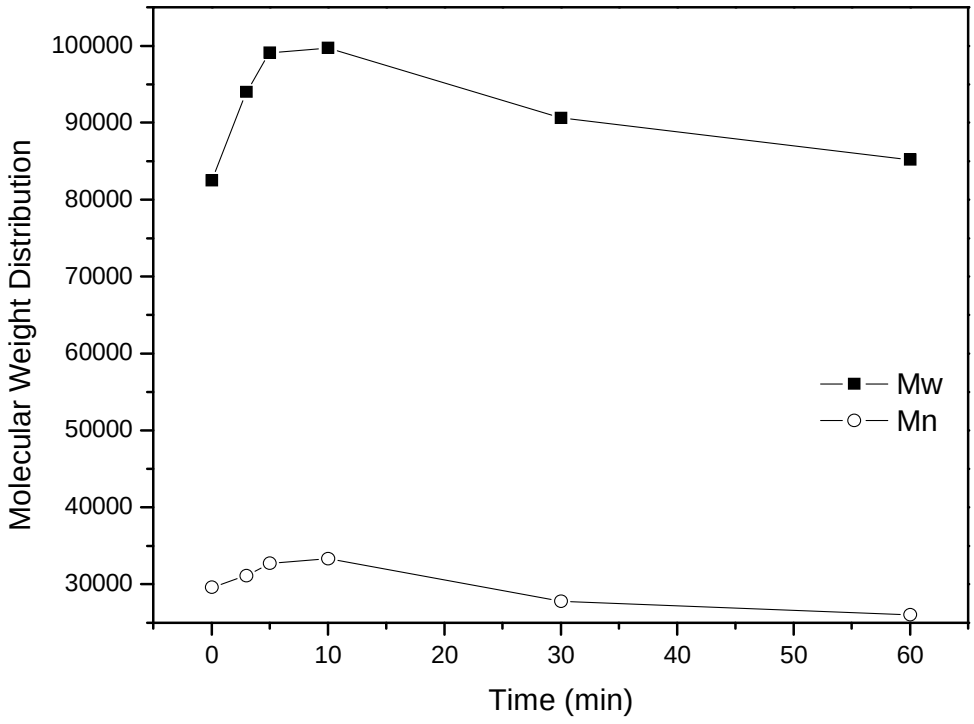

Figure 3.28: Molecular weight development of c-PBT at 190 °C for various polymerisation times

3.2.7 Thermal stability of c-PBT and stannoxane

Thermo gravimetric analysis (TGA), gel permeation chromatography (GPC) and Fourier transform infrared spectroscopy (FTIR) are several common methods which can be used to determine the degradation of polymers [120]. In this study, TGA has been used as a technique to determine the thermal stability of c-PBT and its catalyst (stannoxane). The TGA technique determined the weight loss of the polymer as a function time or temperature. Weight loss due to thermal degradation is an irreversible process. According to Wong and Lam [121], this thermal degradation is largely related to oxidation in which oxygen molecules attack the polymer bonds. The thermal stability of PBT has been extensively studied previously [62, 122, 123] and it has been reported to have thermal stability up to about 300 °C.

Figure 3.29 represents the thermal stability of c-PBT produced from CBT and commercial linear PBT. These TGA traces were recorded from dynamic scans at 10 °C/min from 30 °C up to 800 °C. From the results, c-PBT started to degrade at 280 °C while linear PBT started to degrade at about 300 °C. However, if only the onset is considered then the thermal stability of c-PBT and linear PBT is similar. That suggests that structures or how the PBT is produced (whether from cyclic oligomers or conventional methods) does not have any significance for their stability. The thermal stability of c-PBT by an isothermal method where the sample was held at 190 °C and 240 °C for 60 minutes was also examined as shown in Figure 3.30. The results show that c-PBT has good thermal stability in this temperatures range. The weight loss was found to be below 3 % and which suggests that the temperatures range used in this study is safe for c-PBT prior to

processing. In addition, the PBT chain is known to degrade when held above 250 °C for extended times [14].

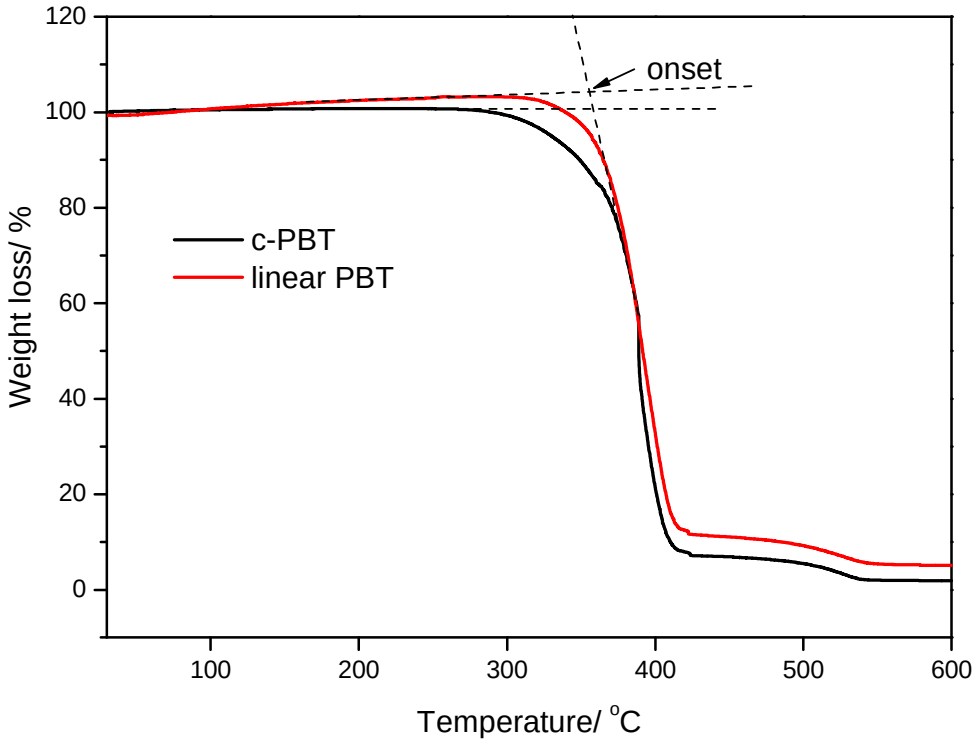

Figure 3.29: Dynamic thermal stability of c-PBT and linear PBT

It was reported that the degradation of catalyst could open the cyclic structure and yield linear polymers [14]. Therefore, it is essential to investigate the degradation temperature of stannoxane. A dynamic scan shows that (Figure 3.31), stannoxane is seen to start degradation above 190 °C and the onset was observed at about 240 °C. The decomposition stage of stannoxane was found to occur in the temperature range of 240 °C to 275 °C, and followed by burning step of carbon at above 300 °C [124].

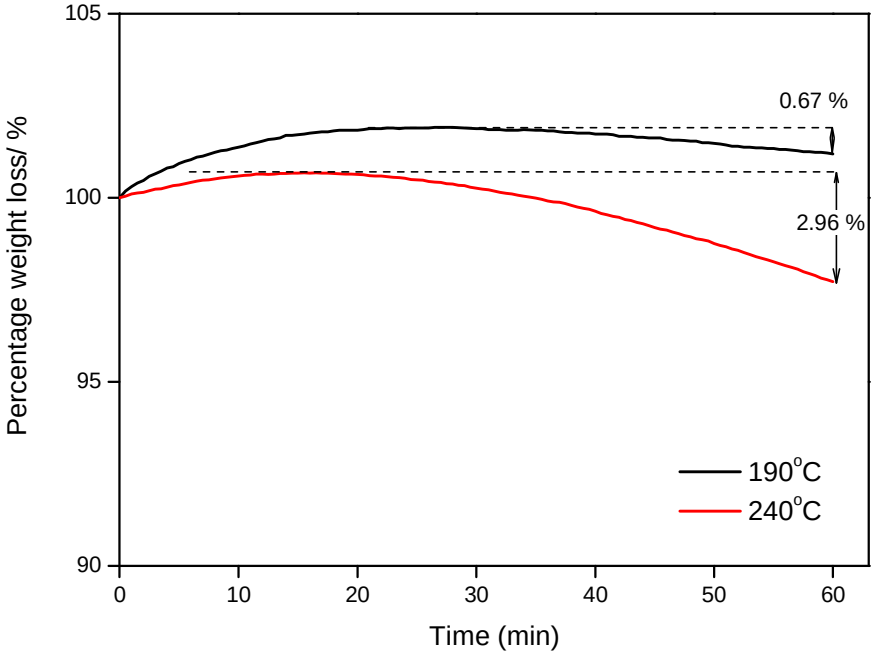

Figure 3.30: Isothermal thermal stability of c-PBT at 190 °C and 240 °C hold for 60 minutes

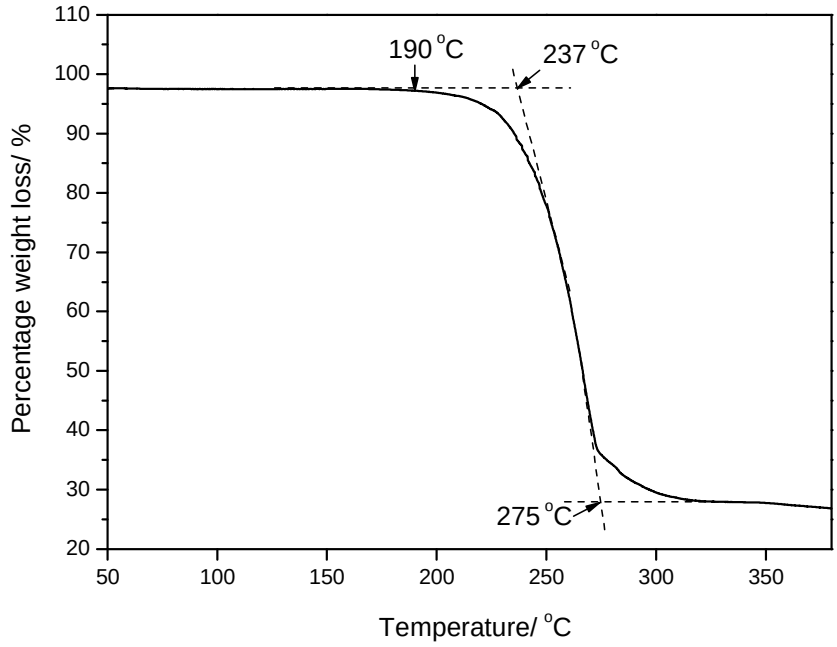

Figure 3.31: Dynamic thermal stability of stannoxane

On the other hand, the isothermal thermal stability of stannoxane at 190 °C shows that it will lose about 8 % weight after 60 minutes. Figure 3.32 also suggests that the *in situ* ring expansion polymerisation at 190 °C is still in a 'safe' region. The best polymerisation time was found to be between 5 to 10 minutes and the weight loss of stannoxane in this time range just below 2 %. However at temperature of 240 °C this catalyst (stannoxane) was observed to have a decomposition phase just in 5 minutes once the temperature is reached.

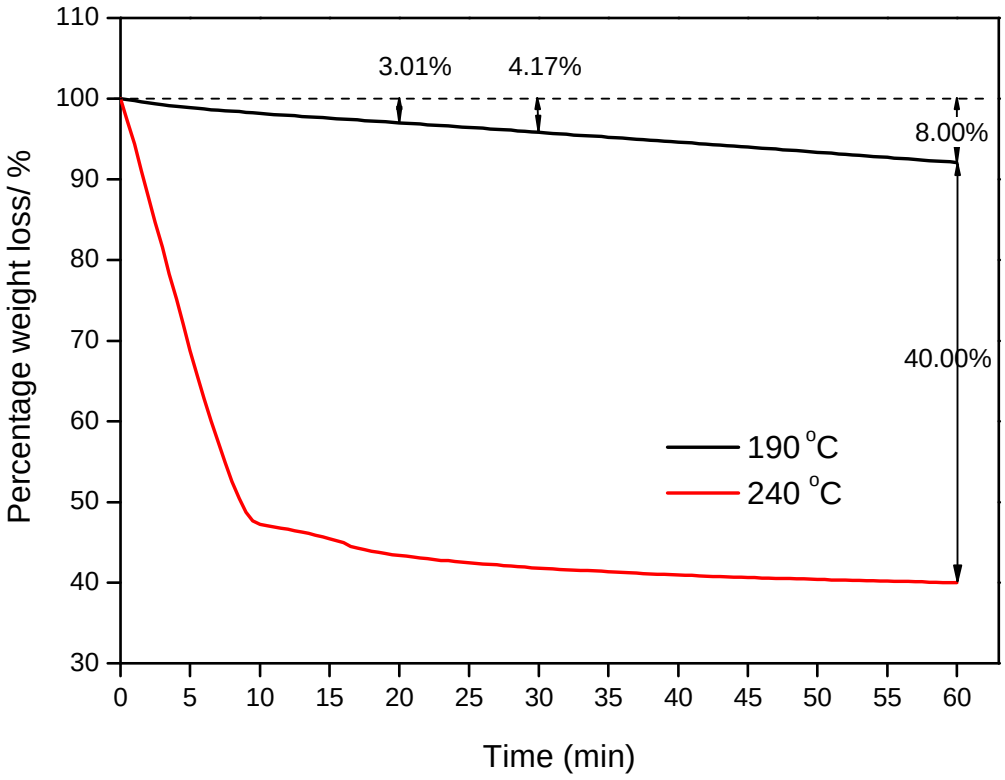

Figure 3.32: Isothermally thermal stability of stannoxane at 190 °C and 240 °C hold for 60 minutes

3.3 Conclusion

The production of polymer from CBT can only be achieved in the presence of a suitable catalyst, i.e. tin catalyst. The use of cyclic catalyst such as stannoxane lead to ring expansion polymerisation and to the production of macrocyclic polymers. The polymerisation is active just after the CBT has fully melted in the range of 160 to 200 °C. The polymer produced in this type of polymerisation was found to have a high degree of crystallinity compared to that produced by conventional methods. Upon production of c-PBT, crystallisation occurred simultaneously. It was found that the simultaneous polymerisation and crystallisation processes could not be separated because both processes occurred rapidly in a short time. It starts with the polymerisation and when the molecular weight reaches an appropriate level the crystallisation process begins. This means that the crystallisation process begins before the polymerisation process is complete. In the assessment of melting behaviour of c-PBT and perfection of crystallites formed, we believed that polymerisation and crystallisation are completed in the same region. From thermal behaviour studies, it could suggest that the best condition to produce c-PBT *via in situ* ring expansion polymerisation was at 190 °C for 5 to 10 minutes.

GPC examination showed that the production of c-PBT began with a low molecular weight material and developed during the polymerisation. The GPC results also indicated that the CBT contain three components, presumably different oligomers. The chromatograms for CBT powder sample and 150 °C only show late retention time peaks which are believed due to cyclic oligomers. For samples heated to 170 °C and, to a lesser extent, 190 °C the chromatograms show earlier retention time peaks due to polymer as

well as peaks due to the oligomers and samples heated at 210, 230 and 240 °C only show polymer. The highest polydispersity was 2.8 when the CBT was heated from 190 to 210 °C. However, the polydispersity reduced after CBT were heated above the melting point of the polymer.

Further investigations using FTIR spectroscopy studied the effect of simultaneous *in situ* polymerisation and crystallisation process of CBT and c-PBT on the absorbtion characterisation of the ester group (i.e. C-O stretching and C=O stretching band). In the region of CBT melting, these bands exhibit an intensity change and a shift as the ring expansion polymerisation occurred. The spectra were found to be more dominant in crystalline arrangement as the c-PBT formed. The C=O band could also show a phase transition during the temperature changes which can be seen upon cooling of c-PBT from the melt and re-heating the sample.

The investigation on stannoxane stability also revealed that the polymerisation of CBT to produce the macrocyclic polymer could only be done below the melting point of the polymer. The results from stannoxane degradation study could also explain the double melting behaviour, the decreased of molecular weight upon polymerisation at high temperature and reduction in peak intensity of the FTIR spectra.

Chapter Four

THE EQUILIBRIUM MELTING AND ISOTHERMAL CRYSTALLISATION OF c-PBT

4.1 Introduction

4.1.1 Background of polymer crystallisation

Crystallisation involves the transformation of a liquid phase into a crystalline phase. Normally, the crystallisation process of a polymer occurs in the temperature range between the glass transition temperature (T_g) and the melting point of the polymer (T_m). In this region the chain segments are sufficiently mobile to rearrange and adopt the required conformation for crystallisation. Below T_g the polymer confirmations are too rigid while above T_m they are too mobile to be placed in a crystalline cell.

However, different polymers have a different ability to crystallise due to chain tacticity, bulkiness and polarity of side groups, and also their microstructure. External factors such as the rate of cooling, nucleating agents and the presence of orientation in the melt also will affect the crystallisation process [125]. Commonly, if the polymer chain is symmetrical and has polar interactions, then crystallisation will occur easily. However, if the polymer chain is branched and has high molar mass, then the crystallisation process will be inhibited. In fact, polymers are never totally crystalline due to chain entanglements, and their long chain nature as well as their high viscosity [125]. In general, there are two processes known to be involved during the crystallisation process, i.e., nucleation, where a new phase is initiated within the parent phase, and the subsequent growth of the new phase [125].

4.1.2 Nucleation

The nucleation process refers to the situation when a polymer is cooled from its melting point there is a tendency for the randomly organised molecules in the melt to become aligned and form small ordered regions, i.e., nuclei. The nucleation process is dynamic and these nuclei will disappear and reform. Wunderlich [125] states that the nucleation process can be divided into two types: homogeneous and heterogeneous nucleation.

The homogeneous nucleation process has a high energy in order to spontaneously create the new surface of a crystal in the interior of a uniform substance. Based on the mode of formation, homogeneous nucleation can be subdivided into primary, secondary and tertiary nucleation. The primary nucleation process describes the process of forming the basic nucleus from which a crystal forms as a polymer is cooled from the melting point. The secondary nucleation process refers to the nucleation that occurs on the face of a pre-existing crystal, while the third nucleation process refers to the nucleation that occurs along an existing crystal edge which involves two crystal faces. Figure 4.1 illustrates schematically the three nucleation steps.

In primary nucleation, a few molecules pack parallel to one another and form an embryo of the crystalline state. Growth of the resulting nucleus occurs by additions of molecule to the crystal face and also chain folding. The crystal surface created in this step has an excess of surface energy proportional to the surface area. However, the free energy decreases during the incorporation of more molecules on the crystal and this is proportional to the crystal volume. The surface-to-volume ratio gives an indication of the free energy change on nucleus formation (ΔG_n).

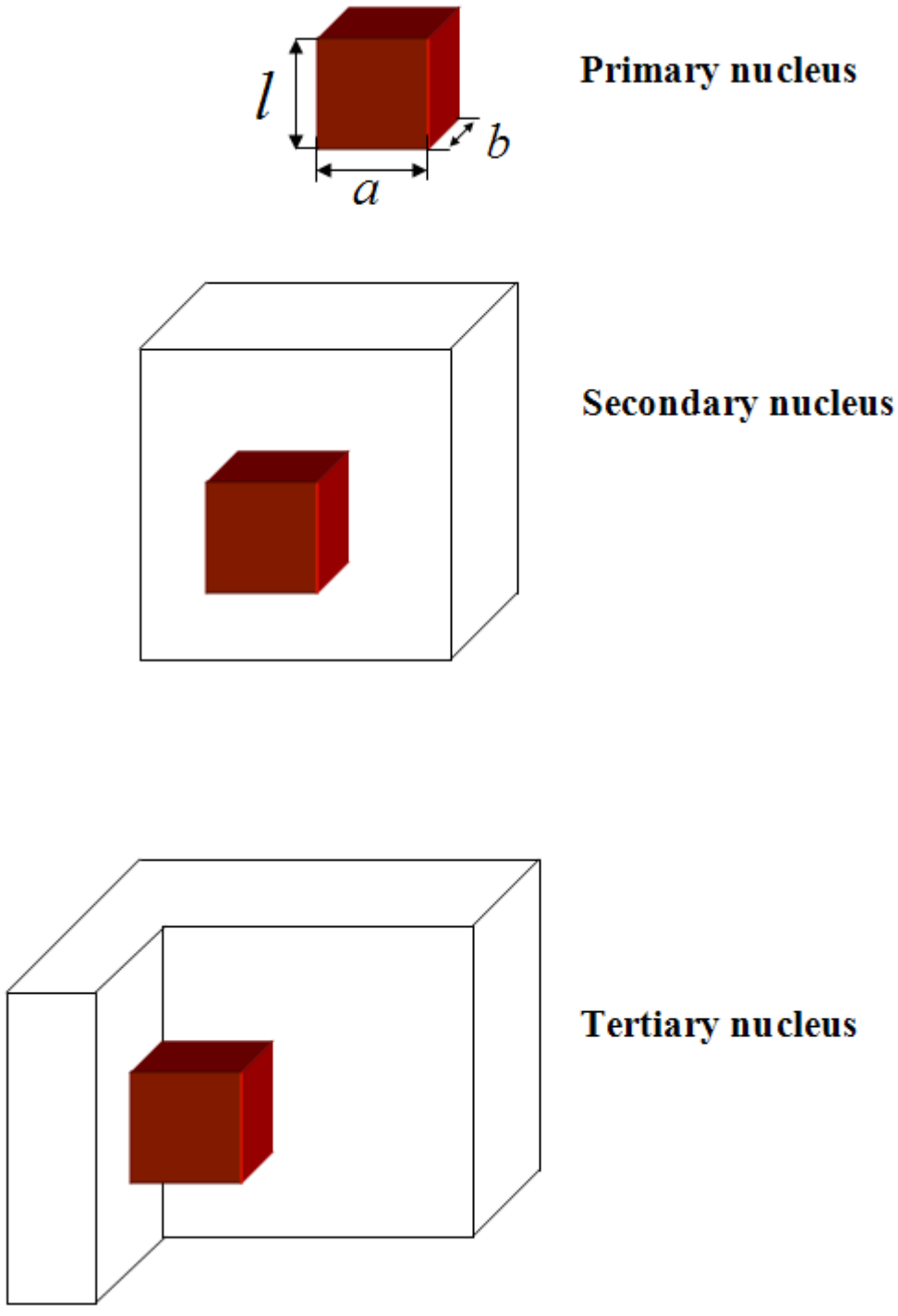

Figure 4.1: Types of crystal nuclei

Figure 4.2 illustrates the variation of free energy with nucleus size for the formation of a stable polymer crystal nucleus. When the nucleus is small the ratio is high and the $\Delta G_n > 0$ (positive) due to excess of surface energy over bulk. Nuclei smaller than the critical size are called subcritical nuclei or embryo. The ΔG_n increases and reaches a maximum corresponding to the critical size of the nucleus. After the critical size, ΔG_n decreases with increasing nucleus size and finally the free energy will be less than that of the melt. Nuclei larger than a critical size are called supercritical as long as ΔG_n is still positive.

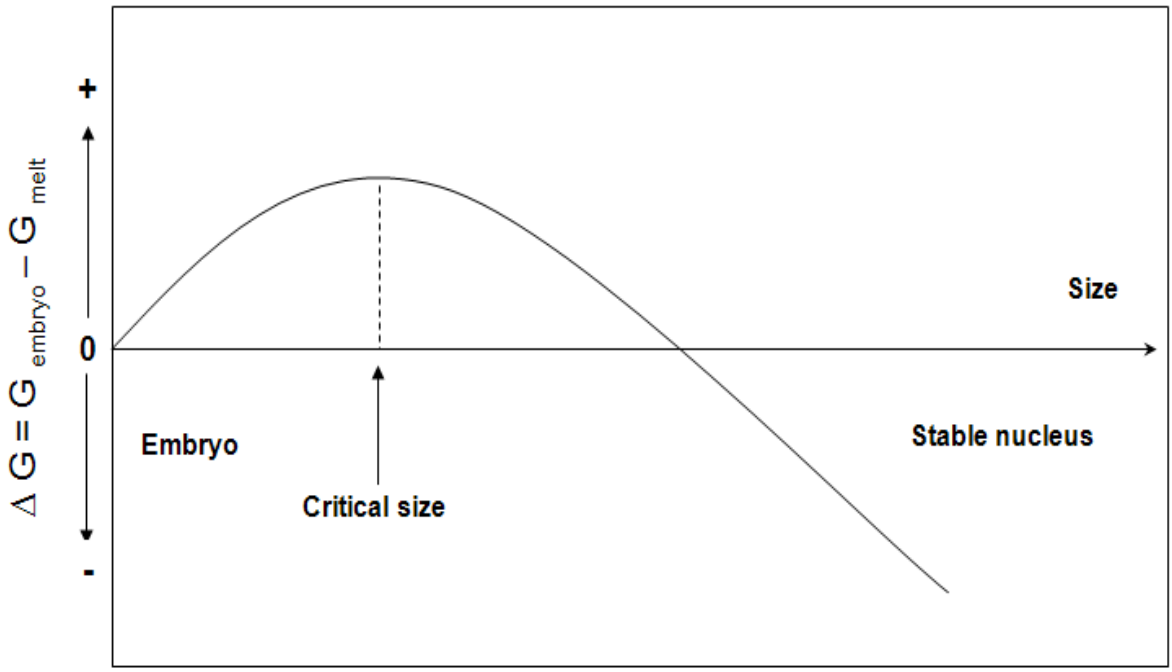

Figure 4.2: The variation of free energy with nucleus size for the formation of a stable polymer crystal nucleus [125]

The overall change in free energy on formation a nucleus (ΔG_n) at constant temperature for primary nucleus with lamellar thickness (l) and width (a) is;

$$\Delta G_n = -a^2 l \Delta G_v + 2a^2 \sigma_e + 4al\sigma \qquad \text{(Equation 4.1)}$$

Where ΔG_v is the bulk free enthalpy change between solid and liquid phase, σ and σ_e are the surface free energy for lateral and folding chain surfaces, respectively [125]. By differentiation with respect to the dimension l and a;

$$\frac{\partial \Delta G_n}{\partial l} = -a^2 \Delta G_v + 4a\sigma \qquad \text{(Equation 4.2)}$$

$$\frac{\partial \Delta G_n}{\partial a} = -2al\Delta G_v + 4a\sigma_e + 4l\sigma \qquad \text{(Equation 4.3)}$$

By setting Equation 4.2 and 4.3 equal to zero, we can obtained the critical nucleus dimensions, l^* and a^*:

$$\left(\frac{\partial \Delta G_n}{\partial l}\right) = \left(\frac{\partial \Delta G_n}{\partial a}\right) = 0 \qquad \text{(Equation 4.4)}$$

The dimensions of the critical nucleus are then;

$$l^* = \frac{4\sigma_e}{\Delta G_v} \qquad \text{(Equation 4.5)}$$

$$a^* = \frac{4\sigma}{\Delta G_v} \qquad \text{(Equation 4.6)}$$

and the critical free energy of formation is;

$$\Delta G_n^* = \frac{32\sigma^2\sigma_e}{\Delta G_v{}^2} \qquad \text{(Equation 4.7)}$$

The bulk free energy change is;

$$\Delta G_v = \Delta H_v - T\Delta S_v \qquad \text{(Equation 4.8)}$$

where ΔH_v and ΔS_v are the enthalpy and entropy of crystallisation. At the equilibrium melting point (T_m^o), the ΔG_v is equal to zero. Therefore,

$$\Delta S_v = \frac{\Delta H_v}{T_m^o} \qquad \text{(Equation 4.9)}$$

If it is assumed that ΔH_v and ΔS_v are temperature independent, then:

$$\Delta G_v = \Delta H_v - T\frac{\Delta H_v}{T_m^o} = \frac{\Delta T}{T_m^o}\Delta H_v \qquad \text{(Equation 4.10)}$$

Hence the free energy of formation of a nucleus of critical size is given by;

$$\Delta G_n^* = \frac{32\sigma^2\sigma_e\left(T_m^o\right)^2}{\left(\Delta H_v \Delta T\right)^2} \qquad \text{(Equation 4.11)}$$

where, ΔT is the degree of supercooling $(\Delta T = T_m^o - T_c)$ and T_c is the crystallisation temperature. From Equation 4.11, it can be observed that the free energy of formation of the critical nucleus is proportional to $(\Delta T)^{-2}$.

After the formation of the primary nucleus, crystal growth can occur by secondary nucleation where a new layer grows on a pre-existing surface. Secondary nucleation occurs with lower free enthalpy barrier since the surface area newly created is smaller. The rate of crystal growth is nucleation-controlled at low supercooling.

Tertiary nucleation determines the rate of covering a nucleated crystal surface with fresh material. It has an even lower surface-to-bulk free energy ratio in comparison with primary and secondary nucleation.

The nucleation process can also occur heterogeneously on a foreign substrate such as bubbles, dust particles and surfaces. Because the free enthalpy barrier to nucleation decreases by nucleation on an existing surface area, heterogeneous nucleation always occurs at lower supercooling than homogeneous [126].

4.1.3 Crystal growth

In the secondary nucleation process, crystals begin to grow on the surfaces once the critical size nucleus is formed [73]. After the initial chain attachment (the chain spreads gradually across the crystal face in secondary nucleation), molecular strands are laid down gradually on a smooth crystal surface. This process is followed by additional chain adhering once more to the interface by a chain folding process where the chains then fold across the surface [99]. Figure 4.3 illustrates a model of the growth of a lamellar crystal through successive laying down of adjacent molecular strands.

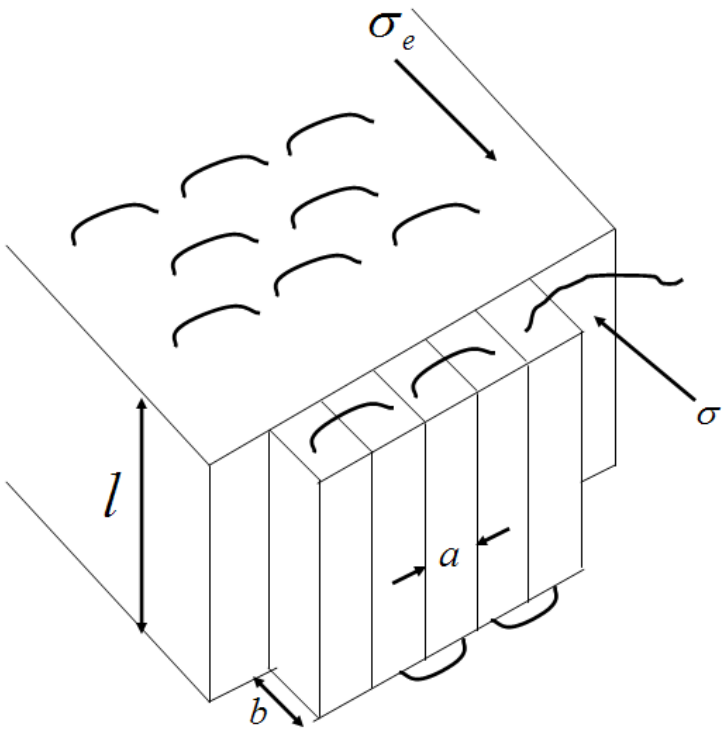

Figure 4.3: Growth model of a lamellar polymer crystal through the successive laying down of adjacent molecular strands

It is assumed that the polymer lamella has a lateral surface energy of σ, a fold surface energy of σ_e, and that the free energy change on crystallisation is ΔG_v per unit volume. By laying down n adjacent molecular strands of length, l with each strand having a cross-section area of $(a \times b)$, the surface energy is:

$$\Delta G_{n(surface)} = 2nab_o\sigma_e + 2b_o l\sigma \qquad \text{(Equation 4.12)}$$

where b_o is the molecular thickness such that the crystal grows one layer after the other. However, there is a reduction in free energy with nucleation incorporation of n molecular strands in crystal:

$$\Delta G_{n(crystal)} = -nab_o l\Delta G_v \qquad \text{(Equation 4.13)}$$

The overall change in free energy when n strands are laid down is;

$$\Delta G_n = -nab_o l\Delta G_v + 2b_o l\sigma + 2nab_o\sigma_e \qquad \text{(Equation 4.14)}$$

From Equation 4.14, it can be observed that for a given n value, ΔG_n is dependent on the length, l where the value of ΔG_n reduces as l increases. A critical length of strand l^* will be achieved and the secondary nucleus will be stable when $\Delta G_n = 0$. The term $2b_o l\sigma$ can be negligible as normally the n value is large. From the combination of Equation 4.10 and Equation 4.14, the critical length of strand l^* is;

$$l^* = \frac{2\sigma_e T_m^o}{\Delta H_v \Delta T} \qquad \text{(Equation 4.15)}$$

The substitution of Equation 4.15 into Equation 4.13 will give the ΔG_n^* for secondary nucleation as;

$$\Delta G_n^* = \frac{4b_o\sigma\sigma_e T_m^o}{\Delta H_v \Delta T} \qquad \text{(Equation 4.16)}$$

It can be seen that the temperature dependence of secondary nucleation is proportional to $(\Delta T)^{-1}$ in comparison with $(\Delta T)^{-2}$ for primary nucleation.

4.1.4 The temperature dependence of growth rate

Turnbull and Fisher [127] proposed that the growth rate of crystals, g, and their dependence on temperature can be represented by the equation below:

$$g = g_o \exp\left(-\frac{\Delta E}{RT}\right)\exp\left(-\frac{\Delta G_n^*}{RT}\right) \qquad \text{(Equation 4.17)}$$

where, g is the steady-state growth rate of a crystal, g_o is a temperature-independent constant (which depends on molecular parameters, and crystal geometry), ΔE is the activation energy for viscous flow, ΔG_n^* represents the free energy of formation of a critical size secondary nucleus and R is the gas constant (8.314 $JK^{-1}mol^{-1}$).

Accordingly, at temperatures near to T_g the first term is dominant and the rate is determined by chain diffusion to the growth front. At higher temperatures close to T_m the second term is dominant and nucleation is the controlling factor. The crystallisation process becomes severely limited by reduced chain mobility when temperatures approach T_g.

The Turnbull-Fisher equation has been rearranged by Hoffman and Lauritzen [125, 128-132] where the spherulitic radial growth rate is expressed as:

$$g = g_o \exp\left(-\frac{U^*}{R(T - T_\infty)}\right)\exp\left(-\frac{K_g}{T\Delta Tf}\right) \qquad \text{(Equation 4.18)}$$

The first exponential term of the equation describes the effect of the temperature dependence of melt viscosity, where, g is the linear growth rate, g_o is a constant, U^* is the activation energy for viscous flow (where Hoffman has assigned a value of 6300 J/mol for this parameter), R is the gas constant, T is the crystallisation temperature and T_∞ is the temperature below which the motions of crystallisable segments to the crystallisation face cease. The T_∞ usually assumed to be 30K below the glass transition temperature ($T_\infty = T_g - 30$).

The second exponential term of this equation (Equation 4.18) describes the effect of primary nucleation on the crystallisation rate at low degrees of supercooling $\left(\Delta T = T_m^o - T\right)$. The parameter f is a correction factor which accounts for the change in the latent heat of fusion that occurs with temperature and can be written as $(\frac{2T}{T + T_m^o})$. T_m^o is the equilibrium melting temperature. The nucleation constant, K_g which appears in this term, is:

$$K_g = \frac{xb_o\sigma\sigma_e T_m^o}{\Delta H_f k} \qquad \text{(Equation 4.19)}$$

This parameter contains the surface free energy product, $\sigma\sigma_e$ (σ is the lateral surface energy and σ_e is the fold surface free energy of the critical size nucleus). ΔH_f is the heat of fusion per unit volume 100% of perfect crystal, b_o is the separation between two adjacent fold planes and k is the Boltzmann constant.

In order to describe crystallisation growth, Hoffman and Lauritzen [128, 133, 134] made several assumptions. The theory assumes that the fold chain length is uniform within the lamellae; there is no imperfect growth at the crystal face and no crystal thickening, and finally that the growth rate is the same on all crystal growth faces. Based on these assumptions, Lauritzen and Hoffman *et al.* [128, 133, 134] proposed three regimes (regime I, regime II and regime III) to define the growth of lamella and the radial growth of spherullites with its dependence on the degree of supercooling. The nucleation constant,

K_g is depends on the nucleation regimes where x=4 for crystallisation in regimes I and III, x=2 for regime II crystallisation.

Regime I occurs at low supercooling and high growth temperatures, where the surface nucleation rate is low. In this regime I, an extended chain is laid down on the growth face of a crystallite. This then followed by an alignment of the segments on to adjacent positions until the surface is completely covered. The crystallite's face grows through the disordered phase because this process occurs repeatedly.

Regime II occurs at lower growth temperature. In this regime, several chain segments are laid down independently on a growth face followed by subsequent addition of chains adjacent to the initial segment. This process (chain addition) will continue until all the growth face is covered.

While, regime III occurs when the degree of supercooling is larger than that in regime II, i.e. where the rate of nucleation is very high and the separation between the nuclei reaches a minimum. Overall, the nucleation constant for all three regimes is:

$$K_{g(III)} = \frac{4b_o\sigma\sigma_e T_m^o}{\Delta H_f k} = K_{g(I)} = 2K_{g(II)} \qquad \text{(Equation 4.20)}$$

Figure 4.4 shows the schematic representation of regime transitions as predicted by the Lauritzen-Hoffman theory [128, 133, 134].

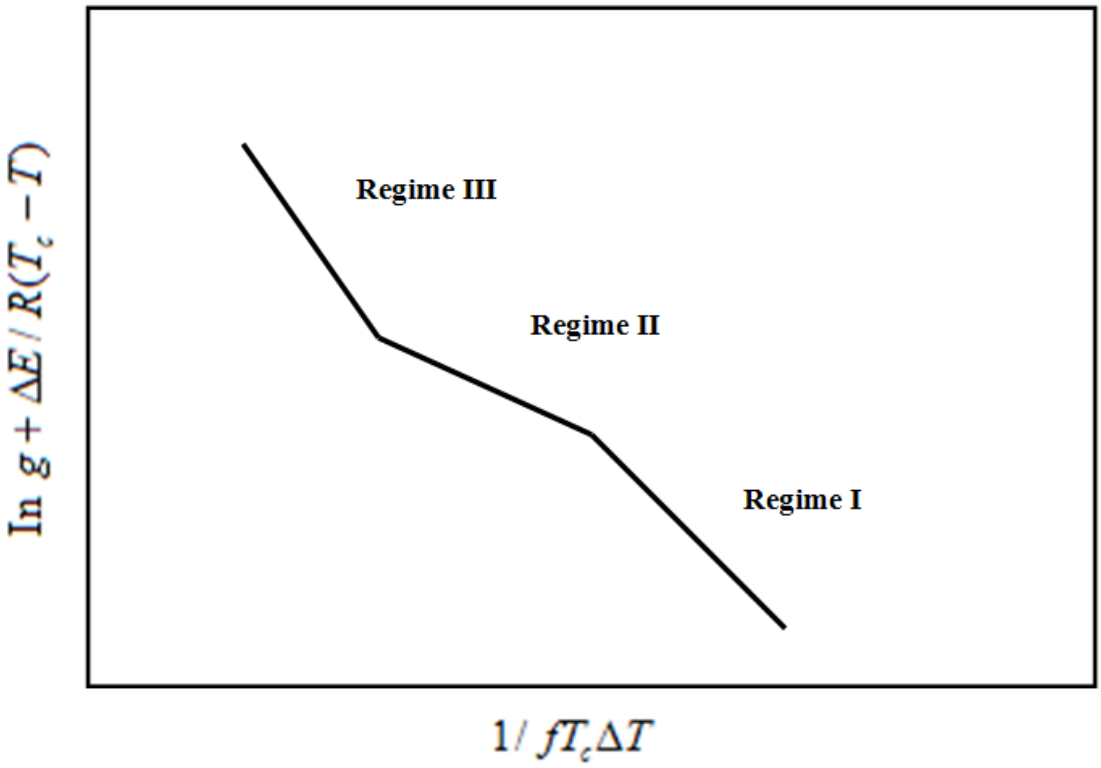

Figure 4.4: Regime transitions based on Lauritzen-Hoffman theory

4.1.5 Crystallisation kinetics by Avrami analysis

The Avrami equation [96-98] is the most widely used to describe the kinetics of crystallisation processes as this approach has been successfully used by many previous researchers [109, 128-131, 134-137] in describing overall kinetics of crystallisation in polymer systems. The deviation of the Avrami equation was simplified by Evans [135] giving;

$$1 - X_t = \exp(-Zt^n) \quad \text{(Equation 4.21)}$$

where, X_t is the fractional crystallinity, which has developed at time, t. Z is a composite rate constant which incorporates nucleation and growth characteristics. The Avrami exponent, n value depends on the crystallisation mechanism and geometry of growth. The corresponding expressions for n and Z value are listed in Table 4.1 [136].

However, the Avrami equation has many limitations. The variations in the crystalline density within the spherulite boundary throughout the crystallisation process give fractional n values and this value assumed to be constant in the Avrami equation. Other assumptions which need to be complied with in the Avrami equation are [124, 140, 141]:

i) random nucleation in a supercooled melt,

ii) the rates of nucleation and growth vary linearly with time,

iii) crystallisation processes occur only by single primary process,

iv) no induction time before starting of crystallisation,

v) when one crystallite impinges upon another growth ceases,

vi) the crystal is still in its original shape in either one, two or three dimension (rods, disc or spheres, respectively) until impingement takes place.

Table 4.1: The physical interpretation of the Avrami parameters for different types of crystallisation mechanism [136]

Crystallisation mechanism		n	Z	**Geometry**
spheres	Sporadic	4.0	$2/3\pi g^3 l$	3 dimensions
	Predetermined	3.0	$4/3\pi g^3 L$	3 dimensions
Discs	Sporadic	3.0	$1/3\pi g^2 ld$	2 dimensions
	Predetermined	2.0	$\pi g^2 Ld$	2 dimensions
Rods	Sporadic	2.0	$1/4\pi glr^2$	1 dimension
	Predetermined	1.0	$1/2\pi gLr^2$	1 dimensions

(g , l are the crystal growth and nucleation rate respectively, while L is density of nuclei; d is constant thickness of discs and r is constant radius of rods)

4.1.6 The equilibrium melting temperatures, T_m^o

The equilibrium melting temperature, T_m^o is defined as the melting temperature of lamellar crystals with an infinite thickness [137]. However, it is not possible to directly measure T_m^o from an experiment. This is because a chain-folded lamellar crystal usually grows with a finite thickness during the crystallisation process. T_m^o is usually determined

from an extrapolation of experimentally observed melting temperatures. It is important to determine T_m^o and establish the degree of super cooling $(\Delta T = T_m^o - T_c)$ in order to understand the temperature dependence of the crystallisation rates.

The Hoffman and Weeks [99] method is the one of the most commonly used procedures to determine equilibrium melting point, T_m^o. They derived a relationship between melting point, T_m, and crystallisation temperature, T_c, which enables T_m^o to be determined, namely;

$$T_m = T_m^o(1-\frac{1}{2\beta}) + \frac{T_c}{2\beta} \qquad \text{(Equation 4.22)}$$

where $\beta = (\sigma_e l / \sigma l_e)$ and σ is the fold surface free energy, l is the lamellae thickness and the subscript e refers to equilibrium conditions. In the absence of re-crystallisation or annealing during melting, β is equal to 1.0 and a plot of T_m against T_c which is linear will give a slope of $1/2\beta$. This line intersects the equilibrium condition of $T_m = T_c$ at T_m^o, but its slope must be 0.5.

4.2 Results and discussion

4.2.1 Equilibrium melting temperature of c-PBT studies

The melting points of the crystals formed by isothermal crystallisation of c-PBT at various temperatures are shown in Figure 4.5. Note that, the melting point was taken as the last trace of crystallinity where Hoffman and Weeks [99] defines the melting point at the temperature of crystals disappearance upon examination by optical miscroscope. These observed melting temperatures, however, are well below this equilibrium value due to the effect of the crystal thickness in depressing the melting point of the lamellae produced at each crystallisation temperature, T_c [99].

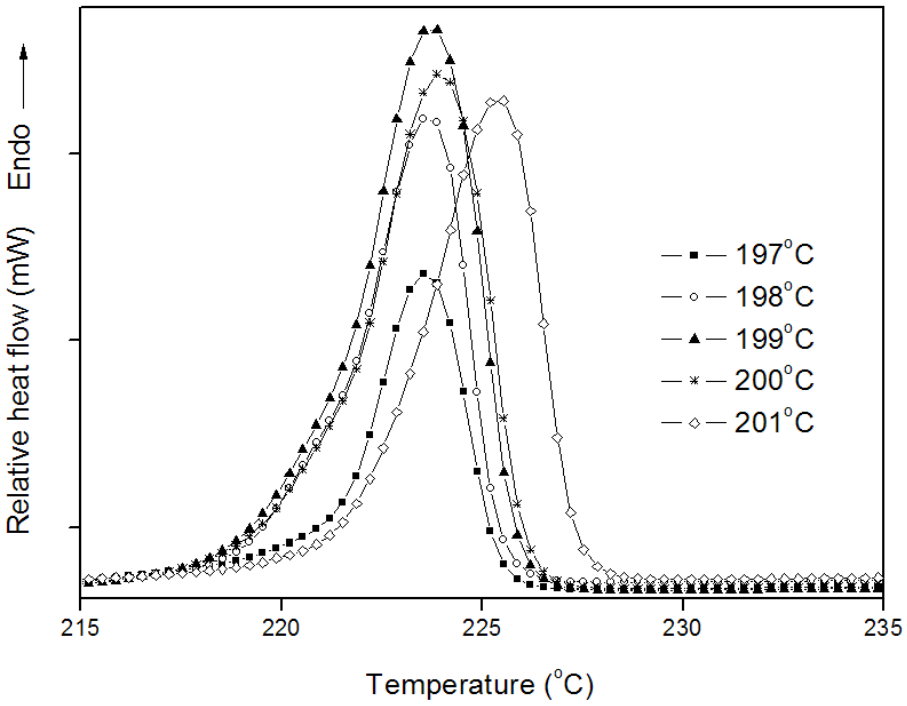

Figure 4.5: Melting peak of c-PBT after held at various crystallisation temperatures 197 °C to 201 °C

Based on the Hoffman and Weeks [99] theory, where the equilibrium melting points (T_m^o) can be determined directly from a plot of T_m against T_c, T_m^o of c-PBT was investigated. The Hoffman and Weeks plot for the c-PBT was shown in Figure 4.6. The linear fit of T_m against T_c gave slope 0.50 ± 0.05 consistent with equilibrium conditions, and on extrapolation to $T_m = T_c$ we observed that the equilibrium melting points (T_m^o) of c-PBT was 529.0 ± 5.0 K. Wu and Jiang [138] in a recent publication (2010), reported that the equilibrium melting points (T_m^o) of c-PBT produced *via* ring opening polymerisation was found to be 257.8 °C (530.8 K). It seems that the T_m^o observed in this study is in agreement with the previous study.

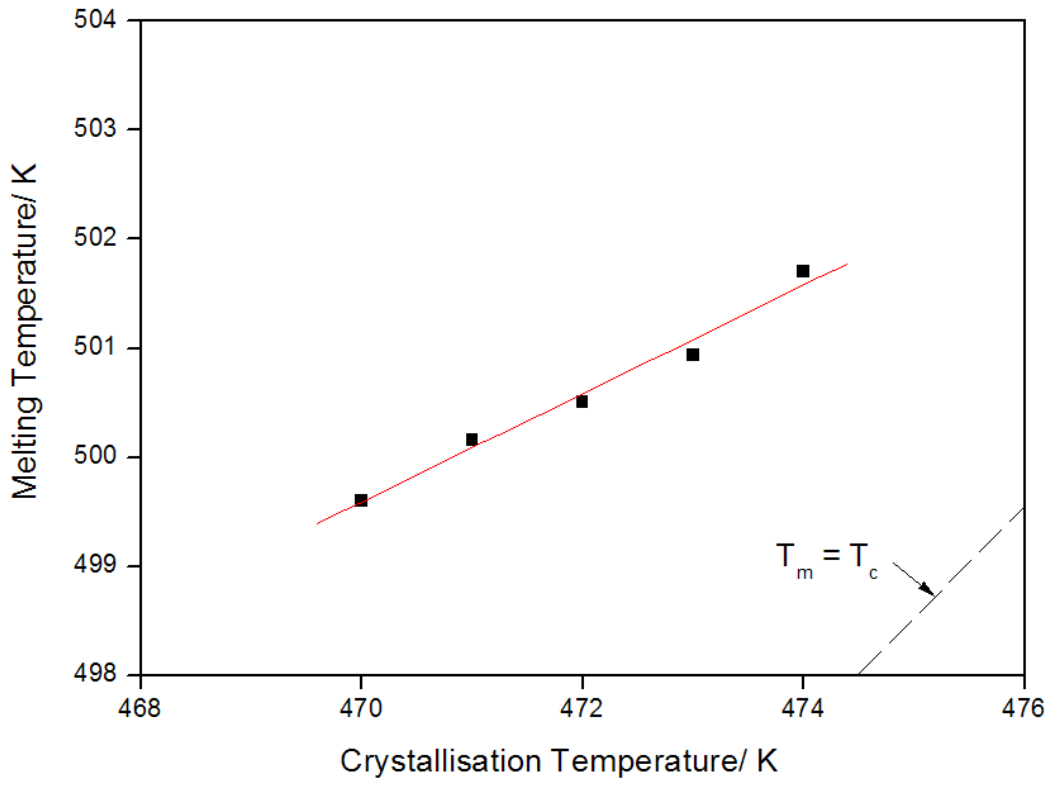

Figure 4.6: A Hoffman-Weeks plot of observed melting temperature against crystallisation temperature for c-PBT

4.2.2 Avrami analysis of c-PBT isothermal crystallisation

Five crystallisation temperatures (T_c) were selected for crystallisation kinetic studies of c-PBT under isothermal experiment conditions ranging from 197 °C to 201 °C. Typical crystallisation curves for c-PBT at different isothermal crystallisation temperatures are measured by rapid cooling to the crystallisation temperature and after correcting for the cooling curve are shown in Figure 4.7. The end of the crystallisation process was taken to be the point where the isothermal curve converged with the horizontal base line [131, 134].

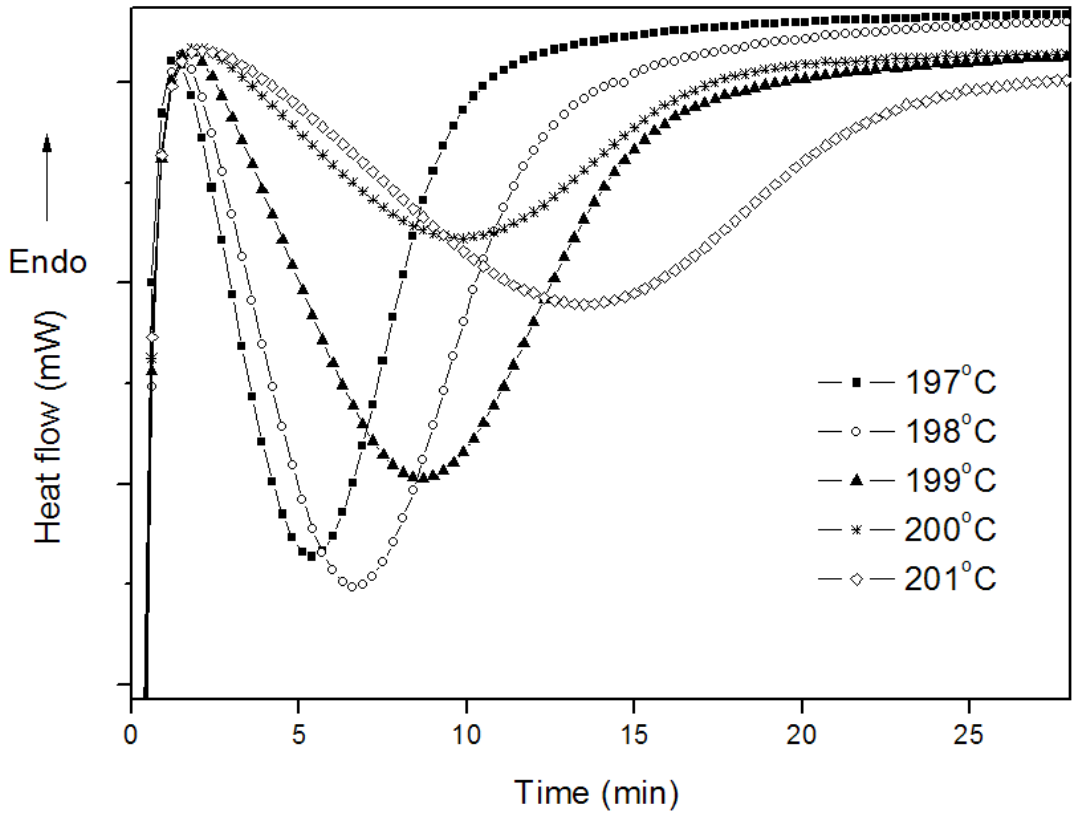

Figure 4.7: DSC exotherms of the isothermal crystallisation of c-PBT at various crystallisation temperatures 197 °C to 201 °C

The early stage of overall crystallisation is normally modelled with the Avrami equation [95-97]. However a number of assumptions are made in the model including the assumption that secondary processes do not occur. Therefore a modified Avrami equation [139, 140] was used to analyze the primary crystallisation process. This modification limited the analysis to the primary process.

The fractional crystallinity, X_t, of the isothermal crystallisation which developed at time t was defined as the ratio of the two areas between the heat flow-time curve and baseline, from t=0 to t=t and from t=0 to t=infinity, i.e [96, 139];

$$\frac{X_t}{X_\infty} = \frac{\int_0^t \left(dH_t / dt \right) dt}{\int_0^\infty \left(dH_t / dt \right) dt} \qquad \text{(Equation 4.23)}$$

The overall development of relative crystallinity with time at selected crystallisation temperature of c-PBT is illustrated in Figure 4.8. From that figure, we can see that all the isotherms show sigmoidal curves and its dependence on the crystallisation temperature selected and time. Jenkins *et al.* [130] found the same trend of the development of relative crystallinity with time for poly(tetramethylene ether glycol) (PTMEG). They believed that the isotherms represent two stages, a primary and secondary process. The primary process consists of the radial growth of the crystallites until impingement and the secondary process involves the growth of subsidiary lamellae or lamella thickening within the crystallites [130].

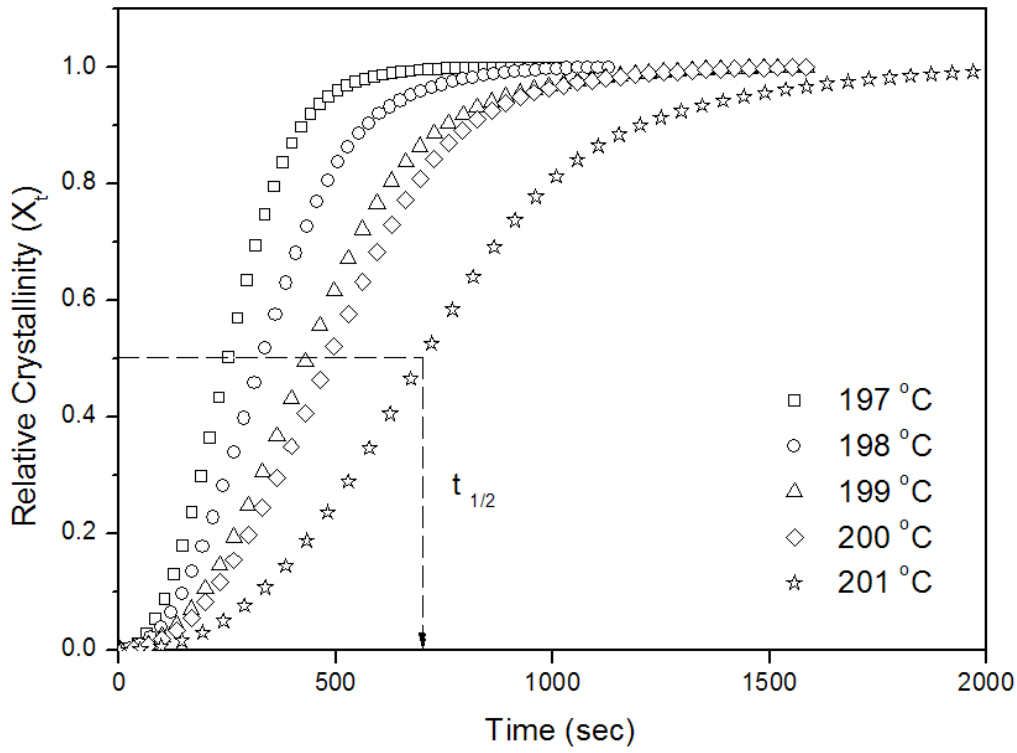

Figure 4.8: Development of crystallinity with time for c-PBT

Rearrange Avrami equation gives;

$$\log\left[-\ln\left(1-\frac{X_t}{X_\infty}\right)\right] = \log Z + n\log t \qquad \text{(Equation 4.24)}$$

An average of the rate constant Z was calculated from the half-life, $t_{1/2}$, and the Avrami exponent n obtained from the slope of the plot of $\log(-In(1-X_t))$ again $\log t$ (Figure 4.9), since;

$$Z = \frac{\ln 2}{(t_{1/2})^n} \qquad \text{(Equation 4.25)}$$

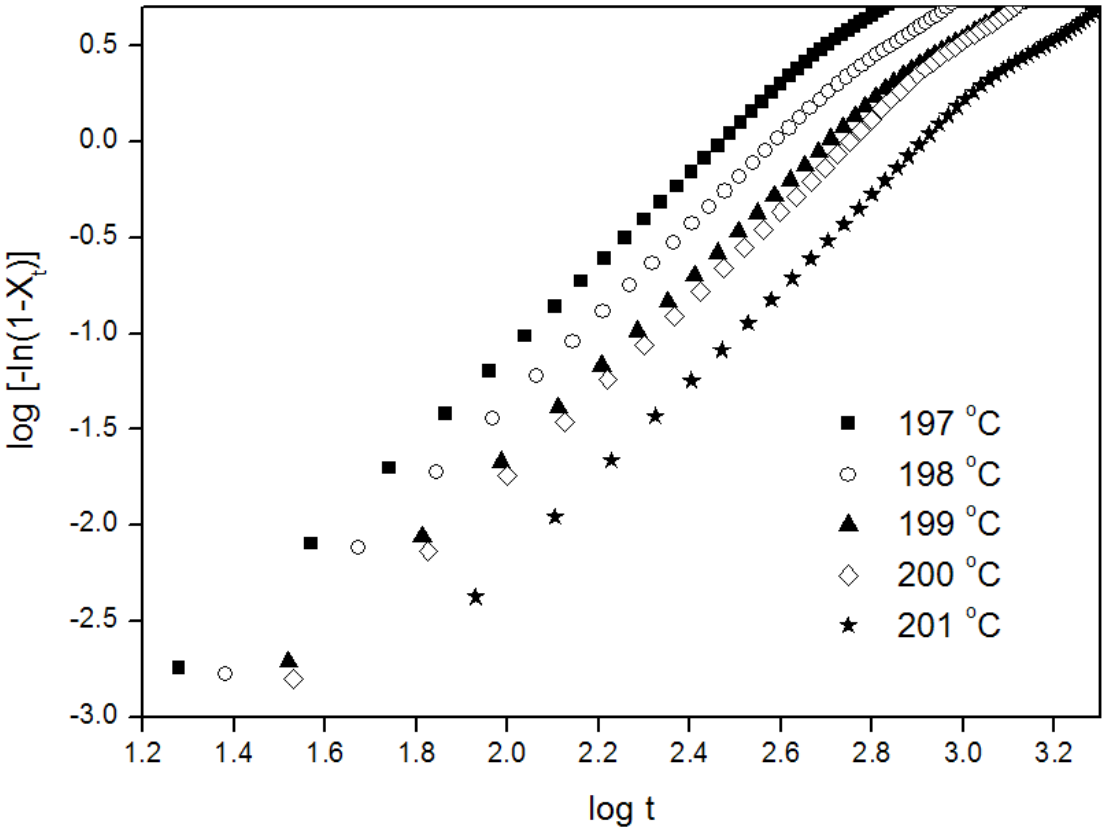

Figure 4.9: An Avrami plot for the isothermal crystallisation of c-PBT

Table 4.2 shows the crystallisation kinetic parameters of c-PBT as modelled by the Avrami equation. In the Avrami equation, if the n value is equal to 4 that means the nucleation mechanism is homogenous while when the n value equal to 3 that shows nucleation mechanism is heterogeneous [141, 142]. The n values of c-PBT was observed in the region of 2.4 to 2.5 (± 0.1) indicating that heterogeneous nucleation of spherulites occurred and growth of spherulites was between two-dimensional and three-dimensional [130, 141, 143]. These results are in agreement with Lehman and Karger-Kocsis [110] work, where they found that for c-PBT the Avrami exponent, n is between 2 and 3. Figure 4.10 illustrates the example of typical variation of instantaneous n value with relative crystallinity for c-PBT at 201 °C.

Table 4.2: The Avrami parameters for c-PBT

Sample ID	Crystallisation Temperature, (^{o}C)	n ± 0.1	Half-life ($t_{1/2}$), min ± 0.1	Z, min^{-n} (x10^{-4}) ± 0.002
c-PBT	197	2.4	2.7	577
	198	2.4	3.7	269
	199	2.4	4.7	155
	200	2.4	6.0	82
	201	2.5	8.4	25

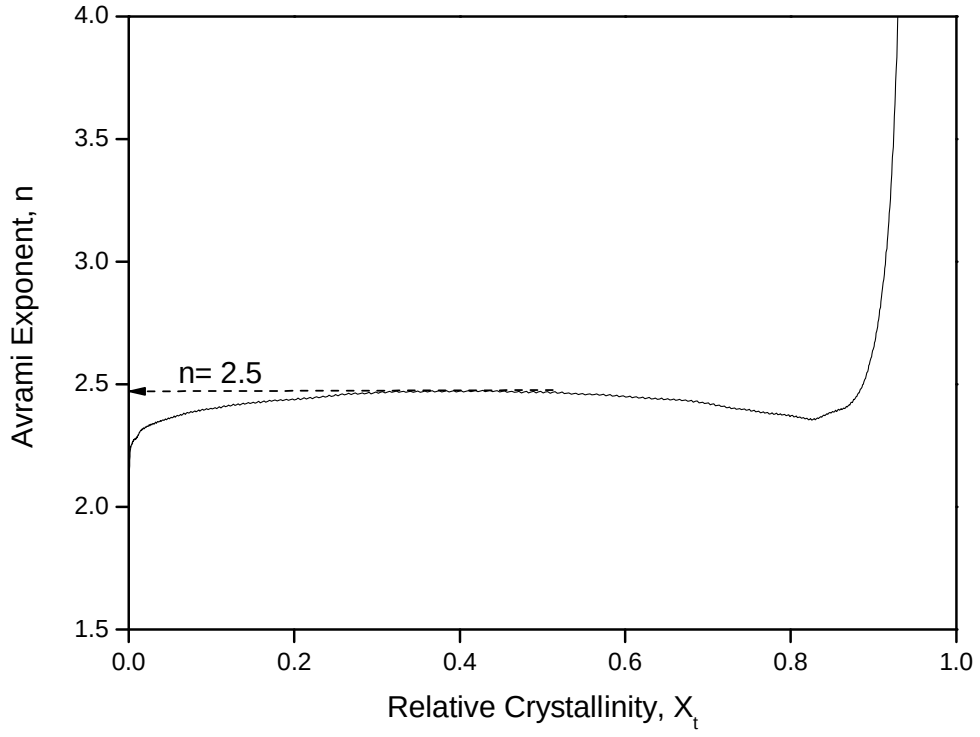

Figure 4.10: Variation of n value for c-PBT primary crystallisation at 201 °C

Since the n value remains essentially constant during the primary crystallisation, the instantaneous change in this value can be used to predict the change in crystallisation mechanism, i.e., primary to secondary [130]. In general, it could be assumed that secondary crystallisation occurs consecutively with primary crystallisation [130], and instantaneous n values can be used to distinguish secondary crystallisation from primary crystallisation since n changes suddenly when the primary process is completed and the secondary process starts.

Taken together, Figure 4.11 and Figure 4.12 depict the variation of half-life $(t_{1/2})$ and rate constant (Z) as a function of degree of supercooling, respectively. The degree of supercooling was used as a function of both $t_{1/2}$ and Z plots in order to compare the data at the same thermodynamic driving force [125, 144].

Both plots are consistent with the general trend of crystallisable polymers where $t_{1/2}$ increases and Z decreases with increasing crystallisation temperature (lower degree of supercooling) as reported in many literature reports [129-132, 145, 146].

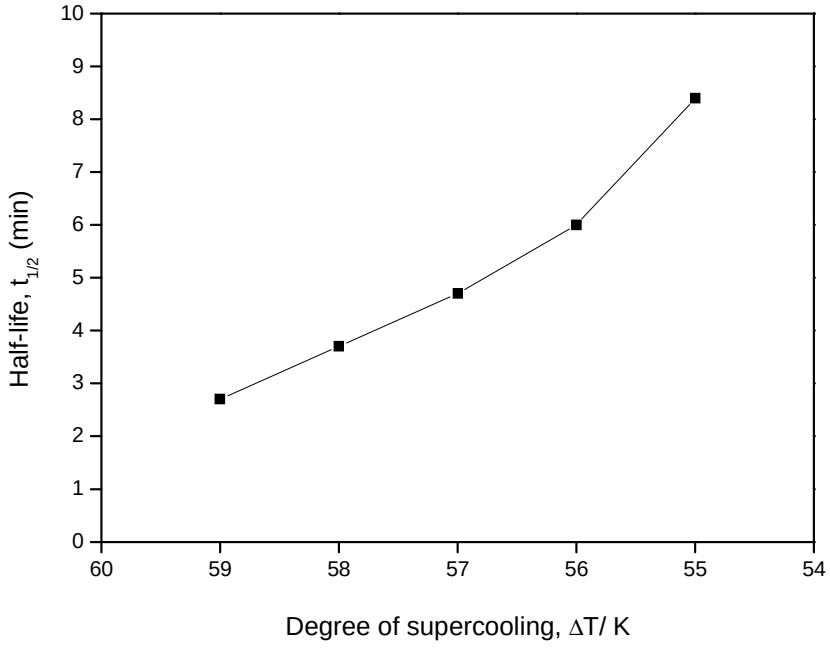

Figure 4.11: Variation of $t_{1/2}$ as a function of degree of supercooling for c-PBT

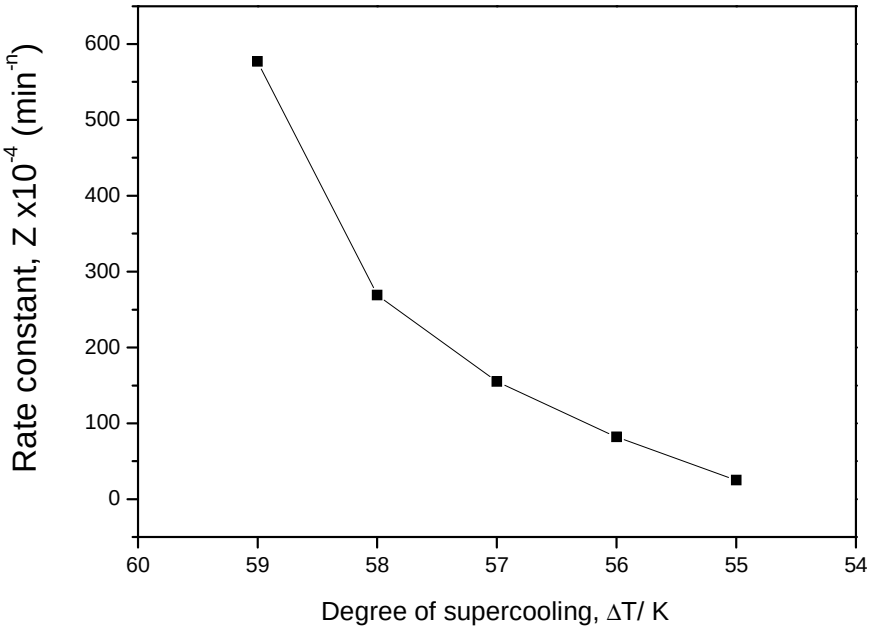

Figure 4.12: Variation of Z as a function of degree of supercooling for c-PBT

4.2.3 Nucleation constant and surface free energy

With the modification of the Hoffman-Lauritzen [125, 128-132] equation (Equation 4.18) where the growth rate has been replaced by the reciprocal of the crystallisation half life, the nucleation constant (K_g) can be determined from the slope of a linear plot of $(In\left(1/t_{1/2}\right)+(U/R(T-T_g+30))$ against $(1/Tf(\Delta T))$ [130]. Figure 4.13 illustrates the Hoffman-Lauritzen plot for c-PBT and it is observed that the K_g value for c-PBT is -5.13 ± 0.02 x 10^5 K^2.

If the K_g values are known, the surface free energy product ($\sigma\sigma_e$) can be calculated from the Equation 4.19;

$$K_g = \frac{nb_o\sigma\sigma_e T_m^o}{\Delta H_f k}$$

where the n value depends on the regime of crystallisation, i.e., $n = 2$ for regime II and $n = 4$ for regime III. As the crystallisation process of c-PBT occurred in regime III, $n = 4$ was applied in Equation 4.19. In order to calculate the $\sigma\sigma_e$, we used 0.580 nm as the b_o value [75]. Based on previous X-ray analysis, it was reported that the c-PBT have the same unit cell as linear PBT [14]. With these values, we found that the surface free energy product ($\sigma\sigma_e$) of c-PBT is 6.44 ± 0.05 x 10^{-4} J^2m^{-4}.

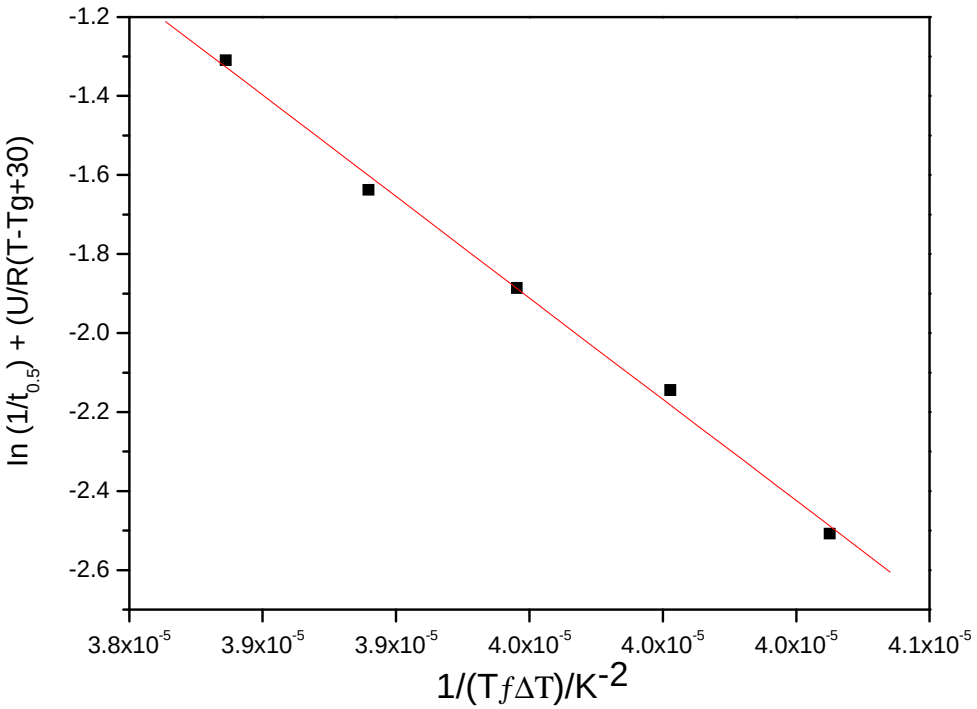

Figure 4.13: A Hoffman-Lauritzen plot for c-PBT

Moreover, Hoffman *et al*. [147] proposed that the value of free energy of the lateral surface (σ) can be estimated using the empirical equation based on Thomas and Staveley relationship [148] as follow :

$$\sigma = \alpha\left(\Delta H^{o}\right)\sqrt{\left(a_o b_o\right)} \qquad \text{(Equation 4.26)}$$

where, a_o is the molecular width (0.496 nm [75]), b_o is the separation between two adjacent fold planes (0.580 nm [75]), ΔH^{o} = 85.75 Jg^{-1} x 1.31 g/cm^3, and α an empirical constant which depends on the chemical structure of the polymers [149]. In general the α parameter varies between 0.1 and 0.3 [150]. It was reported that for high melting polyester

such as PBT, α is usually taken to have the value of 0.25 [137, 143, 150-152]. Taking α=0.25, Equation 4.28 yielded σ = 1.51 ± 0.01 x10^{-2} Jm^{-2}. Thus, the free energy of the chain fold surface (σ_e) can be determined by [150];

$$\sigma_e = \frac{\sigma\sigma_e}{\sigma} \qquad \text{(Equation 4.27)}$$

and σ_e was obtained equal to 4.26 ± 0.01 x10^{-2} Jm^{-2}.

4.3 Conclusions

The equilibrium melting point (T_m^o) and isothermal crystallisation kinetics of PBT which produced from polymerisation of CBT (c-PBT) was investigated. The T_m^o of c-PBT was determined using the Hoffman and Weeks method and it was determined to be at 529.0 ± 1.0 K.

The Avrami crystallisation model has been found to be reliable model for c-PBT crystallisation studies. Crystallisation parameters such as half-life ($t_{1/2}$), rate constant (Z), and Avrami exponent (n) have been found to be sensitive to the T_c values within the range of 197 – 201 °C. The half-life $(t_{1/2})$ was observed to decrease with an increase in the T_c (lower degree of supercooling) while values of rate constant Z decreased in this situation. The mechanistic n values were found to be in the range from 2.4 to 2.5 (± 0.1)

for the primary crystallisation process for c-PBT indicating that heterogeneous nucleation of spherulites occurred and growth of spherulites was between two-dimensional and three-dimensional. The Hoffman-Lauritzen theory was used to determine the nucleation constant (K_g) and surface free energy product ($\sigma\sigma_e$). The K_g and $\sigma\sigma_e$ value for c-PBT was estimated to be -5.13 $\pm$ 0.02 x 10^5 K^2 and 6.44 $\pm$ 0.05 x 10^{-4} J^2m^{-4}, respectively.

This preliminary investigation on isothermal crystallisation of c-PBT will provide useful information for the next step in our studies. The effect blends on the isothermal crystallisation kinetics of c-PBT will be discussed in the following chapter.

Chapter Five

BLENDS OF c-PBT

5.1 Introduction

Different properties in blends can be obtained through changes in morphology which is controlled thermodynamically and kinetically and is composition dependent [153]. This chapter will discuss blends of c-PBT with another polymer, i.e. styrene maleimide (SMI). The blends were prepared by a special route whereby *in situ* polymerisation of CBT takes place inside the blend system. The combination of *in situ* polymerisation with blending is interesting in that it could create novel polymeric materials with properties not attainable through conventional blend processing [91].

5.1.1 Polymer Blends

5.1.1.1 The methods of blending

Preparation of polymer blends can be accomplished by several methods, i.e., mechanical mixing (melt blending), dissolution in co-solvent (solution blending), fine powder mixing (used in this study), use of monomer(s) as solvent for another blend component then polymerisation (e.g. production of IPN or HIPS) and diverse other methods of IPN technology [154]. Mechanical mixing or melt blending predominates for economic reasons. The high viscosity of high molecular-weight polymers in the melt is always a barrier to mixing and miscibility. This can be overcome when strong molecular interactions exist between blend components or when the homopolymers are similar in their chemical structures [155].

Since cyclic oligomers have low molecular weight and melt viscosity (17 centi-poise/ water like) their mixing in blends is more favourable [50]. *In situ* polymerised blends of CBT have been shown to be miscible with PVB where conventionally produced linear PBT blends were not [50]. Unique results, regarding structure, morphology and properties, could possibly be brought about by combining *in situ* polymerisation of cyclic oligomers with blending. The rationale for adoption of the fine powder mixing (solid dispersion) technique is two-fold. Firstly, the blend components exhibit very low viscosity so will disperse easily in the melt. Furthermore, melt extrusion would allow polymerisation to occur during the mixing process which may induce or allow premature phase separation. Conversely, solid dispersion prior to polymerisation allows the phases to be well dispersed prior to polymerisation.

5.1.1.2 Miscibility in polymer blends

Polymer blends can be miscible, immiscible or partially miscible depending on physical and chemical interactions between the chains of the constituent homopolymers [94]. Generally, miscibility of polymer blends is defined in terms of equilibrium thermodynamics, with a range of independent variables (temperature, pressure, molecular weight, chain structure, etc.) under which the free energy of mixing is negative ($\Delta G_m \approx \Delta H_m \leq 0$) [94, 154]. The free energy of mixing expression can be written as [94]:

$$\Delta G_{mix} = \Delta H_{mix} - T\Delta S_{mix} \qquad \text{(Equation 5.1)}$$

where ΔG_{mix}, ΔH_{mix}, and ΔS_{mix} are the Gibb's free energy, the enthalpy and the entropy of mixing at temperature T, respectively. The value of ΔG_{mix} normally depends on the value of ΔH_{mix} since $T\Delta S_{mix}$ is always positive as there is an increase in the entropy of mixing. If ΔG_{mix} gives a negative value, that indicates mixing of polymer pairs will occur simultaneously and lead to miscible blends.

Miscibility also can arise as a result of strong specific interactions between homopolymer chains such as hydrogen bonding, or by way of weaker dispersive interactions [93, 94, 156]. Miscibility or compatibilisation achieved *via* incorporation of hydrogen bonding or ionic groups has long been known by industry [154]. Miscible blends have a homogenous microstructure whereas immiscible blends have a heterogeneous structure with phases of one polymer dispersed in a matrix of another [155]. Both miscible

and immiscible systems can yield synergistic properties as a result of the interactions between the polymer chains and phases in the blends [155, 157].

Furthermore, a relatively rapid way to determined the level of miscibility of polymer blends is by examination of glass transition temperature (T_g) which can be detected using DSC [158]. Miscible polymer blends usually exhibit a single T_g between those of parent polymers. On the other hand, in immiscible blends, each component retains its own individual value; as a result two T_g will appear. In the case of partially-miscible blends, the T_g of the components will shift towards each other where the magnitude depends on the mutual solubility of the phases in each other [154]. Fox [74, 103, 159, 160] suggested that the T_g of miscible blends can be estimated by the equation as follows;

$$\frac{1}{T_g} = \frac{w_a}{T_{g,a}} + \frac{w_b}{T_{g,b}} \qquad \text{(Equation 5.2)}$$

where w_a and w_b represent weight fraction of each polymer and which their glass transition are $T_{g.a}$ and $T_{g.b}$ respectively. However, the Fox's equation seems too simplistic in order to predict the T_g of binary miscible blends system. In the Fox's equation a few assumptions need to be made; mixing occurred in random between the blend components, the change in heat capacity of the blend components between its liquid-like and glassy state are equal i.e., $\Delta C_{p1} = \Delta C_{p2}$, and mixing occurred with no volume expansion between two components [161].

On the other hand, the Gordon-Taylor [162-164] approach could be used to compare with the experiment data where its contain thermodynamic consideration where T_g of the binary blends could be predicted from;

$$T_g = \frac{w_1 T_{g1} + K w_2 T_{g2}}{w_1 + K w_2} \qquad \text{(Equation 5.3)}$$

where, w is the weight fraction of the component, K is an adjustable, fitting parameter which equal to $\Delta C_{p2} / \Delta C_{p1}$, ΔC_p is the change in heat capacity of the blend components between its liquid-like and glassy state. The subscripts 1 and 2 denote the blend components, respectively.

5.1.2 Previous and current work on cyclic oligomers with respect to blending

Although the aim of commercial production of cyclic oligomers is largely for liquid moulding applications, they are also currently receiving some attention in three main areas: polymer blends [50, 58, 66, 91], composites [33, 53-55, 58], and nano-composites [51, 61-63, 165]. Nachlis *et al.* [66] found that the *in situ* polymerisation of bisphenol-A-carbonate cyclic oligomers (BPACY)/styrene-acrylonitrile copolymer (SAN) blends could produce nano-composite structures through liquid-liquid phase separation. There have been few studies looking at combining *in situ* polymerisation of CBT with blending [50, 69, 70]. In all of these studies CBT formed miscible, compatible blends with other

polymers (e.g. PVB). Random and graft copolymers have been suggested to be formed when CBT is *in situ* polymerised to form blends with polycaprolactone and PVB, respectively. Baets *et al*. [58] found the addition of a small amount of polycaprolactone toughened the resulting blend compared with c-PBT. Other work [44] has focused on the crystallisation behaviour of CBT in an attempt to conjecture on *in situ* copolymerisation behaviour.

The interaction of c-PBT with polymers in blends is likely to be complex and differ from that of linear PBT due to the rapid and concurrent polymerisation and crystallisation [13]. It seems likely that the reactive nature of the polymerisation reaction when *in situ* may facilitate and/or accentuate interactions between blend components. Different behaviour of linear and macro-cyclic PBT has been observed in miscible blends with amorphous polymers. In both the miscibility hindered crystallisation in the blends, consistent with other work on other semi-crystalline/amorphous polymer blends [166] and other blends with CBT [50, 58]. In blends of linear PBT with amorphous polyetherimide (PEI), annealing at 200 °C for 10 minutes led to phase separation and crystallisation of linear PBT at all compositions [153]. The crystallinity observed with DSC correlated with a decrease in the obtained infrared wavenumber for the carbonyl groups arising as a result of molecular interactions in the crystalline phase. Tripathy *et al*., (2003) [50] found that annealing CBT/PVB blends at 250 °C for 5 minutes did not promote phase separation and crystallisation at any compositions. It was suggested that the blending process suppressed the crystallinity of PBT due to the formation of a graft copolymer during the reactive ring expansion polymerisation of the CBT. It has been reported that the formation of a graft copolymer suppresses and alters behaviour of PBT crystallinity in blends [167] and that

the degree of grafting affects morphologies [168]. In blends of linear PBT the dispersed phase in immiscible blends can act as a nucleation site for crystallisation [169]. It seems feasible that the reactive nature of the blending of CBT would affect the interface between the phases in immiscible blends.

In this present study, the aim is to investigate the blends behaviour during simultaneous polymerisation and melt blending. To achieve this aim, the other polymers must have melting point (T_m) or glass transition (T_g) below or in the range of polymerisation temperature of the CBT (160 to 200 °C). Blends of CBT with SMI copolymers were prepared by a fine powder mixing (solid dispersion) technique [154]. Then, the *in situ* polymerisation of the CBT in the blend at 190 °C will produce a blend of c-PBT. Another aim is to study the effect of amorphous blend component (i.e. SMI) on crystallisation of c-PBT. Semi-crystalline/amorphous blend systems have achieved much attention in the literature since variations in phase separation and crystallisation behaviour could generate a wide range of morphologies and properties [166, 170, 171].

5.2 Results and discussion

5.2.1 Thermal behaviour of the CBT/SMI and c-PBT/SMI blends

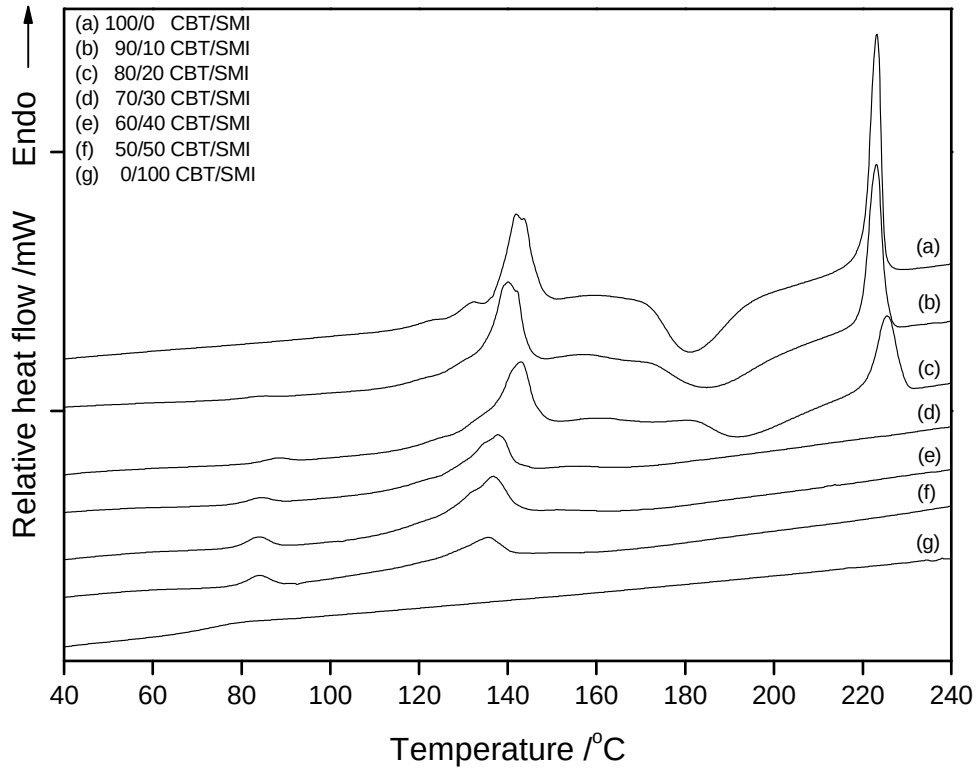

Figure 5.1: Thermal behaviour (heating curve) of various compositions of CBT/SMI blends

Figure 5.1 illustrates the thermal response of CBT, SMI copolymer and its blends in the first DSC dynamic run at 10 °C/min. The thermal response of CBT has already been discussed in Section 3.2.1, while the thermal response of SMI (Figure 5.1 (g)) shows that it only has one thermal transition which is the glass to liquid transition. This transition was observed at 75 °C. SMI can therefore be confirmed as an amorphous polymer. For

CBT/SMI blends, several trends are apparent. Beginning with the T_g of SMI, it is clear that the prominence of the transition increases with increasing SMI content in the blend (as would be expected). A related trend in the melting region of CBT is also apparent, again, this variation with blend composition is due to the effect of a gradually decreasing quantity of CBT in the blend. Examination of the crystallisation region of the CBT component shows that the process is clearly being affected by the addition of the SMI component. The effect is most striking in trace (d) – the 70/30 CBT/SMI blend. At this composition the crystallisation process of c-PBT is being hindered by the presence of the SMI component. Although it should be noted that it cannot be concluded that crystallisation is prevented entirely, only that the crystallisation process cannot occur over the timescale of the DSC experiment in question i.e. the sample is heated over the crystallisation range at 10 °C/min, which is sufficient to prevent crystallisation. The same is true for compositions above 30 wt% SMI. The decrease in the intensity of the melting peak can be explained in terms of a reduction in the quantity of crystalline material in the sample with increasing SMI content. The degree of crystallinity of the blends was shown in Table 5.1 . The degree of crystallinity could only be calculated for compositions up to 20 wt% of SMI because above 30 wt% of SMI no polymer melting peak are found. Given that the variations in the prominence of the SMI T_g and CBT melting peaks have been ascribed to the effect of the compositional variation in the blend, it was deemed important to rule-out these effects in the interpretation of the melting of the melting of the c-PBT component.

Table 5.1: Degree of crystallinity of c-PBT/SMI blends after dynamic heating (10 °C/min) of CBT/SMI blends

Blend Compositions (c-PBT/SMI) (wt %)	100/0	90/0	80/20
Degree of crystallinity (%) (± 1)	57	41	28

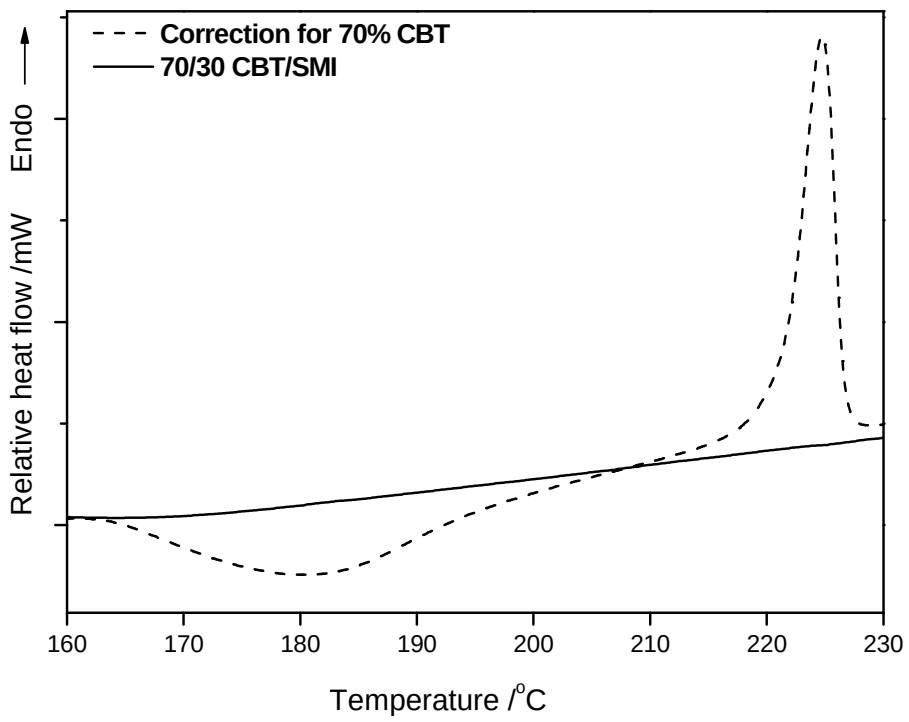

Figure 5.2 : Comparison of first dynamic run between 70/30 CBT/SMI blends and pure CBT

Figure 5.2 shows a comparison of a 20 mg sample of CBT/SMI blend, (identical to the region shown in trace (d)) in Figure 5.1 with a trace obtained from a 14 mg sample of CBT i.e. the actual mass of CBT in both samples was the same and if the crystallisation trend shown in Figure 5.1 was due to a simple variation in mass Figure 5.2 would show a identical melting peak (and some evidence of crystallisation). As this was not the case, it can be concluded that the crystallisation of c-PBT was indeed hindered by the SMI component.

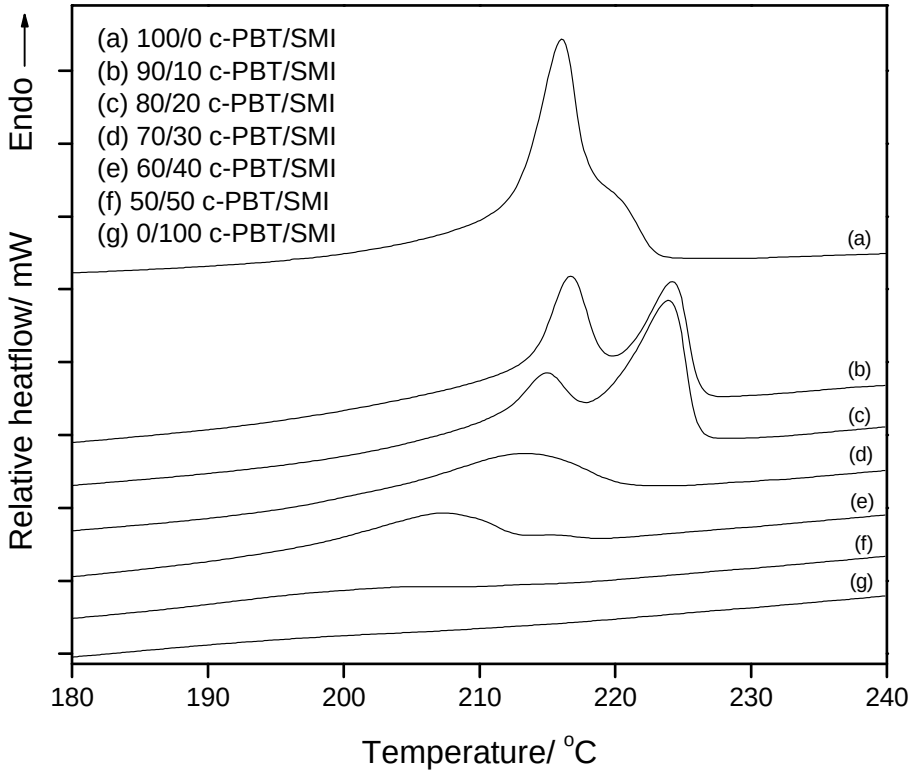

Figure 5.3: Thermal behaviour of re-heating c-PBT/SMI blends

The thermal response of c-PBT/SMI blends produced after the first DSC dynamic run is shown in Figure 5.3. The double melting peak for c-PBT produced after the first dynamic run of CBT was explained in Section 3.2.1. The double melting peak is more obvious with the presence of 10 to 20 wt% SMI in the blend system. The interesting finding is still at trace (d) – the 70/30 CBT/SMI blend, although the crystallisation process cannot occur over the timescale of the DSC experiment, we can still observe the melting transition in the c-PBT melting region which indicates that the polymerisation still occurred although the crystallisation was inhibited. However, the melting transition occurred over a broad region and shifted to lower temperature upon addition of more SMI content.

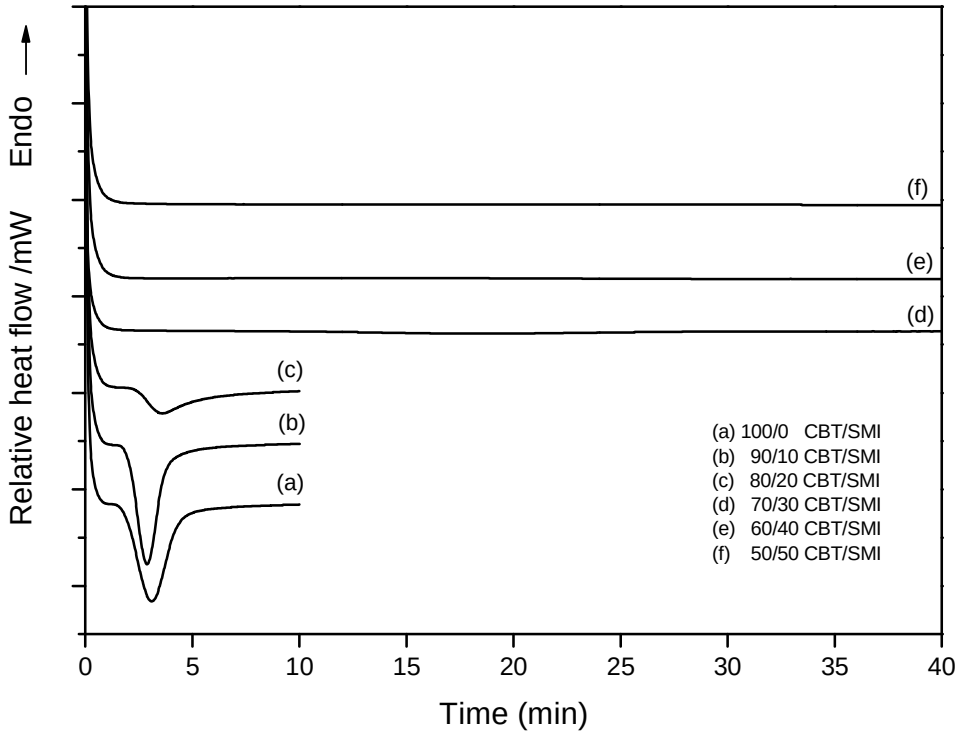

Figure 5.4 : *In situ* polymerisation of CBT/SMI Blends at 190 °C

Supporting evidence for the suppression of crystallisation in c-PBT is also found in the process of *in situ* polymerisation of CBT/SMI blends at 190 °C (Figure 5.4). The crystallisation exotherm cannot be detected above 30 wt% SMI. Again, this suppression only applies in the context of the DSC experiment i.e. at 190 °C; the crystallisation process is either prevented or becomes too slow for the DSC to detect at compositions above 30 wt% SMI. This may be explained in terms of the formation of what is initially a miscible blend. As a result of the development of some degree of miscibility, the crystallisation of c-PBT will require an initial phase separation stage which will hinder the process through an increase in the induction time for the crystallisation. Similar results have been obtained by Tripathy *et al*. [50], where they found that during *in situ* blends of c-PBT with PVB, the crystallinity c-PBT was suppressed by the blending process, which initially created a miscible blend, which in turn affected the crystallisation process.

Figure 5.5 shows the thermal response of c-PBT/SMI blends produced after the CBT/SMI blend was allowed to polymerise at 190 °C for 10 minutes or more. Compared with the results shown in Figure 5.3, the melting transition in Figure 5.5 only produced a single melting peak. It gives the impression that the CBT could still polymerise very well even in the presence of another component (SMI) as long as suitable time is allowed for the in situ polymerisation process. The trend is still the same for more than 30 wt% of SMI in the blend system; the melting transition occurs over a broad region and is shifted to lower temperature. The degree of crystallisation of the c-PBT/SMI blends which polymerised at 190 °C (as shown in Table 5.2) was found to be higher than the results in Table 5.1 .

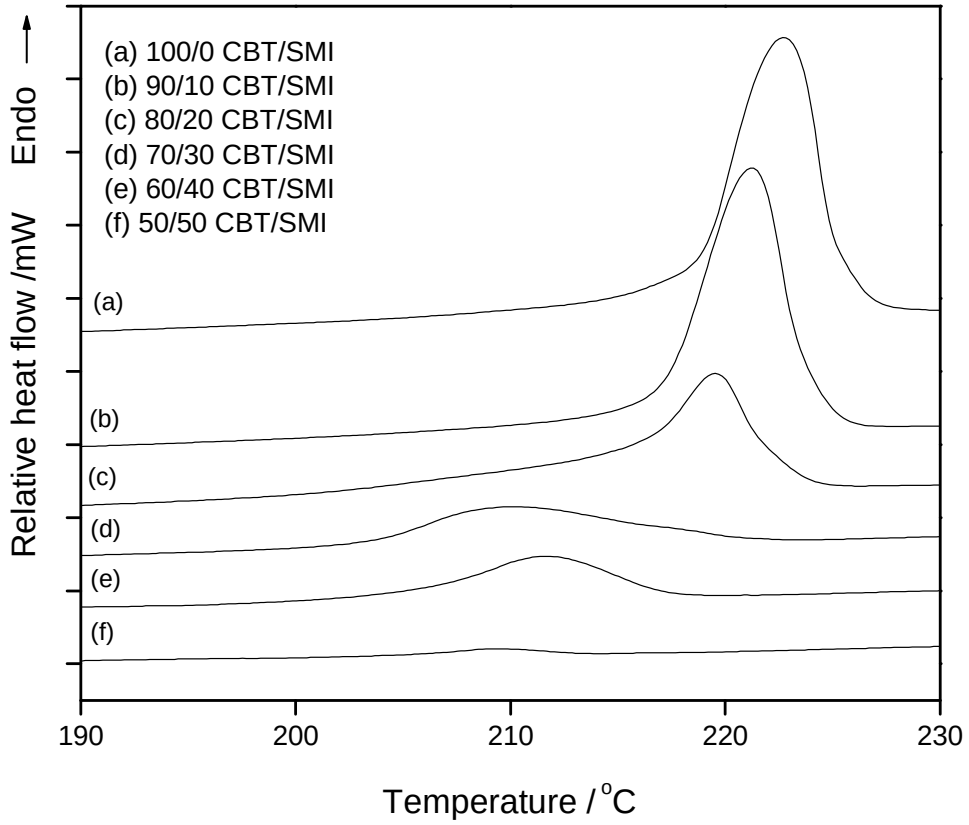

Figure 5.5: Thermal behaviour of various compositions c-PBT/SMI blends after *in situ* polymerisation of CBT/SMI blends at 190 °C

Table 5.2: Degree of crystallinity of c-PBT/SMI after polymerised at 190 °C

Blend Compositions (c-PBT/SMI) (wt %)	Degree of crystallinity (%) (± 1)
100/0	80
90/10	69
80/20	46
70/30	28
60/40	21

5.2.2 Investigation on glass transition temperature (T_g) of the c-PBT blends

Miscibility in a polymer blend can be demonstrated by showing that a single composition dependent T_g is observed in the blend [158]. This was found to be the case in the c-PBT /SMI blend, and some example DSC traces showing the T_g region for the blends are shown in Figure 5.6.

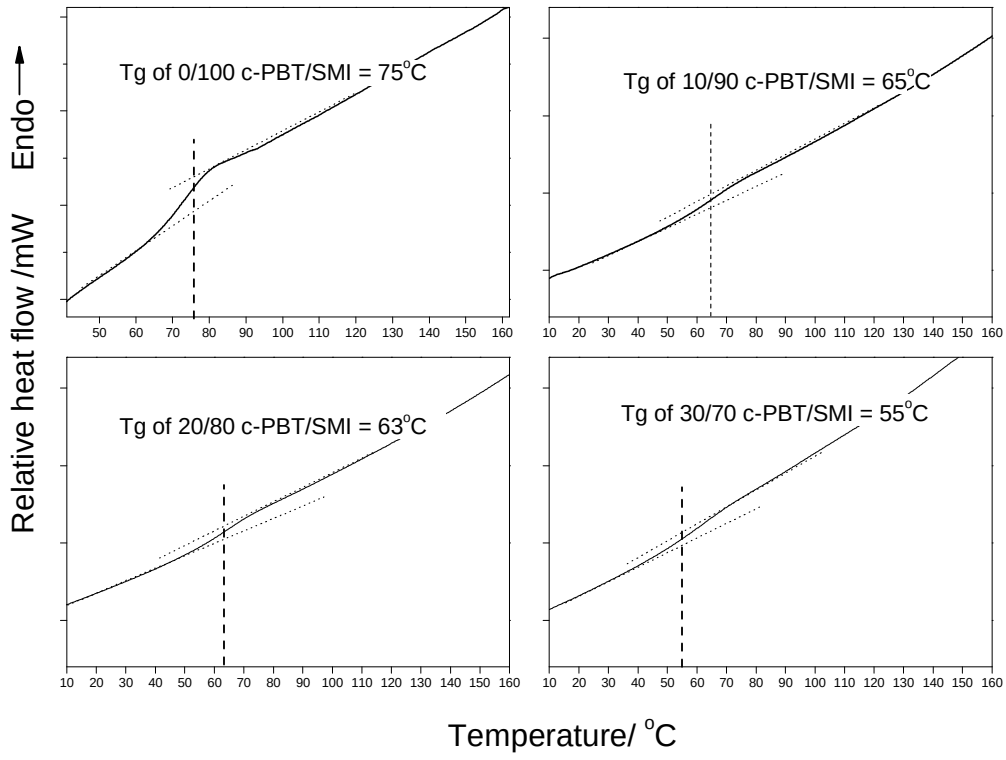

Figure 5.6: Effect of blends composition on SMI T_g

Figure 5.7 illustrates the comparison between the T_g of the c-PBT/SMI blends measured by DSC and the values calculated from the Fox [74, 103, 159, 160] and Gordon-Taylor [162-164]. In order to calculate Gordon-Taylor's equation (Equation 4.3), the ΔC_p value for SMI is 0.159 ± 0.06 $Jg^{-1}K^{-1}$ and c-PBT is 0.099 ± 0.019 $Jg^{-1}K^{-1}$ was used which obtained from DSC experiment.

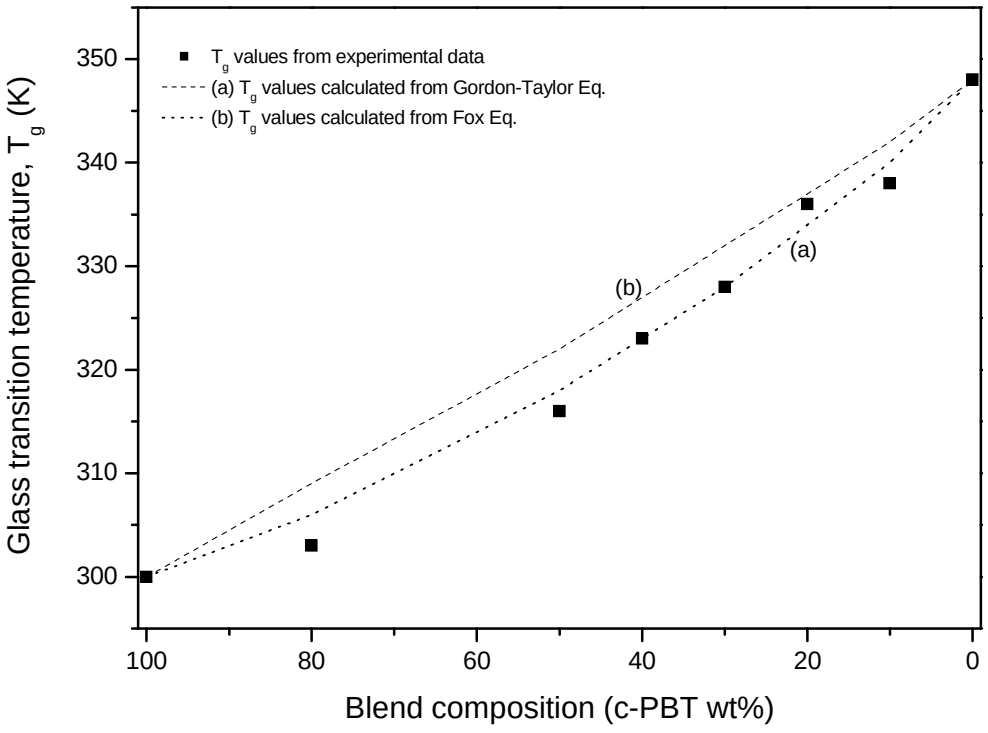

Figure 5.7 : T_g comparison between Fox, Gordon-Taylor and experimental data of c-PBT/SMI Blends

A single, composition-dependent T_g was observed between those of the component polymers. This is further evidence of the development of miscibility in the blend system. In general, each component in immiscible blends retains its own individual properties. Its a consequence they usually exhibit two glass transitions, or melting peaks, in the case of crystalline polymers [120, 154, 158].

5.2.3 FTIR examination on the c-PBT/SMI blends

Figure 5.8 displays the FTIR spectra of CBT and SMI copolymer from a total of 100 scans at a resolution of 2 cm^{-1} by an ATR technique [102]. The peak assignment of CBT was made in Section 3.2.5.1 and the peak assignments of SMI copolymer are listed in Table 5.3 [116, 172-174]. On the other hand, the SMI spectra only show one distinct and very prominent peak corresponding to the carbonyl absorbance (C=O) band from imide [173] centred at 1688 ± 3 cm^{-1} .

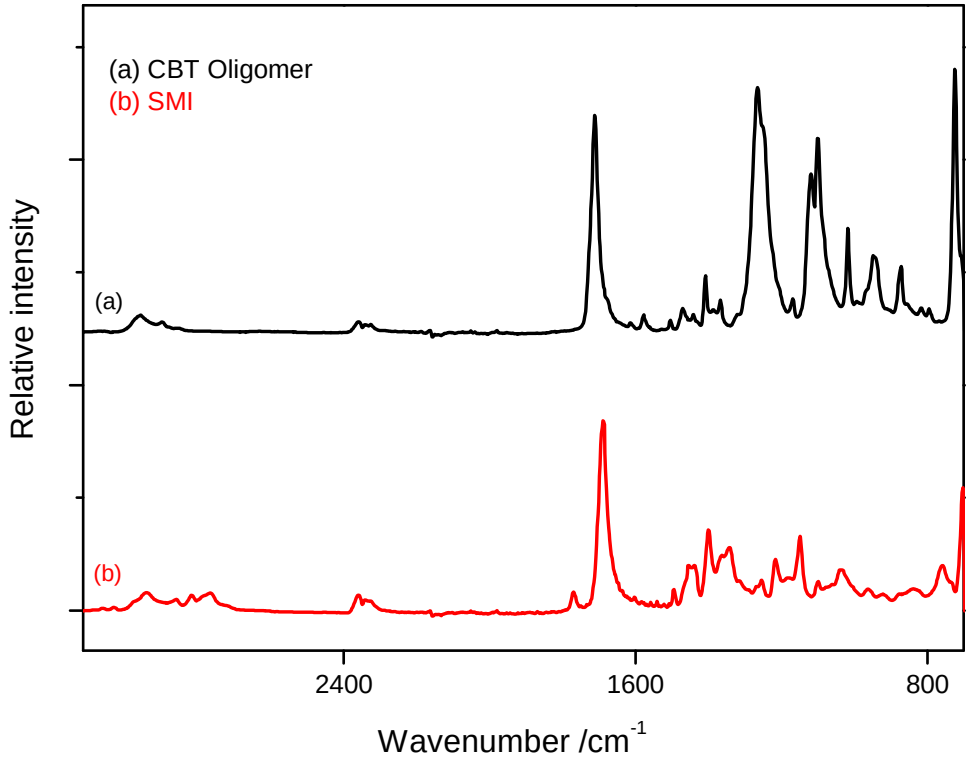

Figure 5.8 : FTIR spectra of CBT and SMI

Table 5.3: Peak assignments for SMI copolymer

Wavenumbers (cm^{-1})	Assignment [116, 172-174]
3600 to 3000	N-H stretching
3000 to 2800	C-H stretching
1750 to 1600	Carbonyl (C=O) stretching
1300 to 1000	Various C-O-, C-C and C-H vibration modes (stretching & bending)
800 to 700	Phenylene bending

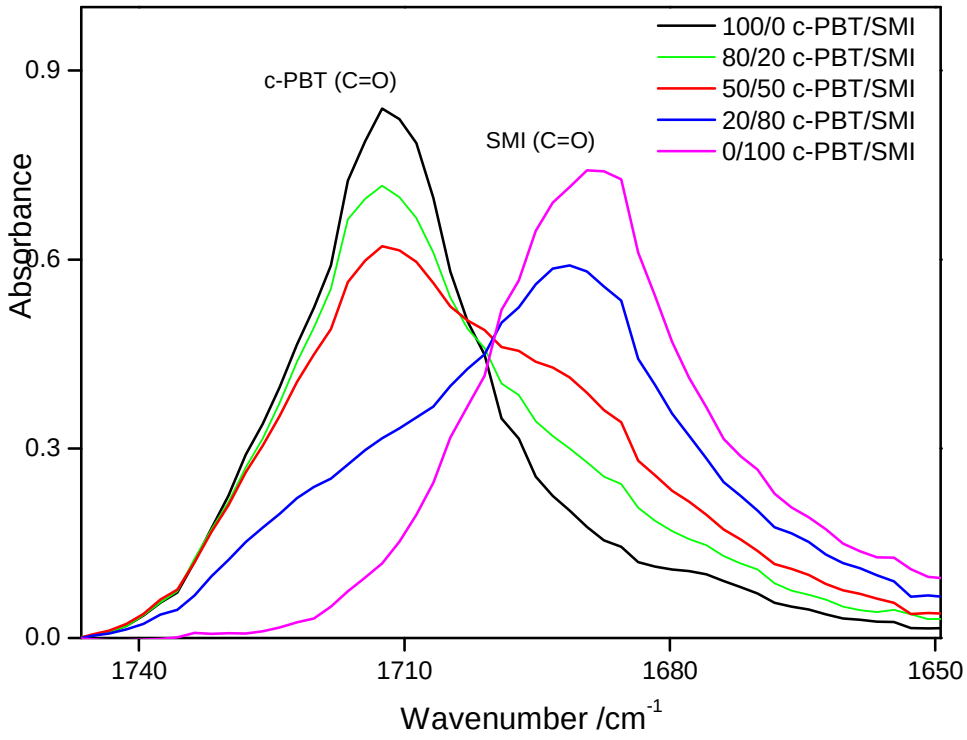

Figure 5.9: Effect of CBT/SMI Blends composition on carbonyl group before *in situ* polymerisation

Since CBT and SMI spectra have prominent peaks corresponding to the carbonyl absorbance (C=O), an investigation were made in this band to study the effect of blend composition and *in situ* polymerisation. Figure 5.9 shows the effect of CBT/SMI blend composition on the carbonyl group before *in situ* polymerisation. Closer inspection of the carbonyl bands of both component polymers shows that the bands appear in different locations, the CBT carbonyl band is centred at 1712 ± 2.5 cm^{-1} and the SMI carbonyl band is centred at 1688 ± 3 cm^{-1}. It can be seen in that figure that for 80/20 and 50/50 CBT/SMI blend composition only the CBT carbonyl band appeared and for 20/80 CBT/SMI only the SMI carbonyl is dominant.

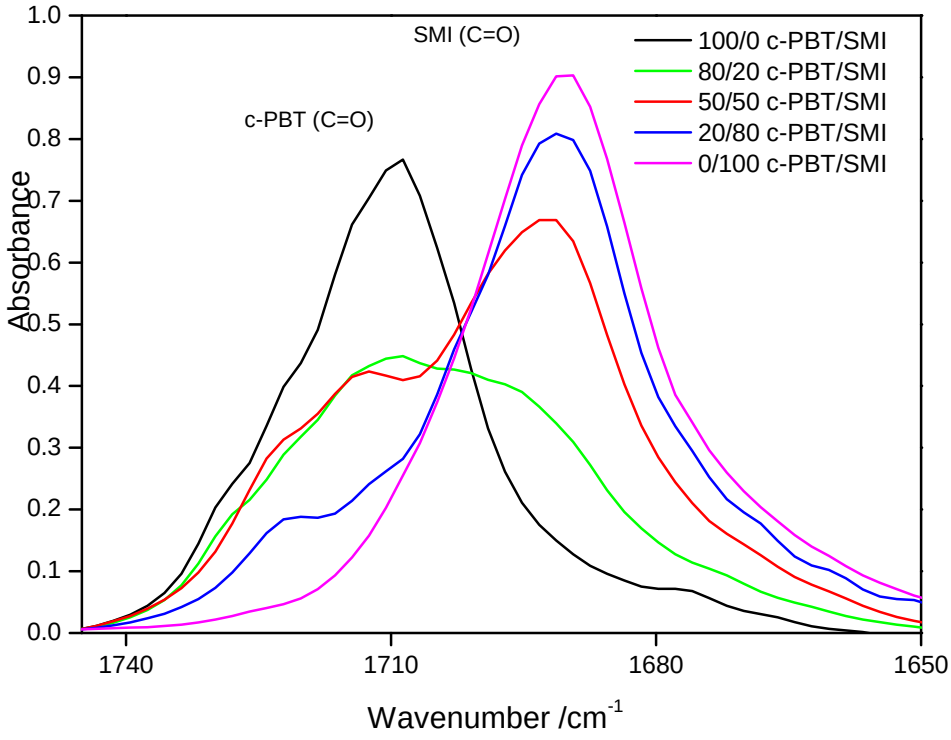

Figure 5.10 : Effect of c-PBT/SMI Blends on carbonyl group

A significant finding was found in the effect on the carbonyl group after *in situ* polymerisation (Figure 5.10). After *in situ* polymerisation the blend spectra consist of both carbonyl bands (c-PBT and SMI). Moreover, a variation in relative intensity of the carbonyl bands with blend composition is apparent (as would be expected in a blend system in which the proportion of each component is altered). There is also a slight variation in peak position of both bands with composition in that there is a shift of both bands to an increased wavenumber. Although the size of the shift is small, it is still significant and can be interpreted in terms of the development of miscibility in the blend system i.e. interaction between the component polymers are likely to involve the carbonyl

bands within both polymers. The interactions change the local environment of these functional groups and hence affect the peak locations.

As the blend composition varied, so did the locations of the carbonyl peaks, as shown in Figure 5.11. Although the variation is most prominent in the SMI (C=O), it can be seen that the peak location of each C=O band shifts towards an increased wavenumber indicating a change in the local environment of the group. This observation can be interpreted in terms of the explanation presented for the suppression of crystallisation and the occurrence of a single T_g, i.e. miscibility.

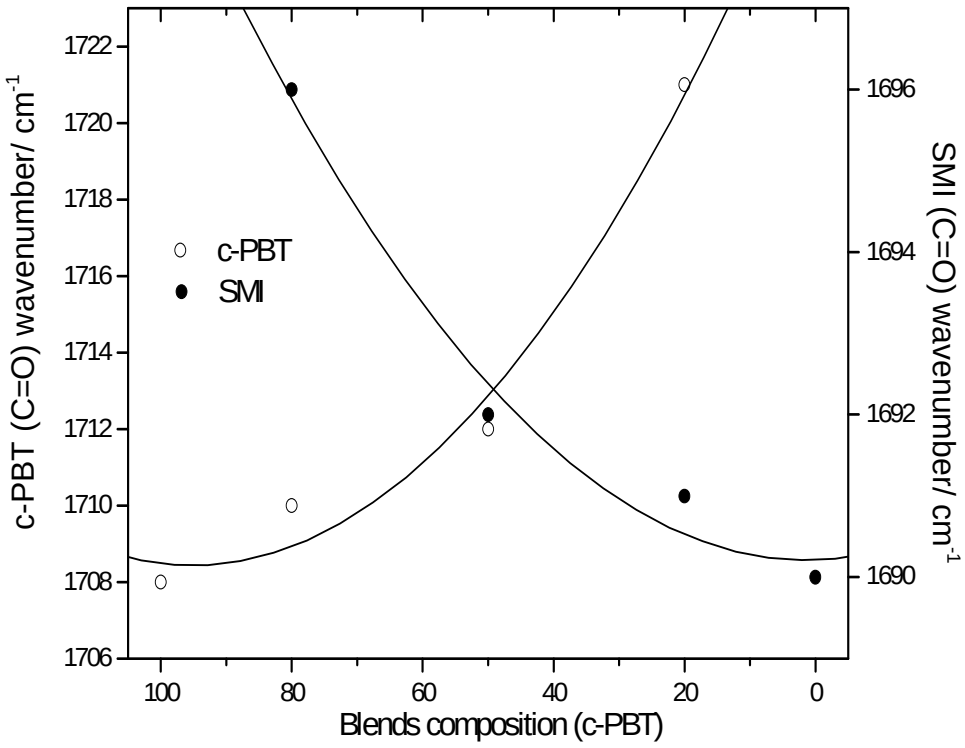

Figure 5.11 : Shift of carbonyl peak by c-PBT/SMI blends composition.

5.2.4 Studies on fracture surfaces of the c-PBT blends

Scanning electron microscopy (SEM) micrographs of the frozen fracture surfaces of c-PBT/SMI blends for the blend composition ranging from 90 to 50 wt% of c-PBT are shown in Figure 5.12. These SEM micrographs showing the effect of c-PBT/SMI blend composition after 30 minutes *in situ* polymerisation. Pure c-PBT shows a ductile fracture surface deformation. Chow [165] obtained a similar type of deformation observed for linear PBT. It could suggest that the production of polyester i.e., PBT via *in situ* polymerisation of its cyclic oligomers still produced ductile material as conventional production of linear PBT.

In this study, we observed that the fracture surface of the c-PBT/SMI blends changed with each 10 wt% SMI content increments. The ductile deformation surface was affected by 10 wt% SMI (90/10 c-PBT/SMI) and completely changed in the presence of 20 wt% SMI and was replaced by appearance of small particles. A closer look (X4000, 5μm) of these small particles showed that actually they had a nodular texture as shown in Figure 5.13. The nodular texture is believed to be crystalline material. The appearance of these possible crystallites reduced with an incremental SMI content and was found to disappear in 50/50 c-PBT/SMI after adequate *in situ* polymerisation time. Phase separation was also not clearly seen at this composition. Furthermore, the homogenous microstructure observed in 50/50 c-PBT/SMI suggesting miscibility.

Moreover, these SEM micrographs are further supporting evidence for the suppression of crystallinity. In summary, suppression of crystallisation in the blends

containing 30 wt% SMI was also observed following examination of the fracture surfaces using SEM which consistent with thermal behaviour (DSC) results.

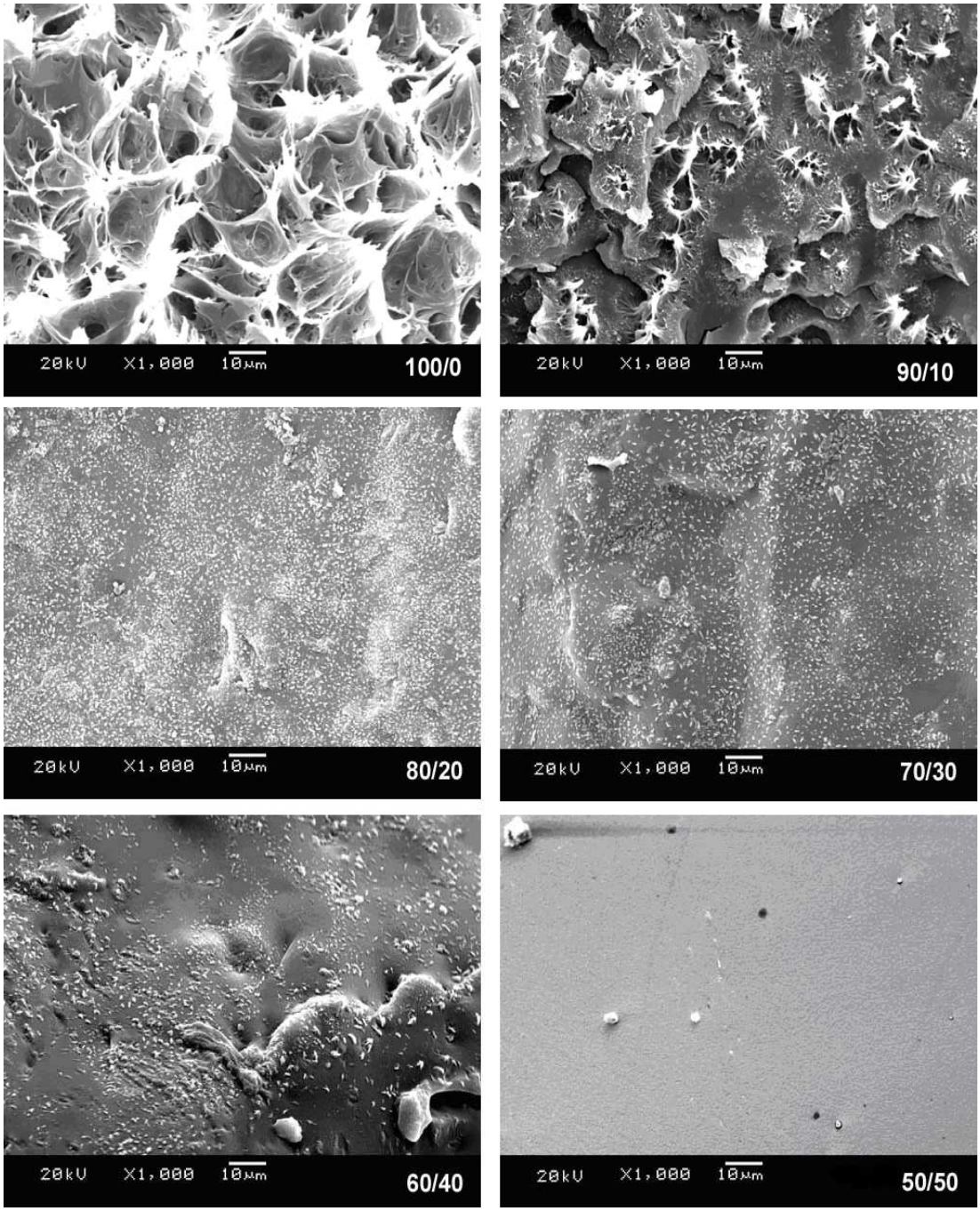

Figure 5.12: Effect of c-PBT/SMI blends composition on fracture surfaces

Investigations to study the effect of *in situ* polymerisation times on the blends fracture surface, are illustrated in Figure 5.13 and Figure 5.14, respectively. The effect of *in situ* polymerisation were studied for various time; 1, 5, 30 minutes. In the case of a c-PBT rich composition (80/20 c-PBT/SMI), we observed that the SEM micrograph showed the presence of small particles which are believed to be crystallites after 1 minute *in situ* polymerisation. These small particles then grow as *in situ* polymerisation times increased to 5 minutes and formed nodular texture which represents the crystalline phase. This nodular texture keep growing as the *in situ* polymerisation reached 30 minutes. The nodular texture observed in the c-PBT/SMI 80/20 blend (Figure 5.13) is indicative of the c-PBT being crystalline rather than immiscibility. This suggestion is in agreement with the thermal behaviour (DSC) results in Figure 5.4.

On the other hand, the SMI rich composition (20/80 c-PBT/SMI) SEM micrograph also shows small particles which appeared after 1 minute of *in situ* polymerisation but do not grow as in the c-PBT rich composition case. It can be seen (Figure 5.14) that the small particles decreased and are missing after the 5 minutes *in situ* polymerisation allowed for SMI rich composition. The 30 minutes *in situ* polymerisation (which is believed complete) of the SMI rich composition resulted in a homogeneous microstructure. This morphology obtained from the *in situ* polymerisation is suggested to produce a miscible c-PBT/SMI blends system above than 30 wt % of SMI.

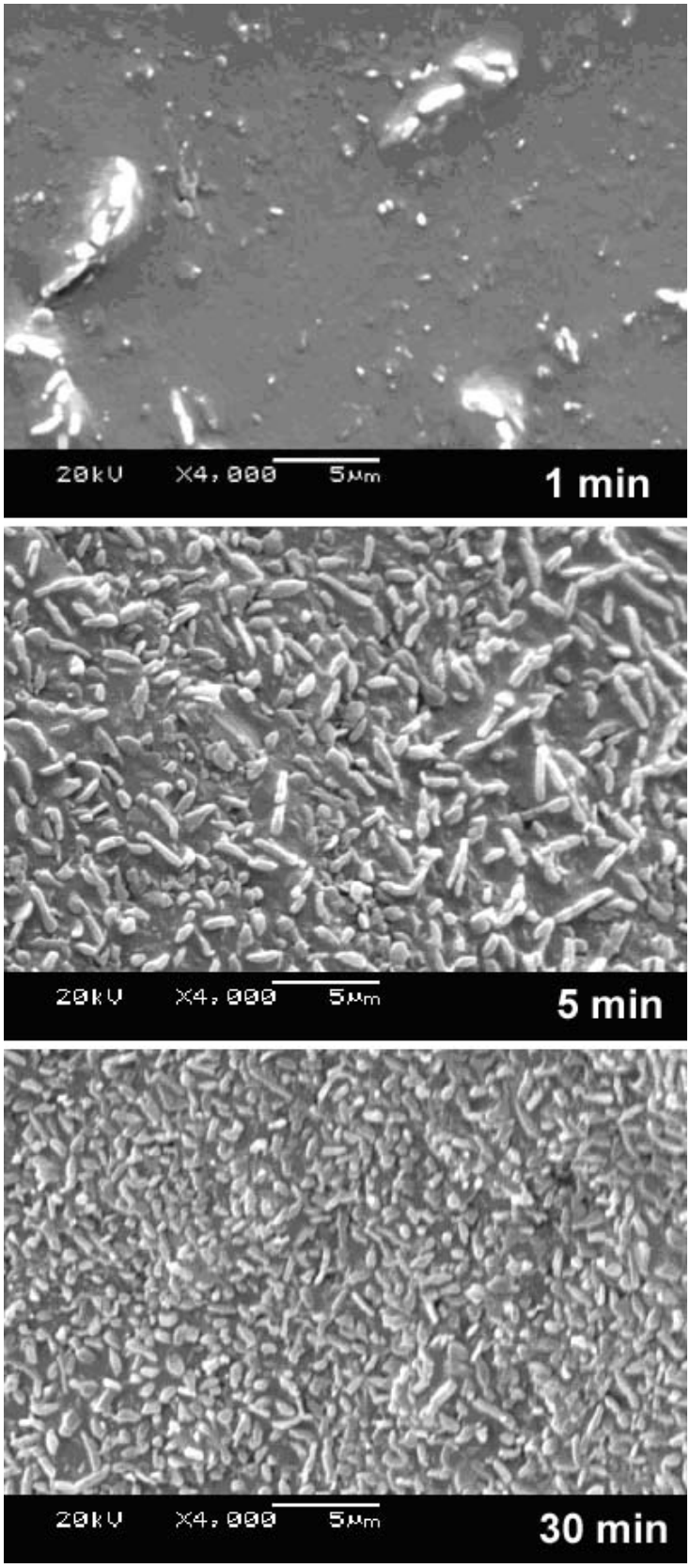

Figure 5.13: Effect of polymerisation time on fracture surface of c-PBT rich blend (80/20 c-PBT/SMI)

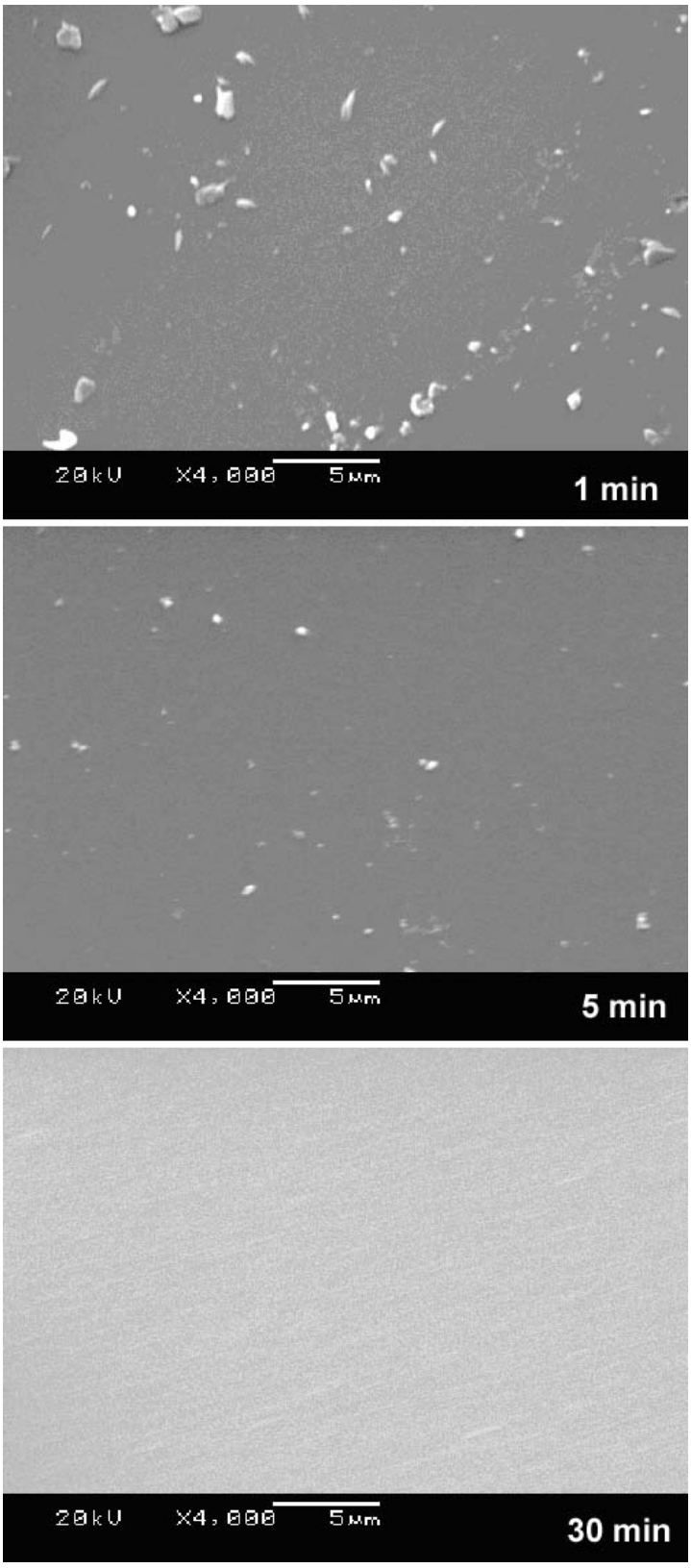

Figure 5.14: Effect of polymerisation time on fracture surface of SMI rich blend (20/80 c-PBT/SMI)

5.2.5 Comparison with the immiscible blends system (c-PBT/PS)

The c-PBT/SMI blends which were prepared *via* the solid dispersion technique and simultaneous *in situ* polymerisation show some evidence of miscibility. As a comparison, we investigated the behaviour and morphology of a blend system which is known to produce immiscible blends with linear PBT. PS was the choice as it has a low T_g (90 to 110 °C) below the range of polymerisation temperature of CBT (160 to 200 °C). PBT/PS blends systems are known to be immiscible blends [175-179]. Note that the c-PBT/PS blends were prepared using the same procedure as that used to prepare c-PBT/SMI blends.

5.2.5.1 Thermal behaviour

Figure 5.15 represents the thermal response of CBT/PS blend during dynamic (10 °C/min) heating. It was expected that the immiscible blends would not interfere with the crystallisation process during production of c-PBT. The crystallisation process still appeared in the case of PS dominant blends (40/60 c-PBT/PS). Signs of crystallisation were not obvious in 20/80 c-PBT/PS as the quantity of CBT in the system decreased. These results be illustrate the difference between thermal behaviour miscible (c-PBT/SMI) and immiscible blends (c-PBT/PS).

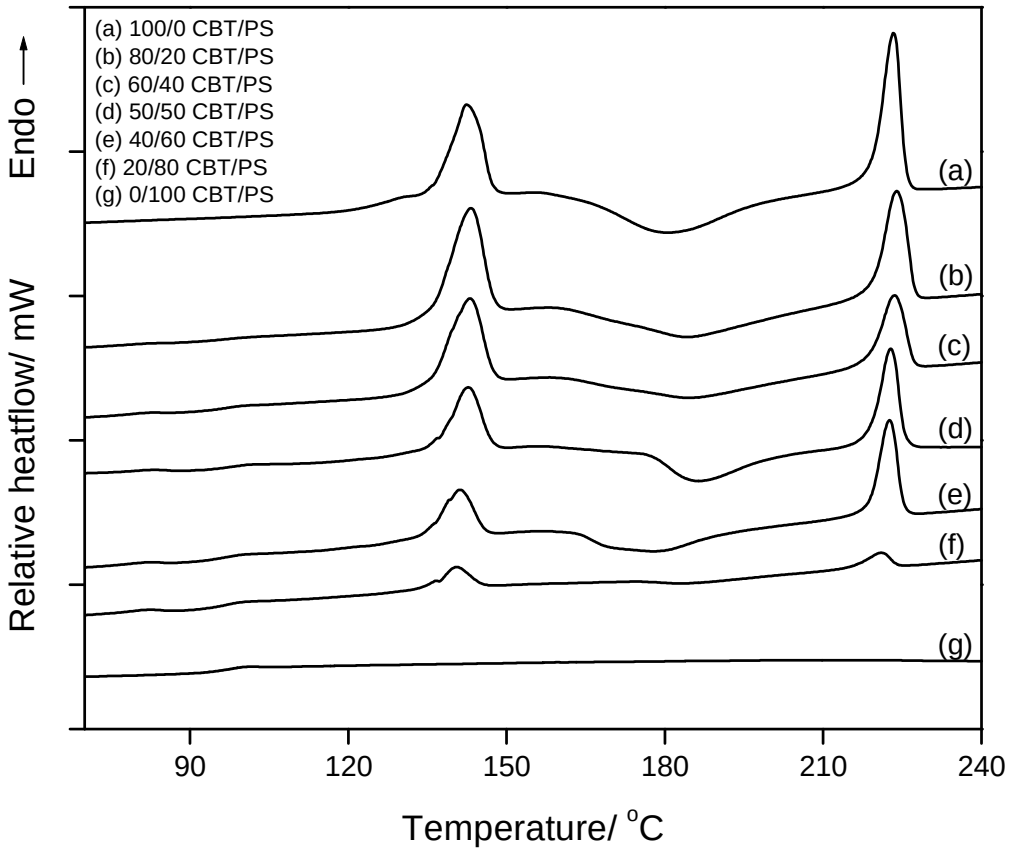

Figure 5.15: Thermal behaviour of various compositions CBT/PS blends

It also clearly seen that the c-PBT/PS heating trace consist of two transitions which belong to glass transition temperature (T_g) of PS above 90 °C and melting point of c-PBT at 225 °C as shown in Figure 5.16. The higher PS content was also found to have ruined the spherulite perfection of c-PBT during fast *in situ* polymerization (trace e.)

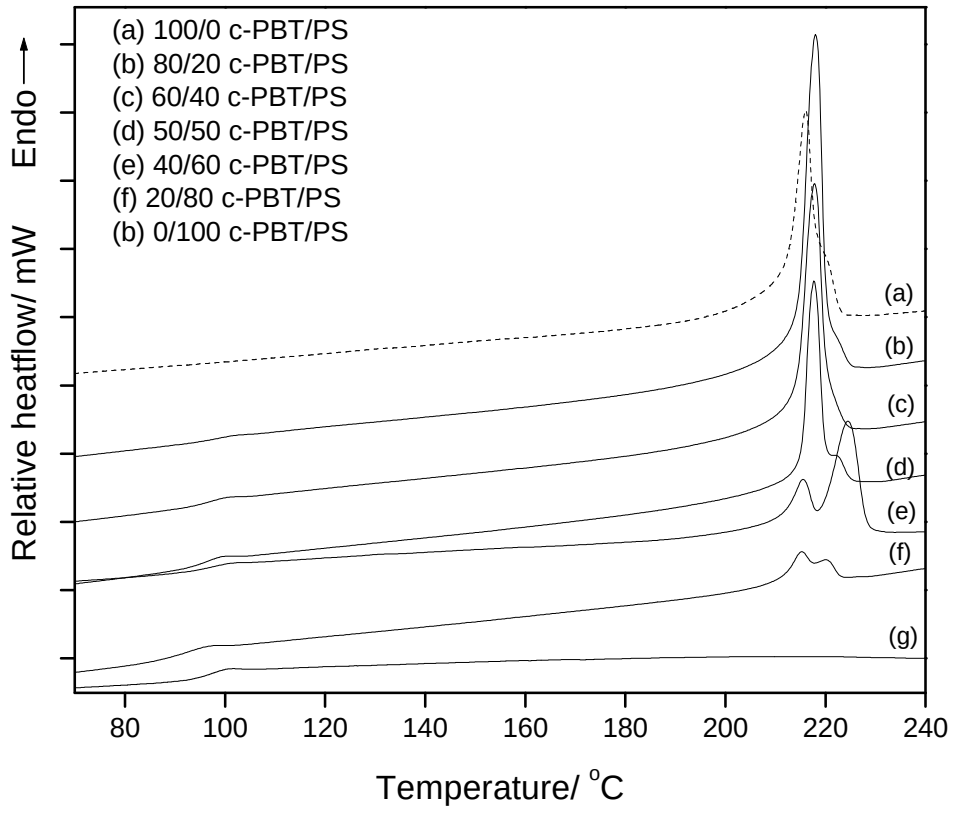

Figure 5.16: Thermal behaviour of re-heating various compositions c-PBT/PS blends

Investigations of the *in situ* polymerisation of CBT/PS blends also reveal that the crystallisation process was not affected by the presence of PS (Figure 5.17). These results are totally different from those for miscible blends (Figure 5.4). The immiscible blends will behave according to their single components [120, 158].

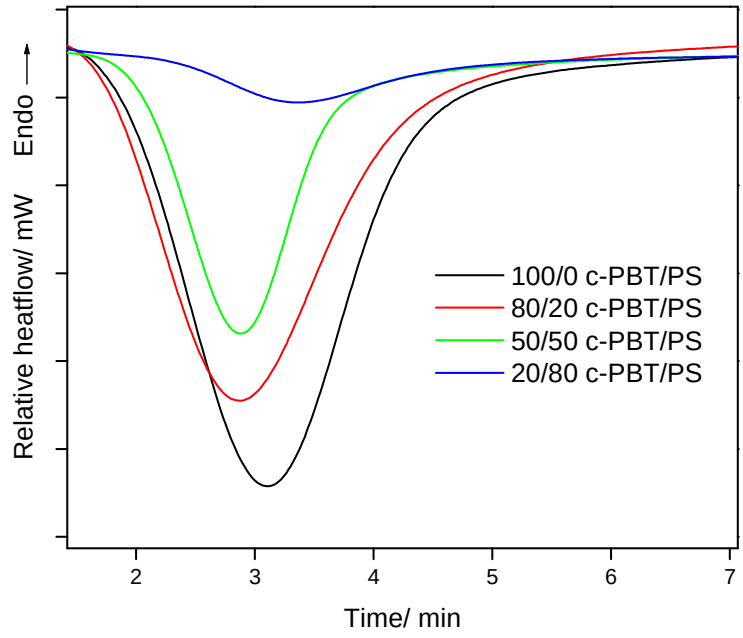

Figure 5.17: *In situ* polymerisation of CBT/PS Blends at 190 °C

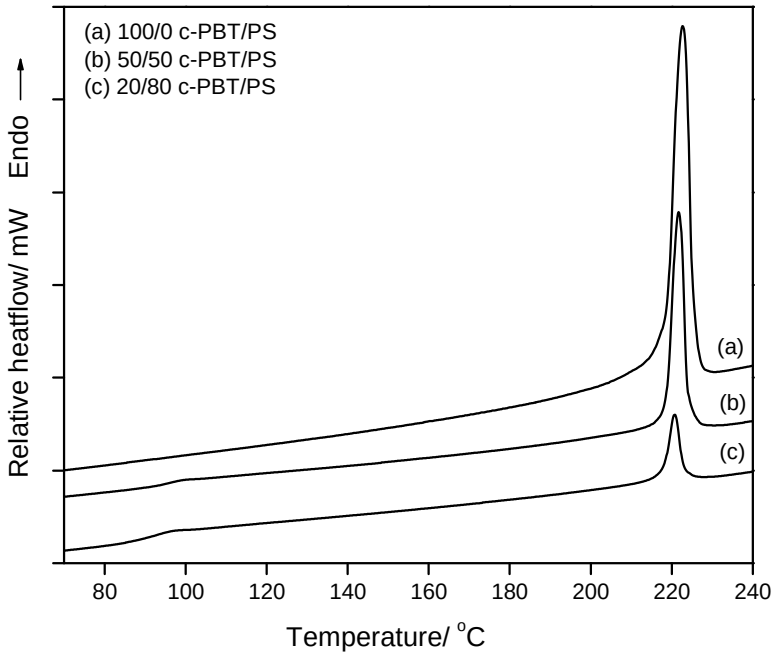

Figure 5.18: Thermal behaviour of various compositions c-PBT/PS blends after *in situ* polymerisation of CBT/PS blends

In Figure 5.18, we can see that the *in situ* polymerisation of CBT/PS which occurred over an appropriate time scale still produced immiscible blend behaviour. The heating traces of c-PBT/PS blends show that two transitions are present, i.e. the T_g of PS and the c-PBT melting point. It reflects that no interaction occurred during the polymerisation process.

Moreover, an observation on T_g of the c-PBT/PS blends clearly indicates two T_g (Figure 5.19) which represent the individual components, c-PBT (27 °C) and PS (90°C), respectively. The Fox's and Gordon-Taylor's equations are not applicable to this system since the system clearly shown immiscible blend characteristics.

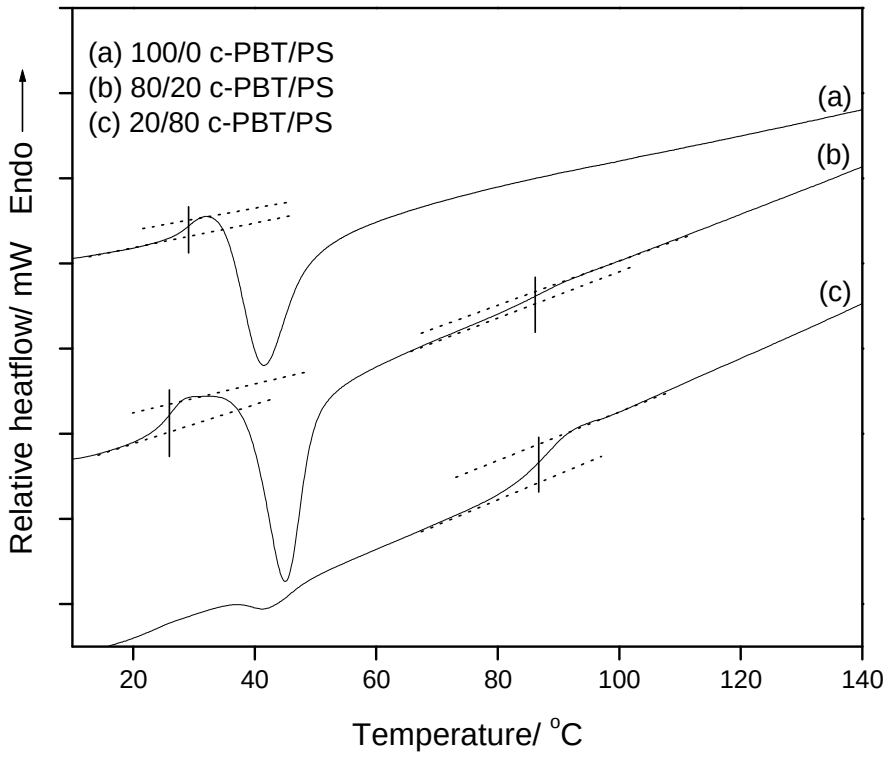

Figure 5.19: T_g of c-PBT/PS blends

5.2.5.2 Fracture surfaces of immiscible blends system (c-PBT/PS)

The morphology of an immiscible polymer blend depends on a variety of factors: the interfacial tension, the viscosity ratio of the components, the volume fraction, the shear, and extensional stresses encountered during processing [180]. An immiscible blend always results in a coarse morphology and a relatively large domain size for the minor component due to high interfacial tension [93, 180]. A coarse surface can be observed in the 20/80 c-PBT/PS blend (produced through same method of production as c-PBT/SMI blends) as shown in Figure 5.20. The SEM micrograph of 20/80 c-PBT/PS blends which went through 10 minutes *in situ* polymerisation shows this sample had a distinct two-phase morphology, i.e., a continuous PS phase with a dispersed c-PBT phase.

Moreover, the effect of phase separation on the samples which had 30 minutes and 60 minutes *in situ* polymerisation can clearly be seen. The samples show a heterogeneous structure with droplets supported in a matrix as found in many cases of immiscible blends previously [155]. This implied poor interfacial adhesion between PS and c-PBT phases as all the spheres and holes are found have smooth surfaces. In summary, it can be said that PS and c-PBT phases in the blend are immiscible, and the interfacial tension between the PS and c-PBT phases was relatively high.

The examination of morphology of c-PBT/PS blends also provides further evidence of miscibility in c-PBT/SMI blends system. There are no droplets or coarse surface found on c-PBT/SMI blends morphology as illustrated in common immiscible blends.

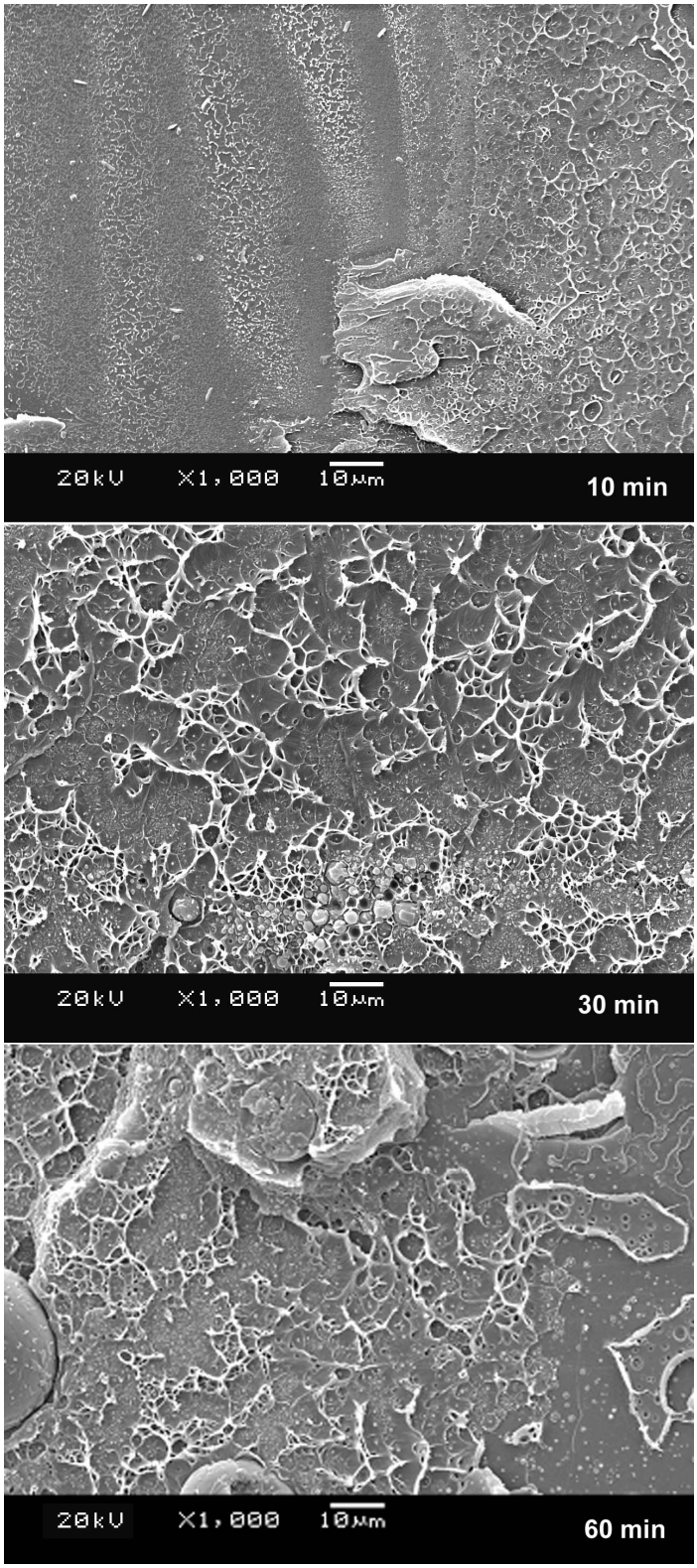

Figure 5.20: Effect of polymerisation time on fracture surface of PS rich blend (20/80 c-PBT/PS)

5.3 Conclusions

Blends of CBT and SMI have been successfully prepared using a solid dispersion technique followed by an *in situ* polymerisation process of the CBT to produce a blend of c-PBT polymer and SMI. Preparation of the blends within the DSC showed that under the conditions of the DSC experiment, the crystallisation of c-PBT was suppressed by the presence of SMI. This was most apparent at compositions in excess of 30 wt% SMI, at which point, the crystallisation process of c-PBT became undetectable within the conditions adopted for the DSC experiment. A single, composition dependent blend T_g was also found which strongly suggested that the blend was miscible. The presence of miscibility offers an explanation of why the crystallisation process in c-PBT became depressed: miscibility necessitated a phase separation process prior to the crystallisation. This manifested itself as an induction time for the crystallisation to such an extent that the crystallisation process became undetectable in the context of the *in situ* polymerisation process adopted in this work.

In contrast, the observation on c-PBT/PS blends system found no suppression of crystallisation processes at all blend compositions. The presence of two T_g in c-PBT/PS blends dynamic DSC heating curve clearly indicates an immiscible blends system. The results found then suggest the further evidence of miscibility c-PBT/SMI blends. The driving force for miscibility between c-PBT and SMI is based primarily on an interaction between carbonyl groups and hydrogen bonding on the component polymers. The morphology investigation also observed that c-PBT/SMI blends have a homogenous microstructure since the SEM micrographs do not show phase separation as in a c-PBT/PS blends.

Chapter Six

THE EFFECT OF c-PBT BLEND COMPOSITION ON THE EQUILIBRIUM MELTING AND ISOTHERMAL CRYSTALLISATION

6.1 Introduction

6.1.1 Semicrystalline/amorphous polymer blends

Figure 6.1 illustrates the possible microstructures of semi-crystalline/amorphous polymer blends on cooling from the melt. It has been reported that there are three possible microstructures which can be formed in the case of miscible semi-crystalline/amorphous polymer blends and where the diluent polymer (amorphous) can reside, i.e. (i) between the crystalline lamellae [181-185], (ii) between fibrils [114, 186] and, (iii) between the spherulites [114, 185-189]. It is also possible that the amorphous polymer location can have combinations of all these (interlamellar, interfibrillar, interspherulitic) arrangements

[114, 185, 186]. The miscible semi-crystalline/amorphous polymer blends could have multiple T_g as multiple locations for the amorphous polymer would be expected to lead to amorphous regions with different composition and, hence, different T_g [93].

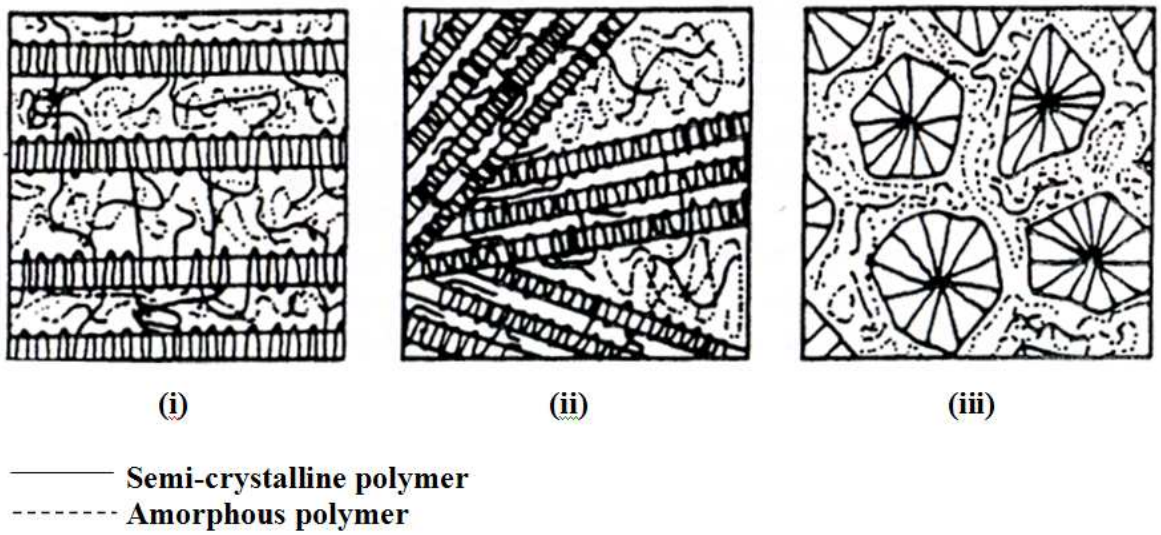

Figure 6.1: The possibility of solid state microstructure of semi-crystalline/amorphous melt miscible blends; (i) interlamellar, (ii) interfibrillar and (iii) interspherulitic (magnification increases from right to left in the drawings)[93]

In general, the amorphous polymer is trapped in interlamellar regions when its T_g is relatively high compared to the T_c of semi-crystalline polymer [93]. On the other hand, when the T_g of amorphous polymer is low relative to T_c, at least some of the amorphous polymer is located outside of the interlamellar regions. The mobility of the amorphous polymer which is determined by its T_g was found as an important factor in diluent segregation. For instance, Talibuddin *et al.* [190] who studied the melt-misciblity of poly

(ethylene oxide) (PEO) blends found that the diluent mobility influence the segregation of weakly interacting blends. They observed that poly (methyl methacrylate) (PMMA) (relatively high T_g) was trapped between PEO lamellae while poly (vinyl acetate) (PVAc) (relatively low T_g) was located partially in interfibrillar regions. However, Wu *et al.* [191] found that the PEO blends with two strongly interacting copolymers (ethylene-methacrylic acid (EMAA) (relatively low T_g) and styrene-hydroxystyrene (SHS) (relatively high T_g)) exhibited approximately the same degree of segregation, regardless of diluent mobility. Moreover, they (Wu *et al*.) reported that EMAA and SHS were excluded into interfibrillar regions at diluent contents of 20% and located at interspherulitic at higher concentration of diluent content. From the both studies of PEO blends, it can be concluded that the strongly interacting SHS showed significant diffusion from the crystal growth front, while the weakly interacting PMMA was trapped within interlamellar regions.

The crystallisation in the semicrystalline-amorphous miscible blends still occur in the range of it's T_g and T_m^o as in neat semi-crystalline polymer [93]. The crystallisation process of miscible semicrystalline-amorphous blends system will involves two types of polymer transport; i.e. diffusion of the crystallisable component toward the crystal growth front and a simultaneous rejection of the amorphous component [143]. This leads to liquid-solid phase separation which give a variety of morphology patterns. According to Chiu *et al.* [143], the morphological formation may be kinetically controlled by composition and thermal history.

6.2 Nishi-Wang Theory

In the previous chapter (Chapter 5), miscibility of the c-PBT/SMI blends was discussed based on the existence of single glass transition temperature, T_g. Furthermore, analysis of the melting behaviour of crystalline polymer blends is also one of the methods of assessing polymer-polymer miscibility [93]. It has been reported that the miscible semi-crystalline/amorphous blends will result in the equilibrium melting temperature, T_m^o depression. The analysis of T_m^o depression is widely used to estimate the Flory-Huggins interaction parameter (χ_{12}) [143, 192-200].

Nishi and Wang [192, 193] who modified the Flory-Huggins theory [201] derived the T_m^o depression of a crystalline phase with amorphous polymer in a miscible blend as;

$$\frac{1}{T^o_{m\,(blend)}} - \frac{1}{T^o_{m\,(pure)}} = \frac{-RV_2}{\Delta H^o_f V_1}\left[\frac{In\phi_2}{m_2} + \left(\frac{1}{m_2} - \frac{1}{m_1}\right)\phi_1 + \chi_{12}\phi_1^2\right] \qquad \text{(Equation 6.1)}$$

where ΔH_f^o is the heat of fusion for the 100% crystallisable component (85.75 J/g [34, 35, 67, 111, 112]), R is the universal gas constant (8.314 $JK^{-1}mol^{-1}$), V is the molar volume of the polymer repeating unit, m is the degree of polymerisation, and ϕ is the volume fraction of the component in the blend. The subscripts 1 and 2 denote the non-crystallisable (amorphous polymer) and crystallisable components (semi-crystalline polymer), respectively.

The volume fraction, ϕ can be evaluated from the weight fractions and densities of the components, where:

$$\phi_1 = \frac{w_1 / \rho_1}{w_1 / \rho_1 + w_2 / \rho_2} \qquad \text{(Equation 6.2)}$$

It is assumed that if the entropy of mixing is negligible in polymer blends $m_1 \approx m_2 \to \infty$ [154, 200], the melting point depression is dominated by an enthalpic term, and Equation 6.1 can be simplified as:

$$\frac{1}{T^o_{m\,(blend)}} - \frac{1}{T^o_{m\,(pure)}} = \frac{-RV_2}{\Delta H^o_f V_1}\left(\chi_{12}\phi_1^2\right) \qquad \text{(Equation 6.3)}$$

Commonly, a plot of $-\Delta H^o_f V_1 / RV_2 (1/T^o_{m(blends)} - 1/T^o_{m(pure)})$ against ϕ_1^2 should result in straight line. Thus, the estimation of χ_{12} is obtained from the slope of this plot [143, 192-200]. Moreover, the interaction energy density, B could be determined from the Equation 6.4 as below [149]:

$$B = \frac{\chi_{12} RT^o_{m(pure)}}{V_1} \qquad \text{(Equation 6.4)}$$

6.3 Results and discussion

6.3.1 The equilibrium melting temperatures, T_m^o

The melting points, T_m of the c-PBT/SMI blends after isothermal crystallisation at various crystallisation temperatures (197 °C to 201 °C) are shown in Figure 6.2 to 6.4. It is observed that as the SMI content increases, the T_m of the blends gradually shifts to lower temperatures which shows that the SMI component causes a depression in T_m . Lim *et al.* [137] suggest that the T_m depression may be attributed to a reduction crystal size or imperfections in the crystalline lattice. Therefore, our observation on c-PBT/SMI blends suggests that the incorporation of SMI will result in less perfect c-PBT crystals.

Again by applying the Hoffman and Weeks [99] approach, the equilibrium melting points (T_m^o) of c-PBT/SMI blends were obtained from a linear fit of T_m against T_c (slope 0.50 ± 0.05), as the intercept of the extrapolated data with the line $T_m = T_c$. Figure 6.5 shows the Hoffman and Weeks plots for the c-PBT/SMI blends.

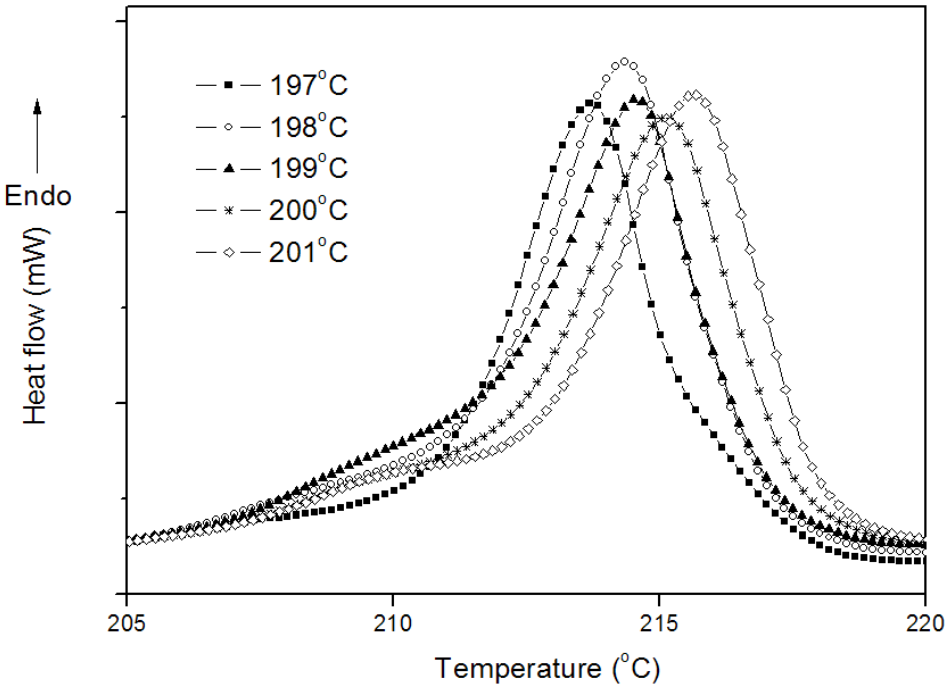

Figure 6.2: Melting peak of 90/10 c-PBT/SMI after being held at various crystallisation temperatures

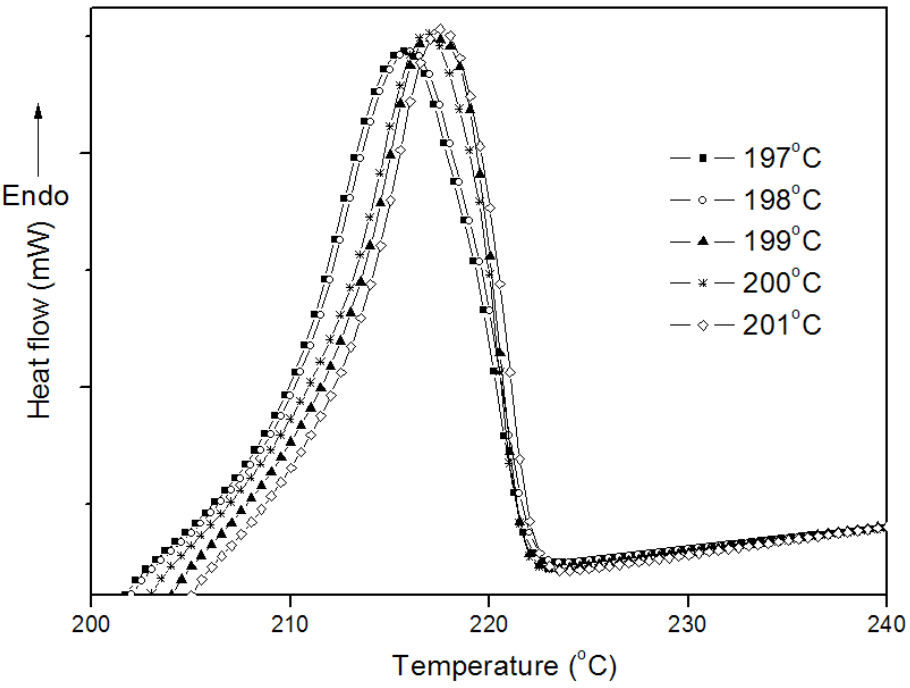

Figure 6.3: Melting peak of 80/20 c-PBT/SMI after being held at various crystallisation temperatures

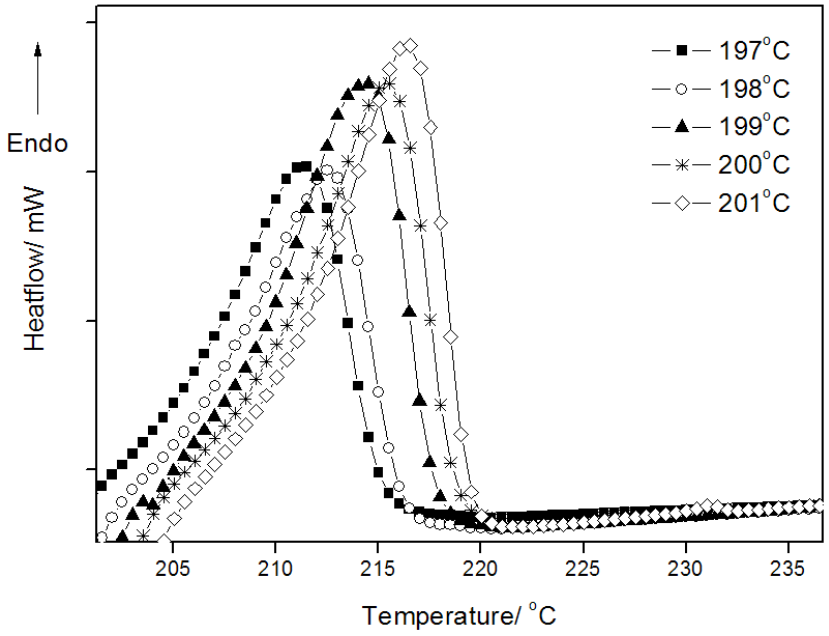

Figure 6.4: Melting peak of 70/30 c-PBT/SMI after held at various crystallisation temperatures

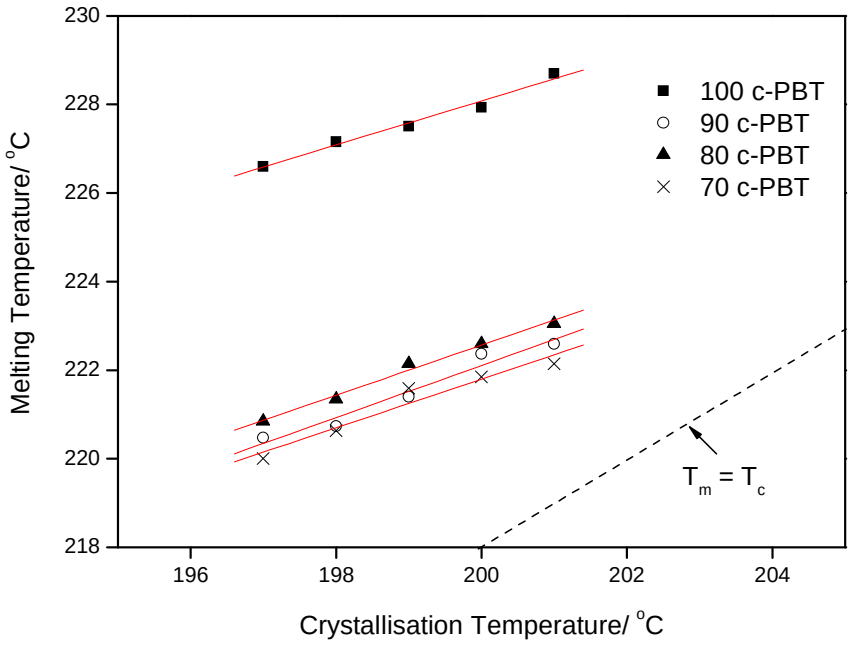

Figure 6.5: Hoffman-Weeks plot of observed melting temperature against crystallisation temperature for c-PBT/SMI blends

Figure 6.6 summarises the T_m^o observed in c-PBT/SMI blends. The results show that the T_m^o values of the blends are lower than those of the c-PBT where the increase of SMI content decreases the T_m^o value. This finding is expected as previous research on miscible crystalline-amorphous polymer blends show a depression of T_m^o [143, 192-200]**.** The depression of T_m^o which lower the degree of supercooling was reported to cause significant reductions in spherulitic growth rates for strongly interacting blends [191].

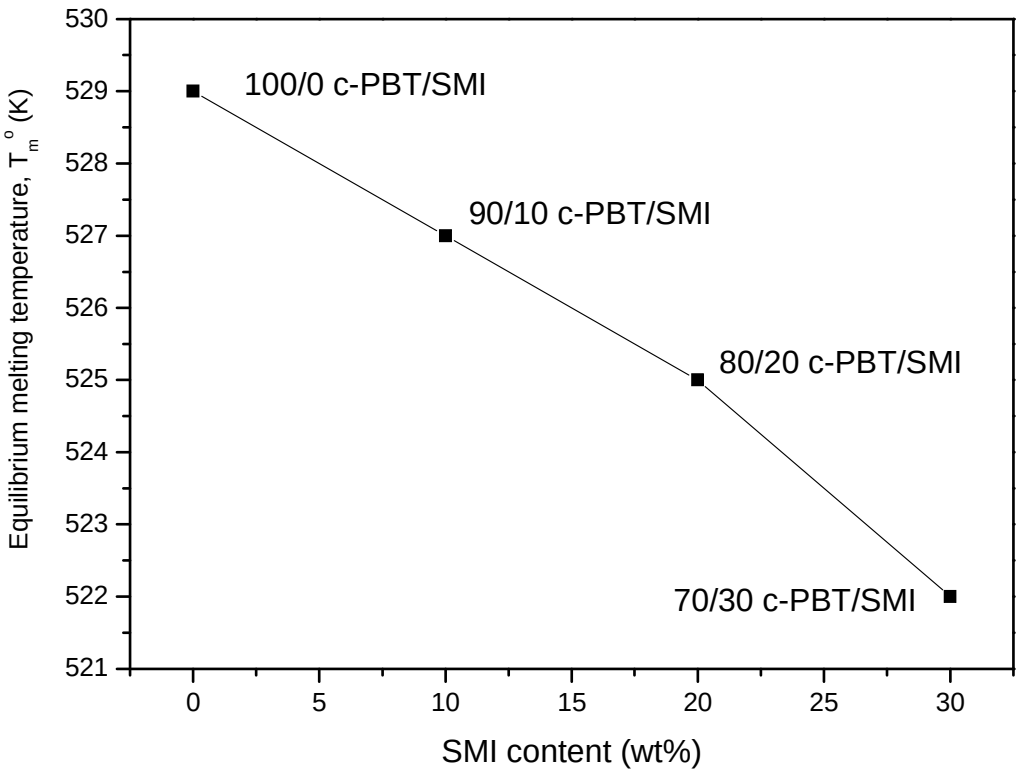

Figure 6.6: The equilibrium melting temperatures of c-PBT/SMI blends

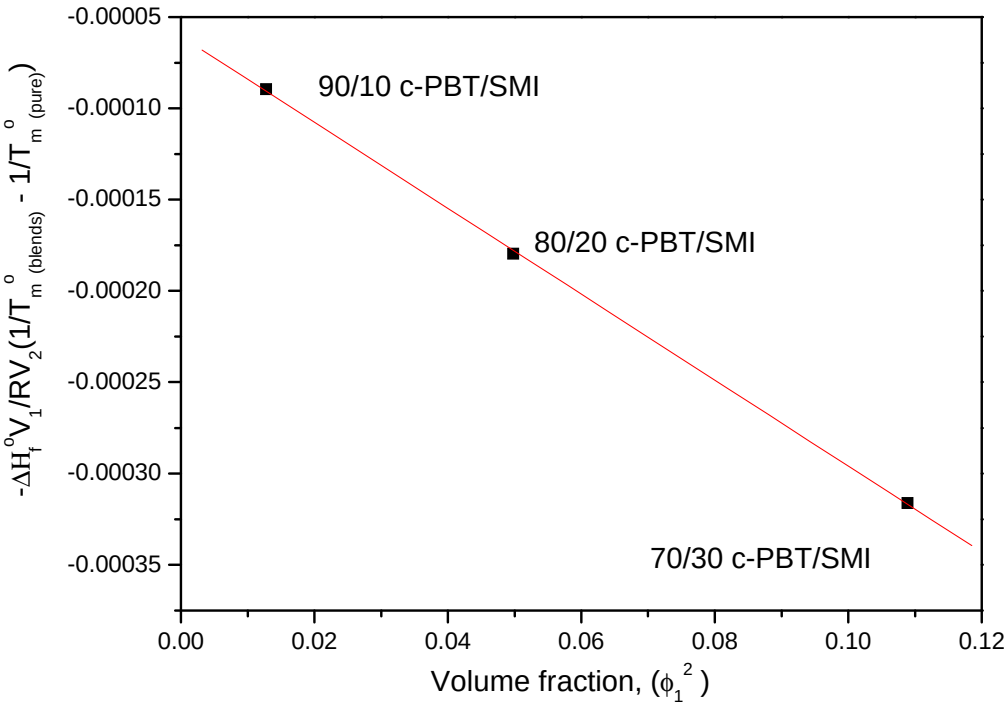

Figure 6.7: Application of Flory-Huggins theory modified by Nishi-Wang equation for c-PBT/SMI blends

By using the Nishi-Wang equation, a plot of the left term $(-\Delta H_f^o V_1 / RV_2(1/T_{m(blends)}^o - 1/T_{m(pure)}^o)$ versus ϕ_1^2 gives a straight line with negative slope as shown in Figure 6.7. The following parameters are used in order to calculate Equation 5.11; ΔH_f^o = 85.75 J/g, R = 8.314 $JK^{-1}mol^{-1}$, V_1 = 251.21 cm^3/mol of monomer, V_2 = 207.73 cm^3/mol of monomer, ρ_1 = 1.14 g/cm^3 [87] and ρ_2 = 1.31 g/cm^3 [75]. It was found that the value of that slope was -2.35 ± 0.15 x 10^{-3} which represents the χ_{12} value.

The negative value of the χ_{12} parameter observed in this study indicates that c-PBT and SMI pairs are thermodynamically miscible in the melt. In general, a negative free energy of mixing can be achieved with interactions between blend components such as intermolecular hydrogen bonding [161, 202]. As discussed earlier in a previous chapter (Chapter 5), an interaction of c-PBT and SMI blends would be expected between the carbonyl groups of the blend components. Moreover, by applying the χ_{12} value which obtained from Nishi-Wang plot in the Equation 6.4, the interaction energy density (B) was calculated as -0.04 Jcm^{-3}. Lee and Woo [149] concluded that reduced B value generally means a stronger intermolecular interaction in the blend. In their work, they found that the B value of poly(4-vinyl phenol)/poly(trimethylene terephthalate) (PVPh/PTT) blend is -32.49 Jcm^{-3} but in other work which studied poly(4-vinyl phenol)/ poly(epsilon -caprolactone) (PVPh/PCL) blends reported that B value of that blend (PVPh/PCL) is -41.11 Jcm^{-3}. This indicates that the PVPh/PCL blends have a stronger intermolecular interaction than PVPh/PTT blends.

6.3.2 Crystallisation of c-PBT/SMI blends

Hot crystallisation (the crystallisation process which occurs during cooling of polymer melts) was studied in the temperature range of 200 to 140 °C to examine the effect of c-PBT/SMI blends on the crystallisation of c-PBT. The overall crystallisation exotherms could be measured when samples were cooled at a rate of 10 °C/min from the melt (after being held at 240^{o}C for 5 min) in the dynamic DSC mode. The effect of blend

composition on the hot crystallisation of c-PBT/SMI blends is shown in Figure 6.8. It is obvious that the presence of SMI shifted the crystallisation of the pure c-PBT (originally found at 190^{o}C) to lower temperature. As predicted and reported by previous researchers [150], the presence of miscible blend components in semi-crystalline polymers will impede the crystallisation process. The possible reason is that the second polymer (amorphous) might reside mainly in the interlamellar and interspherulitic region of crystalline polymer and slow the crystallisation process. From the estimation of Flory-Huggins parameter (χ_{12}) by Nishi-Wang approach, we noticed that the c-PBT/SMI blends are weakly interacting blends as their χ_{12} is a small value and the T_g of SMI is relatively lower than c-PBT T_c. These two characteristics influence the location of second polymer (SMI) in the microstructure of c-PBT/SMI blends as discussed earlier in Section 6.2. On the other hand, Huo *et al.* [114] who studied the location of polyarylate (PAr) in PBT/PAr blends by small-angle X-ray scattering (SAXS) found that PAr (second polymer) location in the interlamellar and interspherulitic region depends on the blend composition, i.e. interlamellar PAr structure holds for blends with PAr < 0.40, while either interfibrillar or interspherulitic structure exists for blends with PAr > 0.40.

Typical crystallisation curves for c-PBT/SMI blends at different isothermal crystallisation temperatures are shown in Figure 6.9, as an example, a 90/10 blend. Note that the end of the crystallisation process was taken to be the point where the isothermal curve converged with the horizontal base line as reported in literature [132, 203].

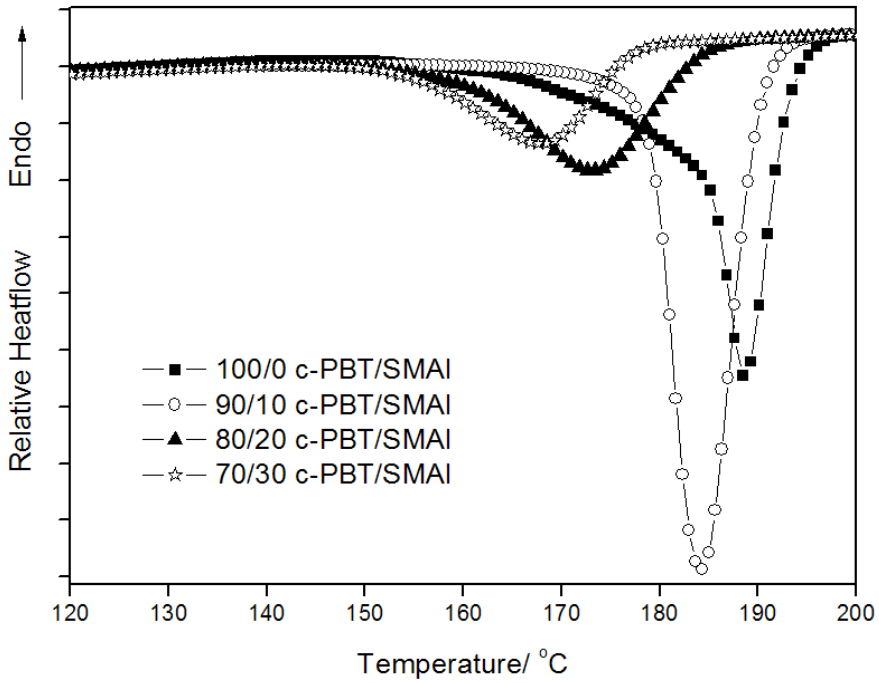

Figure 6.8: Effect of blend composition on hot crystallisation of c-PBT/SMI Blends

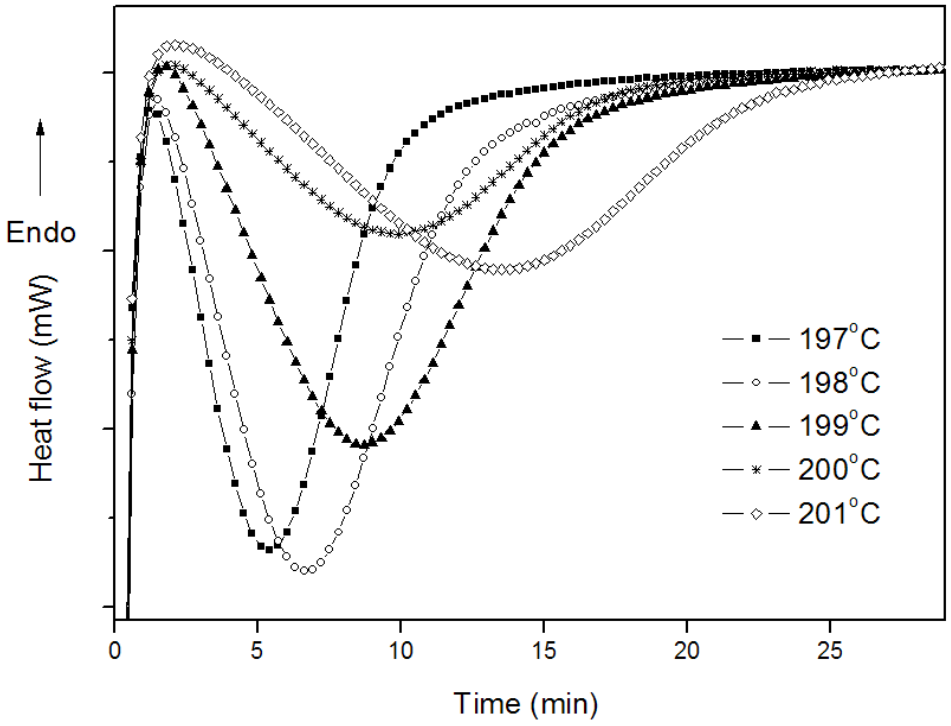

Figure 6.9: DSC exotherms of the isothermal crystallisation of 90/10 c-PBT/SMI blends at various crystallisation temperatures

6.3.3 Avrami analysis

The overall development of relative crystallinity, X_t with time at selected crystallisation temperatures of c-PBT/SMI blends is shown in Figure 6.10. From that figure, we can see that all the isotherms show sigmoidal curves. They depend on the crystallisation temperature selected and time. This trend is in agreement with previous polymer crystallisation studies [130, 143].

In the case of c-PBT/SMI blends, the relative crystallinity versus time plot reveals that higher level of SMI contents slow the crystallisation process of c-PBT. As an example, Figure 6.11 shows that $t_{1/2}$ increases with increasing SMI contents. The $t_{1/2}$ is defined as the time to reach the maximum rate of the crystallisation process [132, 139] and is also known as crystallisation half-life. All the $t_{1/2}$ values for various crystallisation temperatures and blends compositions are listed in Table 6.1.

It could be suggested that the increment of $t_{1/2}$ values with SMI content is attributed to the reduction of molecular mobility, arising from increase of T_g, and the dilution of c-PBT concentration upon blending with SMI. The $t_{1/2}$ also was observed to increase with increasing crystallisation temperature, T_c at given composition which is consistent with the postulate that crystallisation kinetics in the T_c range were dominated by the thermodynamic driving force of crystallisation [143].

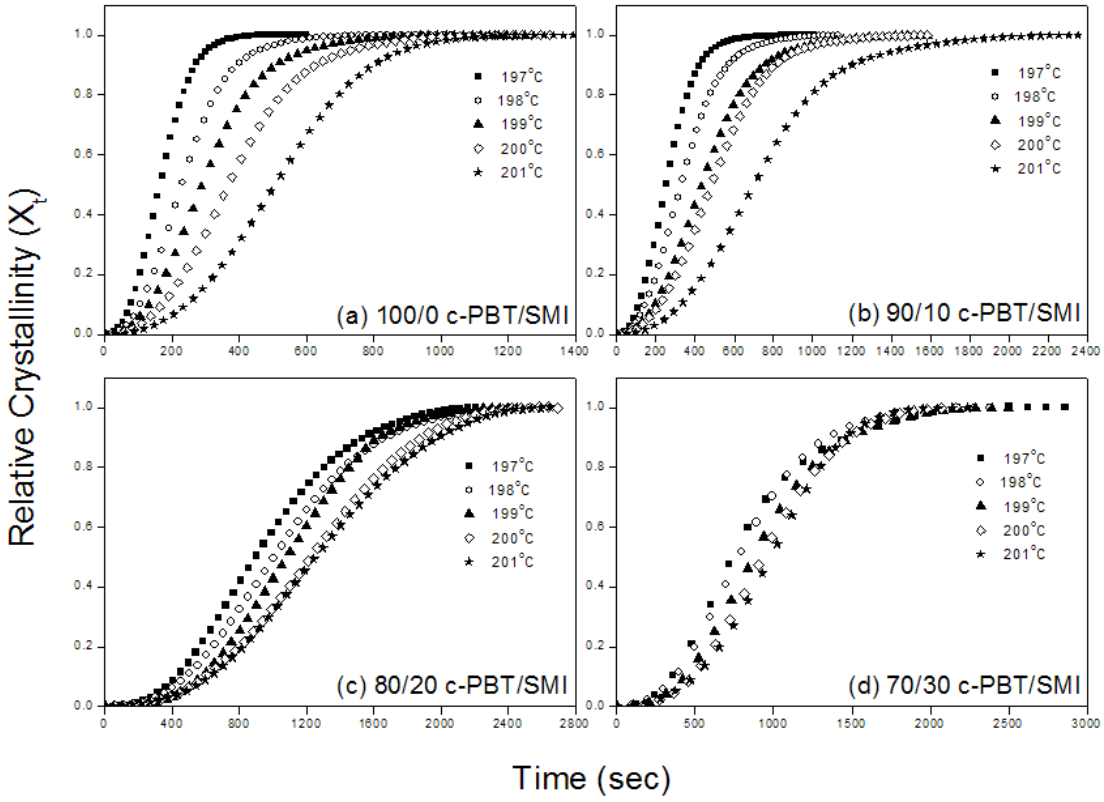

Figure 6.10: Development of crystallinity with time for c-PBT/SMI blends

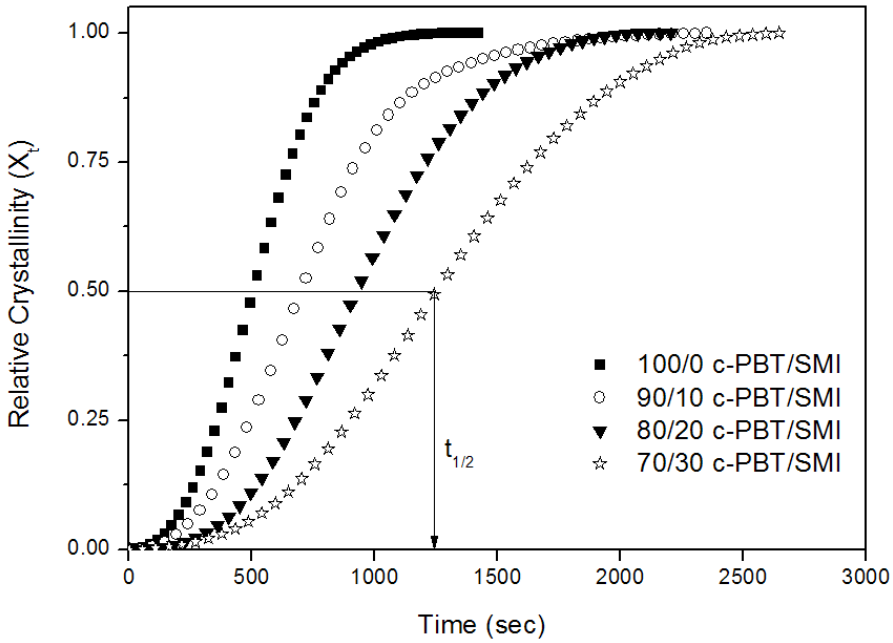

Figure 6.11: Development of crystallinity with time for c-PBT/SMI blends at 201°C

Figure 6.12 illustrates the Avrami plot of c-PBT/SMI blends as an example at 197^{o}C. It clearly shows almost parallel lines at different blend compositions and the lines shifted to higher time as the crystallisation process was impeded with the increasing SMI content into the blend. The parallel lines imply that the crystal growth geometries and nucleation mechanism are similar, although at different blend compositions. This trend was also observed by Chiu *et al.* [143], who worked on the crystallisation kinetics of poly(trimethylene terephthalate)/poly(ether imide) (PTT/PEI) miscible blends. They found that the experimental data closely agree with the Avrami equation at low conversion but deviate from the equation at high conversion which is believed to be due to secondary crystallisation. From this plot ($\log(-In(1-X_t))$ against $\log t$), the Avrami constant, n and the overall crystallisation rate, Z can be obtained from the slope and the intercept, respectively.

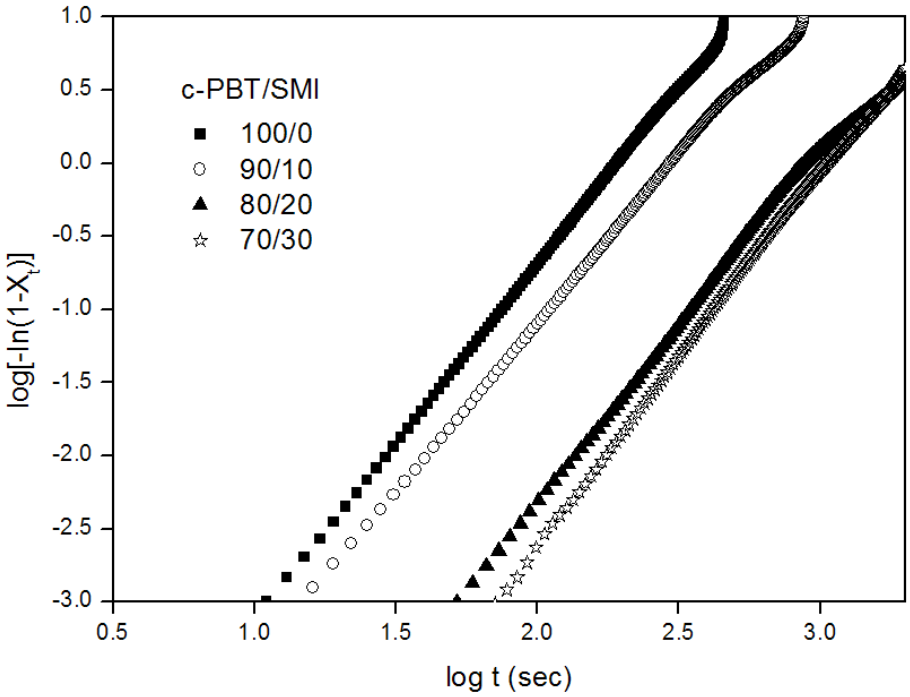

Figure 6.12: Avrami plots of c-PBT/SMI blends at 197 ^{o}C

Table 6.1: The Avrami parameters for c-PBT/SMI blends

Blend composition (c-PBT/SMI)	**Crystallisation Temperature, (^{o}C)**	**n, ±0.1**	**Half-life ($t_{1/2}$), min ±0.1**	**Z , min^{-n} (x10^{-4}) ± 0.002**
100/0 c-PBT/SMI	197	2.4	2.7	577
	198	2.4	3.7	269
	199	2.4	4.7	155
	200	2.4	6.0	82
	201	2.5	8.4	25
90/10 c-PBT/SMI	197	2.5	4.2	235
	198	2.5	5.4	127
	199	2.5	7.2	62
	200	2.5	8.0	46
	201	2.6	11.5	14
80/20 c-PBT/SMI	197	2.7	10.6	10
	198	2.7	11.8	9
	199	2.8	13.5	5
	200	2.8	14.6	3
	201	2.8	16.3	2
70/30 c-PBT/SMI	197	2.6	13.2	8
	198	2.6	16.3	6
	199	2.7	17.3	2
	200	2.7	19.8	2
	201	2.7	20.5	2

It can be observed that the addition of 30 wt% SMI resulted in a drastic increase of $t_{1/2}$ and decrement of Z compared to c-PBT as shown in Figure 6.13 and Figure 6.14, respectively. It is believed that the miscibility effect found in that composition cause the slower crystallisation process of c-PBT. This work focused on the hot-crystallisation of c-PBT, therefore only half of the bell shaped curve is apparent. The growth rate in Avrami equation can be related to the $t_{1/2}$ and the Z. A high growth rate corresponds to a low $t_{1/2}$ and high Z constant. Therefore the temperature dependencies both $t_{1/2}$ and Z are consistent with the Hoffman-Lauritzen theory.

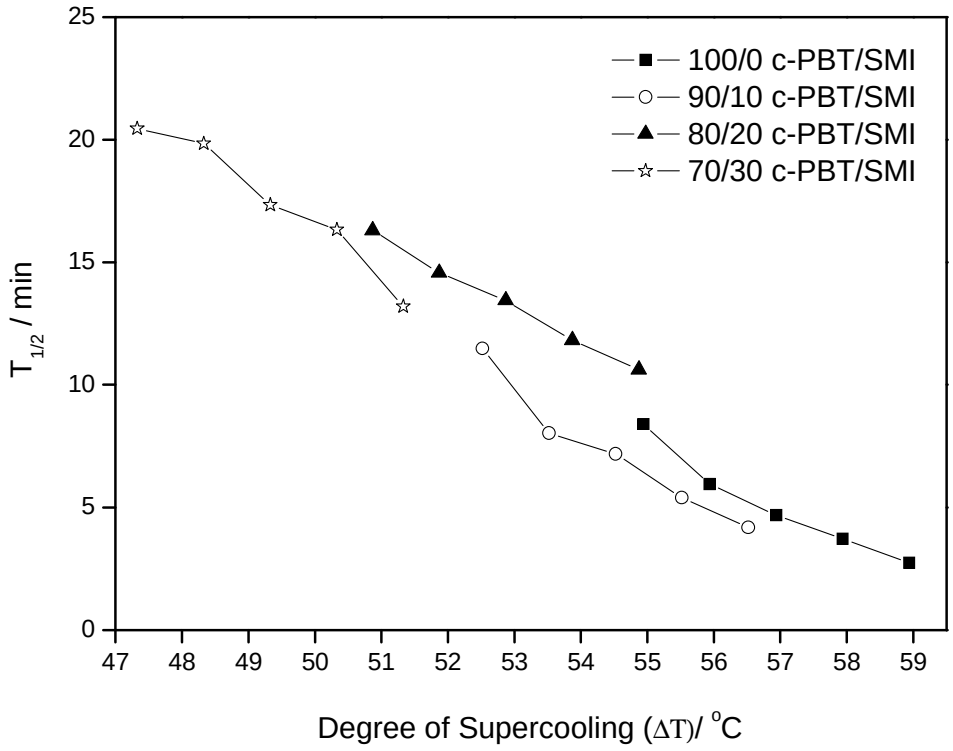

Figure 6.13: Variation of half-life as a function of degree of supercooling of c-PBT/SMI blends

Jenkins [129] in his work on crystallisation in miscible blends of poly(ether ether ketone) (PEEK) and poly(ether imide) (PEI) concluded that the temperature dependence of both the $t_{1/2}$ and the Z can be explained by the existence of two competing effects as described by the Hoffman-Lauritzen theory [125, 128-132] which is modified from Turnbull and Fisher [127]. Competition between the two results in a minimum in the $t_{1/2}$ and a maximum in the Z at a temperature midway between the T_g and T_m.

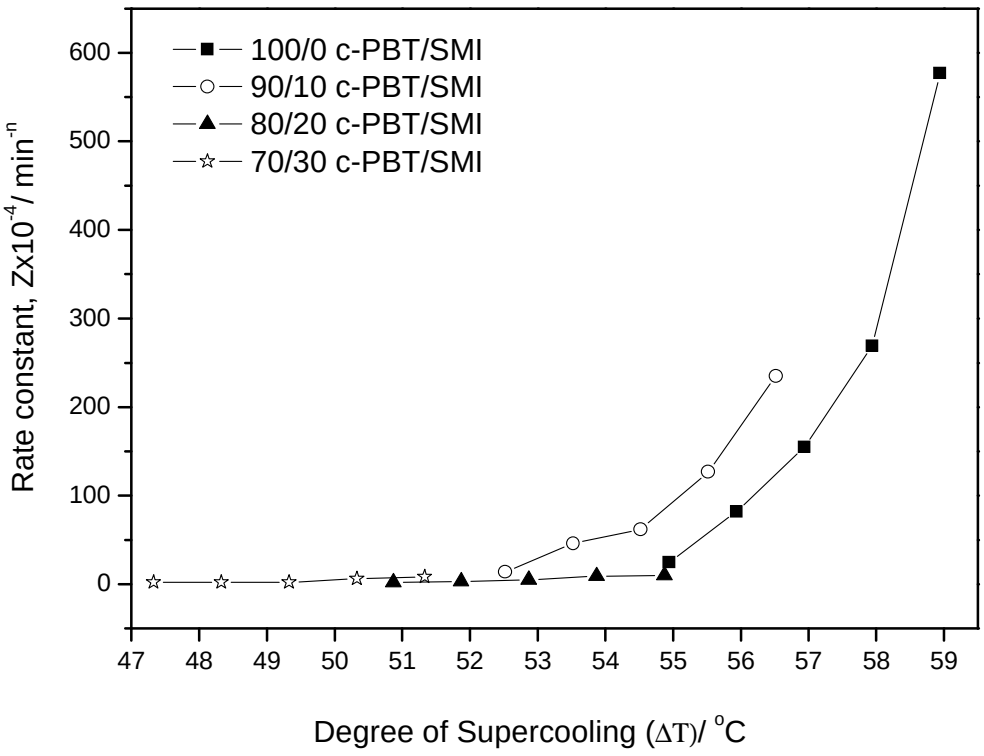

Figure 6.14: Variation of composite rate constant as a function of degree of supercooling for c-PBT/SMI blends

In the case of c-PBT/SMI blends, it is obviously observed that the rate of crystallisation at constant crystallisation temperature decreases with increasing SMI content. The possible reason is the presence of SMI causing increased melt viscosity of the blends. The greater melt viscosity slows the diffusion of the SMI molecules away from the growth front giving rise to a slower crystallisation rate. Information on the phase morphology of the blends can also be inferred from this evidence. As the crystallisation rate of the blend is markedly slower than that of c-PBT, it can be assumed that the components mix at the molecular level and large domains of c-PBT do not exist in the blend.

6.3.4 Effect of the blends on nucleation constant and surface free energy

The effect of the presence of second polymer (SMI) in c-PBT/SMI blends on the nucleation constant (K_g) and surface free energy product ($\sigma\sigma_e$) was also analysed using Hoffman-Lauritzen theory as in Section 4.3.3. Figure 6.15 illustrates the Hoffman-Lauritzen plot for blends of c-PBT/SMI blends. The K_g value was found to decrease (as listed in Table 6.2) and the transition from regime III to regime II was observed as the SMI content increased. The results from this study are consistent with the Hoffman-Lauritzen theory whereas for the c-PBT spherulitic growth occurred in regime III as the degree of supercooling, ΔT is high. The depression of equilibrium melting point (T_m^o**)** which is found in miscible polymer blends will lower the ΔT. As a consequence the spherulitic growth shifted to regime II which occurred at medium ΔT. Avella and Martuscelli [204]

found similar results in PHB/PEO blends where PHB crystallised in regime III but its blends with PEO crystallised in regime II. It was reported that a shift of regime III-II transition to lower temperature with increasing second polymer (amorphous) contents suggest that the secondary nucleation rate was depressed by a larger extent upon blending than the surface spreading rate [194].

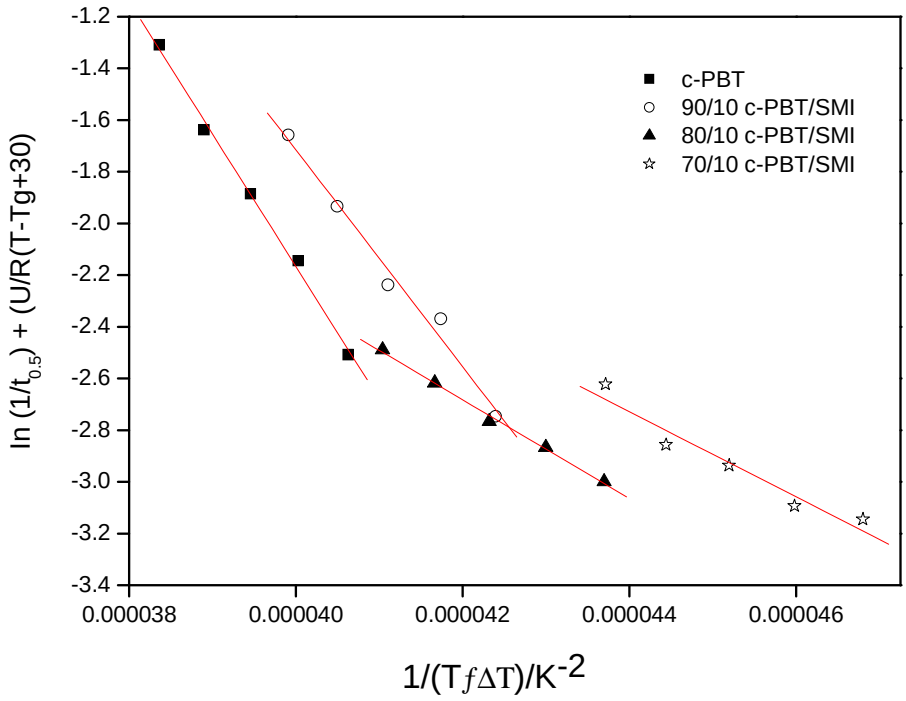

Figure 6.15: A Hoffman-Lauritzen plot for blends of c-PBT/SMI blends

The estimation of surface free energy product, $\sigma\sigma_e$ using Equation 4.19 shows a decrement trend. This is consistent with the melting point depression where the ability of c-PBT to crystallise from melt was reduced with the increased levels of SMI. Jenkins [129] also suggested that the surface free energy product, $\sigma\sigma_e$ is influenced by composition of the blends, i.e., the quantity σ_e is determined by chainfolding, whereas the quantity σ

varies with the nearest neighbours. Hence, the surface energy variation is one of the factors that determine the crystallisation rates of c-PBT. Overall the observation on reduction of K_g and $\sigma\sigma_e$ is in agreement with the previous finding which involved miscible blends of crystallisable polymers [143, 146, 204]. Based on Hoffman-Lauritzen theory (Equation 4.19), it can be seen that the K_g will affect the $\sigma\sigma_e$ in the same regime where the reduction in K_g value will decrease the $\sigma\sigma_e$. It also suggested that reduction of both parameters is due to miscibility of the blends as the crystallisation process has been found to be affected by the blend components especially for the blends which involved a crystalline-amorphous system. It is believed that these amorphous (SMI) components were located in the region of interlamellar and interspherulitic of crystallisable polymer (c-PBT) and as a result they lowered the degree of crystallinity and the crystallisation rate of the semi-crystalline polymer.

Table 6.2: Variation of the nucleation constant and surface free energy product of c-PBT/SMI blends

Sample	$-K_g \times 10^5$ K^2	$\sigma\sigma_e$ ($\times 10^{-4}$ J^2m^{-4})
100/0 c-PBT/SMI	5.13 ± 0.02	6.44 ± 0.01
90/10 c-PBT/SMI	4.18 ± 0.02	5.33 ± 0.02
80/20 c-PBT/SMI	1.88 ± 0.02	4.84 ± 0.01
70/30 c-PBT/SMI	1.62 ± 0.02	4.10 ± 0.05

6.4 Conclusions

The equilibrium melting point (T_m^o) and isothermal crystallisation kinetics of c-PBT blends with SMI were investigated. The T_m^o of c-PBT blends was determined using the Hoffman and Weeks method. Studies on the T_m^o indicate that the presence of SMI content lowers the melting point of c-PBT. It may be attributed to the reduced crystal size or imperfect crystals in the crystalline lattice. We would suggest that the incorporation of SMI will encourage less perfect c-PBT crystals. Moreover, polymer-polymer miscibility could also be investigated by analysing the melting behaviour of crystalline polymer blends. The T_m^o depression is partial evidence that miscibility in the blend system is achieved. The Flory-Huggins interaction parameter (χ_{12}) was calculated using the Flory-Huggins theory modified by Nishi and Wang. In this study, the Flory-Huggins interaction parameter (χ_{12}) was found to have negative values which indicates that c-PBT and SMI pairs are thermodynamically miscible in the melt.

The Avrami plot shows that the crystal growth geometries and nucleation mechanism of c-PBT/SMI blends are similar, although at different blend compositions. Crystallisation parameters such as half-life ($t_{1/2}$), rate constant (Z), and Avrami exponent (n) have been found to be sensitive to the T_c values and blend compositions within the range of 197 - 201 °C. The $t_{1/2}$ was observed to decrease with an increase in the T_c and SMI content while values of Z decreased in this situation. The n values were found to be in the range from 2.4 to 2.8 for the primary crystallisation process for c-PBT and its

blends, indicating that heterogeneous nucleation of spherulites occurred and growth of spherulites was between two-dimensional and three-dimensional.

The Hoffman-Lauritzen secondary nucleation theory was used to estimated the nucleation constant (K_g) and surface free energy product ($\sigma\sigma_e$) of c-PBT/SMI. A shift in the crystallisation process from regime III to regime II was observed with increasing SMI content. The addition of SMI in the c-PBT matrix showed that SMI had some dilution effect on c-PBT where it reduced the crystallisation rate of c-PBT. It is also suggested that the second polymer (SMI) might reside mainly in the interlamellar or interspherulitic regions of the crystalline polymer and impeded the crystallisation process.

Chapter Seven

CONCLUSIONS AND FUTURE WORK

7.1 Conclusion

Thermal behaviour studies have been carried out for CBT and c-PBT, respectively by DSC, FTIR, GPC, TGA and optical microscopy. The GPC results indicated that the CBT contain three components, presumably different oligomers. The production of c-PBT begun with a low molecular weight (M_w) material and it increased during the polymerisation.

A suitable initiator such as tin and titanium catalysts is needed in order to polymerise CBT. The use of a cyclic initiator, i.e., stannoxane is reported [14] to lead to ring-expansion polymerization which produces macro cyclic polymer as a result. It was found that the active temperature range for polymerization is when the CBT was fully melted but below the melting point of the resulting polymer. The c-PBT produced in this

temperatures range has a higher degree of crystallinity than PBT produced by conventional methods.

It is believed that the simultaneous polymerisation and crystallisation processes for the production of c-PBT could not be separated using the thermal analysis behaviour since the polymerisation of CBT is an almost thermo-neutral reaction and also both processes occurred rapidly in a short time. Based on thermal analysis by DSC and GPC it was found that the crystallisation process starts as soon as the M_w of the polymer reaches an appropriate level even though polymerisation still continues. The development of M_w during the crystallisation process suggests that the crystallisation process begins before the polymerisation process was complete. From the assessment of the melting behaviour of the resulting c-PBT and the development of M_w during polymerisation of CBT, it is also believed that polymerisation and crystallisation are completed at the same time.

The polymerisation process of CBT has a significant effect on the C-O stretching and C=O stretching band as the peak intensity changes and the peak location shifts during the ring expansion polymerisation. The spectra were found to be more dominant in crystalline arrangement when the c-PBT formed as the semi-crystalline polymer was produced.

Thermal degradation studies showed that the use of stannoxane as an initiator/catalyst to aid ring-expansion polymerisation however has limitations due to its stability at high temperature. As s consequence, the polymerisation of CBT to produce the macrocyclic polymer should only be done below the melting point of the polymer.

The presence of multiple melting peaks when the polymerisation of CBT is not complete is believed to be due to the existence of mixed spherulites as a consequence of mixed cyclic and linear structures. Furthermore, the polymerisation of CBT at high temperature (> 210 °C) also resulted in multiple melting peaks as the degradation of stannoxane is expected at high temperatures. Degradation of stannoxane will cause mixed cyclic and linear structures. On the other hand, the double melting peak behaviour which is found during re-heating of c-PBT is believed to be due to the melting and re-crystallisation of imperfect crystals.

The c-PBT/SMI blends were successfully prepared by simultaneous *in situ* polymerisation and melt blending of solid dispersion CBT/SMI powder. Note that the blends were prepared without any external force and the miscibility is due to the low viscosities of both component and the potential of SMI to be miscible with polyester. It was found that at compositions in excess of 30 wt % of SMI the crystallisation of c-PBT was suppressed which suggests miscibility occurred.

The sign of miscibility in c-PBT/SMI blends is supported by the existence of a single composition-dependent blend T_g. Moreover, the Flory-Huggins interaction parameter (χ_{12}) which was calculated using the Flory-Huggins theory modified by Nishi and Wang show negative value indicating that c-PBT and SMI pairs are thermodynamically miscible in the melt. It could be suggested that the driving force for miscibility between c-PBT and SMI is based primarily on an interaction between carbonyl groups and hydrogen bonding in the component polymers.

A fracture surface investigation revealed that at higher c-PBT content (> 80 wt %) small particles (which are believed to be crystallites) grow during simultaneous *in situ* polymerisation of CBT and melt blending. This finding is consistent with the DSC result where at 80/20 c-PBT/SMI, the c-PBT still has the ability to crystallise in the blend system. In contrast, at higher SMI (> 50 wt %) content these small particles disappeared with increasing simultaneous *in situ* polymerisation of CBT and melt blending times. The SEM micrographs for these samples show a homogenous microstructure and do not show phase separation.

The effect of the blend components (SMI) on the c-PBT equilibrium melting point (T_m^o**)** and isothermal crystallisation kinetics were also investigated. Studies of the T_m^o indicate that the presence of SMI content lowers the T_m^o of c-PBT. The T_m^o depression is partial evidence that miscibility is achieved in the blend system. It may be attributed to the reduced crystal size or imperfect crystals in the crystalline lattice. It could be suggested that the incorporation of SMI will encourage less perfect c-PBT crystals.

Crystallisation parameters such as half-life ($t_{1/2}$), composite rate constant (Z), and Avrami exponent (n) have been found to be sensitive to the crystallisation temperature (T_c) and blend compositions. The $t_{1/2}$ was observed to decrease with an increase in the T_c and SMI content while values of Z decreased in this situation. The n values of the blends indicate that heterogeneous nucleation of spherulites occurred and growth of spherulites was between two-dimensional and three-dimensional. A shift in the crystallisation process from regime III to regime II was observed with increasing SMI content. The addition of SMI in the c-PBT matrix showed that SMI had some dilution effect on c-PBT where it reduced the crystallisation rate of c-PBT. It is also suggested that the second polymer (SMI) might reside mainly in the interlamellar or interspherulitic regions of the crystalline polymer and impede the crystallisation process.

7.2 Recommendations for future work

Since cyclic polyester, i.e., c-PBT produced from its (CBT) oligomers has interesting properties and a promising future, there is still a great deal of information that needs to be ascertained in order to completely understand the structure-property relationships and the applications of the material. Several recommendations for future interest can be made based on the three major areas as outlined below;

- **Polymerisation of CBT**

The types of catalysts used in polymerisation of CBT have been known to strongly influence the types of polymerisation i.e. ring opening polymerisation or ring expansion polymerisation, as well as the time required for polymerisation and polymer conversion [34]. Therefore the exploration of new catalysts could broaden the application range of CBT. In this study, a cyclic catalyst i.e. stannoxane was used in the polymerisation of CBT through ring-expansion polymerisation in order to produce macrocyclic polyesters. However, stannoxane was found have limitations at high temperature. Therefore it is worth exploring new cyclic catalysts which could initiate production of a macrocyclic polymer.

- **c-PBT Blends**

Since the c-PBT/SMI blends in this study only focused on their thermal behaviour and isothermal crystallisation kinetics, it is suggested that the mechanical properties of the resulted blends such as tensile strength, flexural strength and impact strength also interesting to study.

Moreover, there is the possibility to form nano-composites by liquid-liquid phase separation of *in situ* blend formation by polymerising cyclic oligomers in the presence of another polymer. Nachlis and co-workers [66] outline the key factors to produce nano-composite structures from cyclic oligomers as; (i) the initial mixture of cyclic oligomer and polymer to be blended must be miscible, (ii) the polymerisation kinetic of the cyclic oligomers dispersed through the host polymer must be more rapid than the dynamics of phase separation, (iii) phase separation of the polymers must occur in a sensible timescale to produce immiscible structures and (iv) phase coarsening must be restricted if the nanostructures are to be preserved. Therefore it is suggested to investigate the potential of CBT blends with polymers which comply with the conditions given by Nachlis and co-workers in order to produce nano-composite.

- **Crystallisation kinetics studies of c-PBT and its blends**

In this study crystallisation kinetics study of miscible semi-crystalline/amorphous blends were performed. It would be interesting to investigate the effect of miscible semi-crystalline blend component on the crystallisation of c-PBT. It is also suggested to expand the crystallisation kinetic study of c-PBT and its blends to investigate the crystallisation transition of regime based on Hoffman-Lauritzen theory.

References

1. Scott DW. Equilibria between linear and cyclic polymers in methylpolysiloxanes, Journal of the American Chemical Society, 1946, 68, 11, 2294-2298.
2. Brown JF and Slusarcz GM. Macrocyclic polydimethylsiloxanes, Journal of the American Chemical Society, 1965, 87, 4, 931-932.
3. Carmicheal JB and Winger R. Cyclic distribution in dimethylsiloxanes, Journal of Polymer Science: Part A -General Papers, 1965, 3, 3, 971-984.
4. Carmicheal JB, Gordon DJ, and Isackson FJ. Dilution effects on dimethylsiloxane ring-chain equilibria, Journal of Physical Chemistry, 1967, 71, 7, 2011-2015.
5. Edwards CJC, Stepto RFT, and Semlyen JA. Studies of cyclic and linear poly(dimethyl siloxanes): 5. diffusion behavior in dilute-solution, Polymer, 1980, 21, 7, 781-786.
6. Geiser D and Hocker H. Preparation of macrocyclic polystyrene, Polymer Bulletin, 1980, 2, 9, 591-597.
7. Geiser D and Hocker H. Synthesis and investigation of macrocyclic polystyrene, Macromolecules, 1980, 13, 3, 653-656.
8. Spanagel EW and Carothers WH. Macrocyclic esters, Journal of the American Chemical Society, 1935, 57, 1, 929-934.
9. East GC and Girshab AM. Cyclic oligomers in poly(1,4-butylene terephthalate), Polymer, 1982, 23, 3, 323-324.
10. Brunelle DJ, Macrocyclics for the synthesis of high molecular weight polymers, in *New methods of polymer synthesis*, J.R. Ebdon and G.C. Eastmond, Editors. 1995, Blackie: London.

11. Brunelle DJ and Takekoshi T. Process for preparing macrocyclic polyester oligomers, U.S. Patent, 5,407,984, 1995.

12. Bryant JJL and Semlyen JA. Cyclic polyesters: 7. Preparation and characterization of cyclic oligomers from solution ring-chain reactions of poly(butylene terephthalate), Polymer, 1997, 38, 4531-4537.

13. Brunelle DJ, Bradt JE, Serth-Guzzo J, Takekoshi T, Evans TL, Pearce EJ, and Wilson PR. Semicrystalline polymers *via* ring-opening polymerization: preparation and polymerization of alkylene phthalate cyclic oligomers, Macromolecules, 1998, 31, 4782-4790.

14. Miller S. Macrocyclic polymer from cyclic oligomers of polybutylene terephthalate, Ph. D., University of Massachusetts, 1998.

15. Hall AJ and Hodge P. Recent research on the synthesis and applications of cyclic oligomers Reactive & Functional Polymers, 1999, 41, 1-3, 133-139.

16. Semlyen JA. Cyclic polymers, 2 ed., New York, Boston, Dordrecht, London, Moscow: Kluwer Academic 2000.

17. Brunelle DJ and Bradt JE. Method for preparing and polymerizing macrocyclic poly (alkylene discarboxylate) oligomers, U.S. Patent, 5,039,783, 1991.

18. Brunelle DJ and Shannon TG. Preparation and polymerization of bisphenol A cyclic oligomeric carbonates, Macromolecules, 1991, 24, 11, 3035-3044.

19. Brunelle DJ and Bradt JE. Method for preparation of macrocyclic poly (alkylene discarboxylate) oligomers, U.S. Patent, 5,214,158, 1993.

20. Hall AJ, Hodge P, McGrail CS, and Rickerby J. Synthesis of a series of cyclic oligo(alkylidene isophthalate)s by cyclo-depolymerisation Polymer, 2000, 41, 4, 1239-1249.

21. Brunelle DJ, Synthesis and polymerisation of cyclic polyester oligomers in *Modern Polyesters: Chemistry and Technology of Polyester and Copolyesters*, J. Scheirs and T.E. Long, Editors. 2003, Wiley: New York

22. Weijers C, R.D. de Rooij, Agarwal US, G. de Wit, and Lemstra PJ. Supercritical fluid extraction of cyclic oligomers from depolymerizing PBT Journal of Applied Polymer Science, 2006, 101, 4487-4492.

23. Brunelle DJ. Highlight: Cyclic oligomer chemistry Journal of Polymer Science Part A: Polymer Chemistry, 2008, 46, 1151-1164.

24. Kamau SD, Hodge P, Williams RT, Stagnaro P, and Conzatti L. High throughput synthesis of polyesters using entropically driven ring-opening polymerizations, Journal of Combinatorial Chemistry, 2008, 10, 644–654.

25. Hubbard PA, Brittain WJ, Mattice WL, and Brunelle DJ. Ring size distribution in the depolymerization of poly(butylenes terephthalate), Macromolecules, 1998, 31, 5, 1518-1522.

26. Kricheldorf HR, Lee SR, and Bush S. Polylactones: 36. Macrocyclic polymerization of lactides with cyclic Bu2Sn initiators derived from 1,2-Ethanediol, 2-Mercaptoethanol, and 1,2-Dimercaptoethane, Macromolecules, 1996, 29, 5, 1375–1381.

27. Krabbenhoft HO, Brunelle DJ, and Pearce EJ. “Two component initiator systems for the ring-opening polymerization of oligomeric cyclic bisphenol A carbonates: The *in situ* cleavage of disulfides by triarlyphosphines, Journal of Applied Polymer Science, 1997, 66, 2251–2255.

28. Brunelle DJ and Serth-Guzzo J. Titanate-catalyzed ring-opening polymerization of cyclic phthalate ester oligomers, Abstracts of Papers of the American Chemical Society, 1999, 217, U620-U620.

29. Youk JH, Boulares A, Kambour RP, and MacKnight WJ. Polymerization of ethylene terephthalate cyclic oligomers with a cyclic dibutyltin initiator, Macromolecules, 2000, 33, 3600–3605.

30. Youk JH, Kambour RP, and MacKnight WJ. Polymerization of ethylene terephthalate cyclic oligomers with antimony trioxide, Macromolecules, 2000, 33, 3594–3599.

31. Youk JH, Kambour RP, and MacKnight WJ. Preparation and polymerization of ethylene 2,6-Naphthalenedicarboxylate cyclic oligomers, Macromolecules, 2000, 33, 3606–3610.

32. Hodge P and Colquhoun HM. Recent work on entropically-driven ring-opening polymerizations: some potential applications, Polymers for Advanced Technologies, 2005, 16, 2-3, 84-94.

33. Parton H and Verpoest I. *In situ* polymerization of thermoplastic composites based on cyclic oligomers, Polymer Composites, 2005, 26, 1, 60-65.

34. Tripathy AR, Elmoumni A, Winter HH, and MacKnight WJ. Effects of catalyst and polymerization temperature on the *in situ* polymerization of cyclic poly(butylene terephthalate) oligomers for composite applications, Macromolecules, 2005, 38, 709-715.

35. Mohd Ishak ZA, Gatos KG, and Karger-Kocsis J. On the *in situ* polymerization of cyclic butylene terephthalate oligomers: DSC and rheological studies, Polymer Engineering and Science, 2006, 743-750.

36. Mohd Ishak ZA, Shang PP, and Karger-Kocsis J. A modulated DSC study on the *in situ* polymerization of cyclic butylene terephthalate oligomers, Journal of Thermal Analysis and Calorimetry, 2006, 84, 3, 637-641.

37. Pang K, Kotek R, and Tonelli A. Review of conventional and novel polymerization processes for polyesters Progress Polymer Science, 2006, 31, 1009-1037.

38. Tastard CY, Hodge P, Ben-Haida A, and Dobinson M. Entropically driven ring-opening metathesis polymerization (ED-ROMP) of macrocyclic olefin-containing oligoamides Reactive and Functional Polymers, 2006, 66, 1, 93-107.

39. Hakme C, Stevenson I, Maazouz A, Cassagnau P, Boiteux G, and Seytre G. *In situ* monitoring of cyclic butylene terephtalate polymerization by dielectric sensing, Journal of Non-Crystalline Solids, 2007, 353, 4362–4365.

40. Giuseppina Lanciano, Antonio Grecoa, Alfonso Maffezzoli, and Mascia. L. Effects of thermal history in the ring opening polymerization of CBT and its mixtures with montmorillonite on the crystallization of the resulting poly(butylene terephthalate) Thermochimica Acta, 2009, 493, 61–67.

41. Evans TL, Brunelle DJ, Bradt JE, Pearce EJ, and Wilson PR. Polymerisation of marcocyclic poly(alkylene dicarboxylate) oligomers, U.S. Patent, 5,466,744, 1995.

42. Burch Jr. RR, Dembek AA, Lustig SR, and Spina M. Polymerisations based on cyclic oligomer, U.S. patent, 6,297,330, 2001.

43. Miller S, Donovan J, and MacKnight WJ, Toughness enhancement through conversion of cyclic polybutylene terephthalate to linear PBT, in *ANTEC 2000 Plastics: The Magical Solution*. 2000. p. 1494-1497.

44. Harsch M, Karger-Kocsis J, and Apostolov AA. Crystallization-induced shrinkage, crystalline, and thermomechanical properties of *in situ* polymerized cyclic butylene terephthalate, Journal of Applied Polymer Science, 2008, 108, 1455–1461.

45. Brunelle DJ, Takekoshi T, and Serth-Guzzo J. Titanate catalyst, U.S. Patent, 5,710,086, 1998.

46. Winckler SJ and Takekoshi T. Macrocyclic polyester oligomers and the processes for polymerizing the same, U.S. Patent, 6,420,047, 2002.

47. Winckler SJ and Takekoshi T. Blend material including macrocyclic polyester oligomers and the processes for the same, U.S. Patent, 6,369,157, 2002.

48. Takekoshi T and Pearce EJ. Method for polymerizing macrocyclic poly(alkylene dicarboxylate) oligomers, U.S. Patent, 5,591,800, 1997.

49. Brunelle DJ, ed. Ring-opening polymerization. Hanser Publisher: Munich. 1993.

50. Tripathy AR, Chen W, Kukureka SN, and MacKnight WJ. Novel poly(butylene terephthalate)/poly(vinyl butyral) blends prepared by in situ polymerization of cyclic poly(butylene terephthalate) oligomers, Polymer, 2003, 44, 1835-1842.

51. Tripathy AR, Burgaz E, Kukureka SN, and MacKnight WJ. Poly(butylene terephthalate) nanocomposites prepared by *in situ* polymerization, Macromolecules, 2003, 36, 8593-8595.

52. Al-Zubi R, Wang YF, and Larson P. Rotomoldability of cyclic poly (butylene terephthalate),. in *ANTEC 2003 Plastics: Annual Technical Conference, Volume 1: Processing*. 2003.

53. Parton H, Baetsa J, Lipnikc P, Goderisb B, Devauxc J, and Verpoest I. Properties of poly(butylene terephthatlate) polymerized from cyclic oligomers and its composites, Polymer, 2005, 46, 9871-9880.

54. Mohd Ishak ZA, Leong YW, Steeg M, and Karger-Kocsis J. Woven glass fabric composites *via in situ* polymerized cyclic butylene terephthalate oligomers. in *ANTEC 2006 Plastics: Annual Technical Conference Proceedings*. 2006.

55. Mohd Ishak ZA, Leong YW, Steeg M, and Karger-Kocsis J. Mechanical properties of woven glass fabric reinforced in situ polymerized poly(butylene terephthalate) composites, Composites Science and Technology, 2007, 67, 390-398.

56. Tripathy AR, Farris RJ, and MacKnight WJ. Novel fire resistant matrixes for composites from cyclic poly(butylene terephthalate) oligomers, Polymer Engineering and Science, 2007, 47, 1536-1543.

57. Mader E, Gao SL, Plonka R, and Wang J. Investigation on adhesion, interphases, and failure behaviour of cyclic butylene terephthalate (CBT)/glass fiber composites, Composites Science and Technology 2007, 67, 3140–3150.

58. Baets J, Godara A, Devaux J, and Verpoest I. Toughening of polymerized cyclic butylene terephthalate with carbon nanotubes for use in composites, Composites: Part A, 2008, 39, 1756–1761.

59. Wan C, Zhao F, Bao X, Kandasubramanian B, and Duggan M. Surface characteristics of polyhedral oligomeric silsesquioxane modified clay and its application in polymerization of macrocyclic polyester oligomers, Journal of Physical Chemistry: Part. B, 2008, 112, 11915–11922.

60. Bardash L, Boiteux G, Seytre G, Hakme C, Dargere N, Rybak A, and Melis F. Novel conductive polymer composites based on poly(butylene terephtalate) filled with carbon fibers, E-Polymers, 2008.

61. Berti C, Fiorini M, and Sisti L. Synthesis of poly(butylene terephtahlate) nanocomposites using anionic clays, European Polymer Journal, 2009, 45, 1, 70-78.

62. Wu F and Yang G. Poly(butylene terephthalate)/organoclay nanocomposites prepared by in-situ bulk polymerization with cyclic poly(butylene terephthalate), Materials Letters 2009, 63 1686–1688.

63. Jiang ZY, Siengchin S, Zhou LM, Steeg M, Karger-Kocsis J, and Man HC. Poly (butylene terephthalate)/silica nanocomposites prepared from cyclic butylene terephthalate, Composites: Part A-Applied Science and Manufacturing, 2009, 40, 3, 273-278.

64. Lars Lundquist, Yves Leterrier, Sunderland P, and Månson J-AE. Life Cycle Engineering of Plastics Amsterdam: Elsevier Ltd, 2000.

65. Astrom BT. Manufacturing of polymer composites. London: Chapman & Hall, 1997.

66. Nachlis WL, Kambour RP, and MacKnight WJ. *In situ* polymerization of bisphenoI-A carbonate cyclic oligomers in miscible blends with a styrene-acrylonitrile copolymer: phase separation dynamics and the influence of phase dispersion on ductility, Polymer, 1994, 35, 17, 3643-3657.

67. Tripathy AR, MacKnight WJ, and Kukureka SN. *In situ* copolymerization of cyclic poly(butylene terephthalate) oligomers and caprolactone, Macromolecules, 2004, 37, 6793-6800.

68. Baets J, Dutoit M, Devaux J, and Verpoest I. Toughening of glass fiber reinforced composites with a cyclic butylene terephthalate matrix by addition of polycaprolactone, Composites: Part A, 2008, 39, 13–18

69. Karger-Kocsis J, Felhos D, Barany T, and Czigany T. Hybrids of HNBR and *in situ* polymerizable cyclic butylene terephthalate (CBT) oligomers: properties and dry sliding behavior, Express Polymer Letters, 2008, 2, 7, 520-527.

70. Bahloul W, Bounor-Legare´ V, Fenouillot F, and Cassagnau P. EVA/PBT nanostructured blends synthesized by in situ polymerization of cyclic CBT (cyclic butylene terephthalate) in molten EVA, Polymer, 2009, 50, 2527–2534.

71. Xu D, Karger-Kocsis J, and Apostolov AA. Hybrids from HNBR and *in situ* polymerizable cyclic butylene terephthalate (CBT): Structure and rolling wear properties, European Polymer Journal, 2009, 45, 4, 1270-1281.

72. Nielsen LE and Landel RF. Mechanical properties of polymers and composites, 2nd ed., New York: Marcel Dekker, Inc., 1994.

73. Young RJ and Lovell PA. Introduction to polymers, 2nd ed., London: Chapman & Hall, 1991.

74. Bower DI. An introduction to polymer physics. United Kingdom: Cambridge University Press, 2002.

75. Fakirov S, ed. Handbook of thermoplastic polyesters. Vol. 1:Homopolymer, Copolymers, Blends and Composites. Wiley-VCH: Weinheim. 2002.

76. Chang EP, Kirsten RO, and Slagowski EL. Crystallization studies of polybutylene terephthalate, Abstracts of Papers of the American Chemical Society, 1978, 175, 112-112.

77. Illers KH. Heat of fusion and specific volume of poly(ethylene terephthalate) and poly(butylene terephthalate), Colloid and Polymer Science, 1980, 258, 2, 117-124.

78. Smith JG, Kibler CJ, and Sublett BJ. Preparation and properties of poly(methylene terephthalates), Journal of Polymer Science Part A-1: Polymer Chemistry, 1966, 4, 1851-1859.

79. Farrow G, Mcintosh J, and Ward IM. The interpretation of transition phenomena in polymethylene terephthalate polymers, Makromolekulare Chemie, 1960, 38, 147-158.

80. Van Berkel WM, Van Hartingsveldt EAA, and Van Der Sluijs CL. Handbook of thermoplastics. New York, Basel, Hong Kong: Marcel Dekker, Inc., 1997.

81. Tullo AH, Polymers heat up, in *Chemical and Engineering News*. 2001, American Chemical Society: Washington.

82. Domininghaus H. Plastics for engineers. Munich, Vienna, New York and Barcelona: Hanser Publisers, 1993.

83. Hodge P. Some applications of reactions which interconvert monomers, polymers and/or macrocycles Reactive & Functional Polymers, 2001, 48, 1-3, 15-23.

84. Jacobson H and Stockmayer WH. Intramolecular reaction in polycondensations: 1. The theory of linear systems, Journal of Chemical Physics, 1950, 18, 12, 1600-1606.

85. Ramsden HE, Metuchen, and Banks CK. Polyhydric alcohol-organotin deravatives, U.S. Patent, 2,789,994, 1957.

86. Moore ER. Properties of styrene maleic anhydride copolymers, Industrial & Engineering Chemistry Product Research and Development, 1986, 25, 2, 315-321.

87. Moore ER and Pickelman DM. Synthesis of styrene maleimide copolymers and physical properties thereof, Industrial & Engineering Chemistry Product Research and Development, 1986, 25, 4, 603-609.

88. SMA® Imide Resins SMA® 1000I, 2000I, 3000I and 4000I, http://www.sartomer.com/, 2009

89. Di Lorenzo ML and Righettiaz MC. Crystallization Of Poly(Butylene Terephthalate) Polymer Engineering and Science, 2003, 43, 12, 1889-1894.

90. Stein RS and Misra A. Morphological studies on polybutylene terephthalate, Journal of Polymer Science: Part B-Polymer Physics, 1980, 18, 2, 327-342.

91. Nachlis WL, Bendler JT, Kambour RP, and MacKnight WJ. Topological effects on blend miscibility, Macromolecules, 1995, 28, 23, 7869-7878.

92. Kotnis MA and Muthukumar M. Entropy induced frozen morphology in unstable polymer blends, Macromolecules, 1992, 25, 6, 1716-1724.

93. Paul DR and Bucknall CB. Polymer blends. Vol. Volume 1: Formulation, New York: John Wiley and Sons, Inc., 2000.

94. Paul DR and Newman S. Polymer blends. Vol. 1, New York, San Francisco, London: Academic Press, 1978.

95. Phelps. Species modification in macrocyclic polyester oligomers and compositions prepared thereby, U.S. Patent, 6,436,548, 2002.

96. Avrami M. Kinetic of phase change I: general theory, Journal of Chemical Physics, 1939, 7, 12, 1103-1113.

97. Avrami M. Kinetic of phase change II : Transformation-time relations for random distribution of nuclei, Journal of Chemical Physics, 1940, 8, 212-224.

98. Avrami M. Granulation, phase change and microstructure - Kinetics of phase change III, Journal of Chemical Physics, 1941, 9, 2, 177-184.

99. Hoffman JD and Weeks JJ. Melting process and the equilibrium melting temperature of polychlorotrifluoroethylene, Journal Of Research Of The National Bureau Of Standards—A. Physics and Chemistry, 1961, 66A, 1, 13-28.

100. Pyris software for windows, http://las.perkinelmer.co.uk/ApplicationsSummary/Applications/tea-software-pyris.htm, 2009

101. Pyris Software, www.perkinelmer.com, 2009

102. The Golden Gate™ Single Reflection Diamond ATR Series MkII, www.specac.com, 2009

103. Sperling LH. Introduction to physical polymer science, 4th ed., New Jersey: John Wiley & Sons, 2006.

104. Cirrus™ GPC / Multi Detector Software, http://www.varianinc.com/cgi-bin/nav?products/chrom/polymer/gpc/cirrus/index&cid=LLOHMNQLFO, 2009

105. Software and image capture, http://www.linkam.co.uk/, 2009

106. Brown ME. Introduction to thermal analysis: techniques and applications. London: Chapman & Hall, 1988.

107. Menczel JD and Prime RB, eds. Thermal analysis of polymers: Fundamentals and applications. John Wiley & Sons, Inc: New Jersey. 2009.

108. NETZSCH Proteus® Software for Thermal Analysis, http://www.netzsch-thermal-analysis.com/en/products/software/proteus/, 2009

109. Michler GH. Electron microscopy of polymers. Verlag, Berlin, Heidelberg: Springer, 2008.

110. Lehmann B and Karger-Kocsis J. Isothermal and non-isothermal crystallisation kinetics of pCBT and PBT, Journal of Thermal Analysis and Calorimetry, 2009, 95, 1, 221-227.

111. Yokouchi M, Sakakibara Y, Chatani Y, Tadokoro H, Tanaka T, and Yoda K. Structures of two crystalline forms of poly(butylene terephthalate) and reversible transition between them by mechanical deformation, Macromolecules, 1976, 9, 2, 266-273.

112. Boutevin B, Khamlichi M, Pietrasanta Y, and Robin JJ. Synthesis and characterization of a new block-copolymer - poly(butylene terephthalate-co-olefin) application on PP PBT Blend and PBT homopolymer, Journal of Applied Polymer Science, 1995, 55, 2, 191-199.

113. Nichols ME and Robertson RE. The multiple melting endotherms from poly(butylene terephthalate), Journal of Polymer Science: Part B-Polymer Physics, 1992, 30, 7, 755-768.

114. Huo PP, Cebe P, and Capel M. Dynamic mechanical relaxation and X-Ray scattering study of poly(butylene terephthalate) polyarylate blends, Macromolecules, 1993, 26, 16, 4275-4282.

115. Kong Y and Hay JN. Multiple melting behaviour of poly(ethylene terephthalate), Polymer, 2003, 44, 3, 623-633.

116. Pavia DL, Lampman GM, and Kriz Jr. GS. Introduction to spectroscopy: A guide for students of organic chemistry. Philadelphia: W. B. Saunders Company, 1979.

117. Cole KC, Ajji A, and Pellerin Er. New insights into the development of ordered structure in poly(ethylene terephthalate): 1. Results from external reflection infrared spectroscopy, Macromolecules, 2002, 35, 3, 770-784.

118. Jang J and Sim K. Crystallization behavior in poly(ether Imide)/poly(butylene terephthalate) blends using a spectroscopic method, Polymer Testing 1998, 17, 507–521.

119. Hopfe I, Pompe G, and Eichhorn KJ. Ordered structures and progressive transesterification in PC/PBT melt blends studied by FTIR spectroscopy combined with DSC and NMR, Polymer, 1997, 38, 10, 2321-2327.

120. Cao Y. Studies on the morphology and properties of polycarbonate/polypropylene blends, Ph. D., University of Birmingham, 2008.

121. Wong ACY and Lam F. Study of selected thermal characteristics of polypropylene/polyethylene binary blends using DSC and TGA, Polymer Testing, 2002, 21, 6, 691-696.

122. Samperia F, Puglisib C, Alicatab R, and Montaudob G. Thermal degradation of poly(butylene terephthalate) at the processing temperature, Polymer Degradation and Stability 2004, 83, 1, 11-17.

123. Carroccio S, Rizzarelli P, Scaltro G, and Puglisi C. Comparative investigation of photo- and thermal-oxidation processes in poly(butylene terephthalate), Polymer, 2008, 49, 16, 3371-3381.

124. Jandali MZ and Widmann G. Collected applications thermal analysis: thermoplastic. Bielefeld, Schwerzenbach: Mettler Toledo,

125. Wunderlich B. Macromolecular physics. Vol. Volume 2: Crystal Nucleation, Growth, Annealing, London: Academic Press, 1976.

126. Long Y, Shanks RA, and Stachurski ZH. Kinetics of polymer crystallization, Progress in Polymer Science, 1995, 20, 4, 651-701.

127. Turnbull D and Fisher JC. Rate of nucleation in condensed systems, Journal of Chemical Physics, 1949, 17, 1, 71-73.

128. Lauritzen JI and Hoffman JD. Extension of theory of growth of chain-folded polymer crystals to large undercoolings, Journal of Applied Physics, 1973, 44, 10, 4340-4352.

129. Jenkins MJ. Crystallisation in miscible blends of PEEK and PEI, Polymer, 2001, 42, 1981–1986.

130. Jenkins MJ, Cao Y, and Kukureka SN. The effect of molecular weight on the crystallization kinetics and equilibrium melting temperature of poly(tetramethylene ether glycol), Polymers for Advanced Technologies, 2006, 17, 1-5.

131. Cebe P and Hong SD. Crystallization behaviour of poly(ether-ether-ketone), Polymer, 1986, 27, 8, 1183-1192.

132. Al Lafi AG, Hay JN, and Parker DJ. The effect of proton irradiation on the melting and isothermal crystallization of poly (ether-ether-ketone), Journal of Polymer Science: Part B-Polymer Physics, 2008, 46, 11, 1094-1103.

133. Lauritzen JI and Hoffman JD. Theory of formation of polymer crystals with folded chains in dilute solution, Journal of Research of the National Bureau of Standards: Section a-Physics and Chemistry, 1960, 64, 1, 73-102.

134. Hoffman JD, Frolen LJ, Ross GS, and Lauritzen JI. Growth-rate of spherulites and axialites from melt in polyethylene fractions: Regime-1 and Regime-2 crystallization, Journal of Research of the National Bureau of Standards: Section a-Physics and Chemistry, 1975, 79, 6, 671-699.

135. Evans UR. The laws of expanding circles and spheres in relation to the lateral growth of surface films and the grain-size of metals, Transactions of the Faraday Society, 1945, 41, 7, 365-374.

136. Hay JN. Application of the modified avrami equations to polymer crystallisation kinetics, British Polymer Journal, 1971, 3 2, 74 - 82.

137. Lim JS, Noda I, and Im SS. Effects of metal ion-carbonyl interaction on miscibility and crystallization kinetic of poly(3-hydroxybutyrate-co-3-hydroxyhexanoate)/lightly ionized PBS, European Polymer Journal, 2008, 44, 5, 1428-1440.

138. Wu CM and Jiang CW. Crystallization and morphology of polymerized cyclic butylene terephthalate, Journal of Polymer Science: Part B-Polymer Physics, 2010, 48, 11, 1127-1134.

139. Booth A and Hay JN. Use of differential scanning calorimetry to study polymer crystallization kinetics, Polymer, 1969, 10, 2, 95-104.

140. Hay JN and Mills PJ. The use of differential scanning calorimetry to study polymer crystallization kinetics, Polymer, 1982, 23, 9, 1380-1384.

141. Qin JL, Guo SQ, and Li ZT. Melting behavior and isothermal crystallization kinetics of PP/mLLDPE blends, Journal of Polymer Research, 2008, 15, 5, 413-420.

142. Qin JL, Zhang SQ, and Li ZT. Melting behavior and isothermal crystallization kinetics of polypropylene/metallocene-catalyzed polyethylene elastomer blends, Journal of Applied Polymer Science, 2008, 110, 5, 2615-2622.

143. Chiu HJ, Shu WJ, and Huang JM. Crystallization kinetics of poly(trimethylene terephthalate)/poly(ether imide) blends, Polymer Engineering and Science, 2006, 46, 1, 89-96.

144. Di Lorenzo ML. Spherulite growth rates in binary polymer blends, Progress in Polymer Science, 2003, 28, 4, 663-689.

145. Soccio M, Lotti N, Finelli L, and Munari A. Effect of transesterification reactions on the crystallization behaviour and morphology of poly(butylene/diethylene succinate) block copolymers, European Polymer Journal, 2009, 45, 1, 171-181.

146. Lu J, Qiu Z, and Yang W. Crystallization kinetics and hydrophilicity improvement of biodegradable poly(butylene succinate) in its miscible blends with poly(ethylene oxide), Macromolecular Materials and Engineering 2008, 293, 930–938.

147. Hoffman JD, Davis GT, and Lauritzen Jr. JI, The rate of crystallization of linear polymers with chain folding, in *Treatise on solid state chemistry*, N.B. Hannay, Editor. 1976, Plenum: New York. p. 497.

148. Thomas DG and Staveley LAK. A study of the supercooling of drops of some molecular liquids, Journal of the Chemical Society, 1952, 4569-4577.

149. Lee LT and Woo EM. Miscible blends of poly(4-vinyl phenol)/poly (trimethylene terephthalate), Polymer International, 2004, 53, 11, 1813-1820.

150. Qiu ZB and Yang WT. Crystallization kinetics and morphology of poly(butylene succinate)/poly(vinyl phenol) blend, Polymer, 2006, 47, 18, 6429-6437.

151. Roitman DB, Marand H, Miller RL, and Hoffman JD. Kinetics of crystallization and morphology of poly(pivalolactone): Regime II - III transition and nucleation constants, Journal of Physical Chemistry, 1989, 93, 19, 6919-6926.

152. Marand H and Hoffman JD. Determination of the fold surface free-energy and the equilibrium melting temperature for alpha-phase poly(pivalolactone) crystals, Macromolecules, 1990, 23, 15, 3682-3687.

153. Jang J and Sim K. Spectroscopic studies of the crystallization behaviour in poly(ether imide) poly(ethylene terephthalate) blends, Polymer, 1997, 38, 16, 4043-4048.

154. Utracki LA. Polymer alloys and blends: Thermodynamic and rheology. Munich; Vienna; New York: Hanser Publishers, 1989.

155. Fekete E, Foldes E, and Pukanszky M. Effect of molecular interactions on the miscibility and structure of polymer blends, European Polymer Journal, 2005, 41, 4, 727-736.

156. Paul DR. Polymer-polymer interactions, Pure and Applied Chemistry, 1995, 67, 6, 977-984.

157. Thirtha V, Lehman R, and Nosker T. Morphological effects on glass transition behavior in selected immiscible blends of amorphous and sernicrystalline polymers, Polymer, 2006, 47, 15, 5392-5401.

158. Rim PB and Orler EB. Dependence of Tg on composition for a compatible polymer/oligomer blend, Macromolecules, 1987, 20, 433-435.

159. T. G. Fox. Bulletin of the American Physical Society 1956, 1, 123.

160. Sperling LH. Polymeric multicomponent materials: An introduction. Canada: Wiley, 1997.

161. Xing PX, Dong LS, An YX, Feng ZL, Avella M, and Martuscelli E. Miscibility and crystallization of poly(beta-hydroxybutyrate) and poly(p-vinylphenol) blends, Macromolecules, 1997, 30, 9, 2726-2733.

162. Gordon M and Taylor JS. Ideal copolymers and the 2nd-order transitions of synthetic rubbers .1. non-crystalline copolymers, Journal of Applied Chemistry, 1952, 2, 9, 493-500.

163. An L, Hea D, Jinga J, Wanga Z, Yua D, Jianga B, Jiangb Z, and Mab R. Effects of molecular weight and interaction parameter on the glass transition temperature of polystyrene mixtures and its blends with polystyrene/poly (2,6-dimethyl-p-phenylene oxide), European Polymer Journal, 1997, 33, 9, 1523-1528.

164. Liua Y, Bhandarib B, and Zhou W. Study of glass transition and enthalpy relaxation of mixtures of amorphous sucrose and amorphous tapioca starch syrup solid by differential scanning calorimetry (DSC), Journal of Food Engineering, 2007, 81, 3, 599-610.

165. Chow WS. Cyclic extrusion of poly(butylene terephthalate)/organo-montmorillonite nanocomposites: Thermal and mechanical retention properties, Journal of Applied Polymer Science, 2008, 110, 3, 1642-1648.

166. Dreezen G, Koch MHJ, Reynaers H, and Groeninckx G. Miscible binary blends of poly(ethylene oxide) and an amorphous aromatic polyamide (Aramide 34I): crystallization, melting behavior and semi-crystalline morphology, Polymer, 1999, 40, 23, 6451-6463.

167. Yang HL, Lai MF, Liu WJ, Sun CR, and Liu JJ. Morphology and thermal and mechanical properties of PBT/HIPS and PBT/HIPS-g-GMA blends, Journal of Applied Polymer Science, 2002, 85, 12, 2600-2608.

168. Sun SL, Tan ZY, Zhou C, Zhang MY, and Zhang HX. Effect of ABS grafting degree and compatibilization on the properties of PBT/ABS blends, Polymer Composites, 2007, 28, 4, 484-492.

169. Huang JW, Wen YL, Kang CC, Yeh MY, and Wen SB. Morphology, melting behavior, and non-isothermal crystallization of poly(butylene terephthalate)/poly(ethylene-co-methacrylic acid) blends, Thermochimica Acta, 2007, 465, 1-2, 48-58.

170. Cassagnau P and Michel A. New morphologies in immiscible polymer blends generated by a dynamic quenching process, Polymer, 2001, 42, 7, 3139-3152.

171. Lei YG, Cheung ZL, Ng KM, Li L, Weng LT, and Chan CM. Surface chemical and morphological properties of a blend containing semi-crystalline and amorphous polymers studied with ToF-SIMS, XPS and AFM, Polymer, 2003, 44, 14, 3883-3890.

172. Kemp W. Organic spectroscopy, 3 ed., London: The MacMillan Press Ltd, 1991.

173. Krakovsky I, Lokaj J, Sedlakova Z, Ikeda Y, and Nishida K. Hydrogen bonding interactions of styrene-maleimide copolymers with diaminotriazine derivatives, Journal of Applied Polymer Science, 2006, 101, 4, 2338-2346.

174. Pu H and Qiao L. Proton conductivity of acid doped styrene-maleic imide copolymer with benzimidazole side group, Macromolecular Chemistry and Physics, 2005, 206, 263–267.

175. Su WY, Wang Y, Min K, and Quirk RP. In situ copolymerization and compatibilization of polyester and polystyrene blends. I. Synthesis of functionalized polystyrenes and the reactions with polyester, Polymer, 2001, 42, 12, 5107-5119.

176. Su WY, Min KS, and Quirk RP. In situ copolymerization and compatibilization of polyester and polystyrene blends. II. Thermally and chemically induced reaction and mechanical properties, Polymer, 2001, 42, 12, 5121-5134.

177. Jeon HK and Kim JK. Morphological development with time for immiscible polymer blends with an in situ compatibilizer under controlled shear conditions, Polymer, 1998, 39, 25, 6227-6234.

178. He JS, Bu WS, and Zeng JJ. Co-phase continuity in immiscible binary polymer blends, Polymer, 1997, 38, 26, 6347-6353.

179. Kim JK, Kim S, and Park CE. Compatibilization mechanism of polymer blends with an *in situ* compatibilizer, Polymer, 1997, 38, 9, 2155-2164.

180. Sun QJ, Zhang BY, Yao DS, Yu L, and Jiang ZL. Miscibility enhancement of PP/PBT blends with a side-chain liquid crystalline ionomer, Journal of Applied Polymer Science, 2009, 112, 5, 3007-3015.

181. Russell TP and Stein RS. An investigation of the compatibility and morphology of semicrystalline poly(epsilon-caprolactone)-poly(vinyl chloride) blends, Journal of Polymer Science: Part B-Polymer Physics, 1983, 21, 7, 999-1010.

182. Morra BS and Stein RS. The crystalline morphology of poly(vinylidene fluoride) poly(methylmethacrylate) blends, Polymer Engineering and Science, 1984, 24, 5, 311-318.

183. Russell TP, Ito H, and Wignall GD. Neutron and X-Ray-Scattering studies on semicrystalline polymer blends, Macromolecules, 1988, 21, 6, 1703-1709.

184. Runt JP, Zhang X, Miley DM, Gallagher KP, and Zhang A. Phase-behavior of poly(butylene terephthalate) polyarylate blends, Macromolecules, 1992, 25, 15, 3902-3905.

185. Hsiao BS and Sauer BB. Glass-transition, crystallization and morphology relationships in miscible poly(aryl ether ketones) and poly(ether imide) blends, Journal of Polymer Science: Part B-Polymer Physics, 1993, 31, 8, 901-915.

186. Defieuw G, Groeninckx G, and Reynaers H. Miscibility and morphology of binary polymer blends of polycaprolactone with solution-chlorinated polyethylenes, Polymer, 1989, 30, 4, 595-603.

187. Crevecoeur G and Groeninckx G. Binary blends of poly(ether ether ketone) and poly(ether imide) - miscibility, crystallization behavior and semicrystalline morphology, Macromolecules, 1991, 24, 5, 1190-1195.

188. Lohse DJ and Wissler GE. Compatibility and morphology of blends of isotactic and atactic polypropylene, Journal of Materials Science, 1991, 26, 3, 743-748.

189. Hudson SD, Davis DD, and Lovinger AJ. Semicrystalline morphology of poly(aryl ether ether ketone) poly(ether imide) blends, Macromolecules, 1992, 25, 6, 1759-1765.

190. Talibuddin S, Wu L, Runt J, and Lin JS. Microstructure of melt-miscible semicrystalline polymer blends, Macromolecules, 1996, 29, 23, 7527-7535.

191. Wu LM, Lisowski M, Talibuddin S, and Runt J. Crystallization of poly(ethylene oxide) and melt-miscible PEO blends, Macromolecules, 1999, 32, 5, 1576-1581.

192. Nishi T, Wang TT, and Kwei TK. Thermally induced phase separation behavior of compatible polymer mixtures, Macromolecules, 1975, 8, 2, 227-234.

193. Nishi T and Wang TT. Melting point depression and kinetic effects of cooling on crystallization in poly(vinylidene fluoride) poly(methyl methacrylate) mixtures, Macromolecules, 1975, 8, 6, 909-915.

194. Chen HL and Porter RS. Spherulitic growth kinetics in miscible blends of poly(ether ether ketone) and poly(ether imide), Journal of Polymer Research-Taiwan, 1999, 6, 1, 21-26.

195. El-Shafee E, Saad GR, and Fahmy SM. Miscibility, crystallization and phase structure of poly(3-hydroxybutyrate)/cellulose acetate butyrate blends, European Polymer Journal, 2001, 37, 10, 2091-2104.

196. Qiu ZB, Komura M, Ikehara T, and Nishi T. Miscibility and crystallization behavior of biodegradable blends of two aliphatic polyesters. Poly(butylene succinate) and poly(epsilon-caprolactone), Polymer, 2003, 44, 25, 7749-7756.

197. Qiu ZB, Ikehara T, and Nishi T. Melting behaviour of poly(butylene succinate) in miscible blends with poly(ethylene oxide), Polymer, 2003, 44, 10, 3095-3099.

198. Qiu Z, Komura M, Ikehara T, and Nishi T. Poly(butylene succinate)/poly(vinyl phenol) blends. Part 1. Miscibility and crystallization, Polymer, 2003, 44, 26, 8111-8117.

199. Supaphol P, Apiwarithanakorn N, and Krutphun P. Effect of small amount of poly(ethylene naphthalate) on isothermal crystallization and spherulitic morphology of poly(trimethylene terephthalate), Polymer Testing, 2007, 26, 8, 985-1000.

200. Zhang HL, Ren MQ, Chen QY, Sun SL, Sun XH, Zhang HX, and Mo ZS. Miscibility and crystallization behavior of PBT/epoxy blends, Journal of Polymer Science Part B-Polymer Physics, 2006, 44, 9, 1320-1330.

201. Flory PJ. Principles of polymer chemistry. New York: Cornell, 1953.

202. Gedde UW. Polymer physics. London: Chapman & Hall, 1995.

203. Al-Mulla A, Mathew J, and Shanks R. Isothermal crystallization studies of poly(butylene terephthalate) composites, Journal of Polymer Science: Part B: Polymer Physics, 2007, 45, 11, 1344-1353.

204. Avella M and Martuscelli E. Poly-D(-)(3-hydroxybutyrate) poly(ethylene oxide) blends - Phase diagram, thermal and crystallization behavior, Polymer, 1988, 29, 10, 1731-1737.